Investigating the relationship between hypoxia and the immune tumour microenvironment in muscle-invasive bladder cancer

A thesis submitted to the University of Manchester for the degree of Doctor of Philosophy in the Faculty of Biology, Medicine and Health.

2022

Victoria (Vicky) Z Smith

School of Medical Sciences

Division of Cancer Sciences

Table of Contents

Word count: 62,515

List of figures

List of tables

List of abbreviations

Abbreviation	Definition
5-FU	5-fluorouracil
APC	antigen presenting cell
APZ	apaziquone
Ba/Sq	basal/squamous
BAM	binary alignment and map
BCG	Bacillus Calmette-Guérin
BCON	bladder carbogen and nicotinamide [trial]
BH	Benjamini-Hochberg
BLCA	bladder cancer
bp	base pairs
BRCA	breast invasive carcinoma
CAF	cancer-associated fibroblast
CDx	cluster of differentiation x
CESC	cervical squamous cell carcinoma and endocervical adenocarcinoma
ChIP	chromatin immunoprecipitation
CI	confidence interval
CIS	carcinoma *in situ*
CON	carbogen and nicotinamide
COX-2	cyclodeoxygenase 2
CRUK MI	cancer research UK manchester institute
CSS	cause-specific survival
CTLA-4	cytotoxic T-lymphocyte associated protein 4
DAMPs	danger-associated molecular patterns
DC	dendritic cell
DCA	dichloroacetate
DC-SIGN	dendritic cell type specific C-type lectin
DEG	differentially expressed gene
DMSO	dimethyl sulphoxide
DSP	digital spatial profiling
DSS	disease-specific survival
ECM	extra-cellular matrix
EDTA	ethylenediaminetetraacetic acid
EGFR	epidermal growth factor receptor
EMT	epithelial-to-mesenchymal transition
ESCA	esophageal carcinoma
FACS	fluorescence-activated cell sorting
FBS	foetal bovine serum
FDA	food and drug administration
FDR	false discovery rate
FFPE	formalin-fixed, paraffin-embedded
GEO	gene expression omnibus
GO	gene ontology
GSEA	gene set enrichment analysis
HER2	human epidermal growth factor receptor-2

HIF	hypoxia-inducible factor
HR	hazard ratio
HRE	hypoxia-responsive element
HRP	horseradish peroxidase
ICI	immune checkpoint inhibitor
IFN	interferon
IFNγ	interferon gamma
IHC	immunohistochemistry
iNOS	inducible nitric oxide synthase
IP	immunoprecipitation
LASSO	least absolute shrinkage and selection operator
LPFS	local progression-free survival
LPS	lipopolysaccharide
LumNS	luminal non-specified
LumP	luminal papillary
LumU	luminal unstable
LUSC	lung squamous cell carcinoma
MDS	multidimensional scaling
MDSC	myeloid-derived suppressor cell
MFS	metastasis-free survival
MHC	major histocompatability complex
MIBC	muscle-invasive bladder cancer
MMC	mitomycin C
NCBI	national center for biotechnology information
NE-like	neuroendocrine-like
NHS	national health service
NICE	national institute for health care excellence
NK	natural killer
NMIBC	non-muscle-invasive bladder cancer
O_2	oxygen
OER	oxygen enhancement ratio
OR	odds ratio
OS	overall survival
PAAD	pancreatic adenocarcinoma
PBS	phosphate-buffered saline
PBS-T	PBS-Tween
PCR	polymerase chain reaction
PD-1	programmed cell death protein-1
PD-L1	programmed death ligand 1
PE	phycoerythrin
PFA	paraformaldehyde
PFS	progression-free survival
PGE_2	prostaglandin E_2
PIC	protease inhibitor cocktail
PRAD	prostate adenocarcinoma
PVDF	polyvinyidene difluoride
RB	retinoblastoma protein

RFS	relapse-free survival
ROS	reactive oxygen species
SAM	sequence alignment and map
TAE	tris-acetate-EDTA
TAM	tumour-associated macrophage
TAP	transporter associated with antigen processing
TCC	transitional cell carcinoma
TCGA	the cancer genome atlas
TGF-β	transforming growth factor beta
Th1	T helper 1 cell
Th2	T helper 2 cell
TLR	toll-like receptors
TMA	tissue microarray
TME	tumour microenvironment
TMT	tri-modalilty therapy
TNF	tumour necrosis factor
TNM	tumour, node, metastasis
TPZ	tirapazamine
TRB	translational radiobiology group
Treg	regulatory T cells
TSS	transcriptional start site
TTG	targeted therapy group
TURBT	trans-urethral resection of bladder tumour
UCSC	University of California, Santa Cruz
VEGF	vascular endothelial growth factor
WHO	world health organisation

Abstract

Introduction: Muscle-invasive bladder cancer (MIBC) has high rates of recurrence with poor survival rates. There is a need to improve response to radiotherapy and survival outcomes. Both hypoxia and the immune tumour microenvironment (TME) are therapeutically targetable in MIBC using hypoxia-modifying therapy and immune checkpoint inhibitors (ICIs), respectively. Recent data showed hypoxia drives an immunosuppressive TME via various mechanisms including upregulation of programmed death ligand 1 (PD-L1) and the inhibition and exclusion of cytotoxic CD8 T cells. Published literature also demonstrates hypoxia-driven upregulation of inflammation. There is currently no single biomarker that stratifies MIBC patients for both hypoxia-modifying therapy and ICIs. Therefore, the main thesis aims were to: 1) investigate if hypoxia is associated with upregulation of PD-L1 in MIBC, 2) investigate whether patients with low tumour CD8 T cells benefit from hypoxia-modifying therapy, 3) investigate the role of HIF and hypoxia in immune-related signalling in MIBC, 4) develop a hypoxia-driven immune gene signature that could be used to stratify MIBC patients for hypoxia-modifying therapy and ICIs.

Materials and methods: 1) Three human MIBC cell lines (T24, J82, UMUC3) were cultured in normoxia (20% oxygen) or hypoxia (1% and 0.1% oxygen) for 24 h. Differences in PD-L1 expression were measured using Western blotting, qPCR and flow cytometry. Published gene signatures were used to correlate hypoxia with PD-L1 expression and IFNγ signalling in BCON and TCGA MIBC cohorts. The BCON trial randomised bladder cancer patients to radiotherapy +/- hypoxia-modifying carbogen plus nicotinamide (CON). 2) Tissue microarrays of diagnostic biopsies from 116 BCON patients were stained using multiplex immunohistochemistry (IHC) for CD8, CD4, FOXP3, CD68, and PDL1. Hypoxia was assessed using CA9 IHC. Relationships with overall survival (OS) were investigated using Cox proportional hazard models. 3) ChIPseq and microarray data from MIBC cell lines and the TCGA cohort were used to analyse relationships between HIF/hypoxia and immune-related signalling and to identify prognostic hypoxia-driven immune genes. A LASSO regression model defined a final six-gene signature. Validation and analysis was performed on four bladder cancer cohorts. All *in silico* analyses were carried out using R and RStudio.

Results: 1) Increasing seeding density decreased PD-L1 protein ($p<0.001$) and mRNA ($p=0.001$) expression in T24 cells at 20% and 1% oxygen. Only when 100% confluent were PD-L1 protein and mRNA levels higher in 1% versus 20% oxygen ($p=0.056$ and $p=0.037$). Hypoxia was positively associated with both PD-L1 expression and IFNγ signalling in both BCON ($p=0.003$ and $p<0.001$) and TCGA (both $p<0.001$) cohorts. 2) Low vs high CD8+ T-cell counts were associated with a worse OS across the whole BCON cohort (HR 0.47, $p=0.003$) and in the radiotherapy alone group (HR 0.39, $p=0.005$). Patients with low CD8+ T-cells benefited from CON (HR 0.63, $p=0.05$) and CA9 positive tumours had fewer CD8+ T-cells ($p=0.03$). 3) HIF1/2 bound to ~10% of all immune-related genes in T24 cells and associated with T cell activation signalling. MIBC cells in hypoxia were enriched for myeloid and neutrophil signalling pathways. Hypoxia upregulated both suppressive and anti-tumour immune signalling in MIBC tumours. 4) Low vs high gene signature scores associated with a significantly worse OS in TCGA (HR 2.71, $p<0.0001$), GSE32894 (HR 8.72, $p<0.0001$) and GSE13507 (HR 1.96, $p=0.0054$) cohorts. Signature scores were not prognostic in BCON ($p=0.37$) for the overall cohort, however, patients with high scores benefitted from having CON with radiotherapy (HR 0.57, $p=0.043$). Scores correlated positively with hypoxia scores and associated with basal/squamous and stroma-rich molecular subtypes. Hallmark pathways associated with inflammation were significantly enriched, and TGF-β signalling significantly decreased when gene scores were high vs low.

Conclusions: 1) Hypoxia increases PD-L1 expression in confluent MIBC cells and cell density needs to be considered when studying PD-L1 expression *in vitro*. 2) Low CD8 T cell counts predict benefit from CON and is a potential marker for patient stratification. 3) Hypoxia upregulates both anti-tumour and immune suppressive signalling in MIBC. 4) A derived hypoxia-driven immune gene signature identifies poor prognosis MIBC patients who benefit from having CON with radiotherapy. The signature reflects a hypoxic and inflamed TME and phenotypes that are likely to respond to ICIs.

Declaration

No portion of the work referred to in the thesis has been submitted in support of an application for another degree or qualification of this or any other institute of learning.

Copyright statement

Acknowledgements

I'd like to start by extending my gratitude to Tim Illidge for giving me the opportunity to do this PhD project and for seeing my potential from the beginning. Tim has always been supportive and he has guided me these past four years, for which I am thankful.

I would next like to thank Catharine West who has tirelessly supported me throughout this project. She always provided support when I needed it, pushed me to pursue the project to its full potential, and taught me how to write scientifically. She has been instrumental in publishing the existing paper, submitting the second one and providing the potential for two more. I am extremely grateful for all the help she has given me.

I'd like to thank Ananya Choudhury who has provided me with bladder cancer expertise and helped me with collaborations and proofing documents. I'd also like to thank Peter Hoskin who has been instrumental for the project by allowing me to use the BCON data.

I would like to thank members of the TTG lab especially Debayan Mukherjee, Sapna Lunj, Ellie Cheadle, and Rick Walshaw who helped me along various stages of this project, for which I am very grateful. I'd like to extend my thanks to the rest of the TTG lab group members who made the first year of my PhD so enjoyable and helped me learn various techniques: Ester, Fede, Swati, Tiana, and Rachael - thank you.

Many aspects of this project would not have been possible without the help of various people who provided extensive help along the way. Firstly, thank you to Anna Maria who tirelessly provided support during the multiplex IHC project. Secondly, thank you to Bettina Wingelhoffer who provided essential help and reagents for the ChIPseq experiment. Thirdly, thank you to Sudhakar Sahoo who came up with the model for deriving the gene signature and guided me with various bioinformatics based aspects of this project.

I would like to thank Rob Sellers and Dave Lee, who provided support and help for coding aspects of the gene signature derivation and PD-L1 related ChIPseq analysis, respectively. Thank you to Alex Baker who provided much support for image analysis and microscope use for the multiplex project. I would also like to thank members of the TRB group for their help, especially Brian Lee and Mark Reardon for bioinformatics support.

Thank you to Millie Jones, who has been a good friend from day one and has always been there to lend an ear. She has made this PhD more enjoyable with her as a support and the weekly chats on the way to orchestra provided a much needed outlet. Together, we did it!

I'd like to thank my family for always supporting me throughout my studies. I would also like to thank Claire Pach for encouraging me to become more assertive.

Finally, an immeasurable thank you to Michael Pach, whose love and support knows no bounds. He has continuously supported me throughout this PhD in many different ways, but most noticeably he always listened to my ramblings and helped me to come up with solutions (even when all he wanted to do was enjoy our pints in the sunshine!). I am eternally grateful for him and thankful for all of his support through these last four years.

Last, but definitely not least, I would like to thank Lily and Lotus for all the afternoon cuddles, boundless love and infinite affection (and feathers). Thank you to all!

Preface

Vicky Smith graduated from Queen's University Belfast in 2016 with a first class honours degree in Biomedical Science. She gained lab experience having continued on a summer studentship at the Centre for Cancer Research and Cell Biology in Belfast as her undergraduate research project for the dissertation. She then gained her Master of Research degree in Cancer Sciences from the University of Birmingham in 2017. She started her PhD in 2018 after being awarded a BRC funded PhD studentship with Prof Tim Illidge (Targeted Therapy Group) and Prof Catharine West (Translational RadioBiology group).

Vicky taught herself R coding in 2020 during the first pandemic lock-down and subsequently enrolled with the Translation Manchester scheme to partake in two bioinformatics-related Master's level courses at the University of Manchester. She also partook in the NGS courses run by the Computational Biology Services (CBS) team at CRUK MI to help further her understanding of NGS analysis and bioinformatics.

Statement regarding content

The best science arises from collaboration and this thesis is no exception.

Multiplex IHC was performed with the extensive help from Anna Maria of Richard Byers' group for the initial protocol and immune marker panel, Claire Hart of Mick Brown's group who helped with TMA scanning and processing, and Alex Baker of CRUK MI VIA core facility who helped with microscope use and all image analysis in HALO. CA9 staining of BCON tissue was previously performed by members of the TRB group (Eustace, Irlam, *et al.*, 2013).

ChIP sequencing was only possible because of Bettina Wingelhoffer's tireless help and assistance. The sequencing was performed by the CRUK MI core facilities and subsequent QC and mapping by Sudhakar Sahoo of CRUK MI CBS core facility. The CBS group provided essential help and guidance during the last year of the project. The immune-related ChIPseq analysis was performed by Dave Lee. Rob Sellers and Sudhakar provided the overall model for deriving the gene signature with much help, troubleshooting and question answering along the way.

Microarray gene expression from MIBC cell lines was generated by Rekaya Shabbir in the TRB group who let me use the data for my immune-related analysis.

1 Introduction

1.1 Bladder cancer

1.1.1 Statistics and risk factors

Bladder cancer is the tenth most commonly diagnosed cancer worldwide (Sung *et al.*, 2021). In the UK it is the 11th most commonly diagnosed cancer and the ninth most common cause of cancer mortality, which increases to seventh for males. The disease causes 5,600 deaths every year in the UK, amounting to 15 deaths each day. Bladder cancer disproportionately affects males, which account for 73% of all cases. Incidence rates are also strongly related to age with almost six in ten new cases presenting in people aged 75 and over, and diagnoses peaking at 85-89 years (Office for National Statistics, 2019a; Northern Ireland Cancer Registry, 2020; Public Health Scotland, 2020; Public Health Wales, 2020).

In England, 32.5% of patients have non-muscle-invasive disease at initial presentation, whilst the rest present with disease that has either invaded into the muscle layer of the bladder or the disease stage is unknown (NHS Digital, 2019). Despite bladder cancer survival rates improving by over 10% in the last ten years, the overall ten-year survival rate is only 46% in the UK. Between 2013 and 2017 the five-year survival rates for stage 1 bladder cancer were 79.4%, decreasing to 45.7% and 41.2% for stages 2 and 3 respectively (Office for National Statistics, 2019b).

There are established risk factors associated with bladder cancer. The main risk factor is smoking, which causes 45% of all bladder cancer cases, but also includes exposure to ionising radiation and occupational exposure to aromatic amines, polycyclic hydrocarbons (formed during fossil fuel combustion), paint, mineral oils (aluminium production) and asbestos (Cumberbatch *et al.*, 2018).

1.1.2 Stages and grading

Transitional cell carcinomas (TCCs) account for the majority of all bladder cancers, which are then classified into superficial and invasive subtypes. Superficial tumours are non-muscle-invasive bladder cancers (NMIBC) that are confined to the urothelium, whilst muscle-invasive bladder cancers (MIBC) are tumours that have spread into the surrounding muscle layer of the bladder wall. Less common are bladder cancers arising from other cell types within (adenocarcinoma, squamous cell carcinoma) or outside (e.g. lymphoma, leiomyosarcoma, small cell carcinoma) the urothelium (Reynard 2013, Resnick 2003). The

tumours are staged depending on the extent of invasion into surrounding tissue according to the TNM system (Table 1.1) and graded according to both the 1973 and 2016 World Health Organisation (WHO) systems (Table 1.2) (European Association of Urology, 2018).

Table 1.1. Staging system for bladder cancers

Tumour stage	Description
TIS	Carcinoma *in situ: v*ery early tumour contained to the urothelium ("flat" tumour)
Ta	Non-invasive tumour contained to the urothelium
T1	Tumour has invaded to the subepithelial connective tissue layer
T2	Tumour has invaded to the muscle tissue layer
T2a	Tumour in muscle layer is only superficial (inner half)
T2b	Tumour in muscle layer is deeper (outer half)
T3	Tumour has invaded to the perivesical tissue layer
T3a	Tumour in perivesical layer has invaded microscopically
T3b	Tumour in perivesical layer has invaded macroscopically
T4	Tumour has invaded other organs outside of the bladder
T4a	Tumour has invaded the womb, vagina or prostate
T4b	Tumour has invaded further to the pelvis or abdomen

Information was taken from the European Association of Urology Pocket Guidelines 2018 Edition

Table 1.2. WHO grading systems for bladder cancers

1973 WHO grading	2016 WHO grading (papillary lesions)
Grade 1: well differentiated	Papillary urothelial neoplasm of low malignant potential
Grade 2: moderately differentiated	Low-grade papillary urothelial carcinoma
Grade 3: poorly differentiated	High grade papillary urothelial carcinoma

Information was taken from the European Association of Urology Pocket Guidelines 2018 Edition

1.1.3 Treatment

Treatment for bladder cancer depends on the stage and grade of the cancer and is generally based on whether the tumour has invaded to muscle layer. For NMIBC (stages CIS, Ta, and T1) the treatment depends on the patient's risk category; either low, intermediate or high risk. Risk status is determined by considering the number and size of the tumours, the grade of the cancer cells, and the state of recurrence. Treatments include transurethral resection of a bladder tumour (TURBT), intravesical chemotherapy, a course of Bacillus Calmette-Guerin (BCG) treatment, or a cystectomy to surgically remove the bladder (NHS, 2021).

In the UK, for patients who have MIBC the treatment options are either radical cystectomy, or radiotherapy with a radiosensitiser, depending on the extent of spread into

the surrounding tissue. The National Institute for Health Care Excellence (NICE) guidelines stipulate that intravenous neoadjuvant cisplatin based chemotherapy should be offered to newly diagnosed patients who are suitable (National Institute for Health and Care Excellence, 2015). Radiotherapy is given either in 32 fractions over 6.5 weeks to deliver 64 Gy or in 20 fractions over 4 weeks for 55 Gy. Recently, a meta-analysis was performed on two radiotherapy bladder cancer trial cohorts (n=782) to determine if there is a difference between the two fractionation regimens regarding invasive locoregional control or toxicity. No difference in toxicity was found between the two radiotherapy delivery methods, but 55 Gy delivered in 20 fractions was superior for invasive locoregional control and therefore recommended as the standard-of-care for bladder preserving treatments (Choudhury *et al.*, 2021). Radiosensitisers that are used include mitomycin C (MMC) combined with 5-fluorouracil (5-FU; chemotherapy) or carbogen combined with nicotinamide (CON; hypoxia-modifying therapy) (National Institute for Health and Care Excellence, 2015). A meta-analysis of 10,108 patients in 86 randomised trials investigating the use of hypoxia-modifying therapies as radiosensitisers found that hypoxia-modification significantly improved radiotherapy efficacy for both overall survival (OR = 0.87, 95% CI 0.8-0.95) and locoregional control (OR = 0.77, 95% CI 0.71-0.86) (Overgaard, 2007). Radical cystectomy involves the surgical removal of the bladder, pelvic lymphadenectomy with urinary diversion (Kamat and Black, 2021).

Compared to the UK, treatment approaches differ in the USA where radical cystectomy is the preferred first-line standard-of-care treatment option. Radiotherapy is considered an alternative treatment that is referred to as multi-modality bladder sparing therapy, or some variation thereof, and is usually reserved for patients considered unfit for surgery (Vashistha *et al.*, 2017; European Association of Urology, 2018). A meta-analysis comparing cystectomy to combined modality bladder-preservation treatment (radiotherapy, chemotherapy and TURBT) showed that despite cystectomy being the standard treatment option there was no difference in overall survival between the surgery and combined modality groups (56.2% and 55%, respectively). Further to this, there were fewer major complications attributed to the radiotherapy group (Vashistha *et al.*, 2017).

However, recurrence of disease after treatment is common. The BC2001 trial investigated the benefit of chemoradiation using MMC and 5-FU in MIBC. The two-year relapse-free survival rates were 54% for radiotherapy alone and 67% when patients were

given synchronous chemotherapy (James *et al.*, 2012). The BCON trial showed when patients were given CON concurrently with radiotherapy three-year relapse-free survival rates for tumours stage 2 and above improved from 41% to 52% (Hoskin *et al.*, 2010). These low relapse-free survival rates demonstrate the very high rate of disease recurrence after radiotherapy +/- radiosensitisers, with around 50%-60% of patients relapsing after 2-3 years respectively. Therefore, continuing to improve responses and the efficacy of radiotherapy is vital to decrease rates of recurrence and improve overall survival in MIBC. One such approach is to individualise treatments based on the molecular classification of the tumour.

1.1.4 Molecular subtypes

Molecular subtypes are useful classifications that associate with distinct biological characteristics, differing prognoses and response to treatments. As bladder cancers are highly heterogeneous, molecular subtypes provide useful insight into biological mechanisms underlying the differing survival outcomes between patients. In recent years there have several groups contributing, refining and updating molecular classifications of MIBC, which has led to a number of different of classifications (McConkey and Choi, 2018).

Firstly, the University of North Carolina broadly assigned MIBC into basal and luminal subtypes that reflect the same biological characteristics as seen in breast cancer molecular subtyping. Despite further classifications by other groups increasing the number of molecular subtypes, these all have underlying concordant biological characteristics that broadly associate with either basal or luminal subtypes. Basal tumours reflect those with high expression of basal cell markers such as KRT5/6 and KRT14 and are enriched with squamous features. Luminal tumours reflect those with high expression of luminal differentiation markers such as FOXA1, GATA3 as well as KRT20 and ERBB2 (Fong *et al.*, 2020). MD Anderson cancer centre further classified tumours to include a third group of p53-like tumours, whilst the Lund group created a classification of five molecular subtypes: basal, urobasal B, infiltrated, genomically unstable and urobasal A (Sjödahl *et al.*, 2012, 2017; Choi *et al.*, 2014). Next, The Cancer Genome Atlas (TCGA) created a classification of six subtypes: neuronal, squamous, luminal infiltrated, luminal and luminal-papillary (Robertson *et al.*, 2017). There is underlying concordance between these different classification systems and basal subtypes are generally shown to associate with a worse

prognosis. However, there is currently no predictive value associated with these classifications (Satyal *et al.*, 2019).

Having many different molecular classifications each with distinct nomenclature impedes integration into clinical practice and there is currently no use for molecular subtypes seen clinically. Hence, Kamoun *et al* generated a consensus molecular subtype classification for MIBC using the existing published classification schemes. Their consensus classification has six molecular subtypes each with unique biological and clinical characteristics regarding immune and stromal infiltration, histological and clinical characteristics and oncogenic mechanisms. These six consensus molecular subtypes are: luminal papillary (LumP), luminal non-specified (LumNS), luminal unstable (LumU), stroma-rich, basal/squamous (Ba/Sq), and neuroendocrine-like (NE-like) (Kamoun *et al.*, 2020). The main characteristics of each subtype are summarised in Figure 1.1. Although the consensus classification is based on biological differences and not clinical classes, having a consensus on molecular subtypes for MIBC should aid the identification of biomarkers to help develop personalised treatment for MIBC patients by providing the ability to link clinical findings with specific molecular contexts. Kamoun *et al* have demonstrated this potential by analysing several clinically useful gene signatures that predict response to targeted treatments and showing the expression of each in the context of the molecular subtypes. For example, they show that basal and stroma-rich subtypes have high expression of a hypoxia gene signature that predicts unfavourable response to radiotherapy and that basal subtypes have the highest expression of a CD8 effector gene signature that predicts response to immune checkpoint inhibitors. The relationship between the subtypes and response to treatments needs further elucidation and validation.

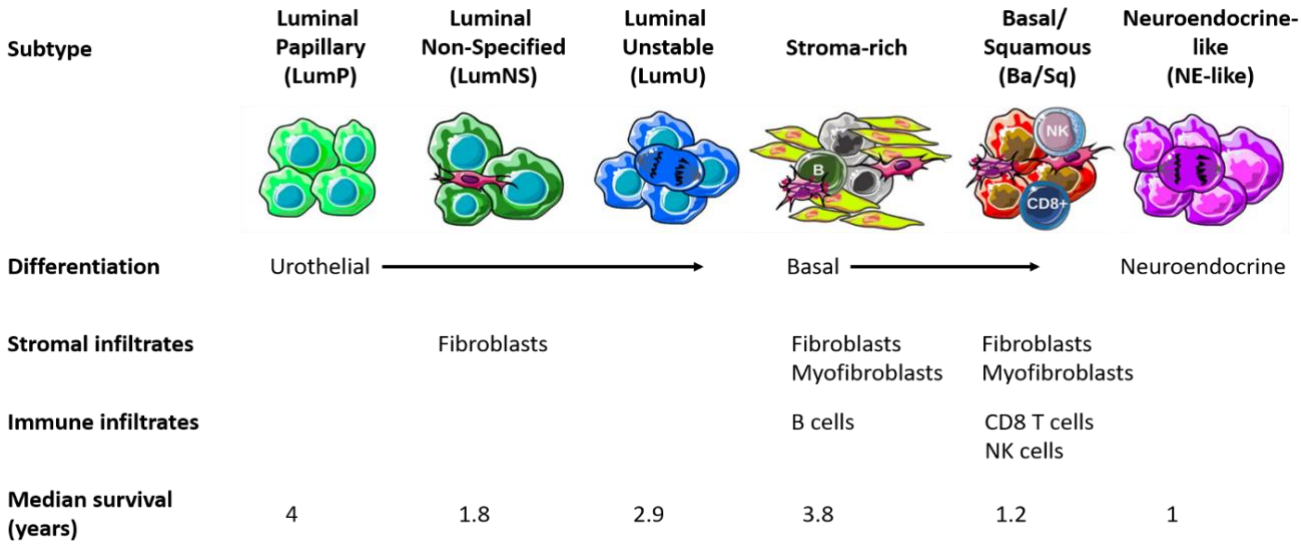

Figure 1.1 Summary of the characteristics of each subtype from the consensus molecular classification of MIBC. Luminal subtypes have urothelial differentiation and both stroma-rich and ba/sq have basal differention, whilst NE-like is uniquely differentiated as neuroendocrine. LumNS and stroma-rich both have higher levels of fibroblasts whilst stroma-rich and ba/sq are characterised by increased levels of myofibroblasts. Stroma-rich and ba/sq have higher levels of immune infiltrates than the other subtypes. NE-like has the worst survival, followed by ba/sq. LumP is associated with the best survival outcome.

1.1.5 Prognostic factors

Due to the particularly poor survival rates of MIBC compared to the more favourable NMIBC, most bladder cancer research focuses on improving the treatment options and patient survival outcomes for MIBC (Sung *et al.*, 2021). Prognostic information is useful as it can be used to inform which patients are likely to have a poor disease outcome and therefore require an intensified treatment regimen. Furthermore, some prognostic biomarkers may also have predictive utility where they can be used to identify which patients are likely to respond to specific treatments (Song *et al.*, 2019). A number of markers have been identified as prognostic factors in MIBC, although none have been successfully implemented into clinical care. Immune and hypoxia prognostic biomarkers are discussed in Section 1.2.4 and Section 1.3.4, respectively. Other prognostic markers include those related to DNA damage response and cell signalling. For example, the presence of altered p53, p21 and phosphorylated RB proteins due to genetic mutations are all independently associated with a poor prognosis and early disease recurrence, and combining them together enhances their prognostic value (Chatterjee *et al.*, 2004). Overexpression of HER2 (ERBB2) protein has been shown to associate with a poor prognosis and disease recurrence, as well as disease aggressiveness (Chakravarti *et al.*, 2005). It has been shown that HER2 overexpression predicts patients likely to fail chemoradiotherapy

and benefit from anti-HER2 antibody, trastuzumab, to enhance their response to chemoradiotherapy (Michaelson *et al.*, 2017). High MRE11 protein expression was shown to associate with better prognosis for radiotherapy, but not for cystectomy treated patients, indicating its potential use as a biomarker for patient treatment selection (Choudhury *et al.*, 2010; Laurberg *et al.*, 2012). However, a subsequent study investigating the validation of the clinical use of an MRE11 IHC scoring assay found no association between MRE11 and survival in three bladder cancer cohorts. There was a lack of concordance between IHC scoring across the centres and a conclusion of a need for alternative scoring methods to be developed (Walker *et al.*, 2019).

1.2 Tumour immune microenvironment in bladder cancer

1.2.1 Tumour immune microenvironment as a hallmark of cancer

A tumour consists of cancer cells and the cellular environment in which the tumour exists. This cellular environment includes cancer-associated fibroblasts (CAFs), pericytes, endothelial cells, and immune cells, which make up the tumour microenvironment (TME) along with blood vessels, the extracellular matrix and signalling molecules. The TME is important because it contributes significantly to the biology of a tumour and affects all stages from tumour initiation to progression and metastasis (Arneth, 2020). The hallmarks of cancer are a set of principles that provide a framework for understanding the biological characteristics of cancer, as established by Hanahan and Weinberg (Hanahan and Weinberg, 2000, 2011). There are eight hallmarks and two enabling characteristics stipulated to enable tumour growth and progression. One of the hallmarks is evading immune destruction. One of the enabling characteristics is the inflammatory state of the tumour, whereby certain immune cells can encourage tumour progression. Therefore, the immune TME appears to have an important role in the initiation, growth, and progression of cancers (Hanahan and Weinberg, 2011).

1.2.1.1 Evading immune destruction

The immune system can mount effective anti-tumour immunity to kill nascent and developing tumour cells, which occurs via the tumour immunity cycle as characterised by Chen and Mellman in 2013 (Figure 1.2). Briefly, cancer cells release neoantigens that are recognised and processed by dendritic cells (DCs) and other antigen presenting cells (APCs)

using MHC I and MHC II molecules. These DCs cross-present the antigens to prime and activate effector T cells (CD8+ T cells). Activated T cells then migrate to the tumour site and infiltrate the tumour. In the tumour, T cells recognise and kill the cancer cells, thereby resulting in cancer cell death that releases neoantigens and initiates the start of the cycle again (Chen and Mellman, 2013).

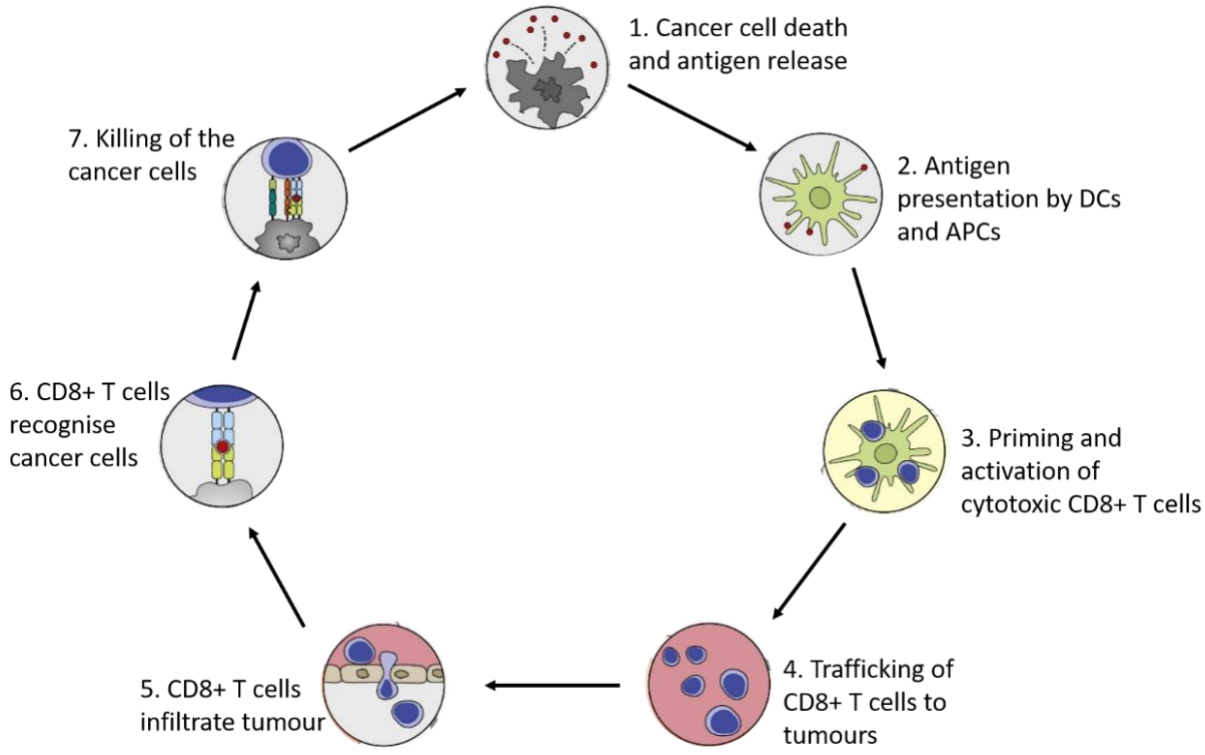

Figure 1.2. The steps involved in the cancer immunity cycle, as described in Section 1.2.1.1. Adapted from Chen and Mellman, 2013.

There is a range of mechanisms that tumours employ to evade destruction by the immune system and disrupt the cancer immunity cycle (Figure 1.3). These include the tumour cell-mediated release of chemokines such as CCL22 and TGF-β that recruit suppressive immune effector cells such as regulatory T cells (Tregs), tumour-associated macrophages (TAMs) and myeloid-derived suppressor cells (MDSCs) to the TME. Together, these cells repress the functionality of T cells to inhibit anti-tumour immune responses and create a pro-inflammatory TME, which will be discussed in Section 1.2.1.2. Another function of tumour cell-mediated TGF-β release is to prevent DCs from maturing and presenting antigens, which inhibits the subsequent cross-presentation and activation of T cells (Vinay *et al.*, 2015). Tumours can also release prostaglandin E_2 (PGE_2), driven by cyclooxygenase 2 (COX-2) signalling, which suppresses anti-tumour immunity and fuels tumour promoting inflammation enabling tumour progression and growth (Zelenay *et al.*, 2015).

Tumour cells can directly inhibit the adaptive immune response by inducing immune tolerance. Tolerance is a necessary mechanism in normal immune function to prevent over-activation of the immune response that results in non-functioning, anergic, T cells. If T cells are engaged without co-stimulation molecules present, such as CD80/CD86 and OX40, then anergy is induced. Many tumour cells therefore exploit this process to directly suppress T cell activity by decreasing the expression of these co-stimulatory molecules. As well as suppressive cytokines and chemokines, and immunoregulatory cells, tolerance is maintained by the presence of checkpoint pathways. Checkpoint molecules expressed on the cell surface, such as PD-L1 and CTLA-4, bind to the complementary receptor on the active T cell, which induces anergy. PD-L1 appears to be a frequently upregulated checkpoint molecule expressed in the TME, causing T cell anergy and deletion (Vinay *et al.*, 2015; Topalian *et al.*, 2016). Targeting the PD1-PD-L1 axis has been a breakthrough in cancer therapy as discussed in Section 1.2.3.

Tumour cells also create a defective antigen presentation mechanism. They downregulate antigen processing machinery, such as components of the MHC I pathway including transporter associated with antigen processing (TAP) protein, tapasin and LMP2 and LMP7. This inhibits the processing and presentation of antigens, to prevent activation of cytotoxic T cells by the recognition of antigens cross-presented to them (Restifo *et al.*, 1993; Vinay *et al.*, 2015).

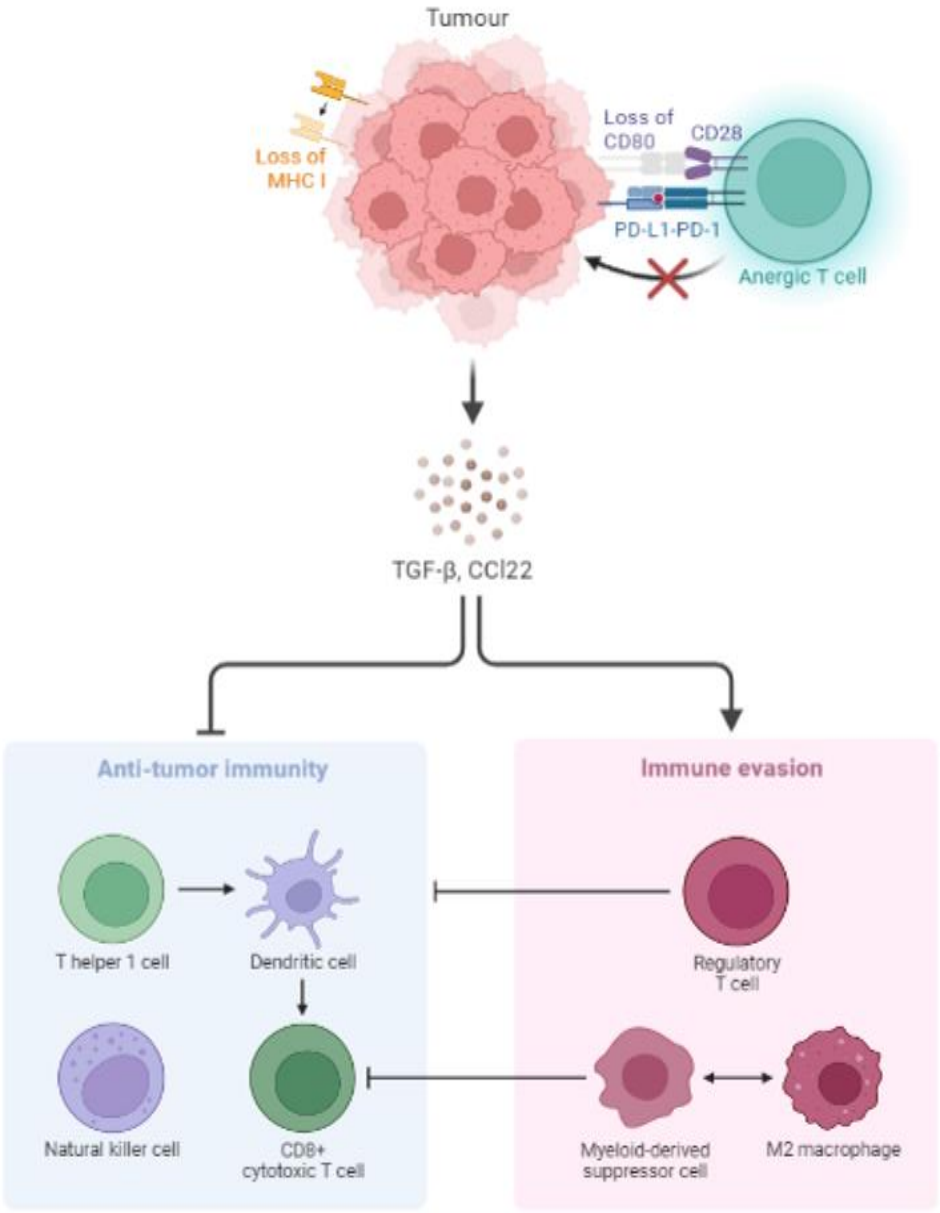

Figure 1.3 A diagram illustrating some of the mechanisms that tumours employ to evade destruction by the immune system as described in Section 1.2.1.1.
Tumour cells downmodulate the expression of MHC I to evade recognition; downmodulate CD80 and increase PD-L1 to induce T cell anergy; and release immune suppressive chemokines such as TGF-B and CCL22 that induce immune evasion by recruiting suppressive immune cells Tregs and MDSCs, which dampen anti-tumour immunity. Created using BioRender.

1.2.1.2 Tumour promoting inflammation

The presence of certain types of immune cells in the TME and their signalling molecules create a niche that is capable of promoting tumorigenesis and tumour progression. These inflammatory cells (TAMs, MDSCs and DCs) mostly belong to myeloid cell lineage of the innate immune system, and are associated with processes such as wound healing and tissue remodelling. Hanahan and Weinberg categorised this tumour-promoting inflammation as an enabling characteristic, as these inflammatory cells release molecules that contribute to multiple hallmark of cancer capabilities. These molecules include: growth factors that

induce tumour cell proliferation signalling; proangiogenic factors that induce formation of new blood vessels; survival factors that inhibit tumour cell death; inductive signals that induce epithelial-to-mesenchymal transition (EMT); and cytokines and chemokines that further the pro-tumour inflammatory state of the TME (Hanahan and Weinberg, 2011).

Macrophages, representing a diverse subset of myeloid cells, are one such population of immune cells that can contribute towards pro-tumour inflammation and appear to have a high degree of plasticity (Qian and Pollard, 2010). Previous dogma regarding macrophage function states that undifferentiated macrophages (M0) can be polarised into one of two types, which contribute towards either pro-tumour or anti-tumour activity as depicted in Figure 1.4. This central idea presents M1 macrophages as classically activated and stimulants of Th1 T cell responses to pathogen and tumour cell killing. They can be characterised by their expression of inducible nitric oxide synthase (iNOS). M2 macrophages are alternatively activated phenotypes that are often characterised by arginase 1 production. M2 macrophages are characterised as stimulants of Th2 T cell responses for wound healing, tissue remodelling and angiogenesis, amongst other functions that stimulate pro-tumour inflammation (Mills *et al.*, 2000; Mantovani *et al.*, 2004).

Recent literature has expanded from the binary dichotomisation of macrophages to instead regard these cells as a continuum of states that broadly reflect phenotype and function of M1 or M2-like macrophages. Furthermore, whilst M1 and M2 polarisation tends to cause opposing inflammatory functions, importantly the TME context can induce either phenotype to be both pro and anti-inflammatory (Rath *et al.*, 2014). In tumours, the TAMs present tend to be polarised towards the pro-tumour M2-like phenotype, which release suppressive cytokines such as IL-10 and TGF-β to recruit more pro-tumour inflammatory cells to the TME via a positive feedback loop. Overall, the M2-like macrophages are tumour-promoting due to pro-angiogenic effects and functions that suppress the adaptive immunity responses allowing for tumour growth and metastatic spread (Mantovani *et al.*, 2008).

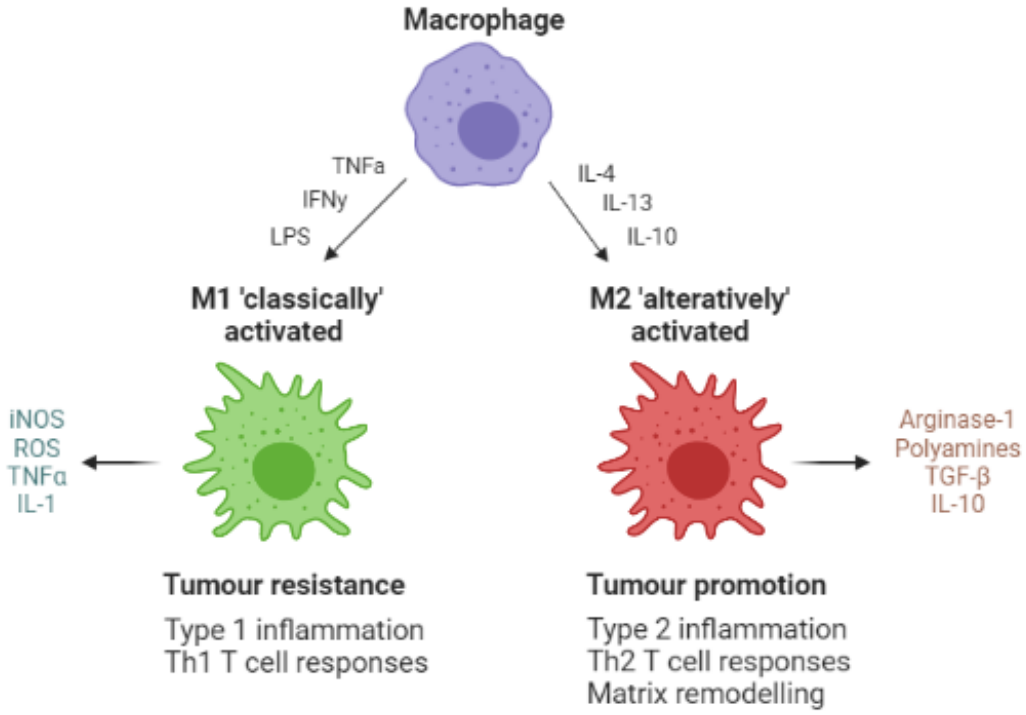

Figure 1.4 Diagram depicting the phenotypic differences between M1 and M2 macrophages as described in Section 1.2.1.2. TNFα = tumour necrosis factor alpha, IFNγ = interferon gamma, LPS = lipopolysaccharide, iNOS = inducible nitric oxide synthase, ROS = reactive oxygen species, IL-x = interleukin x, TGF-β = transforming growth factors beta, Th1 = T helper 1 cell, Th2 = T helper 2 cell. Created using BioRender freely available software.

Neutrophils are a polymorphonuclear phagocytic subset of myeloid cells. These cells have a strong role in tumour angiogenesis, which is essential in promoting tumour progression. They release a number of molecules that promote endothelial proliferation and microtubule formation such as VEGF, CXCL8, and CXCL11. These molecules in turn create a positive feedback loop to recruit more neutrophils to the tumour site which further stimulate angiogenesis. Neutrophils also release MMP9, which is an enzyme that degrades the extra-cellular matrix (ECM), thereby contributing to tumour progression and metastasis (Murdoch *et al.*, 2008).

Myeloid-derived suppressor cells (MDSCs) are a population of functionally immunosuppressive immature myeloid progenitor cells. MDSCs suppress the activity of anti-tumour effector cells such as CD8+ T cells and NK cells by releasing iNOS and arginase 1. They also inhibit DC maturation and promote tumour vascularisation. The significant effect MDSCs have on tumour progression has been well characterised and the presence of these cells strongly correlate with clinical stage and disease progression (Murdoch *et al.*, 2008; Quail and Joyce, 2013).

Whilst B and T cells, cells belonging to the lymphoid lineage, are instrumental in anti-tumour immunity, subclasses of these cell types also have a role in pro-tumour

inflammation. Regulatory T cells (Tregs) are an immune suppressive subset of CD4+ T cells that are characterised by their expression of the transcription factor FOXP3. They are potent suppressors of anti-tumour immunity via different mechanisms, of which the main one is the expression of the checkpoint molecule CTLA-4, which is induced by FOXP3 (Takeuchi and Nishikawa, 2016). CTLA-4 binds to CD80 and CD86 on APCs with stronger avidity than the co-stimulatory molecule CD28 and its binding blocks the maturation and ability of APCs to stimulate anti-tumour CD8+ T cell mediated immunity (Walker and Sansom, 2011). Amongst other mechanisms, Tregs also produce granzyme and perforin, which exhibit direct cytotoxicity against effector CD8+ T cells, and suppressive cytokines such as TGF-β and IL-10, which recruit other suppressive inflammatory cells like macrophages, neutrophils, and MDSCs that overall encourage tumour promotion and inhibit anti-tumour immunity (Takeuchi and Nishikawa, 2016).

The balance and interaction between these different types of immune cells to induce either an anti-tumour or pro-tumour immune TME form the focus of intense current research in tumour immunology and has a vital role in patient prognosis and responses to various treatments, as will be discussed in Section 1.2.4.

1.2.2 Radiotherapy and the immune tumour microenvironment

Radiotherapy can induce profound immunomodulatory effects in the TME, which can have both pro-tumour and anti-tumour effects. Whether the effect of radiotherapy is immunostimulatory or immunosuppressive depends the tumour type, microenvironment and cytokine milieu present (Grivennikov, Greten and Karin, 2010).

1.2.2.1 Anti-tumour immune effects of radiotherapy

Radiotherapy both directly, and indirectly via the induction of reactive oxygen species (ROS), triggers pro-inflammatory cytokines such as IL-1 and tumour necrosis factor alpha (TNFα) to recruit immune cells to the irradiated site. The cellular damage from radiation also exposes damage-associated molecular patterns (DAMPs), which activate the innate immune system via the stimulation of cell survival and pro-inflammatory pathways. The overall result is immunogenic cell death of the tumour cells, which involves the formation of cell debris and apoptotic bodies that are recognised as tumour antigens by the innate immune system. ATP, calreticulin and HBMG-1 are all released as DAMPs and cause the priming and activation of DCs to become antigen presenting cells. These DCs process the tumour-

associated antigens and cross-present them to the T cells of the adaptive immune response, resulting in immunogenic cell death by a tumour-specific T cell response (Barker *et al.*, 2015; Van Limbergen *et al.*, 2017).

Sufficient recruitment and activation of antigen-specific effector CD8+ T cells is essential to elicit an effective anti-tumour immune response. Radiotherapy causes increased production of interferon gamma, IFNγ, which upregulates T cell-recruiting chemokines such as CXCL9 and CXCL10 and stimulates antigen-specific T cell mediated anti-tumour immune responses by enhanced DC priming (Lugade *et al.*, 2008; Burnette *et al.*, 2011). Components of the complement pathway such as C3a and C5a are upregulated by radiotherapy-mediated cell death and promote tumour-specific CD8+ T cell-mediated anti-tumour immunity (Surace *et al.*, 2015). Radiotherapy also makes tumour cells more susceptible to tumour-specific T cell killing by inducing the overexpression of MHC I and NKG2D receptors (Gasser *et al.*, 2005; Reits *et al.*, 2006). Despite this radiation-induced priming of the CD8+ T cell mediated immunity, radiotherapy alone is not always sufficient to create a complete anti-tumour immune response. Therefore, combination therapy strategies are needed to maintain a potentially curative radiotherapy-induced immune response against the tumour (Van Limbergen *et al.*, 2017).

1.2.2.2 Pro-tumour immune effects of radiotherapy

In contrast, the immune suppressive consequences of radiotherapy are potentiated from chemotactic signals that induce extrinsic radioresistance by the recruitment of several myeloid cell populations with distinct roles in T cell suppression, such as Tregs and MDSCs. As outlined in Section 1.2.1.2, these suppressive immune cells contribute towards tumour progression, treatment resistance and disease recurrence. The chemotactic signals induced after radiotherapy include the immunosuppressive cytokine TGF-β, which suppresses DCs and CD8+ T cells, and stimulates the conversion of CD4+ T cells into Tregs. Overall, this increase in TGF-β results in the inhibition of the adaptive immune response that is needed to maximise radiotherapy effectiveness (Demaria and Formenti, 2012).

Sufficient co-stimulation is required for effective activation of the T cells upon antigen presentation, which is hampered by the upregulation of checkpoint pathways (Barker *et al.*, 2015). As discussed in the previous section, IFNγ production is increased by radiation. Alongside its role as a key regulator of T cell mediated tumour killing, IFNγ also upregulates

the expression of the checkpoint molecule PD-L1 on tumour cells. PD-L1 binds to its PD-1 receptor on T cells to induce T cell anergy and deletion, thus dampening T cell-mediated anti-tumour immune responses (Weichselbaum *et al.*, 2017).

Furthermore, pro-tumour radiotherapy-induced effects can occur due to intrinsic radioresistance mechanisms as Tregs are more radioresistant than other lymphocyte cell subsets, resulting in their proportional increase and contribution towards immune evasion during radiotherapy (Kachikwu *et al.*, 2011). Radiotherapy also affects other elements of the TME as well as the immune system. Radiotherapy modulates cancer-associated fibroblasts, which contributes towards ECM remodelling and fibrosis, leading to tumour recurrence. As will be discussed in Section 1.3.3, radiotherapy responses are also affected by hypoxia and lead to tissue revascularisation which contributes towards tumour recurrence and metastasis. All of these elements of the microenvironment interplay together to have a potential overall negative effect on radiotherapy responses (Figure 1.5) (Barker *et al.*, 2015).

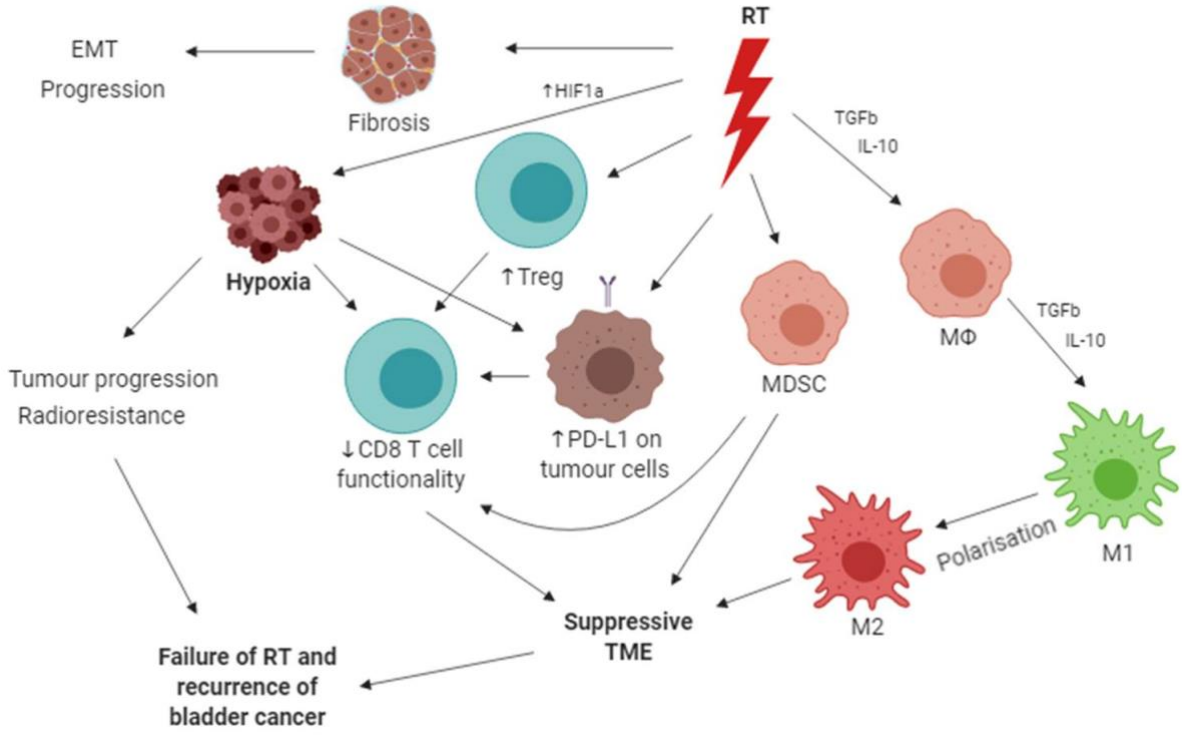

Figure 1.5. A schematic illustrating the potential mechanisms of radioresistance and tumour recurrence in bladder cancer. Radiotherapy (RT) can cause the increased proportion of Treg cells, increased expression of PD-L1 on tumour cells and recruitment of MDSCs, all of which result in decreased CD8 cytotoxic T cell functionality and a suppressive TME. RT can also cause the polarisation of macrophages from M1 phenotype to the immunosuppressive M2 phenotype. RT modulates CAFs which results in fibrosis and tissue remodelling. Hypoxia alters responses to radiotherapy and contributes to tumour progression. Overall, an immunosuppressive environment is created by RT which results in tumour progression and recurrence

A study analysing the gene expression of 136 MIBC tumours showed that a higher expression of genes reflecting CD8+ T cell infiltration and IFNγ signalling was associated with improved disease specific survival for patients who received TMT, but not for patients who had radical cystectomy +/- neoadjuvant chemotherapy (Efstathiou *et al.*, 2019). These results demonstrate that the underlying immune contexture alters the effectiveness of radiotherapy in inducing immune-mediated tumour cell killing and highlights the usefulness of considering the immune contexture in MIBC for predicting radiotherapy responses.

1.2.3 Immunomodulatory agents

There are many immune TME targets that could increase the radiosensitivity of tumour cells by immunomodulation of the TME and extrinsic radioresistance factors to enhance radiotherapy-induced anti-tumour immune responses. Of these, the most prevalent and successful are immune checkpoint inhibitor (ICI) treatments. Other examples of immunomodulatory agents include CD40 and TLR agonists, and CCL2/5 and TGF-β inhibitors.

CD40 is a receptor of the TNF family and its ligation induces DC activation and priming, and stimulates tumoural T cell infiltration. In pre-clinical models, combining radiotherapy with CD40 agonists have resulted in successful anti-tumour immune responses, mediated by DCs and CD8+ T cells (Honeychurch *et al.*, 2003; Rech *et al.*, 2018). In a study using *in vitro* and *in vivo* bladder cancer models, a CD40 agonist activated DCs by the upregulation of CD80 and CD86, and IL-12 production. The CD40 agonist induced the proliferation of antigen-specific T cells and *in vivo* results demonstrated anti-tumour effects (Mangsbo *et al.*, 2015). Phase I clinical trials investigating CD40 agonists with chemotherapy or ICIs in patients with advanced solid tumours have reported well-tolerated toxicities, but limited clinical efficacy (Li and Wang, 2020). A phase II clinical trial investigating the use of a CD40 agonist with chemoradiation in patients with oesophageal or gastroesophageal carcinoma has yet to report results (NCT03165994). There remains clinical potential for CD40 agonists with careful consideration into the scheduling and combination of the therapy, along with robust biomarker selection for patients who will likely see clinical benefit (Colton *et al.*, 2020).

Radiotherapy upregulates the production of CCL2 and CCL5 chemokines in tumour cells, which recruit Tregs and suppressive monocytes (Mondini *et al.*, 2019). The use of a CCL2/5 antagonist with radiotherapy has been shown to reduce intratumoural monocytes and

increase radiotherapy efficacy in pre-clinical models (Connolly *et al.*, 2016). More recently, a study using pancreatic adenocarcinoma murine models showed that a CCL2/5 dual inhibitor used in conjunction with radiotherapy and an ICI increased tumoural effector T cell infiltration and suppressed intratumoural infiltration of Tregs, M2 macrophages and MDSCs resulting in enhanced anti-tumour efficacy of radiotherapy (Wang *et al.*, 2022). Clinical development of CCL2/5 inhibitors are a recent development and a phase I clinical trial using a CCL2 inhibitor in combination with chemotherapy in pancreatic cancer patients confirmed safety and tolerance, and recommended progression to a phase II clinical trial (Nywening *et al.*, 2016). Studies investigating the use of CCL2/5 inhibitors in bladder cancer are lacking.

There are several toll-like receptors, one of which is toll-like receptor-7 (TLR7). TLR7 stimulation is a potent activator of cells of both the innate and adaptive immune response such as MDSCs, macrophages and DCs (Spinetti *et al.*, 2016). In pre-clinical models, TLR7 agonists have been shown to alter the suppressive phenotype of monocytic MDSCs by acquiring APC functionality to induce antigen-specific T cell proliferation and by stimulating their differentiation into tumouricidal M1 macrophages (Wang *et al.*, 2015; Spinetti *et al.*, 2016). Several pre-clinical studies have investigated the use of TLR7 agonists combined with radiotherapy. Radiotherapy was shown to enhance the efficacy of TLR7 agonists to result in long-term anti-tumour immunity via CD8+ T cell activity induced by DCs (Dewan *et al.*, 2012; Schölch *et al.*, 2014; Dovedi *et al.*, 2016). These results led to a phase II clinical trial investigating the use of TLR7 agonist with cyclophosphamide and radiotherapy for breast cancer patients with skin metastases (NCT01421017), the results of which are yet to be published. Many early clinical trials failed due to unacceptable toxicities when the agent was delivered systemically, but improvements in formulations and scheduling has resulted in locally delivered TLR agonists and a renewed interest in their clinical potential (Walshaw *et al.*, 2020). Other research investigating TLR9 agonists have shown similar anti-tumour immunity mediated by CD8+ T cells and NK cells, and synergy with the addition of radiotherapy (Walshaw *et al.*, 2020). To my knowledge, there is currently no research investigating the use of TLR agonists in the bladder cancer setting.

TGF-β inhibitors are another potential immune modulator that could be used in the clinical setting. As discussed in Section 1.2.2, radiotherapy induces TGF-β production, which can alter the balance of radiotherapy-induced immune effects to dampen anti-tumour immune effects and strengthen pro-tumour inflammation. Pre-clinical studies have shown

that the blockade of TGF-β during radiotherapy synergistically resulted in CD8+ T cell-mediated anti-tumour immune responses. Resultant PD-1 upregulation was found to limit tumour rejection and cause recurrence, which was shown to be ameliorated by the addition of ICIs (Vanpouille-Box *et al.*, 2015; Rodríguez-Ruiz *et al.*, 2019). A study investigating the combination of ICIs with TGF-β blockade in a bladder cancer mouse model showed that the combination treatment caused tumoural T cell infiltration, resulting in anti-tumour immunity and subsequent tumour regression (Mariathasan *et al.*, 2018). An early phase I clinical trial of a bifunctional protein, consisting of a monoclonal antibody against PD-L1 fused to a TGF-β trap, in patients with solid tumours showed a tolerable safety profile and early signs of efficacy (Strauss *et al.*, 2018).

Of these immunotherapies, the most prevalent and successful are immune checkpoint inhibitor (ICI) treatments, which work by targeting the immune checkpoint pathways, CTLA-4 and PD-L1, and inhibiting them. This prevents the respective receptors binding with their ligands and initiating their inhibitory effects, thus preventing T cell exhaustion and allowing for successful anti-tumour T cell activity. The first ICIs approved by the Food and Drugs Administration (FDA) were monoclonal antibodies developed for melanoma, with ipilimumab binding to CTLA-4 and pembrolizumab and nivolumab binding to PD-L1. The FDA have since approved more ICIs for a variety of different tumours, including six for advanced bladder cancer: anti-PD-L1 antibodies atezolizumab in 2016, avelumab and durvalumab in 2017; anti-PD-1 antibodies nivolumab in 2017 and pembrolizumab in 2019; and anti-CTLA-4 antibody ipilimumab in 2019 (Wei, Duffy and Allison, 2018; Wołącewicz *et al.*, 2020). Although those patients who respond to ICIs perform well, only between 13% and 24% of bladder cancer patients respond to the treatments (Cheng *et al.*, 2018). Therefore, there is a clinical need to identify those patients who are likely to respond to ICI treatments, as well as to further understand why some patients do not see clinical benefit and identify successful combination strategies.

There are many potential combination strategies for ICIs, including the use of anti-inflammatory drugs that target the COX-2/PGE_2 pathway. Inhibiting the COX-2/PGE_2 pathway was shown to synergise with ICIs to increase intratumoural infiltration of T cells in mouse models as well as patient-derived tumour fragments across different cancer types, although not including bladder (Pelly *et al.*, 2021). Furthermore, pharmacological inhibition of COX-2 was shown to synergise with chemotherapy and ICI to boost efficacy in mouse

models (Bell *et al.*, 2022). Although not investigated in bladder cancer models, the chemotherapy tested included 5-FU, which is routinely given to MIBC patients, highlighting its potential use in this disease. Other combination strategies for potentiating the efficacy of ICIs include hypoxia-modifying agents, which will be discussed in Section 1.4.4.

Many ongoing clinical trials are investigating the use of various ICIs in combination with radiotherapy or chemoradiation in MIBC patients (Tripathi, Khaki and Grivas, 2021). A phase II clinical trial, DUART, investigated the combination of radiotherapy and durvalumab in cisplatin/surgery ineligible MIBC patients and found the treatment was safe and tolerable. Recently, interim efficacy presented at a conference stated that concurrent durvalumab and radiotherapy with adjuvant durvalumab resulted in promising 1-year efficacy with PFS probability of 73% (Joshi *et al.*, 2021). Another study investigating durvalumab with chemoradiation in MIBC patients with locally advanced lymph node positive tumours is ongoing. There are other ongoing clinical trials investigating pembrolizumab (Keynote-992) and atezolizumab concurrently with chemoradiation in MIBC patients (Tripathi, Khaki and Grivas, 2021). If successful, these trials could pave the way for refining bladder-preserving treatment modalities to improve overall survival for MIBC patients. As seen with poor response rates in patients with metastatic advanced tumours, patient selection is likely to improve treatment response rates and the development of biomarkers to predict patient benefit of ICIs is pivotal to this.

1.2.4 Tumour immune cell infiltrates and the potential effects on clinical prognosis

Poor overall survival of MIBC and the need to develop biomarkers to determine efficacy of ICIs has resulted in intense research efforts to identify specific immune cells, or immune contextures, which yield prognostic and predictive value.

1.2.4.1 CD8 T cells

A meta-analysis of 124 published articles was performed by Fridman *et al* to analyse the relationship between T cell infiltration and clinical outcome. It was found that in numerous different cancer types, including bladder, high levels of lymphocyte infiltration are associated with a better clinical outcome. Specifically, high densities of CD8+ (cytotoxic) T cells result in longer disease-free and overall survival (Fridman *et al.*, 2012). Another meta-analysis was performed in 2021 by Li *et al,* associating CD8+ T cell levels with clinical outcome to immunotherapies, namely ICIs. Analysis of 33 studies across cancer types,

including bladder, showed that high numbers of CD8+ T cells significantly associated with better overall survival (HR = 0.52, 95% CI 0.41-0.67, p<0.001), progression free survival (HR = 0.52, 95% CI 0.40-0.67, p<0.001), and overall response rate to ICI treatments. The improved survival and response to ICIs was found to be true regardless of the different treatment approaches: combination (PFS HR = 0.27, 95% CI 0.09-0.81, p=0.019) or mono-therapy (PFS HR = 0.52, 95% CI 0.40-0.68, p<0.001); CD8+ T cell compartmentalisation: stroma (OS HR = 0.41, 95% CI 0.29-0.58, p<0.001) or intra-tumoural (OS HR = 0.59, 95% CI 0.40-0.86, p=0.007); and different cancer types. Higher baseline circulating CD8+ T cells in peripheral blood did not associate with any clinical benefit (Li *et al.*, 2021). Whilst they included two urothelial cohorts in their meta-analysis, other bladder cancer specific studies also corroborated the findings of the meta-analysis. The results from these studies showed a high number of tumour-infiltrating CD8+ T cells correlated with improved survival, patient outcome and response to ICIs (Sharma *et al.*, 2007; Faraj *et al.*, 2015; Deng *et al.*, 2018; Wang *et al.*, 2019). These studies illustrate how the abundance of CD8+ T cells in MIBC can be used not only as a prognostic marker for relapse and recurrence, but also to predict which patients are likely to benefit from ICIs, which is a current unmet clinical need.

Pfannstiel *et al* used immunohistochemistry (IHC) in a Cancer Center Erlangen Metropol Region Nuremberg (CC-EMN) MIBC cohort to analyse tumour-infiltrating lymphocytes (TILs; CD8+, CD4+, NK and B cells) in the TME. They showed that high stromal infiltration of TILs identified patients with a more favourable prognosis and also correlated with a basal molecular subtype. They found that increased levels of stromal TILs correlated with increased macrophages present in the TME. Those patients with high stromal TIL infiltration benefited from platinum-based adjuvant chemotherapy, as seen in a subset of MIBC patients from the CCC-EMN and TCGA cohorts combined (n=102, HR=0.22, 95% CI 0.10-0.47, p<0.001) (Pfannstiel *et al.*, 2019).

1.2.4.2 T helper cells (CD4 and Tregs)

The role of both CD4+ T cells and Tregs is more ambiguous, with comparatively little evidence to conclusively define their impact on clinical outcome in MIBC (Joseph and Enting, 2019). An IHC study performed by Baras *et al* using 67 MIBC tumours found prognostic significance was not associated with the densities of neither CD8+ T cells nor Tregs alone. However, the ratio of CD8+ to Tregs was strongly associated with response to neoadjuvant

chemotherapy, as shown by a significant positive correlation between ratio and response ($p<0.001$). Whilst the authors showed that tumours with a ratio of < 1 comprise 0% of chemotherapy responders, and those with a ratio of > 1 comprise 60% of chemotherapy responders, the study lacked any Cox proportional hazard models or other similar survival analyses to confirm the associations (Baras *et al.*, 2016). A similar study in a cohort of 149 MIBC patients found the same correlation, but associated high CD8:Treg ratios with improved overall survival (HR 1.32, 95% CI 1.06-1.65, p=0.013) after cystectomy (Horn *et al.*, 2016). Shi *et al* used four MIBC gene expression datasets (TCGA, GSE31684, GSE5287, and CIT) and found that a high *CD3D* (CD3 delta chain; marker of T cells) to *CD4* expression ratio had prognostic relevance. They showed that a higher *CD3D*:*CD4* ratio significantly associated with improved survival in the TCGA (n=407, $p<0.001$ by log-rank test, hazard ratios and CIs not shown), GSE31684 (n=78, p=0.02), GSE5287 (n=30, p=0.35) cohorts and non-significantly in the CIT cohort (n=73, p=0.07) (Shi *et al.*, 2019).

However, these studies did not find any prognostic significance for the CD4+ T cells alone. This lack of significance could be due to a lack of in-depth characterisation of the CD4+ T cells and identification of their tumour compartmentalisation, which is essential to glean more conclusive evidence about the roles of these immune cell populations. The importance of further characterisation is demonstrated by a study on prostate cancer patients by Yokokawa *et al*. They found that although the amount of Treg cells did not vary between the cancer and healthy patients, those Tregs present in the cancer patients had a higher immunosuppressive functionality than those found in healthy patients (Yokokawa *et al.*, 2008). Despite Tregs being considered as a suppressive immune cell infiltrate in general, there are some studies that have shown positive associations with Treg abundance and clinical outcome in MIBC (Winerdal *et al.*, 2018). These studies imply a potential paradoxical effect of Tregs in MIBC and highlight the need for further research into the roles of this immune cell population in this disease.

1.2.4.3 Macrophages

The prognostic value of macrophages in bladder cancer is limited by under-characterisation of its phenotype, similar to CD4+ T cells. CD68 and CD163 are used as markers for cells of the monocyte/macrophage lineage, although CD68 is less specific and also detects myeloid cells, DCs and fibroblasts (Harris *et al.*, 2012). A meta-analysis performed by Wu *et al* in

2018 concluded that TAMs identified using CD68 alone had no clinical prognostic relevance in bladder cancer (Wu *et al.*, 2018). There is some evidence that the prognostic relevance of macrophage abundance might increase when investigating just MIBC instead of all bladder cancers as shown by Xu *et al.* They showed that TAMs identified by CD163 had no prognostic significance on overall survival for 134 bladder cancer patients, but for the subgroup of 115 MIBC patients a high versus low CD163+ TAM infiltration associated with a worse survival (p=0.022) (Xu *et al.*, 2018). In general, studies demonstrate that a high number of TAMs associate with a poor prognosis, whereby those tumours with more TAMs are associated with a higher risk of tumour progression as well as worse overall and progression-free survival (Leblond *et al.*, 2021). However, most of these studies gained more relevant and powerful prognostic information from further characterisation of the macrophages, such as whether they express the immune checkpoint molecule CD276 (B7-H3) or DC-SIGN (dendritic cell type specific C-type lectin) (Xu *et al.*, 2018; Hu *et al.*, 2020). A high ratio of CD68+ to CD3+ cells was found to identify patients with a poor prognosis in MIBC (HR = 1.67, 95% CI 1.26-2.21, p<0.001). Interestingly, in this study there were no significant associations with outcome for CD8+ cell counts alone (Sjödahl *et al.*, 2014).

Other studies deconvoluting the immune populations in bladder cancer associated higher numbers of macrophages with higher-risk patients (Fu *et al.*, 2018; P. Li *et al.*, 2021). When analysing the classical phenotypic state of the macrophages, high expression of the M2-like phenotype associated with a poor overall and progression-free survival in MIBC, whilst an M1-like phenotype correlated positively with a favourable prognosis when found in the tumour-draining lymph nodes, but not in the tumour (Asano *et al.*, 2018; Xue *et al.*, 2019; L. R. Jiang *et al.*, 2021). Again, these studies attributed increased prognostic significance to further macrophage characterisation, such as PD-1 expression and specific genomic alterations. One study used bulk single cell RNA sequencing on immune infiltrating cells from MIBC patients and found six different subsets of macrophages. The gene signatures of these subsets did not correlate with existing classical M1-like and M2-like macrophage phenotypes (L. Wang *et al.*, 2021). These studies illustrate the difficulty with analysing macrophages as a prognostic marker due to the complexity of their lineages, plasticity, and the markers used to define them and highlights the need for further investigation into their prognostic and predictive utility in MIBC.

1.2.5 Immune gene signatures

Large scale transcriptomic data sets such as TCGA, ImmGen and Human Immunology Project allow for the characterisation of immune cell contexts. These datasets can be used to develop gene expression profiles to further elucidate the role of immune regulatory genes and tumour-immune cell interactions (Xue *et al.*, 2014; Angelova *et al.*, 2015).

Upon analysing the genes involved with bladder cancer progression, Kim *et al* found an enrichment of genes involving inflammation response and immune cell trafficking (Kim *et al.*, 2011). Mo *et al* also found that when analysing the genes associated with bladder tumour differentiation the most elevated gene enrichments were those involved with immune and inflammatory responses (Mo *et al.*, 2018). Together, the presence and quantity of various immune cell infiltrates influences response to treatment as well as patient prognoses. Therefore, the ability to analyse the cells collectively, rather than individually, is essential to understand the effects of immune TMEs. The use of gene expression profiles to estimate the immune cell population abundance and analyse the landscape of the tumour contexture provides essential information to stratify patient treatments (Becht *et al.*, 2016). For example, immune gene expression profiles could be used to identify which patients will benefit from ICIs checkpoint or immunomodulating therapy to stimulate an anti-tumour immune response (Van Limbergen *et al.*, 2017; Mo *et al.*, 2018).

Nirmal *et al* developed a gene signature that represents seven immune cell types and their immune pathways, including interferon (IFN) response genes. They used transcriptomic analysis to identify co-expressed genes and derive a resultant signature of relevant genes. The study of gene expression signatures is especially useful for the immune microenvironment as there are few markers that are expressed solely to represent one immune cell. The markers change depending on the tissue of origin or activation state. Therefore, a signature is based on the co-expression of markers to represent the overall profile of the immune contexture and this is more applicable than attempting to identify single cells present. The derived signature known as ImSig was validated in metastatic melanoma and showed to be prognostic for survival. ImSig is a very useful tool for analysing the immune TME and exploring the potential to provide prognostic information and predict response to treatments (Nirmal *et al.*, 2016, 2018).

The specific utility of gene signatures predicting response to therapies has been demonstrated by Ayers *et al.,* who have shown that an IFNγ related gene expression profile can be used as a predictive marker for response to PD-1 ICI treatment. They derived a preliminary IFNγ related signature and an expanded one that included genes involved with cytolytic activity, chemokine and cytokines that initiate inflammation, T cell markers and antigen presentation. These two gene signatures were able to differentiate melanoma patients into responders and non-responders to PD-1 pembrolizumab therapy. They further refined the signature and upon testing in head and neck and gastric cancers it highlighted a common biological response that enabled identification of successful response to anti-PD-1 treatment. These results demonstrate that a gene expression profile (gene signature) can be used to analyse whether the immune contexture enables favourable clinical response to ICIs. It was shown to be more robust than immunohistochemistry (IHC) for PD-1 and the authors also showed discrete biology that indicated patient groups unlikely to benefit from the therapy, highlighting its potential for patient stratification (Ayers *et al.*, 2017).

The use of gene signatures for predicting response to ICIs has also been shown with development of a gene profile linked to an immunosuppressive microenvironment via the dysregulation of TGF-β signalling in cancer-associated fibroblasts. The derived signature across cancer types predicted failure of PD-1 ICI, and out-performed the published signatures for stratifying patients for ICIs (Chakravarthy *et al.*, 2018). These results are further supported by a study performed by Mariathasan *et al.,* who found that TGF-β attenuates response to a ICIs by excluding T cells from the tumour. They used a bladder cancer clinical trial cohort treated with atezolizumab, an anti-PD-L1 ICI, and showed that lack of response to the treatment was associated with increased TGF-β signalling in fibroblasts, especially in tumours with an immune-excluded immune phenotype. Conversely, response was shown to be associated with functional CD8+ T cell effector phenotypes (Mariathasan *et al.*, 2018).

1.2.5.1 Immune subtyping in bladder cancer

Classical classification of immunological phenotypes uses histology to stratify solid tumours into three different immune phenotypes: inflamed (“hot”), where there is an abundance of CD8+ T cells in the tumour; desert (“cold”), where there is no presence of CD8+ T cells; or excluded tumours, where CD8+ T cells are confined to the stromal regions of the tumour

(Chen and Mellman, 2013; Hegde, Karanikas and Evers, 2016). In recent years, many studies in MIBC have moved beyond CD8+ T cell measurements alone, combining different immune cell subpopulations using gene expression data to create various unique immune phenotypes that are prognostically significant and can be used to predict response to treatment.

In 2018, Fu *et al* derived a stromal immunotype in MIBC that was prognostic and predicted benefit from adjuvant platinum-based chemotherapy. They used the Cibersort algorithm, which quantifies the fractions of immune cell infiltration into 22 immune cell subpopulations (Chen *et al.*, 2018). Immunotype A represented tumours with a high infiltration of CD8+ T and NK cells and a low infiltration of macrophages, Tregs and mast cells, with immunotype B representing the opposite. Patients with immunotype A tumours had significantly better overall and disease-free survival than immunotype B tumours in the training, testing and validation cohorts (validation cohort: n=287, OS HR 2.065, 95% CI 1.334-3.198, p=0.001). It was also shown that patients with immunotype B tumours who had stage 3 or 4 disease benefitted from adjuvant chemotherapy (OS HR = 0.598, 95% CI 0.394-0.904, p=0.016). Furthermore, immunotype A tumours had significantly higher expression of immune checkpoint molecules PD-L1 and CTLA-4 and an inflamed immune subtype, indicating that these patients are likely to respond to ICIs (Fu *et al.*, 2018).

One study used the TCGA bladder cancer gene expression dataset (TCGA-BLCA) to compare the relationship between different immune subpopulations and prognosis. They separated patients into three subgroups based on hierarchal clustering of immune cell analysis and each subgroup demonstrated distinct prognostic and immune characteristics as discovered using the Cibersort algorithm. In concordance with other published literature previously discussed in Section 1.2.4.1, they found that one subgroup had a higher abundance of CD8+ T cells and NK cells, which associated with better prognosis (p=0.024). Further to this, they found that the abundance of CD8+ T cells decreased as clinical stage increased and that high amounts of CD8+ T cells alone associated with a good prognosis (p=0.005). They also showed that higher abundance of macrophages associated with a poor prognosis (p=0.031) and their abundance increased as clinical stage increased. Interestingly, they also looked at the ratio of CD8+ cells to Tregs and found no prognostic significance (Wang *et al.*, 2020).

Another study demonstrated that a derived risk score based on immune-related gene expression in the TGCA-BLCA dataset correlated with response to ICI and prognosis. They showed that a high score of their signature identified poor prognosis patients in the TCGA dataset (n=406, HR 3.36, p<0.001) and a validation dataset of a cohort treated with an ICI, IMvigor210 (n=348, HR 2.42, p<0.001). Using Cibersort to analyse the differences in immune infiltrates for high versus low risk score groups in both cohorts they found that those patients with a high risk score had a significantly lower abundance of CD8+ T cells, representing an immune desert phenotype, and also higher presence of macrophages. Despite having an ICI treated cohort, they did not show associations between response to treatment and their derived risk scores, although one would hypothesise that the high risk score would predict non-responders (P. Li *et al.*, 2021).

A prognostic signature consisting of seven immune related genes was derived by Qiu *et al* in 2020 using TCGA-BLCA. They showed that patients with a high signature score identified a high risk group with worse overall, cancer specific and progression-free survival compared to those with a lower score (OS HR = 10, 95% CI 5.6-19, p<0.001). However, contrary to other studies, when analysing the differences in immune infiltrates between the groups they found that those in the high risk group had a higher infiltration of CD4+ and CD8+ cells, as well as macrophages, neutrophils and DCs. Whilst they used an external validation dataset from the Gene Expression Omnibus (GEO), they analysed the immune contexture in the TCGA dataset only (Qiu *et al.*, 2020). To analyse the immune contexture they used the TIMER algorithm, an alternative method of deconvoluting the immune populations to Cibersort. TIMER deconvolutes the immune cell infiltration into six different immune cell subpopulations (Li *et al.*, 2016).

Taken together these studies demonstrate the usefulness of analysing the immune infiltrate contexture in MIBC to provide prognostic and predictive value. The current literature also highlights the utility of gene signatures as biomarkers, which is elaborated further in Section 1.3.4.1.

1.3 Hypoxia in the tumour microenvironment

1.3.1 Hypoxia and the effect of hypoxia-inducible factors (HIFs)

Hypoxia is a lack of oxygen availability that occurs when there is an imbalance between the supply of oxygen to the tumour and the oxygen consumption rate (Vaupel and Harrison, 2004). Intratumoural hypoxia is a common feature found in over half of locally advanced solid cancers, such as MIBC (Schito and Semenza, 2014). Hypoxia-induced cellular changes mostly occur due to the transcription factors, hypoxia-inducible factors (HIF), of which there are three isoforms, HIF-1, 2 and 3. HIFs are heterodimers consisting of alpha and beta subunits, but in the presence of oxygen, HIF-α is post-translationally marked for degradation. Therefore, as oxygen levels deplete, the HIF-α subunit is able to bind to the HIF-ß subunit to create the HIF active dimer (Hill *et al.*, 2015; Infantino *et al.*, 2021). HIFs regulate gene expression by binding to hypoxia response elements (HREs) in the genome. HIF-regulated genes are primarily involved in oxygen delivery, angiogenesis and energy preservation that help the tumour cells adapt to the low oxygen environment, but also include a wide variety of other genes (Vaupel and Harrison, 2004) (Figure 1.6). Oxygen delivery is increased by the activation of genes that induce angiogenesis, such as *VEGF*, and those that increase the oxygen uptake of red blood cells, such as *EPO.* Energy preservation is driven by a switch to anaerobic versus aerobic respiration supported by the activation of genes such as *GLUT1* to increase glucose supply and *CA9* to facilitate acid excretion associated with the build-up of lactic acid. These genes act to minimise damage that could be caused by the lack of oxygen and prevent cell death, which ultimately contribute towards tumour cell resistance to radiotherapy, tumour progression and metastasis (Vaupel and Harrison, 2004; Manoochehri Khoshinani, Afshar and Najafi, 2016).

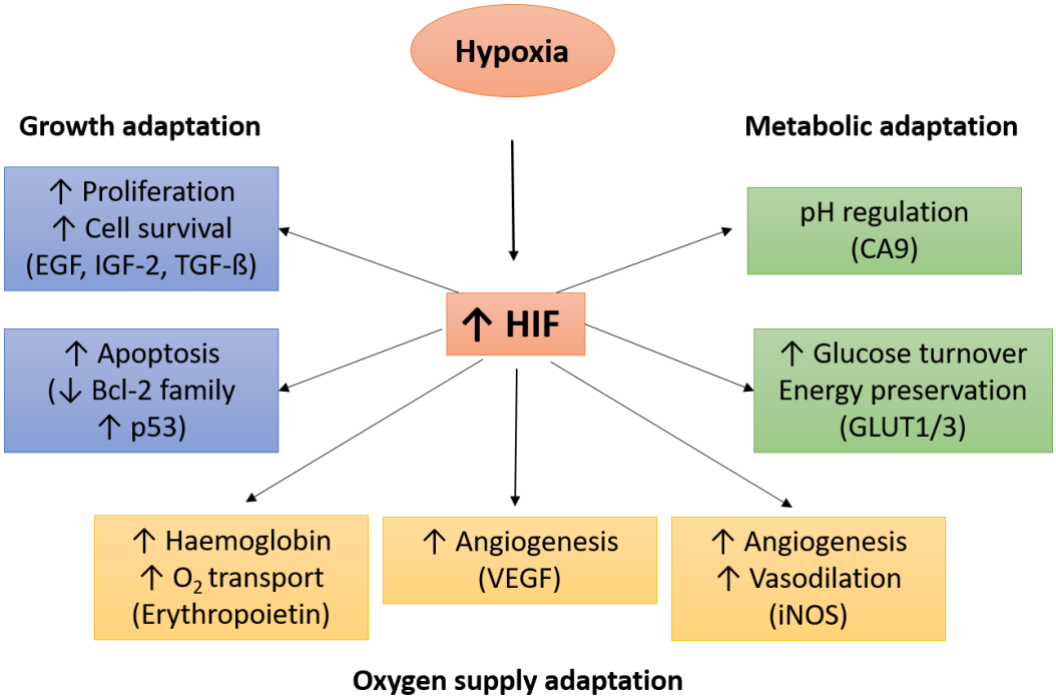

Figure 1.6. Schematic showing how HIF affects growth, oxygen supply, and metabolism adaptation.
Hypoxia results in the stabilisation of HIF, which accumulates and activates a plethora of genes by binding to hypoxia response elements (HREs). The main targets are genes broadly associated with growth, oxygen supply and metabolic adaptations. These include genes that increase proteins involved with proliferation and cell survival (EGF, IGF-2), suppression of apoptosis (BCL2), increase haemoglobin and oxygen transport capacity (EPO), increase angiogenesis and vasodilation (VEGF, iNOS), increase energy preservation and glucose turnover (GLUT), and regulate pH (CA9). Adapted from Vaupel and Harrison, 2004.

1.3.2 Hypoxia in an adverse prognostic factor and contributes to treatment resistance

Hypoxia is an adverse prognostic factor in many cancers including bladder cancer, which is independent from other clinicopathological prognostic features including tumour stage and grade (Schito and Semenza, 2014). Hypoxia contributes to resistance to many different treatments, including chemotherapies, immunotherapies, targeted therapies and radiotherapy (Manoochehri Khoshinani, Afshar and Najafi, 2016). One mechanism of treatment resistance is hypoxia-mediated drug efflux. Chemotherapies and targeted therapies rely upon accumulation of the drug in the tumour cells. A number of genes are involved in drug efflux processes that pump the drug out of the tumour, such a multidrug resistance proteins and multidrug resistance-associated proteins, which have been shown to be upregulated by HIF-1α (Krishnamurthy and Schuetz, 2005; Liu *et al.*, 2008; Xie *et al.*, 2013). Another method of chemoresistance is the inhibition of apoptotic pathways, which hypoxia has been shown to regulate. Hypoxic cells have also been shown to receive a lower drug concentration due to their increased distances from blood vessels (Karakashev and Reginato, 2015). The relationship between hypoxia and immunotherapies will be discussed in Section 1.4.5.

The link between hypoxia and resistance to radiotherapy is well established. Cells are approximately three-fold resistant when irradiated with sparsely ionising radiation in the absence of oxygen (Gray *et al.*, 1953). The oxygen effect is due to oxygen fixation of free radicals produced when radiation interacts with tissue. Radiation damages DNA both directly or indirectly - most damage is indirect for sparsely ionising radiation and the oxygen effect is important for the indirect effects of radiation. The dominant radiolysis species are the •OH and H• radicals formed by interactions with water molecules, because about 80% of cells is water. In the presence of oxygen the radicals formed are 'fixed' into a non-restorable form, that leads to irreparable DNA damage (Grimes and Partridge, 2015). The level of radioresistance due to the oxygen effect can be quantified by the oxygen enhancement ratio (OER), which is the ratio of radiation doses needed under hypoxia compared to normoxia to induce the same effect. Normally, the OER for sparsely ionising radiation is 2.8-3.5 (Hill *et al.*, 2015).

Following seminal work by Thomlinson and Gray highlighting the potential importance of hypoxia in cancer, numerous studies attempted to measure the level of tumour hypoxia and link with radiotherapy outcomes (Thomlinson and Gray, 1955). An important paper in the field was from Höckel *et al* who used oxygen microelectrodes to show that uterine cervical cancer patients with the most hypoxic tumours had a poor outcome following radiotherapy (Höckel *et al.*, 1996). Many studies have since demonstrated that the most hypoxic tumours are associated with a poor prognosis, including in bladder cancer (Theodoropoulos *et al.*, 2004; Chen *et al.*, 2020; M. Jiang *et al.*, 2021; Z. Liu *et al.*, 2021; Z. Zhang *et al.*, 2021).

1.3.3 Treatment options to overcome hypoxia

Methods of overcoming tumour hypoxia have been studied since the 1960s, although few have progressed into clinical treatments, despite many clinical trials. In the twentieth century most work centred on targeting hypoxia to improve the efficacy of radiotherapy. The approaches include increasing oxygen delivery, oxygen mimetic radiosensitisers and use of bioreductive agents (Tharmalingham and Hoskin, 2019). Meta-analyses performed on 86 clinical trials using hypoxia modification in different cancers found that it significantly improved radiotherapy responses for locoregional control (OR = 0.77, 95% CI 0.71-0.86) and overall survival (OR = 0.87, 95% CI 0.80-0.95) (Overgaard, 2007). With increasing recognition of the importance of hypoxia across solid tumours and other treatment

modalities, approaches of overcoming hypoxia have been explored for use without the focus of improving radiotherapy such as targeting hypoxia metabolism, angiogenesis, and HIF-1α activity directly (Table 1.3) (Karakashev and Reginato, 2015).

Table 1.3. Methods of overcoming tumour hypoxia.

Approach	Method	Example
Intratumoural oxygenation	Increase oxygen transfer from lungs	Hyperbaric oxygen
	Improve oxygen diffusion	Carbogen
	Increase vascular perfusion	Nicotinamide
Oxygen mimetics	Mimic radiochemical effects of oxygen	Misonidazole
		Pimonidazole
		Nimorazole
Bioreductive agents	Preferentially destroy hypoxic cells	Tirapazamine
		Apaziquone
HIF-1α indirect targets	HIF-1α synthesis	2ME2
		Topotecan
	HIF-1α DNA binding	Bortezomib
	HIF-1α degradation	17-AAG
		Geldanamycin
		EZN-2968
	HIF-1α transcriptional activity	Echinomycin
Hypoxia metabolism	Inhibition of GLUT1	WZB117
	Inhibition of LDHA	FX11
	Inhibition of PDK3	Dichloroacetate
Hyperthermia	Increase tumoural oxygenation Inhibit DNA repair Induce vascular damage to kill tumour cells	Heat to 39-45°C

1.3.3.1 Targeting hypoxia by increasing oxygen delivery

There are different methods that can be used to overcome tumour hypoxia by increasing intratumoural oxygen availability. These approaches include increasing the oxygen available in the blood using hyperbaric oxygen, improving diffusion of oxygen into the tumour using carbogen, and increasing vascular perfusion using nicotinamide. Although results from the use of hyperbaric oxygen showed clinical efficacy in head and neck and cervical cancers, the technical complexity of delivery concurrent with radiotherapy, as well as late toxicities, limited its acceptance into clinical practice (Tharmalingham and Hoskin, 2019). The meta-analysis mentioned in the above section (1.3.3) investigating the benefit of different methods of hypoxia modification in multiple cancers showed no significant benefit in bladder cancer specifically for locoregional control (OR = 0.82, 95% CI 0.62-1.08) nor overall

survival (OR = 0.88, 95% CI 0.65-1.18) (Overgaard, 2007). However, a trial comparing accelerated radiotherapy with carbogen and nicotinamide (ARCON) with misonidazole or hyperbaric oxygen in bladder cancer patients demonstrated benefit for ARCON. Patients were given CON +/- nicotinamide and the outcomes were compared to patients given misonidazole or hyperbaric oxygen. It was shown that patients given CON, with or without nicotinamide, had significantly improved recurrence free survival ($p<0.001$, no hazard ratios shown) and overall survival ($p=0.04$, no hazard ratios shown) than the other approaches of hypoxia modification (Hoskin, Saunders and Dische, 1999). The combined use of CON with accelerated radiotherapy has been investigated in many phase I and II trials over the years. Although no benefit was seen in gliomas and lung cancers, improved survival was seen in bladder and head and necks cancers leading to further phase III trials in these tumour types (Tharmalingham and Hoskin, 2019).

A phase III clinical trial investigating the use of ARCON in head and neck cancers demonstrated that ARCON significantly improved 5-year regional control rates ($p=0.04$). It was further shown that this benefit of treatment was strengthened when patients with high hypoxia tumours were identified by pimonidazole staining (Janssens *et al.*, 2012). A phase III clinical trial in bladder cancer, BCON, investigated if CON given concurrently with radiotherapy improved patient outcomes. It was found that compared to radiotherapy alone, radiotherapy plus CON improved overall survival ($p=0.03$) and reduced the risk of relapse ($p=0.03$) (Hoskin *et al.*, 2010). Similarly, it has subsequently been shown that this benefit of CON is seen in patients with the most hypoxic tumours as defined using a bladder cancer-specific hypoxia gene signature, which will be discussed in Section 1.3.4.1. A recurring theme in the failure of many of these clinical trials is the lack of patient selection, which is further highlighted by the ARCON and BCON trial analyses. As medicine moves into the era of personalised medicine, the need to stratify patients for those who are likely to benefit from hypoxia-modifying treatments is increasingly clear. Therefore, there is an existing need to be able to quantify tumour hypoxia and select those patients with the most hypoxic tumours for hypoxia-modifying treatments.

1.3.3.2 Targeting hypoxia with hypoxia-specific radiosensitisers

Oxygen mimetics, such as nimorazole, pimonidazole, etanidazole and misonidazole, sensitise tumours to radiotherapy by mimicking the radiochemical effects of oxygen. A

phase III trial for head and neck patients, DAHANCA 5, was conducted in Denmark in which patients were given radiotherapy with either nimorazole or a placebo. The study found that patients who had nimorazole in addition to radiotherapy had significantly improved locoregional control compared to those who received the placebo (Overgaard *et al.*, 1998). Despite these encouraging results, earlier trials of pimonidazole and etanidazole in head and neck and cervical cancers showed no benefit and few investigations have been made further into the use of nimorazole to improve the efficacy of radiotherapy (Tharmalingham and Hoskin, 2019). A phase III trial in the UK, NIMRAD, randomised head and neck cancer patients to receive radiotherapy with either nimorazole or a placebo, which finished recruiting in January 2021 and is yet to publish results (Thomson *et al.*, 2014). In bladder cancer, four clinical trials have investigated the benefit of misonidazole addition to radiotherapy and only one of these showed clinical benefit (Lodhi *et al.*, 2021).

Hyperthermia treatment has been shown to be an effective mechanism for overcoming tumour hypoxia as it increases tumoural blood flow and therefore oxygenation, acts as a radiosensitiser by inhibiting DNA repair, and can both directly and indirectly kill tumour cells by inducing vascular damage. Hyperthermia, which involves heat treatments of 39-45°C, has been shown to improve response to radiotherapy in many clinical trials for various tumour types, including bladder, yet it remains unused as a treatment option in most countries despite these successes (Elming *et al.*, 2019).

1.3.3.3 Targeting hypoxia with small molecular inhibitors

Developing direct inhibitors of HIF-1α has been unsuccessful. However, many compounds indirectly affecting HIF-1α showed preclinical potential and progressed through to clinical trials in advanced, metastatic solid tumours, but with limited success (Karakashev and Reginato, 2015). HIF-1α can be indirectly targeted by promoting proteasomal degradation (17-AAG/geldanamycin) (Mabjeesh *et al.*, 2002), blocking DNA binding ability (bortezomib) (Shin *et al.*, 2008), inhibiting transcriptional activity (echinomycin) (Kong *et al.*, 2005), promoting mRNA degradation (EZN-2968) (Jeong *et al.*, 2014), and disrupting synthesis (2ME2 and topotecan) (Mabjeesh *et al.*, 2003; Matei *et al.*, 2009; Kummar *et al.*, 2011). None of these indirect HIF-1α targets have been trialled so far in bladder cancer.

Targeting hypoxia driven changes in metabolism is another therapeutic method for exploiting tumour hypoxia. Small molecule inhibitors that target GLUT1 and LDHA,

downstream effectors of HIF, have shown to work synergistically with chemotherapies including cisplatin, paclitaxel and daunorubicin in various *in vitro* and *in vivo* mouse models to improve tumour killing and ameliorate hypoxia-induced treatment resistance (Cao *et al.*, 2007; Le *et al.*, 2010; Zhou *et al.*, 2010). No small molecular inhibitors targeting GLUT1 or LDHA have currently progressed into clinical trials.

An inhibitor of the hypoxia-induced molecule PDK3, dichloroacetate (DCA), has progressed through to clinical trials. DCA was shown to overcome hypoxia-induced apoptosis inhibition and enhance the efficacy of chemotherapies by inducing apoptosis in *in vivo* preclinical models (Cairns *et al.*, 2007). Phase II trials have been conducted in both glioblastoma and head and neck cancers and showed the treatment was safe. In head and neck cancer, there was no significant survival differences between the groups given DCA or placebo with cisplatin and definitive radiation (Powell *et al.*, 2015, 2022).

Hypoxia activated pro-drugs preferentially destroy hypoxic cells as their activation is inhibited by molecular oxygen and thus are only activated under hypoxic conditions. The most notable hypoxia pro-drug is tirapazamine (TPZ). Compared to normoxia TPZ has a 300-fold higher toxicity under hypoxia and *in vivo* models combing TPZ with radiotherapy and chemotherapies showed potential, leading to a phase III clinical trials in head and neck, lung, and cervical cancers. However, toxicities were high and the results of these trials that concluded no clinical benefit was seen from the addition of TPZ, which has limited its use clinically (Williamson *et al.*, 2005; Rischin *et al.*, 2008; DiSilvestro *et al.*, 2014). It is noted that patient selection to enable the targeting of hypoxic tumours is likely to improve overall response. Other hypoxia pro-drugs include PR-104 and apaziquone. PR-104 showed efficacy in phase II trials for lung cancers, but the phase III trial progression was terminated due to discovery of a new mechanism of action (NCT00544674). Apaziquone (APZ) failed to show clinical efficacy in phase II trials due to drug delivery barriers. However, as bladder cancer treatments can be delivered intravesically it can circumvent potential drug delivery problems (Phillips *et al.*, 2013). Therefore, two phase III clinical trials investigated the benefit of apaziquone after TURBT in NMIBC where patients were randomised to either APZ or a placebo after TURBT. A combined analysis was performed on these trials and no significant difference in survival was seen between the two treatment groups. However, when split into subgroups based upon the time APZ was given post-TURBT, significant differences in disease recurrence were seen. No difference between the two treatment

groups was seen when patients were given the compound less than 30 minutes post-TURBT (n=455), but when it was given a minimum of 30 minutes after (n=690) there was a 25.5% relative reduction in the 2-year recurrence rate compared to those given the placebo (HR 0.61, p=0.001), as well as a reduction in time to recurrence by 33% (HR = 0.67, p<0.001). This benefit in time to recurrence was even stronger for those who received APZ 30-90 minutes post-TURBT (HR 0.48, p<0.001) (Karsh *et al.*, 2018).

1.3.4 Measuring tumour hypoxia

The development of methods to measure tumour hypoxia have been studied since the 1960s, but each has various drawbacks and limitations (Table 1.4). No approach has been integrated into routine clinical practice for MIBC, although many are used for clinical research (Lodhi *et al.*, 2021).

Table 1.4. Methods used to measure tumour hypoxia in muscle-invasive bladder cancer.

	Advantages	**Limitations**	**Use in MIBC**
Electrodes	• Prognostic	• Accessible tumours only • Larger than 3cm • Invasive	Not studied
Histopathology (necrosis)	• Cheap • Simple	• Robustness • Reproducibility	Prognostic Predicted benefit of CON
Endogenous markers (HIF-1α, CAIX, GLUT-1)	• Cheap • Simple	• Robustness • Reproducibility • Not hypoxia specific	Prognostic (HIF-1α - borderline, CAIX, GLUT-1) Predicted benefit of CON (HIF-1α)
Gene signatures	• Well validated • Sensitive • Multiple tests in one	• Tumour specific	Prognostic Predicted benefit of CON
Imaging	• Repeat tests through treatment • Whole tumour	• Expensive • Lack of standardisation	Limited to none

Oxygen sensing electrodes were first used in cervical cancer by Kolstad in 1960 and were refined to fine needle microelectrodes by Vaupel in 1974 to minimise bleeding and tissue damage (Kolstad, 1964; Vaupel and Kelleher, 2013). Whilst this approach provides useful information on the oxygen levels, it is limited due to it being highly invasive and restricted to accessible tumours that are more than 3 cm in diameter. This technique is also limited due to not being applicable to any retrospective clinical material and therefore can only be used

prospectively (Bosco and Varesio, 2014). Studies using the microelectrodes in soft tissue sarcomas and prostate, cervical and head and neck cancers showed that hypoxia correlated with a poor prognosis after radiotherapy (Thiruthaneeswaran *et al.*, 2021). The use of oxygen sensing electrodes has not been studied in bladder cancer.

Another method of measuring tumour hypoxia is with the use of exogenous hypoxia markers that can be detected by infusion of tracers, an example of which is pimonidazole. Tracers are compounds that are either injected or given orally, which form covalent bonds with macromolecules at oxygen levels below 1.3% and can be visualised using subsequent IHC on biopsies (Ragnum *et al.*, 2015). The level of pimonidazole staining was found to correlate well with electrode measurements and be successfully applied to formalin-fixed paraffin-embedded (FFPE) tumours (Raleigh *et al.*, 1999). In bladder cancer it was shown that pimonidazole staining correlated well with GLUT-1 and CAIX protein expression in FFPE sections (Hoskin *et al.*, 2003).

Endogenous hypoxia markers have also been used on tumour biopsies as a method of measuring tumour hypoxia such as HIF-1α and its downstream targets, GLUT-1 and CAIX. These markers are limited as accurate measures of true hypoxia because they can be upregulated by external factors such as oncogenes and cytokine signalling (Datta *et al.*, 2021). Nonetheless, a meta-analysis from 147 studies across multiple cancers analysed the relationship between CAIX expression and survival and showed that high expression of CAIX associated with worse overall survival (HR = 1.76, 95% CI 1.58-1.98, $p<0.001$) as well as progression-free survival (PFS), disease-specific survival (DSS), metastasis-free survival (MFS) and locoregional control (Van Kuijk *et al.*, 2016). In bladder cancer, various studies have shown the prognostic and predictive value of hypoxia assessment using HIF and its downstream targets (Table 1.5).

Table 1.5. Protein expression of HIF-1α and its downstream markers evaluated for prognostic potential in bladder cancer.

Study	Protein	Prognostic	Predictive
Hunter *et al.*, 2014	HIF-1α	No	Yes - benefit of CON
Chai *et al.*, 2008	HIF-1α	Yes for DFS (p=0.009)	Not studied
Deniz *et al.*, 2010	HIF-1α	Significantly related to stage and grade	Not studied
Theodoropoulos *et al.*, 2005	HIF-1α	No for PFS (p=0.058)	Not studied
Younes *et al.*, 2001	GLUT-1	Yes for OS (p=0.0064)	Not studied
Boström *et al.*, 2016	GLUT-1	Yes for DSS (p=0.0085) – cohort 1 No for DSS (p=0.15) – cohort 2	Not studied
Hoskin *et al.*, 2003	GLUT-1	Yes for CSS (p=0.016) Yes for OS (p=0.0045)	Yes - benefit of CON
Hunter *et al.*, 2014	CAIX	No	Yes – benefit of CON
Hoskin *et al.*, 2003	CAIX	Yes for CSS (p=0.041) Yes for OS (p=0.034)	Yes - benefit of CON
Klatte *et al.*, 2009	CAIX	Yes for RFS (p=0.001) – TURBT cohort Yes for OS (p=0.003) – cystectomy cohort	Not studied
Turner *et al.*, 2002	CAIX	No	Not studied

DFS = disease specific survival, PFS = progression free survival, OS = overall survival, CSS = cause specific survival, RFS = recurrence free survival, CON = carbogen and nicotinamide.

The utility of both exogenous and endogenous hypoxia markers are limited by their qualitative nature, which makes them difficult to use as an objective and reproducible measure of tumour hypoxia. Furthermore, their application is limited to biopsies, which may not provide an accurate reflection of hypoxia levels in the whole tumour (Bosco and Varesio, 2014; Datta *et al.*, 2021).

Positron emission tomography (PET) and magnetic resonance imaging (MRI) are imaging techniques that can be used to measure tumour hypoxia. These methods are advantageous as they can provide non-invasive hypoxic measurements for the whole tumour, including inaccessible tumours, and can be used repeatedly as treatment progresses to monitor response. However, these approaches are limited by a lack of standardisation in image acquisition, analysis and reporting, and validation is needed to adopt these methods into routine clinical practice (Thiruthaneeswaran *et al.*, 2021). Studies in bladder cancer using dynamic contrast enhanced MRI have shown benefit in assessing tumour stage, grade and extent of angiogenesis (Tuncbilek *et al.*, 2012; Rabie *et al.*, 2016; Hassanien *et al.*, 2019).

1.3.4.1 Hypoxia gene signatures

In recent years, assessing hypoxia by the expression of a collection of hypoxia-associated genes has shown promising utility as a method of measuring tumour hypoxia with prognostic value, resulting in numerous existing prognostic hypoxia gene signatures for various cancers (Table 1.6). Not all of the published hypoxia signatures compare the derived signature scores with other measures of hypoxia but those that do report a good concordance between the two, indicating the hypoxia gene signatures are accurately reflecting levels of tumour hypoxia (Suh *et al.*, 2017; Yang, Forker, *et al.*, 2017; Nie, Qin and Zhang, 2022; Salberg *et al.*, 2022). Some of these signatures also demonstrate predictive value by predicting benefit from hypoxia-modifying treatments, as outlined in Table 1.6.

Methods to derive the gene signature vary between studies as do methods of applying a score to each sample and stratification methods for splitting cohorts into low and high expression. Although most of these signatures are limited by their cancer-specific nature, there are some pan-cancer hypoxia signatures, most notably a 51-gene common hypoxia gene signature developed by Buffa *et al,* which was shown to be prognostic in lung, breast and head and neck cancers (Buffa *et al.*, 2010). In the last two years there has been an increasing number of hypoxia/immune-associated gene signatures being published. The majority of the newly derived hypoxia signatures also analyse the differences in immune infiltrates between hypoxia high and low tumours due to the increasing recognition that hypoxia affects the immune TME which will be discussed further in Section 1.4.

Hypoxia-associated gene signatures have high clinical feasibility in theory as routine biopsies are easily available for calculating the signature scores at a reasonable cost compared to other approaches such as imaging. Gene signatures also allow for the application of multiple tests from a single method (Yang and West, 2019). However, the use of biopsies is also one of their limitations as these do not incorporate the heterogeneity of the tumour and the resulting scores may reflect sampling bias and not the hypoxia status of the whole tumour. Furthermore, there are many hurdles to overcome for the transition of a gene signature based biomarker from research to clinical use such as multiple cohort validation, platform validation and consistency across different centres. Despite this, the prognostic and predictive potential of these sensitive hypoxia gene signatures mean they have exciting potential for clinical application.

Table 1.6. Published cancer-specific hypoxia gene signatures

Derived by	Cancer	Size	Prognostically derived	Score application	Signature stratification	Predictive
M. Jiang et al., 2021	Bladder	4	Yes	Formula	Median	No
Z. Liu *et al.*, 2021	Bladder	16	Yes	Formula	Median	No
F. Zhang *et al.*, 2021	Bladder	8	Yes	Formula	Mean	No
Yang, Taylor, *et al.*, 2017	Bladder	24	Yes	Median	Median	Yes - CON
Fardin et al., 2010	Brain	62	No	K-means clustering	Binary score	No
Gao et al., 2021	Brain	26	No	Formula	Median	No
Ghazoui et al., 2011	Breast	70	No	Median	Median	No
Hu et al., 2009	Breast	13	No	Mean	X-tile	No
Seigneuric et al., 2007	Breast	14	No	Unknown	Unknown	No
Fjeldbo et al., 2016	Cervix	6	Yes	Formula	Binary score	No
Halle *et al.*, 2012	Cervix	31	Yes	Mean	Clustering	No
Nie, Qin and Zhang, 2022	Cervix	9	Yes	Formula	Median	No
Dekervel et al., 2014	Colorectal	6	No	Formula	ROC curve	No
Suh *et al.*, 2017	Head and neck	21	No	Mean	Quartiles	No
Toustrup et al., 2016	Head and neck	15	No	Formula	Binary score	Yes - nimorazole
Winter et al., 2007	Head and neck	99	No	Median	Upper quartile	No
Eustace et al., 2013	Head and neck	26	No	Median	Median	Yes - ARCON
Lane *et al.*, 2022	Lung	28	No	Shrunken centroids	Shrunken centroids	No
Van Malenstein et al., 2010	Liver	7	Yes	Formula	ROC curve	No
Q. Zhang et al., 2021	Liver	21	No	GSVA	X-tile	No
Luo and Du, 2021	Lung	6	Yes	Formula	Median	No
Mo et al., 2020	Lung	4	Yes	Formula	Median	No
Khouzam et al., 2021	Pancreas	8	No	Formula	Specific	No
Ragnum et al., 2015	Prostate	32	No	Median	Unknown	No
Yang, Roberts, *et al.*, 2018	Prostate	28	Yes	Weighted mean	Median	Yes - CON (bladder)
Yang, Forker, *et al.*, 2018	Soft tissue sarcoma	24	No	Formula	Formula	No

1.3.4.1.1 Bladder cancer hypoxia gene signatures

The bladder cancer hypoxia gene signature published by Yang *et al* was shown to have both prognostic and predictive value. The signature was derived using a list of 611 known hypoxia related genes gleaned from literature and then further analysed by generating a co-expression network in the discovery TCGA bladder cancer cohort. Two genes were considered connected if positively correlated (Spearman correlation ≥ 0.5), and hypoxia signature genes were selected as being prognostic ($p < 0.05$) and associated with poor prognosis (HR < 1). A 24-gene signature was derived and tested for associations with survival outcomes by stratifying into hypoxia high or low using the median signature score of a cohort as a cut-off. The final 24-gene signature was prognostic in a meta-analysis of six bladder cancer cohorts for overall survival (n=679, HR = 2.32, 95% CI 1.73-3.12, p<0.001) and in the radiotherapy alone arm of the BCON cohort for local relapse-free survival (n=75, HR = 2.37, 95% CI 1.26-4.47, p=0.008). Prognostic significance was retained in multivariable analyses. The signature also predicted patients who would benefit from having hypoxia-modifying CON addition with radiotherapy (n=76, HR = 0.47, 95% CI 0.26-0.86, p=0.015) (Yang, Taylor, *et al.*, 2017). A test for interaction between hypoxia signature score and treatment arms was significant (p=0.0094).

More recently, a 14-gene bladder cancer miRNA signature was developed that was prognostic for overall survival in a MIBC cohort using the median as stratification (n=62, HR = 2.56, 95% CI 1.19-5.48, p=0.01) and whose performance was improved when using the upper quartile as stratification (n=62, p=0.0002, hazard ratios and CIs not stated). Using the same upper quartile value from the 62 patient MIBC cohort, the signature was shown to predict benefit from CON in the BCON cohort when signature scores were high for both overall survival (HR = 0.44, 95% CI 0.19-1.00, p=0.044) and local relapse free survival (HR = 0.45, 95% CI 0.21-1.01, p=0.048). Whilst benefit was shown to be significant, the strength is somewhat limited by large confidence intervals. There was no significant benefit from CON seen when using the median as cut-off, or in multivariable analyses (Khan *et al.*, 2021).

Three other hypoxia-associated bladder cancer gene signatures have been recently developed and the resulting differences in immune contexts between signature score high and low have been evaluated in all of them. None of the three hypoxia gene signatures were tested for the ability to predict benefit from hypoxia-modifying treatment, but all of them were shown to be prognostic. They will be discussed further in Section 1.4.5.1.

1.4 Hypoxia and the immune tumour microenvironment

Hypoxia results in the regulation of a multitude of genes - roughly 1.25% of the human genome (Denko *et al.*, 2003). Research has shown that hypoxia-induced gene changes, either direct or indirect effect of HIFs, can affect tumour immune responses and contribute towards an immunosuppressive TME by altering the phenotypes and activities of immune cells (Manoochehri Khoshinani, Afshar and Najafi, 2016).

1.4.1 Hypoxia and its effects on myeloid immune cells

Elia *et al* demonstrated that hypoxia inhibits immature DCs from taking up antigens and diminished their antigen-presenting functionality by the downmodulation of pathways involved in the processing of antigens. They showed that hypoxia changed the cytokine and chemokine expression of DCs to decrease expression of CCL18, which is involved in recruiting and promoting migration of T cells and DCs. Hypoxic DCs were also shown to increase production of CXCL1 and CXCL8, both of which recruit neutrophils and stimulate VEGF production. Overall, they showed that hypoxia changes the DC-mediated mechanisms by which leukocytes are recruited to create an inflammatory and pro-angiogenic TME (Elia *et al.*, 2008).

A study by Corzo *et al* demonstrated that under hypoxic conditions MDSCs inhibited T cell proliferation due to, amongst other things, the increased production of arginase 1. Hypoxia exposure caused the differentiation of MDSCs to TAMs, which was shown to be dependent on HIF-1α expression (Corzo *et al.*, 2010). I*n vivo* murine studies demonstrated that the inflammatory ability of macrophages and neutrophils was dependent on HIF-1α expression. They further showed that loss of HIF-1α resulted in decreased invasion of these myeloid cells (Cramer *et al.*, 2003). Neutrophils are regulated by apoptotic mechanisms to prevent prolonged inflammation. A study by Walmsely *et al* showed that HIF-1α increases the expression of NF-kB in human and mouse neutrophils, which inhibits apoptosis and prolongs neutrophil survival under hypoxic conditions (Walmsley *et al.*, 2005). Most of the studies investigating the effect of hypoxia on neutrophils used murine inflammation models and there is little data on the human immune TME. Furthermore, the studies have frequently used a marker that targets both macrophages and neutrophils (LysM). Further studies with a neutrophil-specific marker (MRP-8 or Ly-6G) are needed to elucidate the relationship

between hypoxia and neutrophils, as well studies in human MIBC (Riera-Domingo *et al.*, 2020).

It has been shown that TAMs are found in the highest densities in hypoxic or necrotic regions of a tumour where they have an altered M2, pro-tumour phenotype (Murdoch *et al.*, 2004). Numerous studies of various cancers, including bladder, found a strong positive correlation between the expression of HIF-2α and presence of TAMs (Talks *et al.*, 2000). Doedens *et al* investigated the role of HIF expression in macrophages using a murine breast cancer model and demonstrated that deletion of HIF-1α in macrophages inhibited tumour growth and progression. They showed that in hypoxia macrophages inhibit CD8+ T cell proliferation and response to stimulation due to HIF-1α dependent induction of arginase 1, a hallmark of M2-like macrophages (Doedens *et al.*, 2010). Hypoxia is likely to have a similar effect in bladder cancer where HIF-1α expression correlates positively correlates with increased macrophage infiltration, angiogenesis and a worse prognosis (Chai *et al.*, 2008). HIF-1α in macrophages has been found in numerous studies to increase angiogenesis by both direct and indirect upregulation of VEGF (Riera-Domingo *et al.*, 2020). Taken together, there is increasing evidence that hypoxia potentiates the suppressive effects of myeloid immune cells by both HIF-dependent and independent mechanisms. There is little evidence elucidating the relationship between hypoxia and DCs, MDSCs and neutrophils in bladder cancer specifically.

1.4.2 Hypoxia and its effects on tumour infiltrating lymphocytes

A study performed by Doedens *et al* used mouse models with *VHL* deficient T cells to investigate hypoxia and HIF-dependent changes in CD8+ T cells. Using this model they showed that hypoxia, in a HIF-dependent manner, upregulated the expression of effector and co-activation molecules such as granzyme-B and 4-1BB, GITR and OX40, respectively, as well as inhibitory molecules such as LAG-3 and CTLA-4. They also showed an increased abundance of IFNγ mRNA, amongst other soluble factors, at early time points, but their expression was not sustained indicating a role of paracrine signalling to other immune cells. Overall, they found that HIF signalling limits terminal differentiation of CD8+ T cells and enhances their effector functions under hypoxia, despite the increased expression of checkpoint molecules (Doedens *et al.*, 2013). The notion that hypoxia enhances CD8+ T cell effector functions is further supported by a study investigating HIF expression in CD8+ T

cells. It was shown showed HIF-1α, but not HIF-2α, was essential in maintaining effector functions and states of CD8+ T cells by the expression of the same effector and co-activation molecules found in the Doedens *et al* study (granzymbe B, GITR, OX40) as well as checkpoint molecules (LAG-3, PD-1 and TIM-3). It was shown that CD8+ T cell tumour infiltration and killing was reduced as a result of HIF-1α loss (Palazon *et al.*, 2017). As HIF activity in myeloid cells was shown to suppress T cell responses (Doedens *et al.*, 2010), this highlights the importance of considering immune infiltrates altogether to fully elucidate the effects of hypoxia in the immune TME due to homeostatic cross-talk that occurs between the immune cells present.

The work described above shows that hypoxia can have a positive impact to promote CD8+ effector T cells. However, hypoxia can also negatively regulate CD8+ T cells by HIF-independent mechanisms such as via adenosine accumulation. Hypoxia increases extracellular ATP release resulting in the accumulation of extracellular adenosine (Bowser *et al.*, 2017). A study by Sun *et al* showed hypoxia induced apoptosis in human T cells, which was mediated by the binding of adenosine to its receptors and downstream signalling of the adenosine receptor signalling pathway. This pathway was also shown to significantly inhibit the expression of CCR7 under hypoxic conditions, which is a chemokine essential for T cell migration, differentiation and anti-apoptotic signalling (Sun *et al.*, 2009). Previous studies also support this adenosine-mediated, hypoxia-associated role of CD8+ T cell inhibition using a tumour murine model as well as in the context of myocardial infarction (Yang *et al.*, 2005; Ohta *et al.*, 2006). Adenosine binding to the A2AR receptor on NK cells has been shown to negatively regulate their maturation and functional cytotoxic abilities against tumour cells (Raskovalova *et al.*, 2005; Young *et al.*, 2018).

Hypoxia associated adenosine accumulation also affects other immune cell populations such as DCs. Extracellular adenosine was shown to bind to the adenosine receptor and increase expression of co-stimulatory molecules CD80/86, MHC I and HLA-DR cell surface molecules in both immature and mature DCs thereby increasing their antigen presenting ability. However, in this study the overall result of adenosine increase was to inhibit CD4+ T cells from differentiating to Th1 helper cells, resulting in the shifting of the balance between Th1 and Th2 subpopulations towards the more suppressive Th2 phenotype (Panther *et al.*, 2003).

Another HIF-independent mechanism that can alter immune cell phenotypes as a result of hypoxia is the hypoxia transcription factor Nanog. A murine melanoma model was used to investigate the role of Nanog in immune suppression. The study confirmed that Nanog was selectively induced in hypoxic tumour areas and its inhibition reduced Treg and macrophage levels, which led to a subsequent increase in tumour infiltrating CD8+ T cells. It was shown that Nanog increased expression of TGF-β by its direct binding to the *TGF-B1* gene under hypoxic conditions (Hasmim *et al.*, 2013). TGF-β was shown to induce naïve CD4+ T cells to differentiate into Tregs by the HIF-driven expression of Foxp3 in inflammatory bowel disease (Clambey *et al.*, 2012). There are other studies elucidating the relationship between hypoxia and CD4+ cells, but many have been performed in the context of inflammatory hypoxia and not the nuanced context of an hypoxic TME. Overall, the studies indicate an hypoxia-mediated increase in suppressive Th2 and Treg cells, and inhibition of Th1 cells, although further studies are needed for clarification, especially in the context of bladder cancer (Riera-Domingo *et al.*, 2020).

1.4.3 Hypoxia and its effects on other aspects of the immune TME

Some studies have demonstrated the upregulation of PD-L1 in response to HIF-1α. A study by Barsoum *et al* demonstrated that HIF-1α binds to the HRE on the PD-L1 promoter region in the DU145 prostate cancer cell line and that the hypoxia-induced upregulation of PD-L1 was dependent on HIF-1α expression. They used a murine model to show that hypoxia caused resistance of cytotoxic T cell-mediated tumour lysis via a mechanism that is dependent on the HIF-1α induction of PD-L1 (Barsoum *et al.*, 2014). Another study investigating the hypoxia-related expression of PD-L1 in a panel of murine and human cancer cell lines showed that melanoma cell lines had increased PD-L1 expression under hypoxic conditions. Further to this, HIF-1α was shown to upregulate PD-L1 expression in MDSCs, DCs, and macrophages. In MDSCs, HIF-1α was shown to bind to the HRE on the PD-L1 promoter region and subsequent blocking of the PD-L1 under hypoxic conditions increased MDSC-mediated T cell activation and decreased the release of the immunosuppressive cytokine IL-10 (Noman *et al.*, 2014).

Hypoxia has been shown to downregulate MHC I on the surface of tumour cells, thus providing a mechanism of immune escape by evading detection as discussed in Section 1.2.1.1. A study using prostate cancer cell lines demonstrated that hypoxia exposure causes

tumour cell shedding of MHC I via impaired nitric oxide signalling (Siemens *et al.*, 2008). Another study demonstrated that hypoxia-associated downregulation of MHC I was HIF-dependent using various renal cell carcinoma cell lines (mouse and human) and *in vivo* tumour studies. It was shown that hypoxia, via HIF, decreased antigen presenting proteins such as TAP 1/2 and LMP7. Hyperoxia (60% O_2) reversed this effect as MHC I, TAP 1/2 and LMP7 protein and RNA expression levels were all increased in hyperoxia compared to hypoxia (Sethumadhavan *et al.*, 2017). This reversal of hypoxia-mediated immune evasion mechanisms highlights the importance of overcoming hypoxia to improve immune-mediated tumour killing with implications for immune-based therapies. An HIF-independent mechanism of hypoxia-mediated tumour cell MHC I shedding was demonstrated in a subsequent study by Murthy *et al*. They used murine melanoma and colon tumour cell lines and showed that tumour cells downregulated MHC I in hypoxia due to decreased IFNγ signalling, which also decreased chemokines CXCL9 and CXCL10 essential for immune cell infiltration. They found that this mechanism was independent of HIF and that *in vitro* CD8+ T cells had reduced ability to proliferate and generate IFNγ in hypoxia (Murthy *et al.*, 2019). There are no studies investigating the effects of hypoxia on PD-L1 or MHC expression in bladder cancer.

1.4.4 How hypoxia treatments affect the immune TME

Studies have investigated how increasing tumour oxygenation affects the immune TME. In mouse melanoma models, Hatfield *et al* showed breathing hyperbaric oxygen (60% O_2) decreased tumoural levels of both hypoxia and extracellular adenosine. They showed that respiratory hyperoxia increased the expression of MHC I on tumour cells, tumour killing by cytotoxic T cells and overall survival (Hatfield *et al.*, 2014). The mechanisms of this effect was further elucidated by the same group in a study using hyperbaric oxygen breathing on mouse melanoma and lung tumour models. They demonstrated that respiratory hyperoxia resulted in tumour regression and increased survival in both tumour models. Tumour regression was shown to result from anti-tumour killing effects of NK and T cells, which were shown to avoid hypoxic areas of the tumour and increase tumour infiltration after treatment. They demonstrated a resultant decrease in TGF-β and increase in pro-inflammatory cytokines after respiratory hyperoxia. It was further shown that hyperoxia weakened the immunosuppressive effects of Tregs by decreasing the amount of tumoural

Tregs; reducing their levels of Foxp3 expression; decreasing their expression of enzymes that generate adenosine (CD39/CD73); and reducing their expression of CTLA-4 (Hatfield *et al.*, 2015). These results suggest that concurrent hypoxia-modifying treatments would improve response to immunotherapies such as ICIs.

This hypothesis is supported by work showing that in murine prostate tumours the hypoxia activated pro-drug TH-302 reduced/eliminated hypoxia, led to an influx of T cells and resulted in >80% cures when combined with ICIs (CTLA-4 and PD-1 combination). The study demonstrated that the combination treatment increased CD8+ T cell proliferation, cytotoxic potential (shown by granzyme B release), activation (shown by CD44 expression), and effector cytokine production (shown by IFNγ and TNF-α). Combination treatment also reduced the density of MDSCs and their capacity to inhibit CD8+ T cells (Jayaprakash *et al.*, 2018).

That reversing hypoxia could improve responses to ICIs is also supported by a study using a combination of hyperbaric oxygen and an anti-PD-1 ICI in breast, pancreas and liver tumour mouse models, as well as patient derived hepatocellular carcinoma cells. It was shown that combining hyperbaric oxygen with an ICI promoted delivery of the ICI and T cell infiltration into the tumour and elicited robust anti-tumour CD8+ T cell response that inhibited tumour relapse (X. Liu *et al.*, 2021).

Further support comes from work developing a novel approach to increase oxygen delivery to tumours using oxygen-generating cryogels. The approach was shown to successfully deliver oxygen, which inhibited expression of genes regulated by HIF and reduced adenosine accumulation *in vitro* and *in vivo* melanoma models. These oxygen cryogels were shown to enhance the secretion of cytotoxic proteins in T cells and restore their tumour killing ability (Colombani *et al.*, 2021). Further studies are needed into the effects of hypoxia reversal on the immune TME in human tumours, and there is no current research in the context of bladder cancer.

1.4.5 Hypoxia and its effects on the whole immune TME

Whilst hypoxia, via HIF-dependent and -independent mechanisms, has differential effects on individual immune cells, the overall effect on the immune TME is due to how the immune cells interact with each other. As discussed above, the activation of CD8+ T cells by HIF-dependent mechanisms is contrasted with hypoxia-associated mechanisms of CD8+ T cell

inhibition. These mechanisms of CD8+ T cell inhibition include the hypoxia-associated adenosine-mediated inhibition of CD8+ T cells; the hypoxia-mediated PD-L1 expression that reduces CD8+ T cell tumour killing by inducing an exhausted phenotype; and hypoxia-mediated myeloid cell inhibition of CD8+ T cell tumour migration, activation and tumour killing. Therefore, it is useful to look at associations between hypoxia and the inflammatory state of the whole TME. One approach is to use transcriptional information as it can potentially provide better information to reflect the complex interactions between the two aspects than protein level information as discussed in Section 1.2.5.

A study by Chen *et al* used ten different cancer types from TCGA (bladder, breast, colon, brain, liver, lung, pancreas, rectal, stomach, and thyroid) to investigate the associations between *HIF1A* gene expression and tumour immunity, microenvironment and clinical outcomes. Firstly, they found a positive correlation between *HIF1A* gene expression and anti-tumour immune signatures in multiple cancer types (between 8-10, bladder included) such as CD8+ T cells, B cells, NK cells, M1 macrophages and IFN response as well as immune suppressive signatures such as PD-L1, Tregs, M2 macrophages, TGF-ß, T cell exhaustion and MDSCs. They next looked at correlations between *HIF1A* gene expression and the ratio of *CD8A* to *PD-L1* and found a significant negative correlation in eight individual cancer types (bladder included) as well as in the pooled pan-cancer expression data. Although HIF associates with increased inflammation overall, the low *CD8A:PD-L1* ratio indicates that it associates more strongly with suppressive (PD-L1) than anti (CD8+ T cells) tumour immunity. As high levels of inflammation and checkpoint molecules indicate benefit from ICIs (see Section 1.2.4 and 1.2.5), they investigated *HIF1A* RNA expression in an ICI treated renal cell carcinoma cohort and found that tumours with high *HIF1A* expression had better response than those with low *HIF1A* expression (Chen *et al.*, 2020). Although renal cell carcinomas are associated with VHL mutations that drive high HIF levels a clear benefit was seen for higher *HIF-1a* expression compared to low (Gao *et al.*, 2017). The original study also showed that deficiency in the gene PBRM1 associated with clinical benefit of ICI and those tumours had high transcriptional JAK/STAT, hypoxia and immune signalling (Miao *et al.*, 2018). Chen *et al* showed that all ten cancer types, and the pan-cancer dataset, had a significant positive correlation with ESTIMATE stromal scores and vice versa for ESTIMATE tumour purity. Surprisingly, they did not report on associations with ESTIMATE immune

scores. In five of the cancer types, including bladder, there was an enrichment of TGF-β signalling in the high versus low *HIF1A* expression group (Chen *et al.*, 2020).

The results presented by Chen *et al* provide further support for the notion that HIF enables tumour progression and metastasis and is an adverse prognostic factor in many cancers. Tumours with a stem cell-like phenotype have been previously associated with progression, metastasis, immunosuppression and treatment resistance (Miranda *et al.*, 2019). Chen *et* al demonstrated that a signature representing tumour stemness positively correlated with *HIF1A* expression in eight of the cancer types, including bladder cancer. Signatures reflecting EMT also positively correlated with *HIF1A* expression in nine cancer types (bladder included), as well as the pan-cancer dataset. Survival analyses showed higher *HIF1A* expression conferred a worse prognosis as seen in the pan-cancer dataset for overall survival (n=3038), progression-free survival (n = 2963) and disease specific survival (3041; log-rank test $p<0.001$ for all, no CIs provided) (Chen *et al.*, 2020). This study provides useful insights into the relationship between HIF expression and the immune TME contexture, although it is limited by its use of transcriptomics alone. Further studies elucidating the findings of this study at protein level in human cancers are needed.

1.4.5.1 Immune-related hypoxia gene signatures

As discussed in Sections 1.2.5 and 1.3.4.1, gene signatures are useful tools for patient stratification and can provide further elucidation between hypoxia and the immune TME. Recent studies have used gene signatures to combine information on hypoxia and the immune TME. Brooks *et al* developed a combined hypoxia and immune classifier for head and neck cancer that was shown to be prognostic. They combined a 26-gene hypoxia signature (Eustace, Mani, *et al.*, 2013) and a 28-gene immune response gene signature (Lal *et al.*, 2015) to make a 54-gene combined classifier that clustered TCGA head and neck cohort into three distinct groups: hypoxia^{high}/immune^{low}, hypoxia^{low}/immune^{high}, and mixed. They showed that of the groups the hypoxia^{low}/immune^{high} subgroup had the best prognosis and this was validated on two external head and neck cancer datasets. Using both gene expression analysis and protein staining by IHC they demonstrated that their classifier accurately stratified tumours reflective of their names, that is hypoxia^{low}/immune^{high} tumours had high expression of immune molecules, low expression of hypoxia-associated molecules, and were represented by the classical inflamed immunphenotyping as shown by

CD3 IHC staining. The opposite was true of hypoxia^{low}/immune^{high} tumours, and mixed tumours had a mixture of hypoxia and immune signalling. Although this classifier has implications for benefit of treatment, the study did not extend to investigating this.

Chang *et al* also developed a gene signature from a mixture of hypoxia and immune-associated genes. They first identified a 45-gene signature in liver cancer that was prognostic in three liver cohorts, but then refined this to an 8-gene signature that was also prognostic in head and neck, kidney, lung, pancreas and endometrial cancer. The hypoxia genes were identified by using the common hypoxia gene signature from Buffa *et al* and a ChIPseq dataset generated from human liver cancer cell lines to identify genes bound by HIF. They then determined those common hypoxia genes that were significant across 25 TCGA cancer types (n=29) and which of these genes overlapped with identified HIF targets from their ChIPseq dataset (n=23). For the immune-related genes they identified hypoxia-driven immune suppressive genes by using literature to determine genes associated with Tregs and exhausted CD8+ T cells and which of those genes overlapped with identified HIF targets (n=79). To derive the initial 45-gene signature they used a liver cancer training dataset to find which of those immune-related genes were upregulated >1.5 fold (n=26) and combined them with the hypoxia genes to derive a signature for testing (n=45; 4 gene overlap between two sets). A final 8-gene signature was derived following Cox regression to analyse the prognostic significance in three liver cohorts and found an overlap of eight genes. The study found their 8-gene signature was highly prognostic in multiple cancers, including in multivariable analyses, and that it outperformed current TNM staging in three of them. Whilst they show a significant positive correlation between their 8-gene signature and hypoxia scores in all of the examined cancer types they did not correlate their signature with the immune contexture of the tumours (Chang, Forde and Lai, 2019). Although the signature is derived from immune genes associated with Tregs and exhausted CD8 T cells, no analyses were performed to examine the differences in immune landscapes between patients stratified into high and low gene signature scores. The lack of any subsequent reflection of their score and the immune TME is a limitation of their study.

In 2021 three studies were published for *de novo* hypoxia signatures in bladder cancer that were prognostic and reflected differences in the immune TME contexture. Jiang *et al* identified a four gene hypoxia signature using the 200 hypoxia-related genes from GSEA. The signature was prognostic in three external bladder cancer cohorts (aside from the

training dataset) for disease-specific survival and overall survival, although no confidence intervals were stated. It was found to be prognostic in multivariable analyses for two of the cohorts. They compared their gene signature with the immune TME using previously established signatures for 28 immune cell infiltrates and ESTIMATE scores and found that high versus low score correlated with increased abundance of immune cells and ESTIMATE immune and stromal scores. The authors investigated the differences in checkpoint molecule expression between high and low score tumours and found that high score tumours had increased expression of *CTLA-4*, *LAG-3*, *PD-L1* and *PD-1.* They further analysed 14 bladder cancer samples using IHC and showed that CTLA-4 and LAG3 protein expression (assessed by positive frequencies of German immunoreactive scores) was higher in the high versus low signature score tumours (M. Jiang *et al.*, 2021). Whilst this study highlights the prognostic potential of their derived four-gene hypoxia signature in bladder cancer and indicates that there are potentially important differences in the immune infiltrates between high and low score tumours, more robust elucidation is needed to confirm the results. An established method of deconvoluting the tumour immune cell populations such as ImSig, TIMER or Cibersort would improve the study alongside analysis of IHC staining on an increased sample number and associations with molecular subtypes. The signature was derived from the 200 genes in the Hallmark hypoxia gene list, but no subsequent correlations between their derived signature and Hallmark hypoxia scores, or other measures of hypoxia, were shown (M. Jiang *et al.*, 2021).

Published in the same month as Jiang *et al.,* another group developed a prognostic hypoxia-related gene signature in bladder cancer using the GSEA hypoxia-associated genes and TCGA-BLCA dataset (F. Zhang *et al.*, 2021). The validation datasets from GEO were the same and both signatures were trained on prognosis with slight differences in subsequent signature generation. Zhang *et al* had eight genes in their final signature, of which one overlapped with Jiang *et al* (HS3ST1). Their signature was prognostic in all three cohorts, although no hazard ratios or confidence intervals were shown. The group investigated the relationship between the signature and clinical parameters in all three cohorts and found that the signature was prognostic regardless of age, stage, gender and grade subgroups. In multivariable analyses the signature maintained independent prognostic significance, although this was only stated for the TCGA cohort. Using Cibersort they showed that high score tumours had higher infiltration of M0 and M1 macrophages, and activated memory

CD4+ T cells in all of the cohorts. GSEA was used to identify an enrichment of immune-related pathways as seen by KEGG pathway analysis, such as cytokine and complement signalling pathways. None of the top pathways enriched in the high score tumours related to hypoxia signalling and no correlation was made between the derived signature and hypoxia measurements. The authors used the Genomics of Drug Sensitivity in Cancer database to associate their gene signature scores with prediction of response to chemotherapies. They found that certain drugs used in bladder cancer treatments (methotrexate, vinblastine, doxorubicin, gemcitabine and cisplatin) had higher IC50s when the score was high, in specific cohorts, indicating a potential for those tumours to develop chemoresistance (F. Zhang *et al.*, 2021).

Liu *et al* also derived a prognostic hypoxia immune signature using the GSEA 200 hypoxia-associated genes in bladder cancer. They demonstrated that the signature was prognostic in two external bladder cancer cohorts. They used literature and knowledge-based signatures corresponding to the cancer immunity cycle and demonstrated a positive correlation between their score and anti-cancer immune responses such as T cell and NK cell recruitment. The methodology behind this is not very clearly explained in their publication. They then used Cibersort and TIMER, alongside four other algorithms, to compare correlations between immune infiltrates and their gene signature. Upon analysing both the training cohort and a validation cohort they found positive correlations between the gene signature score and levels of immune infiltrates such as CD8+ T cells, NK cells and DCs, although the data shown suggests little concordance between the algorithms, making it difficult to draw conclusions (Table 1.7).

Table 1.7. Correlations between gene signature score and immune infiltrates from different algorithms

Algorithm	Cohort	CD8 T cells	NK cells	Dendritic cells
TIMER	Training	0.42	Null	Myeloid: 0.57
	Validation	0.53	Null	Myeloid: 0.49
TIP	Training	Null	0.10	0.25
	Validation	0.31	Ns	Ns
Cibersort	Training	0.20	Null	Activated: -0.23 Resting: 0.10
	Validation	Ns	Ns	Activated: Ns Resting: Ns
QuanTIseq	Training	0.25	-0.11	-0.20
	Validation	Ns	Ns	-0.26
X-cell	Training	-0.15	Ns	Activated: 0.55 Myeloid: 0.32
	Validation	-0.32	Ns	Activated: 0.55 Myeloid: 0.36
MCP-counter	Training	0.25	0.25	Myeloid: 0.31
	Validation	Ns	0.49	Myeloid: 0.53

Modified from Liu et al., 2021. Ns = not significant. Stated to be either Pearson's or Spearman's correlations.

Lui *et al* also correlated scores for their gene signature with those for other signatures from literature that predict ICI efficacy and with checkpoint molecule gene expression. They found a positive correlations, although the figure presented is difficult to decipher. They used seven different methods of molecular stratification, including the consensus method, and saw that high risk score for their signature associated with basal subtypes and low scores with luminal subtypes (Z. Liu *et al.*, 2021). Similarly to Jiang's gene signature, whilst the results of this study indicate the potential for their gene signature to reflect different immune TME contexts, further validation and more robust analyses are needed to clarify this. There are currently no prognostic gene signatures in bladder cancer combining hypoxia and immune genes that clearly define tumours with distinct hypoxia status and immune landscapes and predict response to treatments.

1.5 Summary, aim and objectives

1.5.1 Rationale

Bladder cancer is a highly prevalent disease with poor survival rates (Sung *et al.*, 2021). Radiotherapy with radiosensitisers is given as a bladder-preserving alternative to surgery, but there are high rates of relapse after treatment (Vashistha *et al.*, 2017). There is a current need to develop biomarkers to identify patients likely to relapse after standard-of-care treatment and those who will benefit from additional therapeutic agents to improve radiotherapy responses and overall survival (Flaig, 2019).

Hypoxia is a common feature of many solid tumours and is also an adverse prognostic factor in bladder cancer (Theodoropoulos *et al.*, 2004; Chai *et al.*, 2008; Hunter *et al.*, 2014; Yang, Taylor, *et al.*, 2017). An immunosuppressive tumour microenvironment is known to be a negative prognostic factor contributing to recurrence of disease and tumour progression (Hanahan and Weinberg, 2011). In MIBC both hypoxia and an immunosuppressive TME contribute to the failure of radiotherapy and are targetable by hypoxia-modifying treatments and immune checkpoint inhibitors, respectively. (Höckel *et al.*, 1996; Barker *et al.*, 2015). Both are therefore of interest as potential biomarkers. There is growing evidence that hypoxia drives a suppressive immune tumour microenvironment, but this is yet to be fully elucidated in bladder cancer. Therefore, the relationship between immunosuppression and hypoxia is of interest when developing biomarkers to guide the management of MIBC

Gene signatures can be used as biomarkers to stratify patients into groups that are likely to fail radiotherapy and would therefore benefit from other therapeutic approaches in combination. Independently, existing hypoxia and immune gene signatures have shown both prognostic and predictive value. As both of these factors are targetable in MIBC, a prognostic gene signature that also provides predictive information regarding treatment strategy would be clinically useful to stratify patients into different groups for combination therapeutic approaches to improve treatment outcomes and overall survival. Currently there are no gene signatures that evaluate the hypoxia status of the tumour alongside the immune TME contexture for MIBC that predicts benefit of treatment.

1.5.2 Hypothesis

As hypoxia drives an inflammatory TME in MIBC, which contributes towards an immunosuppressive TME leading to failure of radiotherapy, a prognostic and predictive gene signature can be developed as a biomarker that identifies poor prognosis patients likely to benefit from hypoxia-modifying treatments and/or ICIs.

1.5.3 Aim and objectives

The overall aim of the project is to investigate the effects of hypoxia on the immune tumour microenvironment in muscle-invasive bladder cancer and develop biomarkers that could be used to individualise the use of concurrent treatments with radiotherapy. The specific objectives of this thesis were the following:

1. Investigate the effects of hypoxia on PD-L1 expression in MIBC using *in vitro* and *in silico* approaches.
2. Investigate the association between hypoxia and CD8+ T cells (amongst other immune markers) at the protein level using tissue available from the BCON study.
3. Investigate the relationship between HIF-binding, hypoxic conditions, and immune-related signalling in MIBC using *in vitro* studies and at the gene expression level using *in silico* approaches.
4. Develop an hypoxia-driven immune gene signature that can identify poor prognosis MIBC patients and predict benefit of treatment.

2 Materials and Methods

2.1 Cell culture

2.1.1 Cell lines and reagents

Three human muscle-invasive bladder cancer cell lines were used for *in vitro* experiments: T24, J82 and UMUC3. They are all adherent transitional cell carcinoma cell lines and were cultured in Eagle's Minimum Essential Media (Gibco; ThermoFisher Scientific, Loughborough, UK) supplemented with 10% filtered foetal bovine serum (Gibco) and 2 mM L-glutamine (Gibco). The cell lines were authenticated by the Cancer Research UK Manchester Institute core facilities every six months and tested for mycoplasma monthly. Cells were kept in an humidified incubator (37°C, air plus 5% CO_2). To prevent exhaustion of nutrients the cell media were replaced every two or three days after removing the previous media and washing the cells with phosphate buffered saline (PBS; made by in-house services) to remove dead cells and debris before replacing with fresh warmed culture media. Cells were grown to sub-confluence and passaged either to keep cells growing for future use or for seeding an experiment. Cells were passaged by removing media and washing the cells with PBS before using 0.25% Trypsin-EDTA (Gibco) to dissociate the cells from the culture flask in the incubator for no longer than five min. Media with 10% FBS was used to neutralise the trypsin and the cells were collected into a Universal centrifuge tube and centrifuged at 400 g for five min at room temperature to obtain a cell pellet. The supernatant was discarded and the pellet resuspended in fresh culture media. To maintain the cell line for future use the cell solution was reseeded at a desired concentration (usually around 1:10) in a new labelled T-75 flask (Corning, New York, USA) containing warmed culture media and kept in the incubator. For use in experiments the cell solution was counted using a haemocytometer and trypan blue (Sigma-Aldrich, Missouri, USA) to detect and discount dead cells and the desired amount seeded for the experiment in relevant culture plates or dishes.

2.1.2 Treating cells with pharmacological agents

Human recombinant interferon gamma (IFNγ; Peprotech, London, UK) was reconstituted in dimethyl sulphoxide (DMSO) to make a working stock solution of 20 µg/ml. It was diluted in medium to a working concentration of 10 ng/ml.

2.1.3 Exposure to hypoxia

Cells were counted and plated appropriately, usually at a density of $1x10^5$ per well in 6-well cell culture plates (Corning) unless otherwise stated, and left to adhere for 24 h in an incubator (37°C, air plus 5% CO_2). Plates were then transferred to a hypoxia cabinet (Baker-Russkin®, Bridgend, Wales), washed with PBS and fresh media added as appropriate. Both the PBS and fresh media were pre-equilibrated to the required oxygen concentration in the appropriate hypoxia cabinet for 24 h.

2.2 Western blotting

Western blotting was performed to visualise the amount of a protein expressed by cells subjected to different conditions.

2.2.1 Protein extraction

The cells were lysed *in situ*. Lysis buffer solution was made by using a 1:10 dilution of lysis buffer (Cell Signalling Technology, Massachusetts, USA) in ddH_2O and 1:100 protease inhibitor cocktail (Cell Signalling Technology) and an appropriate amount added to the culture dish after aspiration of media and two PBS washes. The dishes were left at 4°C, or on ice in the hypoxic workstation, for 10 min and then scraped into labelled 1.5 ml Eppendorf® tubes (Sigma-Aldrich). From this stage onwards all samples were kept on ice to minimise protein degradation. Samples were sonicated at 10 amplitude microns for 10 s using a Soniprep 150 (MSE, UK). They were then centrifuged at 14,000 g for 15 min at 4°C and the lysate transferred into a new labelled Eppendorf tube. Quantification was carried out using BCA protein assay kit (ThermoFisher Scientific, Massachusetts, USA) according to the protocol. Lysates were diluted with ddH_2O to 30 µg/ml of protein and Laemmli SDS sample buffer (Alfa Aesar, Massachusetts, USA) was added to make 24 µl volume in a new labelled Eppendorf tube. The lysates were boiled for 5 min on a hot block at 95°C and briefly centrifuged for ~3 s using a MiniSpin (Merck, Darmstadt, Germany) to collect the entire sample.

2.2.2 Electrophoresis and transfer

XCell SureLock™ Mini-Cell Electrophoresis System (ThermoFisher Scientific) was used with Novex™ WedgeWell™ 4-20% Tris-Glycine Protein Gels (ThermoFisher Scientific). Running buffer (Alfa Aesar) was added down the middle with a 2 cm overflow. Lysate samples were added to the relevant wells, a protein ladder (ProSieve® Color Protein Markers; Lonza, Basel,

Switzerland) in the first well and water in empty wells to prevent “smiling”. The gel was run for 1.5 h at 125V using a power pack (Bio-Rad, California, USA). The gels were removed from the cassettes and transferred to a membrane using XCell II™ Blot Module (ThermoFisher Scientific) transfer system with. Sponges, filter paper (Bio-Rad), nitrocellulose membrane (Immun-blot PVDF membrane, Bio-Rad) and the gels were layered together in a transfer cassette. The transfer cassettes were placed in the tank with transfer buffer (Alfa Aesar) down the middle and overflowing to 2 cm at the bottom and run at 25V for 2 h using the same power pack. The box was surrounded by ice to keep the transfer cool and minimise blurring.

2.2.3 Antibody staining and membrane visualisation

5% milk (Marvel) in 0.1% Tween 20 (Sigma-Aldrich) PBS (0.1% PBS-T) was used to block the membranes for 1 h on a rocker. All antibodies were diluted using 5% milk in 0.1% PBS-T. Table 2.1 lists the antibodies and dilutions used. The membranes were cut using either the visible ladder as a guide or by staining with Ponceau S (Sigma-Aldrich) for 5 min and then washed after cutting by three 5 min washes in 0.1% PBS-T on a rocker. The sections of membranes were incubated with diluted antibody and left overnight at 4°C. The following morning the membranes were washed twice for 10 min in 0.1% PBS-T on a rocker and incubated in secondary antibody for 1 h on a rocker at room temperature. The membranes were then washed four times for 5 min in 0.1% PBS-T on a rocker.

Table 2.1 List of antibody dilutions used for western blotting

Target	Raised in	Dilution	Supplier	Code
PD-L1	Rabbit	1:2000	Cell Signalling Technology	13684
HIF1a	Mouse	1:500	BD	610959
CA9	Rabbit	1:500	Abcam	184006
GAPDH	Rabbit	1:2500	Cell Signalling Technology	2118
Mouse-HRP	Goat	1:7500	Invitrogen	62-6520
Rabbit-HRP	Goat	1:5000	Invitrogen	65-6120

Membranes were viewed using a ChemiDoc™ XRS+ imager (Bio-Rad) and Pierce™ enhanced chemiluminescent kit (ThermoFisher Scientific). Membrane images were acquired using optimised settings for each target of interest to obtain a clear image without overexposure.

2.2.4 Quantification by densitometry

Densitometry analysis was performed using ImageJ software in order to quantify the relative expression of proteins. Protein densities were calculated relative to the control untreated samples, for both proteins of interest and loading control proteins. Protein densities were then calculated relative to the loading control samples. Relative protein densities were plotted using GraphPad Prism software.

2.3 Flow cytometry

Changes in the surface expression of proteins were measured at the single cell level using flow cytometry.

2.3.1 Sample acquisition and staining

Cells were plated in triplicate in 12-well plates (Corning) and placed in a hypoxia cabinet for 24 h (see Section 2.1). The cells were then trypsinised and collected into labelled FACS tubes (Corning). All proceeding steps were performed with refrigerated reagents and the centrifugation step throughout the protocol was 400 g for 3 min at 4°C. The cells were centrifuged, washed in FACS buffer (1% FBS in PBS) and resuspended in 100 µl per sample of live/dead fixable cell stain (Invitrogen, Massachusetts, USA) diluted at a 1:1000 dilution in PBS. The cells were left in the dark at room temperature for 30 min before being centrifuged. The supernatant was discarded and the cell pellets were washed twice in FACs buffer. The cells were then resuspended in 100 µl per sample of human FcR (Miltenyi Biotec, Bergisch Gladbach, Germany) diluted at a 1:100 dilution in FACs buffer to block non-specific binding and left at 4°C for 15 min. The samples were centrifuged, supernatant discarded, and resuspended in 100 µl per sample of phycoerythrin (PE) conjugated PD-L1 antibody (Invitrogen) diluted at a 1:100 dilution in FACs buffer. To check the specificity of the binding a control of PE mouse IgG1 k isotype antibody (BD Biosciences, New Jersey, USA) was added to each repeat of each sample using the same dilution. Samples were then left for 30 min at 4°C, centrifuged, washed twice in FACs buffer, resuspended in 100 µl of 1%

paraformaldehyde (PFA) (Biolegend, California, USA) to fix the cells. Samples were left at 4°C for a maximum of 3 days before being analysed.

2.3.2 Analysing samples

Data were acquired using an LSRII flow cytometer (BD Biosciences). Compensation controls were used to minimise spectral overlap of the channels: unstained cells, cells stained only with the PD-L1 PE antibody and cells stained only with the live/dead fixable dye. Compensation samples were analysed first and the resulting compensation applied to all samples. At least 10,000 cells were acquired per sample. The data were analysed using FlowJo software (version 10.6.1). Statistical analysis was performed using GraphPad Prism 8 software. Mean values were compared using 2-way ANOVA with Tukey's multiple comparison test.

2.4 Quantitative Polymerase Chain Reaction (qPCR)

The mRNA expression of target genes was measured using qPCR. RNAse free water and filter tips were used throughout to prevent RNA degradation.

2.4.1 RNA extraction and quantification

Cells were seeded onto 6 cm cell culture dishes (Corning) and treated as previously described. RNA was extracted from the samples using the RNeasy mini kit (Qiagen, Hilden, Germany) as follows. The cells were lysed *in-situ* with 350 µl Buffer RLT after removal of media and a wash with PBS. The cells were scraped using a cell scraper and collected into 1.5ml Eppendorf tube and mixed thoroughly by pipetting. The samples were homogenised using a 19-guage needle and syringe and passing the lysate through at least five times. 350 µl of 70% ethanol was added to each lysate and mixed by pipetting. The sample was then transferred to an RNeasy spin column in a 2 ml collection tube and centrifuged at 8000 g for 15 s at room temperature. The flow through was discarded, 700 µl Buffer RW1 added to each spin column, and the centrifuge step repeated. This was repeated again with 500 µl Buffer RPE twice, with the second centrifuge step being for 2 min to dry the spin column to ensure no ethanol was carried over. To further ensure the dryness and non-contamination of the samples, the optional additional drying step was always included and the spin columns were placed into new collection tubes and centrifuged at 20,817 g for 1 min at room temperature. The spin columns were then placed into new 1.5ml collection tubes, 30 µl RNAse-free water added, and samples centrifuged at 8000 g for 1 min at room

temperature to elute the RNA. The RNA samples were quantified immediately using 1 µl of sample and a NanoDrop™ spectrophotometer (ThermoFisher Scientific). The purity was determined using 260/280 ratio values. RNA was stored at -80°C until further use.

2.4.2 cDNA synthesis

cDNA was obtained from the RNA samples using OmniScript RT kit (Qiagen) to make 1 µg per sample. These steps were all performed on ice and reagents thawed on ice prior to use to prevent premature cDNA synthesis and minimise RNA degradation. An aliquot of 10x buffer RT was diluted to a 1x working concentration. RNase Inhibitor (New England Biolabs, Massachusetts, USA) was diluted to 10 units/µl in ice cold 1x buffer RT. A master mix was prepared using the supplied OmniScript RT kit reagents and random hexamer primers (ThermoFisher Scientific; Table 2.2). 8 µl was added to separate RNase free 0.2ml tubes on ice. RNA samples were made up to 1 µg/µl based on the quantification in the previous step and diluted with ddH_2O to make 12 µl per sample then added to tube with the master mix to make a 20 µl final volume per reaction. Samples were vortexed for ~3 s, centrifuged in a MiniSpin for ~3 s to bring all of the tube's contents down, and incubated for 60 min at 37°C. Resulting cDNA was either used straight away in the next step, or stored at -20°C until further use.

Table 2.2 Reverse transcription reaction master mix components for 1 sample

Component	Volume (µl)
10x Buffer RT	2
dNTP mix (5 mM)	2
Random hexamer primers	2
Omniscript reverse transcriptase	1
RNase inhibitor (10 units/µl)	1

2.4.3 Designing primers

Primers for the target genes were chosen following guideline advice on primer selection. First the gene sequence was found using National Center for Biotechnology Information (NBCI) and then Primer-BLAST software and Primer3 software was used to find suitable forward and reverse primers (Table 2.3). The primers were checked using Beacon Designer software (Premier Biosoft) to ensure their suitability. Primers were ordered from Eurofins Genomics (Ebersberg, Germany) and resuspended as stated on the data sheet in the relevant amount of TE buffer (VWR International Ltd, Lutterworth, UK).

Table 2.3 Primer sequences used for qPCR and their properties

Primer	Sequence	Temperature (°C)	GC-content (%)
PD-L1 forward	TATGGTGGTGCCGACTACAA	57.3	50
PD-L1 reverse	TGGCTCCCAGAATTACCAAG	57.3	50
SDHA forward	CATCCACTACATGACGGAGCA	59.8	52.4
SDHA reverse	ATCTTGCCATCTTCAGTTCTGCTA	59.3	41.7

2.4.4 Preparing the plate, running the reaction and analysing the results

cDNA was diluted in water as desired for the experiment: serial dilutions were used for primer validation and 1:100 dilution used for other experiments to make a final concentration of 10 ng/µl cDNA. Primer mixes were made using 1 µl forward primer, 1 µl reverse primer and 5 µl PowerUp SYBR Green Master Mix (ThermoFisher Scientific) per well. A 384-well PCR plate was used as supplied by the CRUK MI molecular biology core facilities. 7 µl of the prepared primer mix was added to the desired well with 3 µl of cDNA dilution. A no template control consisting of 3 µl nuclease-free water instead of cDNA was plated in triplicate in every plate to monitor contamination and primer-dimer formations. An adhesive sticker was placed on top to seal the plate, which was centrifuged for ~3 s to remove bubbles and pull down any liquid to the bottom of each well. The plate was run on a QuantStudio 5 Real-Time PCR System (ThermoFisher Scientific) for 384-well plates as shown in Table 2.4. A melting curve was generated after the cycling programme as described in Table 2.5.

Table 2.4 Thermal cycling protocol used for qPCR

Step	Temperature (ºC)	Duration (s)	Cycles
UDG activation	50	120	Hold
Dual Lock DNA polymerase	95	120	Hold
Denature	95	15	40
Anneal	60	15	
Extend	72	60	

Table 2.5 Dissociation curve conditions used for melt curve stage of qPCR

Step	Ramp rate (°C/s)	Temperature (°C)	Time (s)
1	1.6	95	15
2	1.6	60	60
3 (dissociation)	0.15	95	15

Data were analysed using QuantStudio Design & Analysis software (ThermoFisher Scientific) by analysing the Ct values and melt curve peaks. For primer efficiencies all the graphs were created and the goodness of fit R^2 values calculated using GraphPad Prism 8 software.

2.5 Multiplex Immunohistochemistry

Immunohistochemistry (IHC) allows for the visualisation of proteins of interest in tissue sections. Multiplex IHC was used to visualise multiple proteins on the same tissue section, with each protein being represented by a different colour to allow for visualisation of the interaction and co-localisation between the different proteins in one tissue section. This allows for the visualisation of the spatial distribution of immune cells in context to the tumour microenvironment. Opal™ detection was used to allow for the use of antibodies of the same species without cross-reactivity occurring and for the optimised simultaneous measurement of five targets in a single section. All multiplex protocols had been previously optimised on a different tissue type by Anna Maria, a member of Prof Richard Byers' group (Tsakiroglou *et al.*, 2020, 2021). The protocol was re-optimised for bladder cancer tissue.

2.5.1 BCON tissue

BCON was a prospective multicentre phase III clinical trial that recruited patients in the UK from 2000 to 2006 (registered as CRUK/01/003). Patients with bladder cancer were randomised to radiotherapy alone or radiotherapy with concurrent carbogen (2% CO_2 + 98% O_2) and nicotinamide (40 or 60 mg kg^{-1}). At the time of recruitment, patients provided written informed consent for the use of their diagnostic biopsies in future research. Approval was obtained by a local ethics committee for research using the samples (LREC 09/H1013/24) and. The primary end point was cystoscopic control at six months and the secondary end points were overall survival, local relapse free survival, urinary and rectal morbidity (Figure). The trial protocol and results are described in further detail elsewhere (Hoskin *et al.*, 2010). FFPE diagnostic biopsies were available to use for the optimisation and spectral library creation. Tissue microarrays (TMAs) were previously created by the Histology Facility of the Cancer Research UK Manchester Institute using the muscle-invasive tumour FFPE tissue blocks and these were used for the final staining protocol (Eustace, Irlam, *et al.*, 2013; Hunter *et al.*, 2014). For these TMAs, 1 mm cores of up to three per tumour region from two regions were taken from tumour areas that had been marked out by a histopathologist (Dr Helen Denley).

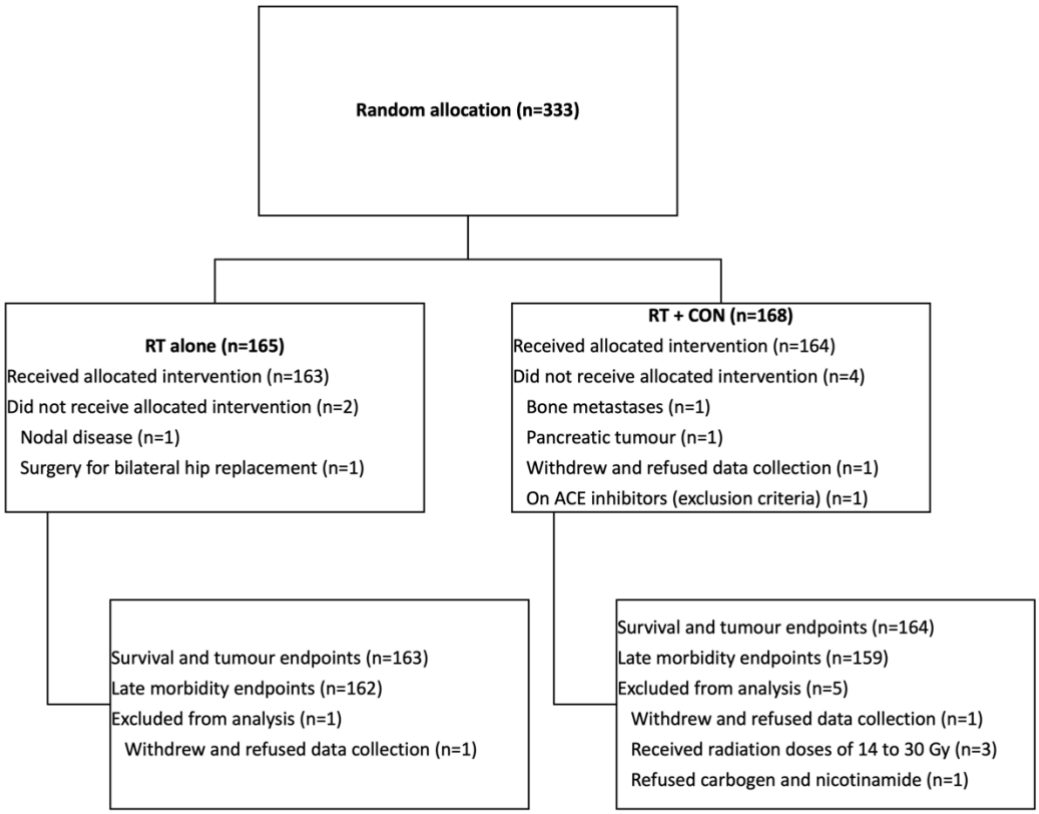

Figure 2.1 BCON trial CONSORT diagram.

2.5.2 Protocol optimisation and spectral library creation

The Ventana Discovery Ultra (Roche, Basel, Switzerland) system was used for the automated IHC. Each marker was paired with a specific fluorophore (Table 2.6). The protocol was optimised by using a variety of primary antibody dilutions and Opal dilutions on both the single plex and multiplex slides until there was a clear and specific signal for each marker with a good signal:background ratio of <1:15. Final reagent concentrations are listed in Table 2.6. Single plex slides of each marker at the same concentrations were used for spectral library creation, along with a slide with no stain to detect autofluorescence and a slide with DAPI.

Table 2.6 Suppliers and dilutions for reagents used during the multiplex immunohistochemistry staining.

Target	Raised in	Dilution	Supplier	Code	Opal™	Dilution
CD4	Rabbit	Pre-diluted	Roche	790-4423	620	1:300
CD8	Mouse	1:300	DAKO	C8/144B	540	1:600
CD68	Mouse	1:40	Abcam	ab955	650	1:400
FOXP3	Mouse	1:60	Abcam	ab20034	520	1:400
PD-L1	Rabbit	Pre-diluted	Roche	790-4905	570	1:1000

2.5.3 Multiplex staining protocol

Final staining was performed on tissue microarray slides from BCON. The staining protocol involved initial deparaffinisation and epitope retrieval at pH 8.5 followed by multiple cycles of incubation with primary antibody, secondary antibody and opal detection. The cycles were separated by a short denaturation at pH 6. UltraMap anti-rabbit/mouse HRP conjugated secondary antibodies were used (Roche). Antibody and Opal™ concentrations are listed Table 2.6. After the automated protocol the slides were manually washed by three 5 min cycles of a 1:10 dilution of EZ preparation (Ventana Medical Systems) before being counter-stained with a 1:120000 dilution of DAPI (ThermoFisher Scientific) for 5 min. The slides were then cover-slipped with ProLong™ Gold Antifade Mountant (ThermoFisher Scientific).

2.5.4 Multispectral scanning and unmixing

A Vectra 3 microscope (Akoya Biosciences) was used to scan the slides with a Vectra Fluorescence Illuminator 200 watt Metal Halide Bulb set to 10%. Manual annotation of TMA core locations was performed using a low resolution scan at 4x magnification. A multi-spectral image of each core was then acquired at 20x magnification using DAPI, AF488, TRITC, AF594 and AF647 filters. After multispectral scanning, the slides were spectrally unmixed using inForm software 2.4.9 (Akoya Biosciences) and the pre-prepared spectral library.

2.5.5 Image analysis

Image analysis was done in HALO 3.2 with the TMA Module (Indica Labs, Albuquerque, USA) to manually exclude artefacts and then obtain counts of each marker per core. The marker quantification was then exported to R where normalisation was performed by calculating the percentage of each marker from the total cell count across all cores of each patient (n=116). This method was chosen to account for cores of different sizes and different numbers of cores per patient. CA9 IHC scores previously generated were used to assign patients a CA9 status of present or absent (n=111) (Eustace, Irlam, *et al.*, 2013). CA9 status was used instead of our hypoxia signature as using the hypoxia signature was not significant due to constricted patient numbers (n=86). Gene expression data previously generated (Yang, Taylor, *et al.*, 2017) was used to assign each patient a molecular subtype using the "consensusMIBC" package in R (Kamoun *et al.*, 2020).

2.5.6 Statistical analysis

All the analyses were performed using R version 4.0.5 and RStudio version 1.3.1093 and associated packages used to analyse data and calculate significance. Non-parametric statistics (Wilcox test) were used due to the non-normal distribution of each marker. Relationships with overall and local progression-free survival for 16-year follow up were assessed in R using Cox proportional hazard models and Kaplan-Meier curves via the "survival" and "survminer" packages which uses a log-rank test to calculate p values. Tables of characteristics were tabulated using "table1" package in R. Cumulative incidence curves were plotted and the significance calculated using "cmprsk" package. Multivariable analysis and statistical tests were performed using the "survival" package and the results were tabulated using "gtsummary" package.

2.6 Chromatin Immunoprecipitation sequencing (ChIPseq)

Chromatin immunoprecipitation Sequencing, ChIPseq, can be used to identify the association of proteins with specific genomic regions. It was used here in a bladder cancer cell line, T24, to investigate the binding patterns of HIF1a, HIF2a and HIF1b transcription factors. The process involves cross-linking the protein-DNA interactions before lysing the cells and shearing the chromatin into smaller fragments. Immunoprecipitation uses antibodies specific to the protein of interest and magnetic beads to isolate the protein-DNA complexes. The fragments are then de-cross-linked and the DNA eluted and sequenced.

2.6.1 Preparing antibody/magnetic bead mixture

Dynabeads Protein G (ThermoFisher Scientific) were used at a concentration of 100 µl per 100 million cells. The beads were washed three times in ice cold blocking mixture of 5 mg/ml Bovine Serum Albumin (Sigma-Aldrich) in PBS using a magnetic stand (Diagenode, New Jersey, USA). The beads were resuspended in 500 µl blocking solution, split into enough tubes per antibody, topped up to 500 µl total volume with blocking solution and left rotating overnight at 4°C. Negative and positive controls were used alongside the antibodies of interest. Table 2.7 lists the antibodies and concentrations used.

Table 2.7 List of antibodies and dilutions used for ChIP experiment.

Target	Raised in	Concentration	Supplier	Code
HIF-1α	Rabbit	1mg/ml	Abcam	Ab2185
HIF-2α	Rabbit	1mg/ml	Abcam	Ab199
HIF-1β	Mouse	1mg/ml	Novus Biologicals	H1beta234
CTCF	Rabbit	1mg/ml	Diagenode	C01010170
IgG control	Rabbit	1mg/ml	Millipore	12-370

2.6.2 Cross-linking and cell collection

Cells were cultured in hypoxia as previously described (Section 2.1.3), using 15 cm culture dishes (Sarstedt, North Carolina, USA). Cells were dual cross-linked directly in the hypoxia cabinet using 10 ml PBS/$MgCl_2$ and 40 µl ChIP cross-link gold (Diagenode) for 10 min followed by 15 ml of 1% formaldehyde (Sigma) in PBS for 10 min. The reaction was quenched by adding 0.125 M glycine. The dishes were removed from the hypoxia cabinet and placed on ice. The cells were manually scraped using ice-cold PBS + Protease Inhibitor Cocktail (PIC; Promega, Wisconsin, USA) before being centrifuged at 300 g for 3 min at 4°C. The resulting cell pellets were washed twice with PBS + PIC.

2.6.3 Fragmenting chromatin samples and performing ChIP

Everything in this step was performed on ice. Lysis buffer 1 (50 mM Hepes-KOH, pH7.5; 140 mM NaCl; 1 mM EDTA; 10% glycerol; 0.5% NP-40/Igepal CA-630; 0.25% Triton™ X-100; ddH2O) + PIC was added to each sample and incubated for 10 min at 4°C and then centrifuged at 300 g for 3 min at 4°C. The supernatant was removed and the resulting pellet was resuspended in lysis buffer 2 (10 mM Tris-HCl, pH 8.0; 200 mM NaCl; 1 mM EDTA; 0.5 mM EGTA; ddH2O) + PIC. These were incubated for 5 min at 4°C and the centrifugation step repeated. The pellet was resuspended in lysis buffer 3 (10 mM Tris-HCl, pH 8; 100 mM NaCl; 1 mM EDTA; 0.5 mM EGTA; 0.1% Na-deoxycholate; 0.5% N-lauroylsarcosine; ddH2O) + PIC and the sample split into microtubes for sonication (Diagenode). Sonication was previously optimised per cell line to obtain optimal size fragments of 200-300 bp. For T24 cell line this was 16 cycles of 30 s on and 30 s off using a Biorupter Pico (Diagenode). Each time the experiment was performed the fragment sizes were checked using agarose gel electrophoresis, as described below (Section 2.6.4). 50 µl of chromatin was removed for input reference and stored at -20°C. The rest of the chromatin samples was then incubated with the pre-prepared magnetic bead/antibody mixes, as previously described in Section 2.6.1, overnight on a rotator at 4°C.

2.6.4 Agarose gel electrophoresis

The samples were prepared by adding 1 µl of proteinase K (ThermoFisher Scientific) to 10 µl of chromatin sample, incubating them at 65°C for 20 min, and adding 1 µl of 10% Triton™ X-100. Samples were centrifuged at 20,817 g for 5 min at room temperature, transferred to new Eppendorf tubes and 10 µl H_2O added with 6 µl gel loading dye (Promega). The samples were run on a 1.5% agarose gel made using agarose powder (Invitrogen), TAE buffer (ThermoFisher Scientific) and SYBR safe gel dye (ThermoFisher Scientific). 6 µl prepared DNA ladder (Promega) was added into the first well and 24 µl of each prepared sample into subsequent wells. The gel was run at 130 V for 30 min using a power pack (Bio-Rad) and TAE running buffer (ThermoFisher Scientific). The gel was visualised using ChemiDoc UV light viewer (Bio-Rad).

2.6.5 Reverse cross-link and harvest chromatin

The IP samples were washed in RIPA buffer (50mM HEPES pH 7.6, 1mM EDTA, 0.7% Na deoxycholate, 1% NP-40, 0.5M LiCL) five times. Samples were then washed with TE buffer and all residual TE buffer removed. Odom lab elution buffer (50mM TrisHCl, pH8, 10mM EDTA, 1% SDS) was added to each sample, including the input sample, and vortexed to mix thoroughly. Samples were incubated overnight for a maximum of 16 h on a shaker at 65°C to reverse the protein-DNA cross-link. The supernatant was then collected using a magnetic stand and transferred to a fresh Eppendorf. After adding 200 µl of TE buffer and 8 µl of 10 mg/ml RNAse A (Merck) to each sample, the samples were incubated for 1 h at 37°C. 4 µl of proteinase K was then added to each sample prior to incubating at 55°C for 2 h. 400 µl phenol: chloroform: isoamyl alcohol (25:24:1; ThermoFisher Scientific) was then added and samples vortexed and then centrifuged at 10,000 g for 5 min at room temperature. The top aqueous layer containing DNA was removed into a new Eppendorf and the process repeated with chloroform: isoamyl alcohol (24:1; Merck). 16 µl of 5 M NaCl (Cambridge Biosciences Limited, Cambridge, UK) was added to make a final concentration of 200 mM which was mixed with 2 µl of 20 µg /µl glycogen (Merck) to give a visible pellet. Next, 800 µl 100% ethanol was added to each sample, which were then placed in a -80°C freezer for a minimum of 30 min to improve precipitation. After the freezing step, the samples were centrifuged at 20,817 g for 20 min at 4°C to precipitate out the DNA. The resulting pellet was washed in 500 µl ice cold 70% ethanol and the centrifugation process was repeated. The pellet was air dried at room temperature for 5 min and resuspended in ~30 µl 10mM

Tris-HCl pH 8.0 (ThermoFisher Scientific), depending on pellet size, and quantified using NanoDrop™ (ThermoFisher Scientific). Samples were stored at -20°C until further use.

2.6.6 qPCR verification of ChIP samples

The IP samples were verified via qPCR using primers for negative and positive loci enrichment. EGLN3, UGP2 and TTLL2 were used as positive controls and beta-actin as a negative control for the HIF samples (Eurofins genomics). Table 2.8 lists the primer sequences and properties. Pre-made primer pairs of H19 and myoglobin were used from the iDeal ChIPseq for transcription factors kit (Diagenode; C01010170) as a positive and negative control for CTCF, respectively. For each primer pair the input DNA was run alongside the IP samples and the negative Ig control. Samples were diluted 1:10 in H_2O to make enough diluted DNA for 5 µl per well and the primer mixes were prepared using a 1:1 ratio with enough primer mix for 1 µl per well. Primer master mixes were made for each primer using 10 µl SYBR Green master mix (ThermoFisher Scientific), 1 µl primer mix and 4 µl H_2O per well, scaled for the number of wells needed. The thermal cycling conditions are given in Table 2.4 followed by a melt curve stage as per Table 2.5 (see Section 2.4.4).

Table 2.8 Primer sequences used for qPCR validation of ChIP and their properties

Primer	Sequence	Tm (°C)	GC-content (%)
EGLN3 forward	AGTGTCCGTTCCCAGCTCAG	61.4	60
EGLN3 reverse	TAGGCACAGTAAACAGGCC	56.7	52.6
UGP2 forward	GGACTGTTGGGAAGCTTTA	57.3	50
UGP2 reverse	GACGCAAACCACGTACACA	56.7	52.6
TTLL2 forward	CTCTGTATCACCCGCCTAGC	61.4	60
TTLL2 reverse	TTTCACTGGGGTGAGGTAGC	59.4	55
Beta-actin forward	ACCATGGATGATGATATCGCC	57.9	47.6
Beta-actin reverse	GCCTTGCACATGCCGG	56.9	68.8

IP sample enrichment was then calculated by the following formula:

$$\% \text{ recovery} = 2\text{^}((Ct_{input}\text{-compensatory factor})-Ct_{sample})*100\%$$

Where Ct_{input} and Ct_{sample} are the threshold values from the exponential phase of qPCR, 2 is the amplification efficiency (assumed to be 100%), and the compensatory factor corrects for the input dilution. Compensation factor was calculated by $\log_2[X\%]$ where X is the dilution factor. If there was an enrichment over the positive loci with a low background, with no enrichment on the negative control then the IP was considered successful and sent for sequencing.

2.6.7 Sequencing

Sequencing was performed by the core facilities at CRUK MI. ChIPseq libraries were prepared using 1ng of ChIP DNA and 12 cycles of amplification with the NEBNext Ultra II DNA Library Prep Kit for Illumina (New England BioLabs). Where applicable a double-sided size selection of libraries were performed using AMPure XP Reagent (Beckman Coulter, California, USA) with volumes of 0.47x and 0.45x (total 0.92x) of the library volume. Library quality was checked using the Agilent Bioanalyzer/Fragment Analyzer (Agilent Technologies, California, USA). Libraries were quantified by qPCR using a KAPA Library Quantification Kit for Illumina (Roche). Paired-end 100bp sequencing was performed by loading 180-200pM pooled libraries on a NovaSeq 6000 sequencer with XP loading (Illumina, California, USA).

2.6.8 Analysing and mapping samples

Analysis was performed by the computational biology support team of the CRUK MI. First, the sequencing reads from ChIP and input samples were quality checked using FASTQC. All bases with a Phred quality score ≤ 20 and any adapter sequences present in the data were removed using Trim Galore. Second, the cleaned and trimmed FASTQ files from previous steps were mapped to the hg19 reference assembly using bowtie2.v2.2.1. Third, the resulting alignment SAM files were processed using samtools v1.3.1 to remove unmapped reads, and to retain reads that mapped in proper pair with a mapping quality >= 20. The SAM files were then converted into BAM files and indexed. Fourth, the alignment results (BAM files) were used in MACS2 v2.1.2 (with –keep-dup 1 -q 0.01 parameters for narrow peaks and with --broad-cutoff 0.1 for broad peaks) for peak calling to identify the ChIP signal enriched genomic regions. Last, Homer v4.10 was used to annotate the significant peaks and TSS/gene body profiles were generated by ngsplot v2.61. Different filtering parameters were then applied to the annotated peaks using the assigned genomic regions. The filtering parameter are as follows: 1) All significant peaks (no subsequent filtering); 2) peaks assigned to protein coding regions; 3) peaks assigned to near transcriptional start site (TSS) promoter regions; and 4) both protein coding and near TSS. For visualising tracks bigWig files were produced from BAMs using the bamCoverage function and these were subsequently subset according set of peaks chosen by MACS2 and visualised using the University of California, Santa Cruz (UCSC) genome browser. All processing was performed using the CRUK MI high-performance computing service (Phoenix) with packages deepTools (3.5.1), bedops (2.4.39) and ucscsuite (20150630).

2.7 Microarray cell line data generation

Microarray gene expression data from four MIBC cell lines (T24, J82, UMUC3, and HT1376) exposed to four different oxygen concentrations (21%, 1%, 0.2%, and 0.1%) was generated by Rekaya Shabbir in the TRB group.

2.7.1 Cell lines and seeding

The cell lines and media that was used for this experiment are described in Section 2.1.1, with the addition of the MIBC cell line HT1376, and exposure to hypoxia performed as detailed in Section 2.1.3. For this experiment $5x10^5$ cells were seeded in 10 cm cell culture dishes (Corning) and exposed to each oxygen concentration for 24 h.

2.7.2 Harvesting RNA

The cells were manually scraped in PBS and transferred to a 1 ml RNAse free microfuge tube (Ambion, Texas, USA) before being centrifuged at 10,000 rpm for 10 min at 4°C. Supernatant was discarded and the remaining cell pellet used for RNA extraction using RNeasy Plus Mini Kit (Qiagen) as described in Section 2.4.1, with QIAshredder (Qiagen) homogenisation method instead of needle and syringe. The cell suspension with buffer RLT was transferred to a QIAshredder spin column and centrifuged at 10,000 rpm for 1 min at room temperature. The lysate was transferred to a gDNA eliminator spin column and centrifuged at 10,000 rpm for 30 s at room temperature before continuing from the addition of ethanol as described in Section 2.4.1. The RNA quantity was measured using a NanoDrop™ spectrophotometer (ThermoFisher Scientific) and purity measured using a Qubit 4 Fluorometer (ThermoFisher Scientific).

2.7.3 Affymetrix Clariom S microarray

Gene expression arrays were prepared using 8 ng/µl in 9 µl of the RNA and the Clariom S pico HT human assay (ThermoFisher Scientific). The sample hybridisation was performed by Yourgene Health (Manchester, UK) and batches of Affymetrix CEL files were normalised by signal space transformation with probe guanine cytosine count correction using Affymetrix Array Power Tools (ThermoFisher Scientific). Batch correction was performed using the ComBat function from the R package "sva" to generate $\log_2$ summarised gene level expression.

2.8 Bioinformatics

Bioinformatics was used for general *in silico* analyses to analyse transcriptomic data available from the BCON trial and publicly available cohorts such as TCGA. It was also used to analyse the microarray and ChIPseq datasets that were generated. R and RStudio were used throughout, the versions were updated throughout the project but ranged from 4.0.3 – 4.0.5 and 1.3.1093 – 2022.02.2, respectively. The package "tidyverse" was used in all analyses.

2.8.1 Cohorts used

RNAseq data from the TCGA bladder cancer cohort (n=405) was obtained using the R packages "TCGAUtils" and "curatedTCGAData". Bladder cancer cohort microarray data from the gene expression omnibus (GEO) were obtained using the R package GEOquery. GSE32894 (n=224) was fresh-frozen resection samples treated with TURBT and GSE13507 (n=187) was fresh-frozen resection samples treated with TURBT +/- BCG as appropriate. BCON transcriptomic data were generated by the TRB group (n=152) and the updated long-term clinical outcomes were used throughout (Song *et al.*, 2021). Further details are outlined in Section 2.5.1. TCGA (n=401) and BCON (n=141) datasets were filtered to include only tumours stage 2 and above, i.e., MIBC.

2.8.2 Assigning molecular subtypes

Consensus molecular subtypes were applied using the R package "consensusMIBC" (Kamoun *et al.*, 2020). First order subtyping was applied by assigning all three luminal subtypes (LumP, LumNS and LumU) to luminal and basal/squamous and stroma-rich subtypes to basal. NE-like were removed from the first order analyses due to numbers being small.

2.8.3 Assessing relationships with survival

Relationships between generated biomarkers and survival were assessed using Cox proportional hazard models via the "survival" and "survminer" packages, which generates Kaplan-Meier curves and uses a log-rank test to calculate p values. Multivariable analyses and statistical tests were also performed using the "survival" package and the results were tabulated using "gtsummary" package.

2.8.4 LASSO regression model

Z scores were calculated from the TCGA expression scores using the scale function from the R package "glmnet". The optimal lambda was calculated using the package "pcoxtime" and the lambda.min was used. LASSO model was applied and those genes with a coefficient shrunken to 0 were removed from the list before running the model again. The final coefficients were used to apply the weighted mean to each sample using the predict function from the package "glmnet".

2.8.5 Immune cell deconvolution analysis

ImSig was applied using the R package "ImSig" (Nirmal *et al.*, 2016). First, the optimal correlation threshold was chosen for each dataset using the function gene_stat to choose a value that retains a large number of genes after feature selection with a reasonably high correlation value across the cell types. For the BCON dataset this value was set at r=0.6, and for TCGA dataset it was r=0.65. TIMER deconvolution was performed using the website http://timer.cistrome.org/ with BLCA as the cancer type (Li *et al.*, 2016). Immune cell fractions were also imputed using the Cibersort algorithm (Chen *et al.*, 2018). All of the cohorts used LM22 as the mixture file with 100 permutations and no batch corrections. Only for the TCGA cohort was the quantile normalisation disabled, as recommended by Cibersort for RNAseq data. Significance between groups is shown as the adjusted p values from BH method using the t_test function to correct for multiple testing.

2.8.6 Use of other gene signatures

Hypoxia scores were assigned using the Yang *et al* bladder cancer hypoxia gene signature by calculating the median score across the genes in the signature and stratifying into low and high groups using the median score of the cohort (Yang, Taylor, *et al.*, 2017). All other gene signatures were assigned by calculating the mean score across the genes in the signature. The genes in each signature are listed in Table 2.9.

Table 2.9 Lists of the genes in each respective gene signature.

Signature	Genes						
Hypoxia [1]	*CAV1*	*THBS4*	*LDLR*	*GULP1*	*GLG1*	*FUT11*	*SLC2A3*
	DAAM1	*CYP1B1*	*CAD*	*AHNAK2*	*SAV1*	*PDLIM2*	*LRP1*
	TRAM2	*SRPX*	*DPYSL2*	*TGFBI*	*SLC16A1*	*P4HA2*	*ITGA5*
	DSC2	*SYDE1*	*COL5A1*				
IFNγ signalling [2]	*IDO1*	*CXCL10*	*CXCL9*	*STAT1*	*IFNG*		
CD8 signalling [2]	*CD3D*	*TAGAP*	*CXCL13*	*GZMB*	*STAT1*	*CXCL10*	*LAG3*
	NKG7	*IL2RG*	*CD2*	*GZMK*	*CCL5*	*CD3E*	*CIITA*
	CXCR6	*IDO1*					
B cells [3]	*BLK*	*CD19*	*FCRL2*	*MS4A1*	*KIAA0125*	*TNFRSF17*	*TCL1A*
	PNOC	*SPIB*					
Cytotoxic [3]	*PRF1*	*GZMA*	*GZMB*	*NKG7*	*GZMH*	*KLRK1*	*KLRB1*
	CTSW	*GNLY*	*KLRD1*				
DCs [3]	*CCL13*	*CD209*	*HSD11B1*				
Exhausted CD8 [3]	*LAG3*	*CD244*	*EOMES*	*PTGER4*			
Macrophages [3]	*CD68*	*CD84*	*CD163*	*MS4A4A*			
Mast cells [3]	*TPSB2*	*TPSAB1*	*CPA3*	*MS4A2*	*HDC*		
Neutrophils [3]	*FPR1*	*SIGLEC5*	*CSF3R*	*FCAR*	*FCGR3B*	*CEACAM3*	*S100A12*
NK cells [3]	*NCR1*	*XCL1*	*XCL2*				
T cells [3]	*CD6*	*CD3D*	*CD3E*	*SH2D1A*	*TRAT1*	*CD3G*	
Checkpoint [4]	*CD274*	*PDCD1LG2*	*CTLA4*	*PDCD1*	*LAG3*	*HAVCR2*	*TIGIT*
TGFb ECM [5]	*FN1*	*POSTN*	*SULF1*	*COL3A1*	*COL1A2*	*COMP*	*VCAN*
	MFAP2	*COL5A3*	*COL7A1*	*COL5A1*	*ITGAX*	*MMP12*	*TIMP1*
	ADAM8	*FAP*	*SPP1*	*ACAN*	*ADAM12*	*LOXL2*	*MMP9*
	MMP1	*COL11A1*	*COL10A1*	*SERPINH1*	*ADAMTS14*	*MMP11*	*TGFB*
	COL5A2	*COL1A1*					
M1 TAMs	*CCL2*	*CCR2*	*CD36*	*CD80*	*CD86*	*CXCL10*	*IL1B*
	NFKBIA	*NOS2*	*TNF*	*CXCL16*	*CXCL9*	*IL6*	
M2 TAMs	*ARG1*	*CCL17*	*CCL22*	*CHI3L1*	*CD163*	*IGF1*	*EGR2*
	MRC1						

1 = (Yang, Taylor, *et al.*, 2017), 2 = (Ayers et al., 2017), 3 = (Danaher et al., 2017), 4 = (Mariathasan *et al.*, 2018), 5= (Chakravarthy et al., 2018).

2.8.7 Over representation analysis

The top 20 Gene Ontology (GO) biological processes were identified using the R package "clusterProfiler" and represented graphically using "enrichplot". Significance was set as adjusted p value < 0.05 (BH).

2.8.8 Gene Set Enrichment Analysis (GSEA)

The R package "limma" was used to identify differentially expressed genes (DEGs; $p<0.1$). The goana function was used with the DEGs to investigate gene ontologies that were significantly ($p<0.05$) enriched. Hallmark pathways were downloaded using "msigdb" and the package "fgsea" was used to perform GSEA to see which Hallmark pathways were significantly increased/decreased (Subramanian *et al.*, 2005).

2.8.9 Statistics and other bioinformatics tests

Parametric statistics (t-test, Pearson) were used when data were normally distributed and non-parametric statistics (Wilcox test, Spearman) were used when the data were non-normally distributed. Data distributions were calculated using the Shapiro-Wilks test. Cumulative incidence curves were plotted and the significance calculated using "cmprsk" package. Tables of characteristics were tabulated using "table1" package.

3 The effect of hypoxia on PD-L1 expression in bladder cancer

The work in this chapter was published in BMC Cancer on 25th November 2021 and was re-formatted and edited for this thesis. The original article can be found using the DOI: https://doi.org/10.1186/s12885-021-09009-7.

Smith, V., Mukherjee, D., Lunj, S. *et al.* The effect of hypoxia on PD-L1 expression in bladder cancer. *BMC Cancer* 21, 1271 (2021). https://doi.org/10.1186/s12885-021-09009-7

3.1 Abstract

Introduction: Recent data has demonstrated that hypoxia drives an immunosuppressive tumour microenvironment (TME) via various mechanisms including hypoxia inducible factor (HIF)-dependent upregulation of programmed death ligand 1 (PD-L1). Both hypoxia and an immunosuppressive TME are targetable independent negative prognostic factors for bladder cancer. Therefore we sought to investigate whether hypoxia is associated with upregulation of PD-L1 in the disease.

Materials and methods: Three human muscle-invasive bladder cancer cell lines (T24, J82, UMUC3) were cultured in normoxia (20% oxygen) or hypoxia (1% and 0.1% oxygen) for 24 h. Differences in PD-L1 expression were measured using Western blotting, quantitative polymerase chain reaction (qPCR) and flow cytometry (≥3 independent experiments). Statistical tests performed were unpaired t tests and ANOVA. For *in silico* work an hypoxia signature was used to apply hypoxia scores to muscle-invasive bladder cancers from a clinical trial (BCON; n=142) and TCGA (n=404). RStudio was used for analyses and statistics performed were linear models and one-way ANOVA.

Results: When T24 cells were seeded at <70% confluence, there was decreased PD-L1 protein ($p=0.009$) and mRNA ($p<0.001$) expression after culture in 0.1% oxygen. PD-L1 protein expression decreased in both 0.1% oxygen and 1% oxygen in a panel of muscle-invasive bladder cancer cells: T24 ($p=0.009$ and 0.001), J82 ($p=0.008$ and 0.013) and UMUC3 ($p=0.003$ and 0.289). Increasing seeding density decreased PD-L1 protein ($p<0.001$) and mRNA ($p=0.001$) expression in T24 cells grown in both 20% and 1% oxygen. Only when cells were 100% confluent, were PD-L1 protein and mRNA levels higher in 1% versus 20% oxygen ($p=0.056$ and $p=0.037$). *In silico* analyses showed a positive correlation between hypoxia signature scores and PD-L1 expression in both BCON ($p=0.003$) and TCGA ($p<0.001$) cohorts, and between hypoxia and IFNγ signature scores ($p<0.001$ for both).

Conclusion: Tumour hypoxia correlates with increased PD-L1 expression in patient derived bladder cancer tumours. *In vitro* PD-L1 expression was affected by cell density and decreased PD-L1 expression was observed after culture in hypoxia in muscle-invasive bladder cancer cell lines. As cell density has such an important effect on PD-L1 expression, it should be considered when investigating PD-L1 expression *in vitro*.

3.2 Introduction

Bladder cancer is the tenth most common cause of cancer death in the UK with an overall ten-year survival rate of only 46% in England (Cancer Research UK, 2022). Stages two, three and four are classified as muscle-invasive bladder cancer (MIBC) for which the five-year survival rates are 45%, 40% and 10% respectively (Office for National Statistics, 2019b).

The two definitive treatment approaches for MIBC are cystectomy, or radiotherapy with a radiosensitiser. Neoadjuvant chemotherapy can be given with either, but has a limited contribution to improved survival (Song *et al.*, 2019). Immunotherapy for bladder cancer has an extensive history, with the first immunotherapy (Bacillus Calmette–Guérin) for non-MIBC being approved in 1990 (Morales, Eidinger and Bruce, 2002). In the last five years, six new immunotherapies were approved for advanced urothelial carcinoma, most targeting the PD-1/PD-L1 pathway. However, despite initial successes the rates of durable responses remain low with generally only around one in five patients showing a sustained response (Wołącewicz *et al.*, 2020).

An immunosuppressive tumour microenvironment (TME) is known to be a negative prognostic factor contributing to recurrence of disease and tumour progression (Hanahan and Weinberg, 2011). Hypoxia is a common feature of many solid tumours and is also an adverse prognostic factor in bladder cancer (Theodoropoulos *et al.*, 2004; Chai *et al.*, 2008). Both an immunosuppressive TME and hypoxia contribute to the failure of radiotherapy, therefore, the relationship between them is of interest for developing biomarkers to guide treatment choices (Höckel *et al.*, 1996; Barker *et al.*, 2015).

Hypoxia inducible factor (HIF1)-1α is a transcription factor that regulates ~1.25% of the human genome in response to decreased oxygen availability (Denko *et al.*, 2003). Recently, it was shown that hypoxia-induced gene changes affect tumour immune responses and contribute towards an immunosuppressive TME (Manoochehri Khoshinani, Afshar and Najafi, 2016). The mechanisms involved include direct effects on immune cells that alter their functions and indirect effects due to altered cytokine and chemokine expression that impact the recruitment and migration of immune cells (Murdoch *et al.*, 2004; Sitkovsky and Lukashev, 2005).

Specifically, hypoxia via HIF-1α was shown to increase expression of the immune checkpoint gene PD-L1 in human and mouse cancer cell lines (Barsoum *et al.*, 2014; Noman

et al., 2014). The effect of hypoxia on PD-L1 expression in bladder cancer has not previously been reported.

The aims of this chapter were to investigate the effects of hypoxia on PD-L1 expression in bladder cancer using *in vitro* and *in silico* approaches.

3.3 Materials and methods

3.3.1 Cell culture

Human MIBC cell lines (T24, J82, UMUC3) were cultured in Eagle's Minimum Essential Media supplemented with 10% foetal bovine serum and L-glutamine as detailed in Section 2.1.1. Cell lines were authenticated by the Cancer Research UK Manchester Institute core facilities services every 6 months and tested for mycoplasma monthly. Cells were seeded at a density of $1x10^5$ per well, unless otherwise stated, onto 6-well cell culture plates in a humidified atmosphere of air plus 5% CO_2 (here termed normoxia) and left to adhere for 24 h. Some plates were then transferred to a hypoxia cabinet, washed with PBS and fresh media added with/without the addition of human recombinant IFNγ to media culture to a working concentration of 10 ng/ml. Both the PBS and fresh media were pre-equilibrated to the required oxygen concentration for 24 h. The other plates were processed in the same way but in normoxia. See Sections 2.1.2 and 2.1.3 for further details.

3.3.2 Western blotting

Western blotting was performed as detailed in Section 2.2. In brief, cells were lysed *in situ* and sonicated at 10 amplitude microns for 10 s before centrifugation at 14,000 g for 15 min. Protein concentrations of the lysates were measured using a BCA Protein Assay kit and the solution resolved on 4-20% Tris-Glycine Protein Gels prior to transference to a nitrocellulose membrane. The membrane was then incubated with the primary and secondary antibodies with PBS washes in between.

3.3.3 qPCR

As described in Section 2.4, RNA was extracted using a Qiagen RNeasy Mini Kit and quantified using a NanoDrop™. cDNA was obtained using OmniScript RT Kit with random hexamer primers and RNase Inhibitor. Primers were designed by Primer-BLAST and Primer3 software, checked using Beacon Design Software and made by Eurofins Genomics before being resuspended in Tris – EDTA (TE) buffer. Serial dilutions of primers were used for

validation experiments and primer mixes were made with SYBR Green Master Mix. 384-well PCR plates were run using a QuantStudio 5 Real-Time PCR System and appropriate controls.

3.3.4 Flow cytometry

Flow cytometry was performed as detailed in Section 2.3. In brief, cells were trypsinised, placed in fluorescence-activated cell sorting (FACS) tubes, washed in FACS buffer (1% FBS in PBS), centrifuged and resuspended in a series of solutions with FACS buffer washing steps in between. In order, the cells were resuspended in a live/dead fixable cell stain (1:1000), human FcR blocking solution (1:100), then either PD-L1 PE antibody (1:100) or control PE mouse IgG1 k isotype antibody (1:100) before being fixed in 1% paraformaldehyde. Samples were acquired on a LSRII flow cytometer with 10,000 viable cells collected per sample. Flow cytometry was performed in either duplicate or triplicate wells as stated and each well was split into two FACS tubes for immunoglobulin control alongside a target of interest. The data collected were then processed using FlowJo software (version 10.6.1).

3.3.5 Bioinformatics and statistics

BCON is a clinical trial registered as CRUK/01/003 of which the details and conclusions are outlined in the initial findings report (Hoskin *et al.*, 2010). Gene expression data from the BCON cohort were obtained as detailed in Section 2.8.1 (Yang, Taylor, *et al.*, 2017). The TCGA-BLCA data were obtained using the R packages "TCGAUtils" and "curatedTCGAData". Both datasets were filtered to include only tumours of a known stage and stage 2 and above. *In silico* data were tested by linear regression, Pearson's correlation and ANOVA using R (version 4.0.3) and RStudio (version 1.3). *In vitro* data were tested by unpaired t test or ANOVA using GraphPad Prism 8 software.

3.4 Results

3.4.1 Hypoxia decreases expression of PD-L1 in T24 human bladder cancer cells

To investigate the effects of hypoxia on PD-L1 expression in T24 MIBC cells they were cultured at 0.1% oxygen and 20% oxygen and the differences in PD-L1 expression examined. PD-L1 expression significantly decreased in hypoxia (0.1% oxygen for 24 h) at both the RNA (qPCR) and protein (Western blotting, flow cytometry) level in T24 human bladder cancer cells (Figure 3.1). IFNγ is a known stimulant of PD-L1 and its addition led to the expected stimulation of PD-L1 (Garcia-Diaz *et al.*, 2017). However, when IFNγ stimulated cells were cultured in hypoxia, the IFNγ-driven PD-L1 increase was reduced (Figure 3.1). This finding

further highlights the negating effects of hypoxia on PD-L1 expression in T24 cells. HIF-1α protein expression was present in all the samples cultured in hypoxia (0.1% oxygen) and absent in those under normoxia, confirming the cells are responding to the hypoxic conditions (Figure 3.2). Comparison of the proportion of viable cells between samples showed hypoxia did not induce excessive cell death (Figure 3.3).

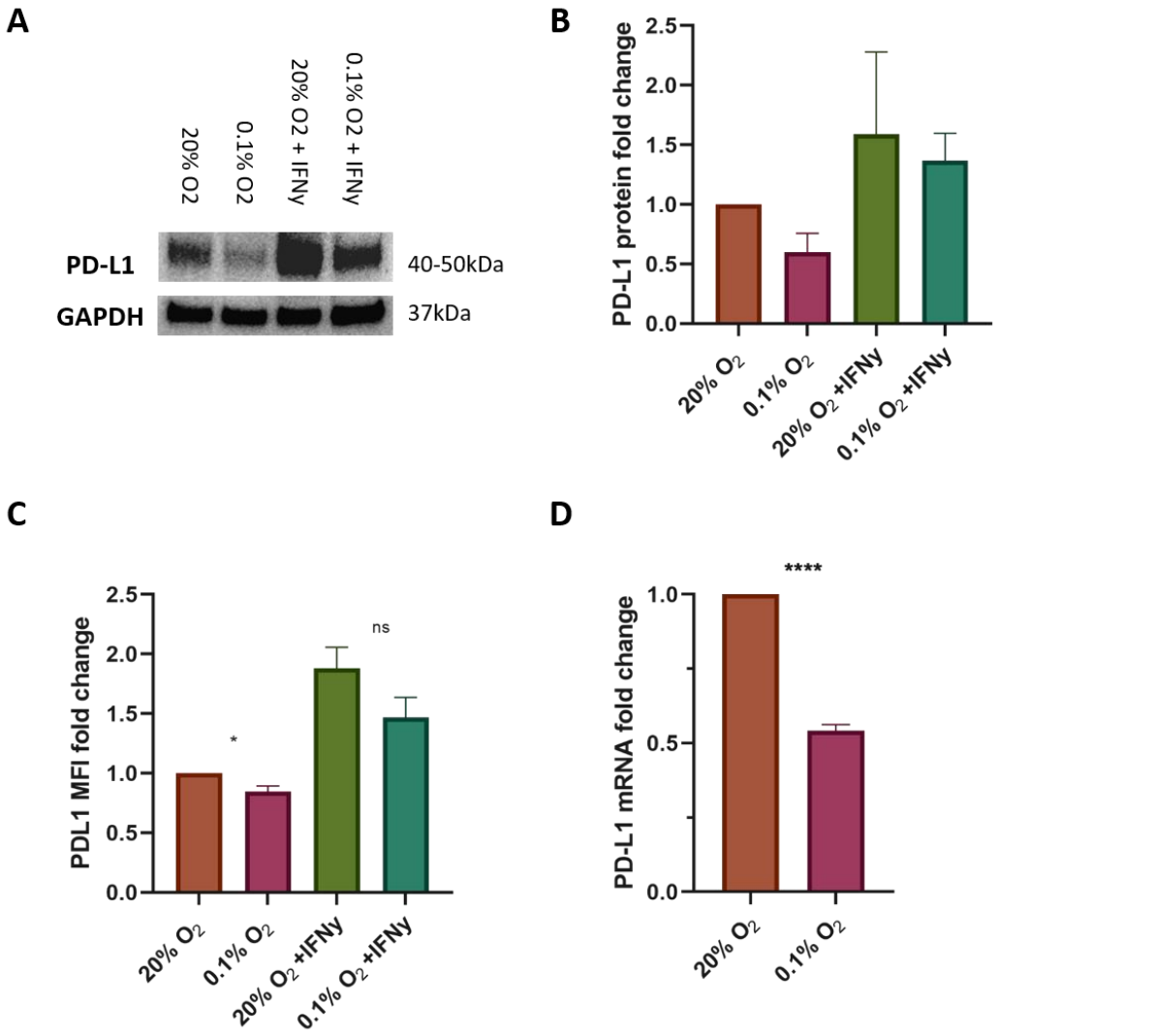

Figure 3.1. Hypoxia (0.1%) decreases the expression of PD-L1 in T24 bladder cancer cells.
PD-L1 expression decreased in T24 cells after 24 h culture in 0.1% oxygen. IFNγ stimulation increased expression of PD-L1 in 20% O_2, but the IFNγ-driven increase was attenuated in cells grown in 0.1% O_2. Cells were seeded and left to adhere for 24 h before placing into a hypoxia chamber for 24 h and/or 10 ng/ml IFNγ added to the culture media. A) Western blotting shows the change in protein levels of PD-L1 with GAPDH used as a loading control. Three independent experiments were carried out and a representative image is shown. B) Quantification by densitometry analysis was performed using ImageJ by calculating the relative densities of both the loading control and the samples to the control untreated lane. These values were then scaled to the relative density values to find adjusted relative values from three independent experiments. C) Flow cytometry shows the change in surface expression of PD-L1. Data are the mean ± standard error of the mean (SEM) of the mean fluorescence intensity of 10,000 viable cells from replicates of four independent experiments normalised to normoxia untreated condition to show the relative fold change. D) qPCR shows changes in mRNA levels relative to the mRNA levels of T24 cells cultured in 20% O_2. Data are the mean ± standard error of the mean (SEM) from three independent experiments plated in triplicate with differences calculated using the delta-delta Ct method relative to the expression of reference gene SDHA. Statistical tests are unpaired t tests performed in GraphPad Prism with p values represented as follows: ns = not significant, * < 0.05, ** < 0.01, *** < 0.001, **** < 0.0001.

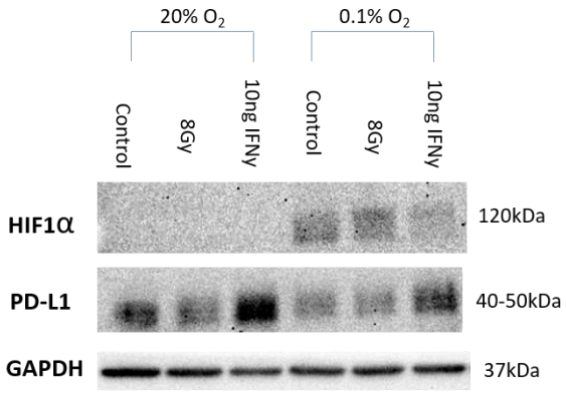

Figure 3.2. HIF-1α is present in T24 cells cultured in hypoxia and absent when cultured in normoxia.
Western blot showing the presence/absence of HIF-1α across different experimental conditions alongside the changes in PD-L1 expression. GAPDH was used as an experimental loading control. Independent experiments were performed three times and a representative blot shown.

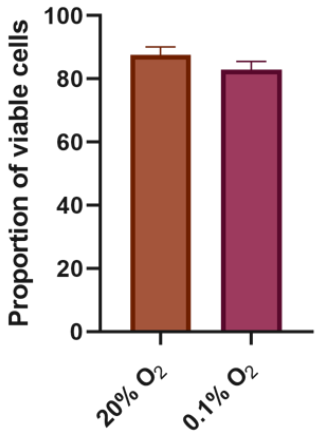

Figure 3.3. Hypoxia does not induce excessive cell death in T24 cells.
Flow cytometry shows there is no excessive cell death induced by culture in 0.1% O_2. A live/dead stain was incorporated into the assay, which only enters cells with compromised membranes. Gating around cells with no dye uptake and comparing with total population allows for the analysis of the proportion of viable cells. Data are the mean ± standard error of the mean (SEM) from at least three independent experiments performed in duplicate, of which each sample had 10,000 viable cells analysed.

3.4.2 Both 0.1% and 1% hypoxia decreases PD-L1 expression in human MIBC cells

To investigate whether the decrease in PD-L1 might be cell line or oxygen concentration dependent, two other human MIBC cell lines were investigated (J82 and UMUC3) and a less severe level of hypoxia (1% oxygen). There was a consistent significant decrease in PD-L1 protein expression after exposure to hypoxia in all three bladder cancer cell lines and at both 0.1% and 1% oxygen concentrations (Figure 3.4; Table 3.1). Across the three cell lines there was also a continued attenuation of the IFNγ-driven PD-L1 induction in hypoxia (Figure 3.4; Table 3.1).

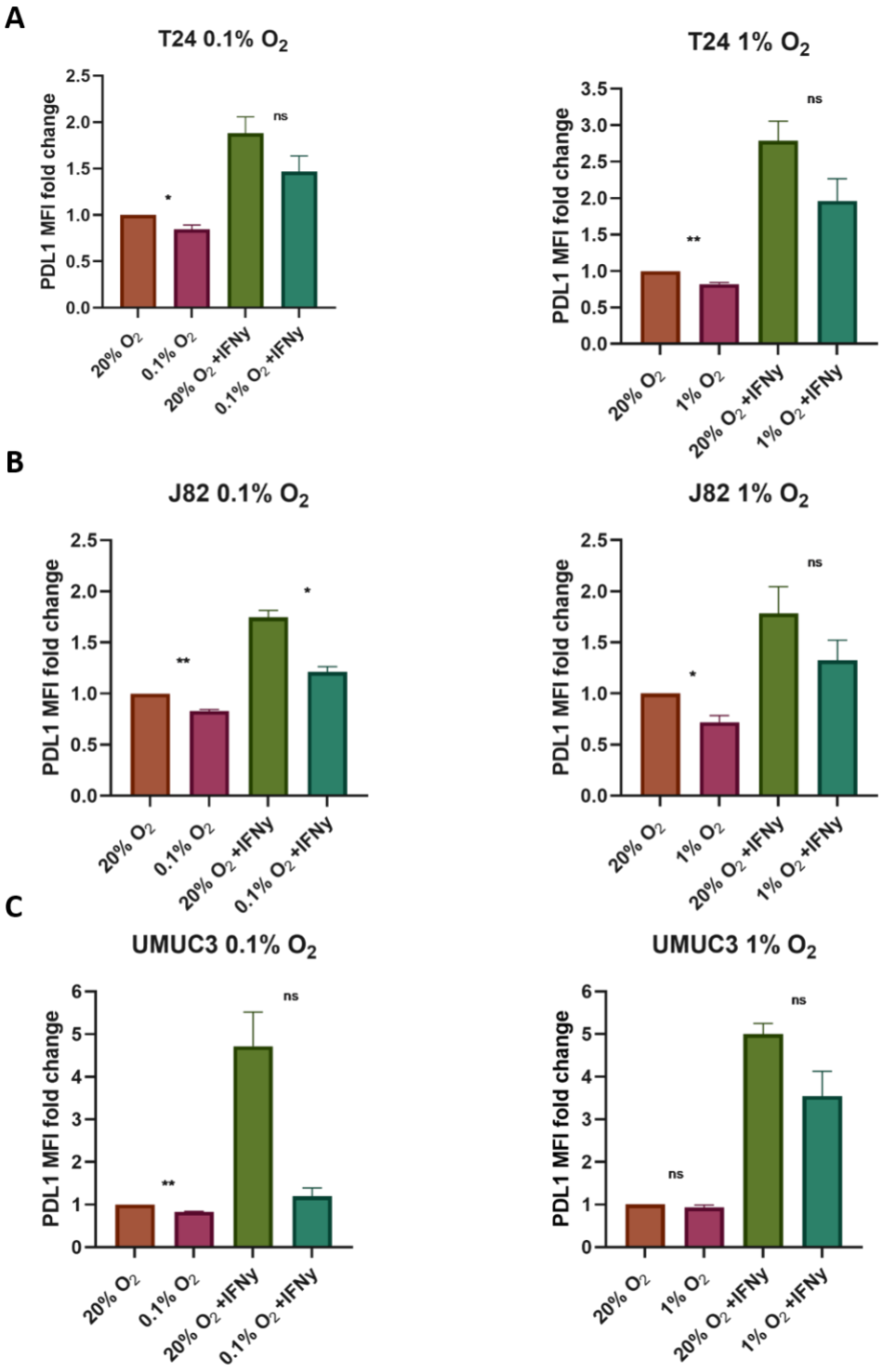

Figure 3.4. Hypoxia (0.1% and 1%) decreases PD-L1 expression in a panel of human bladder cancer cells.
Flow cytometry analyses show the surface expression of PD-L1 decreases after culture in hypoxia. Culture in 0.1% and 1% O_2 for 24 h decreases the expression of PD-L1 compared with the levels present when cultured under 20% O_2 in T24 (**A**), J82 (**B**), UMUC3 (**C**) bladder cancer cells. Cells were seeded and left to adhere for 24 h before placing in 0.1% or 1% O_2 for 24 h and 10 ng/mL IFNγ added to the relevant wells. Data are the mean ± standard error of the mean (SEM) of the mean fluorescence intensity of 10,000 viable cells from replicates of at least two independent experiments normalised to the normoxia untreated condition to show the relative fold change. Statistical tests are unpaired t tests performed in GraphPad Prism with p values represented as follows: ns = not significant, * < 0.05, ** < 0.01, *** < 0.001, **** < 0.0001.

Table 3.1. Tabulated data from the graphs shown in Figure 3.4.

	0.1% O_2				**1% O_2**		
	T24	J82	UMUC3		T24	J82	UMUC3
20% O_2	1.00	1.00	1.00	20% O_2	1.00	1.00	1.00
0.1% O_2	0.85	0.83	0.83	1% O_2	0.82	0.72	0.93
20% O_2 + IFNγ	1.88	1.74	4.72	20% O_2 + IFNγ	2.79	1.78	5.00
0.1% O_2 + IFNγ	1.47	1.21	1.20	1% O_2 + IFNγ	1.96	1.33	3.55

Data are the mean fluorescence intensity of 10,000 viable cells from replicates of at least two independent experiments normalised to the normoxia untreated condition to show the relative fold change.

3.4.3 PD-L1 levels decrease as cell density increases and a PD-L1 increase in hypoxia occurs only when cells are highly confluent

The effects of cell density on hypoxia-induced changes in PD-L1 expression were explored in T24 cells. This cell line was used due to its fast proliferation rate, with a doubling time of around 20 h (Bubeník *et al.*, 1973; Masters *et al.*, 1986), which facilitated the assessment of increasing cell density. As similar effects were seen in both 0.1% and 1% hypoxia, the less severe 1% hypoxia was taken forward for further experiments to minimise stress on the cells. Density gradient experiments showed PD-L1 protein and mRNA expression decreased significantly with increasing cell density in both normoxia and hypoxia (Figure 3.5, Figure 3.6). A significant hypoxia-induced increase in PD-L1 expression was only seen in cells seeded at the highest densities (Figure 3.5). Increasing cell density had no effect on viability (Figure 3.7).

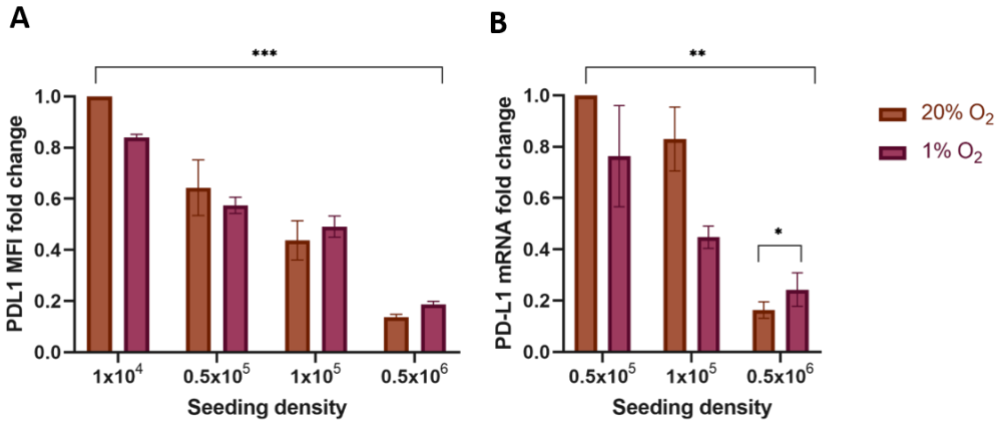

Figure 3.5. PD-L1 expression decreases with increasing cell density and hypoxia-induced PD-L1 increase occurs only in high-density cells.
As T24 cell seeding density increases, the protein and mRNA expression of PD-L1 decrease in both normoxia and hypoxia conditions ($p<0.001$ and $p=0.0011$ respectively). When the cells are cultured at higher densities (100% confluence) PD-L1 protein and mRNA expression increases after culture in hypoxia compared with normoxia ($p=0.05576$ and $p=0.03721$ respectively). Cells were counted and seeded at different densities, left to adhere for 24h and then incubated for 24h. A) Flow cytometry shows the change in surface expression of PD-L1. Data are the mean ± standard error of the mean (SEM) of the mean fluorescence intensity of 10,000 viable cells from replicates of three independent experiments normalised to normoxia untreated condition to show the relative fold change. B) qPCR shows changes in mRNA levels relative to the mRNA levels of T24 cells cultured in a 20% O_2 incubator. Data are the mean ± standard error of the mean (SEM) from three independent experiments plated in triplicate and the difference calculated using the delta-delta Ct method relative to the

expression of reference gene SDHA. Statistical tests are linear models and ANOVA performed using R and RStudio with p values represented as follows: ns = not significant, * < 0.05, ** < 0.01, *** < 0.001, **** < 0.0001.

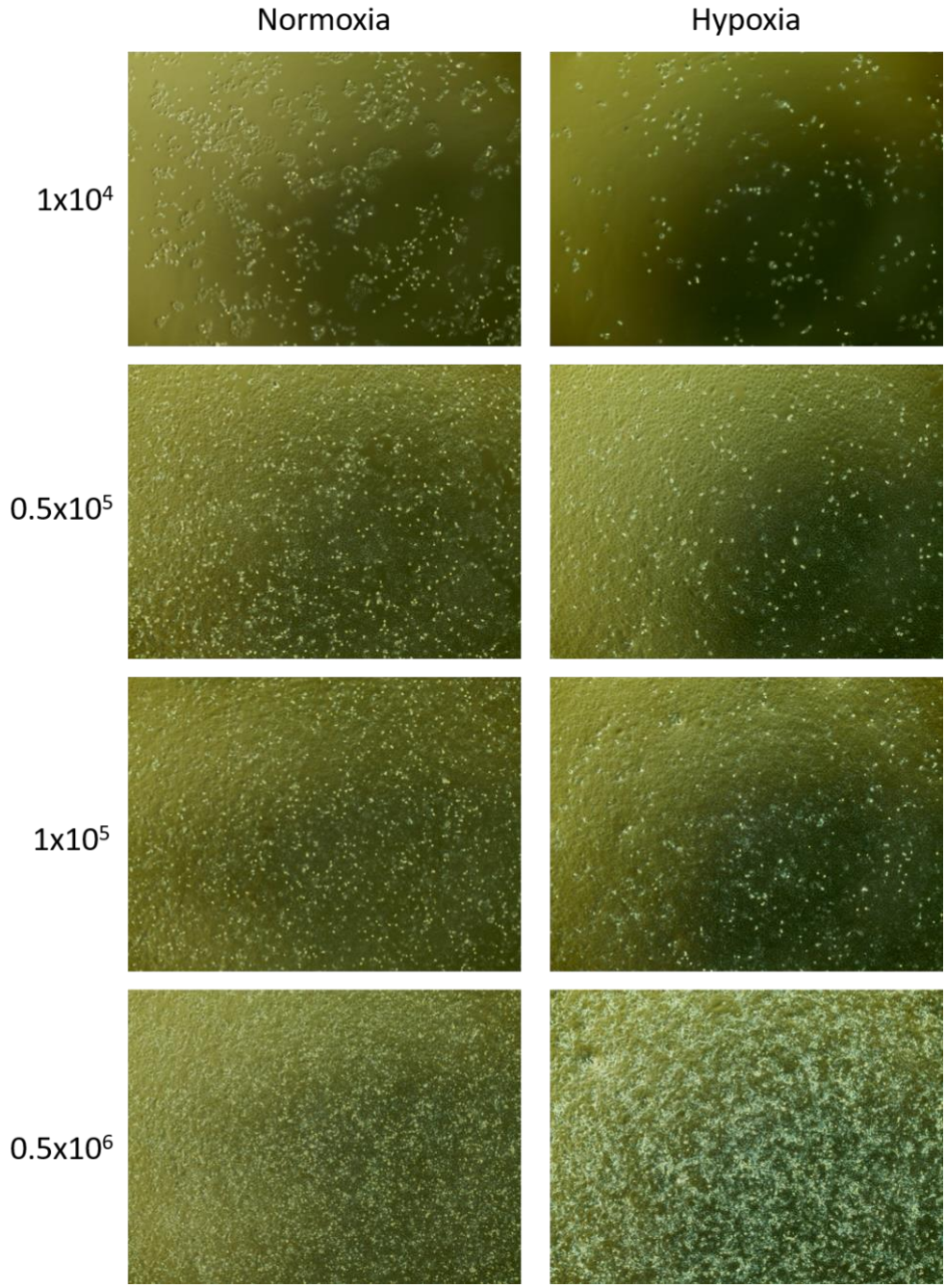

Figure 3.6 Phase contrast microscopy pictures of the different seeding densities after 24 h incubation in each condition.

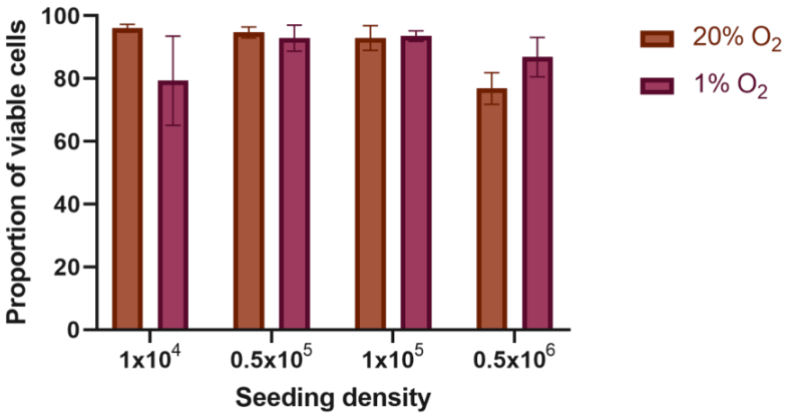

Figure 3.7. Increased cell seeding density does not induce excessive cell death in T24 cells.
Flow cytometry shows no increase in cell death neither by culture in 0.1% O_2 nor as the cell seeding density increases. A live/dead stain was incorporated into the assay, which only enters cells with compromised membranes. Gating around cells with no dye present and comparing with total population allows for the analysis of the proportion of viable cells. Data are the mean ± standard error of the mean (SEM) from at least three independent experiments performed in duplicates, with 10,000 viable cells analysed per sample.

3.4.4 PD-L1 gene expression correlates positively with hypoxia in MIBC patients

To elucidate further the potential relationship and clinical relevance between hypoxia and PD-L1, *in silico* analyses were performed using gene expression datasets from two bladder cancer cohorts. A bladder cancer specific hypoxia signature previously published was used to assign hypoxia scores, which were then correlated with the RNA expression of PD-L1 (*CD274*) (Yang, Taylor, *et al.*, 2017). A significant positive correlation was seen between hypoxia signature scores and the expression of PD-L1 in both cohorts (Figure 3.8 A, B). The median hypoxic score across each cohort stratified patients into low and high hypoxia groups. In both cohorts, the high hypoxia tumours had a significantly higher expression of PD-L1 compared with low hypoxia tumours (Figure 3.8 C, D).

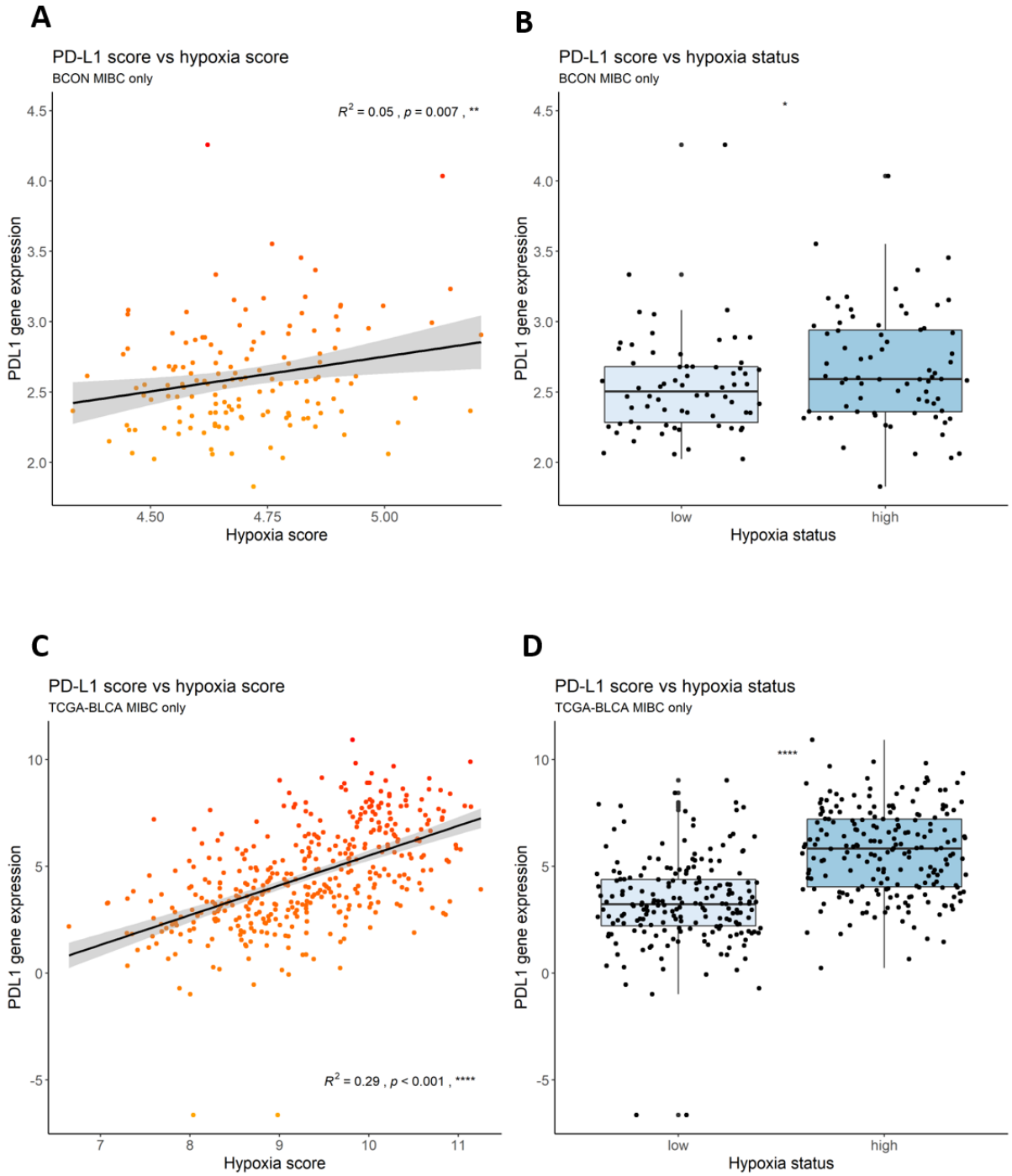

Figure 3.8. In silico analyses show a positive association between hypoxia and PD-L1 in muscle-invasive bladder tumours. Analyses involved microarray data from the BCON trial normalised previously using aroma package and filtered to include only tumours stage 2 and above (n=142) and the TCGA-BLCA RNASeq2GeneNorm dataset downloaded using the Bioconductor package TCGAutils and filtered to include only tumours of a known stage 2 and above (n = 404). Hypoxia scores were applied to each tumour sample using a previously published 24-gene bladder cancer hypoxia signature. Hypoxia signature scores were plotted against the expression of PD-L1 in A) BCON and C) TCGA cohorts. R^2 values were calculated using Pearson's correlation coefficient and the p values represent a linear model analysis. Tumours were stratified into hypoxia low or high using the median of the hypoxia scores for each cohort, and plotted against the PD-L1 expression in the B) BCON and D) TCGA cohorts. P values were calculated using a t-test between the two groups. p values are represented as follows: ns = not significant, * < 0.05, ** < 0.01, *** < 0.001, **** < 0.0001.

3.4.5 Hypoxia and IFNγ-signalling signature scores correlate positively in muscle-invasive bladder cancer patients

A published IFNγ gene signature representing the extent of IFNγ signalling was used to attribute IFNγ scores to the BCON and TCGA cohorts (Ayers *et al.*, 2017). There were positive correlations between hypoxia and IFNγ signature scores (Figure 3.9 A, B). The tumours were again stratified into low and high hypoxia and in both cohorts the high hypoxia tumours showed significantly higher IFNγ scores compared with the low hypoxia tumours (Figure 3.9 C, D).

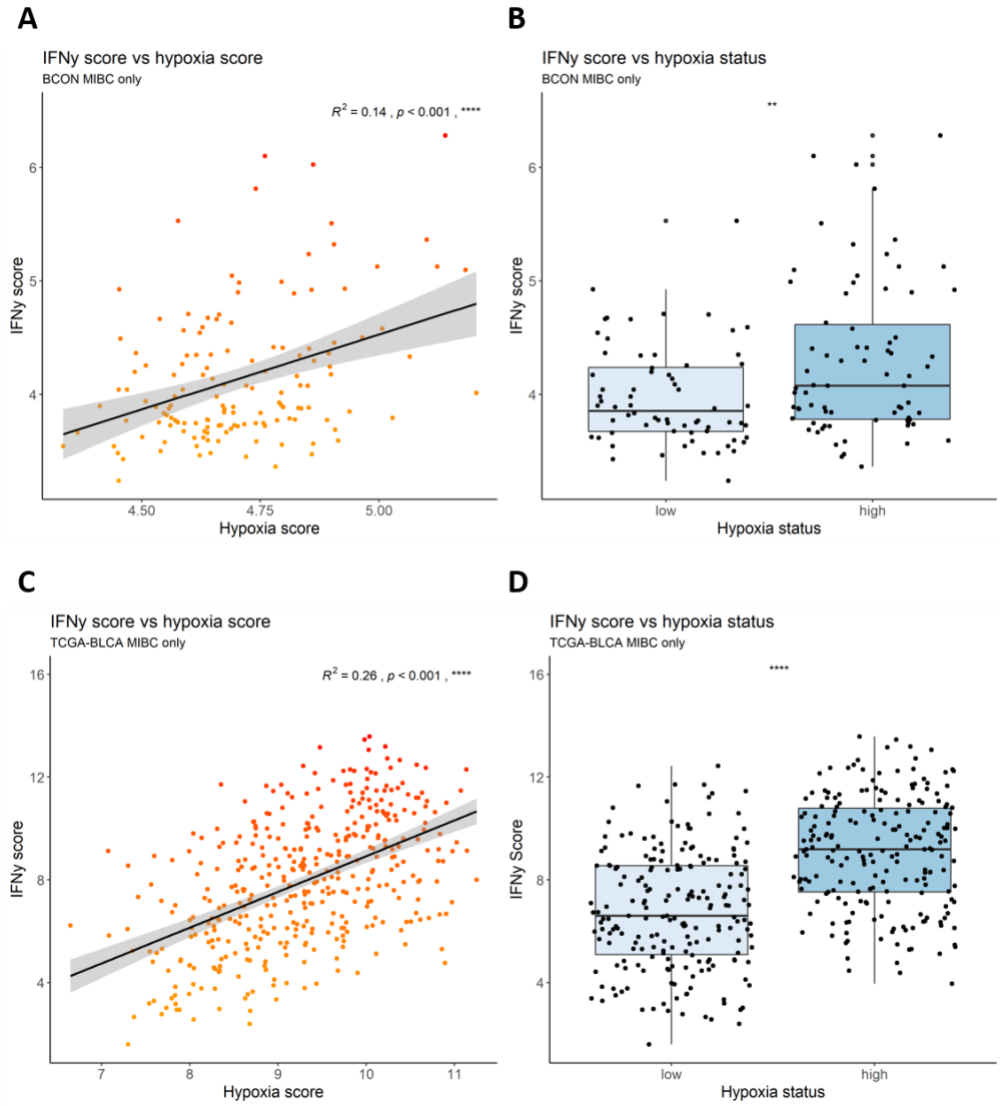

Figure 3.9. In silico analyses show a positive association between hypoxia and IFNγ-signalling in muscle-invasive bladder tumours.

Hypoxia scores were applied to tumours from BCON and TCGA cohorts filtered to include stage 2 and above only. A published 6-gene IFNγ gene signature was used to attribute an IFNγ score to each tumour. These scores were plotted against the hypoxia scores in the **A)** BCON and **C)** TCGA cohorts. R^2 values were calculated using Pearson's correlation coefficient and the p values represent a linear model analysis. Tumours were stratified into hypoxia low or high using the median of the hypoxia score from each cohort, and plotted against the IFNγ signature score in the **B)** BCON and **D)** TCGA cohorts. P values were calculated using a t-test between the two groups. p values are represented as follows: ns = not significant, * < 0.05, ** < 0.01, *** < 0.001, **** < 0.0001.

3.5 Discussion

Several new findings emerged from this study. First, hypoxia decreased PD-L1 expression and abrogated IFNγ-induced increases in PD-L1 in bladder cancer cells. Second, PD-L1 expression decreased with increasing cell seeding density, which was pronounced in cells cultured in normoxia versus hypoxia. Third, a hypoxia-induced increase in PD-L1 was only seen with the highest cell seeding densities when there was a marked down-regulation of PD-L1 in cells grown in normoxia. Fourth, PD-L1 gene expression, as well as IFNγ-signalling expression, correlated positively with hypoxia in bladder cancers *in silico*.

The observation that hypoxia decreases PD-L1 expression initially appears to conflict with conclusions made in published literature. Noman *et al.* (Noman *et al.*, 2014) concluded that hypoxia induced an upregulation of PD-L1 in a panel of murine and human cell lines. However, the finding appears to be tissue-type specific as only one (B16-F10) of four murine cell lines (B16-F10 melanoma; LLC lung; CT26 colon; 4T1 mammary) studied showed an increase in the percentage of PD-L1 positive cells after culture in 0.1% oxygen. There was a minimal increase at 72 h in the lung, no change in the colon, and a non-significant decrease in the mammary cell line. In the human cell lines, there was a marked hypoxia-induced increase in PD-L1 in melanoma (T1, M4T), a small significant increase in lung (IGR-Heu), and no change in breast (MCF-7). In addition, all the hypoxia results (24 h, 48 h, 72 h) were compared with 72 h normoxia data. Interestingly, across the cell lines, there were no significant changes observed at 24 h, except for the murine melanoma cell line, and most of the significant changes were seen at the 72 h time-point. As cell density will increase at the later time-point, the results might be affected by the cell density effect we found here.

Barsoum *et al.* (Barsoum *et al.*, 2014) also reported hypoxia-induced upregulation of PD-L1 expression. They incubated cells in 0.5% oxygen for 24 h and showed an increase in PD-L1 expression in human prostate (DU145) and breast (MDA-MB-231) cancer cells. The authors stated that all their experiments were conducted using cultures that did not exceed 70% confluence. The study also used siRNA knockdown experiments to show that PD-L1 upregulation was HIF1α dependent. HIFs bind to gene promoter regions known as hypoxia response elements (HREs). In 2011, Schödel *et al.* used chromatin immunoprecipitation sequencing (ChIPseq) to perform high resolution mapping of HIF binding sites in MCF-7 cells; PD-L1 was not in their 300+ list of high stringency HIF1 and HIF2 binding sites (Schödel *et al.*, 2011). Given that Noman *et al.* also saw no effect of hypoxia on the expression of PD-L1 in

MCF-7 cells, but Barsoum *et al.* identified HREs in the PD-L1 gene in DU145 cell lines as well as an hypoxia-induced increase in PD-L1 expression, it is possible that the hypoxia-induced upregulation of PD-L1 is tissue specific (Barsoum *et al.*, 2014; Noman *et al.*, 2014). To our knowledge this is the first documentation of the effects of hypoxia on PD-L1 expression in bladder cancer cell lines. The current literature outlines a discrepancy between the effects of hypoxia on the expression of PD-L1 across cell lines of different tissue origins and further comprehensive characterisation across an extensive panel of other cancer cell lines is required for more definitive conclusions.

Hypoxic cells preserve energy by reducing metabolic processes via HIF regulation of various genes (Vaupel and Harrison, 2004). Decreases in cellular metabolism also occur as a result of increasing cell density, and a recently published report underlines the importance of considering cell density in *in vitro* experiments and how cell density affects cellular metabolic changes (Wright Muelas *et al.*, 2018; Trajkovic *et al.*, 2019). Therefore, the PD-L1 decrease we found in cells cultured in hypoxia could be due to reduced cellular metabolism. Furthermore, cells proliferate faster in normoxia than in hypoxia due to having higher cellular metabolism. Therefore, in the highly dense cells, a cell density-mediated reduction in metabolism should occur faster and be more pronounced in normoxia. The observed effect, therefore, might be an abrogated decreased PD-L1 expression occurring in the densely packed hypoxic conditions, rather than a true cellular hypoxia-driven increase and warrants further investigation. In support of this suggestion, several publications showed that increasing cell density results in decreased expression of cell surface markers including transforming growth factor beta (TGF-β) receptor in fibroblast cells, epidermal growth factor receptors (EGFRs) in breast cancer cells, and tumour necrosis factor (TNF) receptors in HeLa epithelial and myeloid HL-60 cell lines (Kuszynski, Miller and Rizzino, 1993; Pocsik *et al.*, 1994; Petridou *et al.*, 2000).

Increasing cell density leads to contact inhibition and cell cycle arrest via the Hippo/YAP pathway (Gérard and Goldbeter, 2014), and interacts with multiple intracellular signalling pathways (Lallemand *et al.*, 1998; Yuan *et al.*, 2011; Pavel *et al.*, 2018) that regulate cyclin D expression (Duronio and Xiong, 2013). PD-L1 expression is also affected directly by the cell cycle via cyclin D regulation (Zhang *et al.*, 2018) and via interactions with multiple cell signalling pathways, e.g., via PI3K/AKT, JAK/STAT3, WNT, NFkB and MAPK (Shen *et al.*, 2019; Han, Liu and Li, 2020). This complex interplay between cell density, cell cycle, cell signalling

and PD-L1 expression is yet to be fully elucidated and more research is needed to understand how hypoxia affects the interactions. Although we showed cell density affects the expression of PD-L1, we have not identified whether it is a direct effect, or due to cell density-mediated changes in cell cycle or cell signalling. The discrepancy in some of the *in vitro* results could potentially be explained by further investigations into the cell cycle and cell signalling pathways to determine how these affect the changes in PD-L1 expression in response to hypoxia.

To further explore the relationship between hypoxia and PD-L1 beyond the *in vitro* cell culture experiments I performed *in silico* analyses in patient tumours. The BCON trial randomised patients to receive either radiotherapy or radiotherapy plus hypoxia-modifying carbogen and nicotinamide (CON). TCGA-BLCA is a cohort of bladder cancer patients who underwent surgery and the gene expression dataset from these tumours is publicly available. The positive correlations seen between hypoxia signature scores and PD-L1 expression in both cohorts indicates that, despite the cell line findings, there is a relationship between the extent of hypoxia and increased PD-L1 expression in bladder cancer. This has implications for the treatment of MIBC whereby some patients may potentially benefit from a combination of hypoxia-modifying therapy with immunotherapy agents. In the same cohorts, we saw a positive correlation between hypoxia and IFNγ-signalling signature scores. IFNγ is known to stimulate PD-L1 and increased PD-L1 expression in the more hypoxic tumours could be a direct result of increased IFNγ signalling (Garcia-Diaz *et al.*, 2017). Current *in silico* investigations have shown more immune infiltrates present as tumour hypoxia increases. As IFNγ is a central immune signalling molecule that is produced by many immune infiltrates, this provides an explanation for the increased IFNγ-signalling in the more hypoxic tumours. This suggestion needs investigating further. Taken together, our *in vitro* and *in silico* findings show that, although hypoxia-mediated cellular PD-L1 upregulation is not seen in bladder cancer cell lines, there is an overall increased expression of PD-L1 as tumour hypoxia increases in bladder cancer, which could be a result of increased IFNγ-signalling in the more hypoxic TMEs leading to an increased PD-L1 expression. These results highlight the importance of including patient sample analysis alongside cell line work when investigating immune-related contexts to provide translatable findings that account for the immune tumour microenvironment.

In conclusion, I report for the first time that in bladder cancer cells the *in vitro* cell density affects PD-L1 expression in contrast to an absence of hypoxia-induced increase in PD-L1 expression. These findings underlie the importance of cell density on the expression of PD-L1 *in vitro* and the need to address this in further publications. The clinical data provide evidence that hypoxia may induce an immunosuppressive TME in bladder cancer and highlight the importance of further studies to investigate the underlying mechanisms.

4 Low CD8 T cell counts predict benefit from hypoxia-modifying therapy in muscle-invasive bladder cancer

The results presented in this chapter are based on a manuscript that is currently under consideration in the International Journal of Radiation Oncology, Biology and Physics, which has been re-formatted and edited for this thesis.

4.1 Abstract

Background: In the tumour microenvironment, hypoxia has been shown to inhibit CD8+ T cells and affect other immune cell populations, such as macrophages and Tregs, and the immune checkpoint molecule PD-L1. For this study, protein level analysis was used to see if patients with low tumour CD8+ T-cells benefitted from hypoxia-modifying therapy.

Methods: The BCON trial randomised patients with muscle-invasive bladder cancer (MIBC) to radiotherapy alone or with hypoxia-modifying carbogen plus nicotinamide (CON). Tissue microarrays of diagnostic biopsies from 116 patients were stained using multiplex immunohistochemistry (IHC) with immune-related markers (CD8, CD4, FOXP3, CD68, PD-L1). Hypoxia was assessed using CA9 IHC (n=111). Linked transcriptomic data (n=80) identified molecular subtype. Relationships with overall survival (OS) were investigated using Cox proportional hazard models.

Results: Low vs high CD8 T-cell counts associated with a worse OS across the whole cohort (n=116; HR 0.47, 95% CI 0.28-0.78, p=0.003) and also in the radiotherapy alone group (n=61; HR 0.39, 95% CI 0.19-0.76, p=0.005). Patients with low CD8+ T-cells benefited from CON (n=87; HR 0.63, 95% CI 0.4-1.0, p=0.05), but those with high CD8 T cells did not (n=27; p=0.95). CA9 positive tumours had fewer CD8+ T-cells (p=0.03). Prognostic significance of low CD8+ T-cells in the whole cohort remained after adjusting for clinicopathologic variables (HR 0.33, 95% CI 0.18-0.59, p<0.001). Basal vs luminal subtype had more CD8+ cells (p=0.02) but was not prognostic (n=80; p=0.26). Exploratory analyses with other immune markers did not improve on findings obtained with CD8 counts.

Conclusions: In MIBC low CD8+ T-cell counts predicted benefit from CON addition to radiotherapy.

4.2 Introduction

Hypoxia and an immunosuppressive tumour microenvironment (TME) are both poor prognostic factors that contribute to radiotherapy and chemotherapy resistance in MIBC (Theodoropoulos *et al.*, 2004; Walshaw *et al.*, 2018). They are targetable by hypoxia-modifying therapy and immune checkpoint inhibitors (ICIs) respectively and are therefore of interest as potential biomarkers. Adding hypoxia-modifying carbogen and nicotinamide (CON) to radiotherapy improves survival outcomes in bladder cancer patients (Hoskin *et al.*, 2010; Song *et al.*, 2021). We showed previously this benefit is only seen in patients with the most hypoxic tumours (Yang, Taylor, *et al.*, 2017).

There is growing evidence that hypoxia contributes to a suppressive immune tumour microenvironment (TME). Specifically, hypoxia decreases CD8+ T cell activity and proliferation in the TME (B. Wang *et al.*, 2021). In mouse models, systemic oxygenation and locally delivered oxygen ameliorated this effect, restored the anti-tumour cytotoxic effects of CD8+ T cells and improved the efficacy of ICIs (Hatfield *et al.*, 2014, 2015; Colombani *et al.*, 2021; X. Liu *et al.*, 2021). Therefore, patients with low tumour CD8+ T cell counts might benefit from hypoxia-targeting CON given with radiotherapy.

There is a need to find biomarkers that predict ICI response (Cheng *et al.*, 2018; Wołącewicz *et al.*, 2020). A systematic review and meta-analysis of 33 studies involving multiple cancers, including bladder, showed high tumour infiltrating CD8+ T cells associated with benefit from ICIs whether given as single-agents or as part of combination treatments (F. Li *et al.*, 2021).

Hypoxia can also drive an immunosuppressive TME by increasing pro-tumour immune infiltrates, such as regulatory T helper cells (Tregs; CD4+FOXP3+) and macrophages (CD68+), and the immunosuppressive immune checkpoint molecule PD-L1 (Aouali *et al.*, 2017). In the previous chapter, I showed that in MIBC the more hypoxic tumours had increased expression of PD-L1. PD-L1 is also of current interest as a potential biomarker and predictor of response to ICI treatment (van Wilpe *et al.*, 2020).

Therefore, the primary objective in this chapter was to investigate whether patients with low tumour CD8+ T cell counts benefited from having CON with radiotherapy. The study involved tumour samples collected from patients enrolled in the BCON trial that randomised MIBC patients to radiotherapy alone (RT) or with CON (RT+CON). Secondary objectives were to (1) carry out additional exploratory analyses to investigate other suppressive

immune markers (CD4, FOXP3, CD68, PD-L1) in the context of hypoxia and prognosis; and (2) compare findings with molecular subtypes as an emerging biomarker for bladder cancer.

4.3 Materials and methods

4.3.1 BCON Cohort

BCON was a prospective multicentre phase III clinical trial that randomised patients to radiotherapy alone or radiotherapy with carbogen and nicotinamide (CON). Tissue microarrays (TMAs) were previously made from diagnostic biopsies of muscle-invasive tumour samples as described in Section 2.5.1. The updated long-term clinical outcomes were used in all analyses (Song *et al.*, 2021).

4.3.2 Multiplex Staining Protocol

As detailed in 2.5, multiplex immunohistochemistry (IHC) was performed using the Opal™ detection system for CD8, CD4, CD68, FOXP3, and PD-L1. The protocol involved multiple cycles of incubation with primary antibody, secondary antibody and Opal™ detection separated by a short denaturation. The slides were washed, counter-stained with DAPI and then cover-slipped. A multi-spectral image of each core was then acquired at 20x magnification on a Vectra microscope. After multispectral scanning, the slides were spectrally unmixed using inForm software with a pre-prepared spectral library. The library was prepared using single-plex controls to acquire the individual spectrum of each fluorophore, alongside DAPI and autofluorescence, under the same experimental parameters as the multiplexed slides.

4.3.3 Data Analysis

Image analysis was performed in HALO 3.2 with the TMA Module to manually exclude artefacts and then obtain counts of each marker per core. The marker quantification was then exported to R where normalisation was performed by calculating the percentage of each marker from the total cell count across all cores of each patient (n=116). This method was chosen to account for cores of different sizes and different numbers of cores per patient. CA9 IHC scores previously generated were used to assign patients a CA9 status of present or absent (n=111) (Eustace, Irlam, *et al.*, 2013). CA9 status was used instead of our hypoxia signature as using the hypoxia signature was not significant due to constricted patient numbers.

4.3.4 Statistical analysis

Analyses were performed using R and RStudio with associated packages, as detailed in Section 2.5.6. Non-parametric statistics (Wilcox test) were used. Kaplan-Meier curves and multivariable analysis were generated via Cox proportional hazard models using R packages "survival" and "survminer". Cumulative incidence curves were plotted and the significance calculated using "cmprsk" package.

4.4 Results

4.4.1 Study cohort

The study cohort comprised 150 patients and TMAs with 353 cores. Following staining and filtering out poor quality cores due to folds/dropouts/scanning errors, cores (n=301) from 116 patients were available for analysis (Figure 4.1). Each patient had 1-3 different 1 mm cores analysed, with an average of 2 cores per patient. A representative multiplex IHC image of a core is shown in Figure 4.2. Table 4.1 shows no differences in the clinicopathologic characteristics of the study cohort compared with the BCON trial cohort.

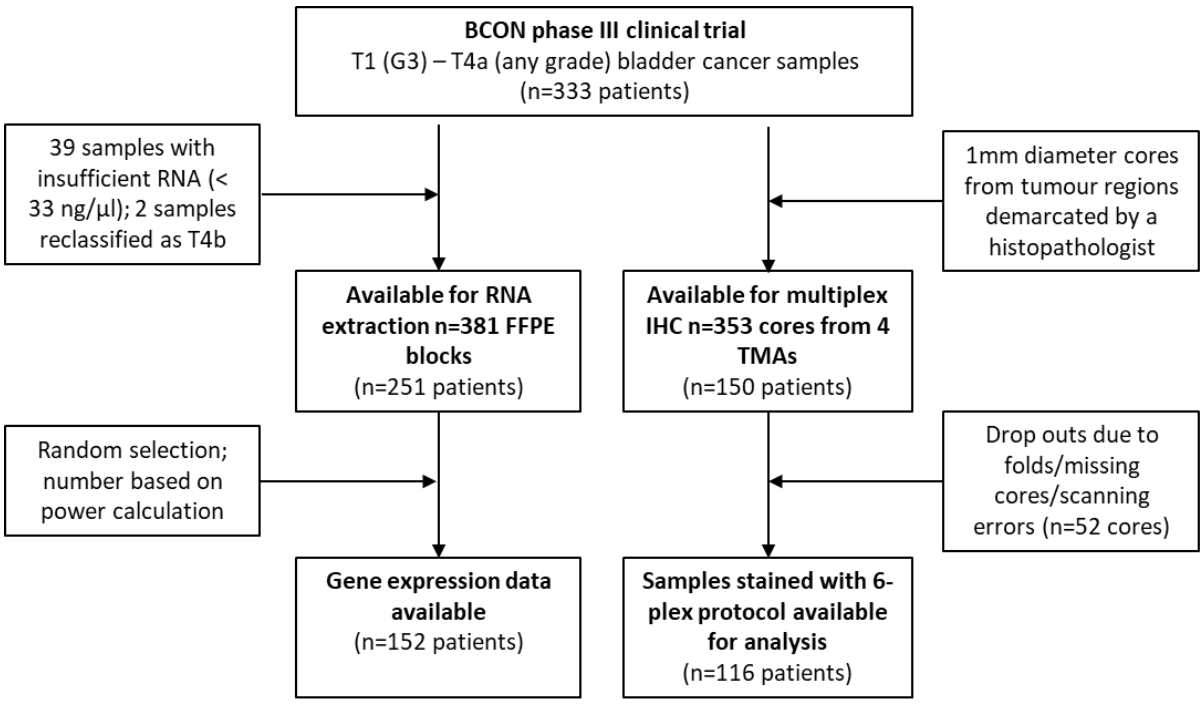

Figure 4.1. Study consort flowchart.
Abbreviations: TMA=Tissue Microarray; FFPE=Formalin Fixed Paraffin Embedded; IHC=immunohistochemistry.

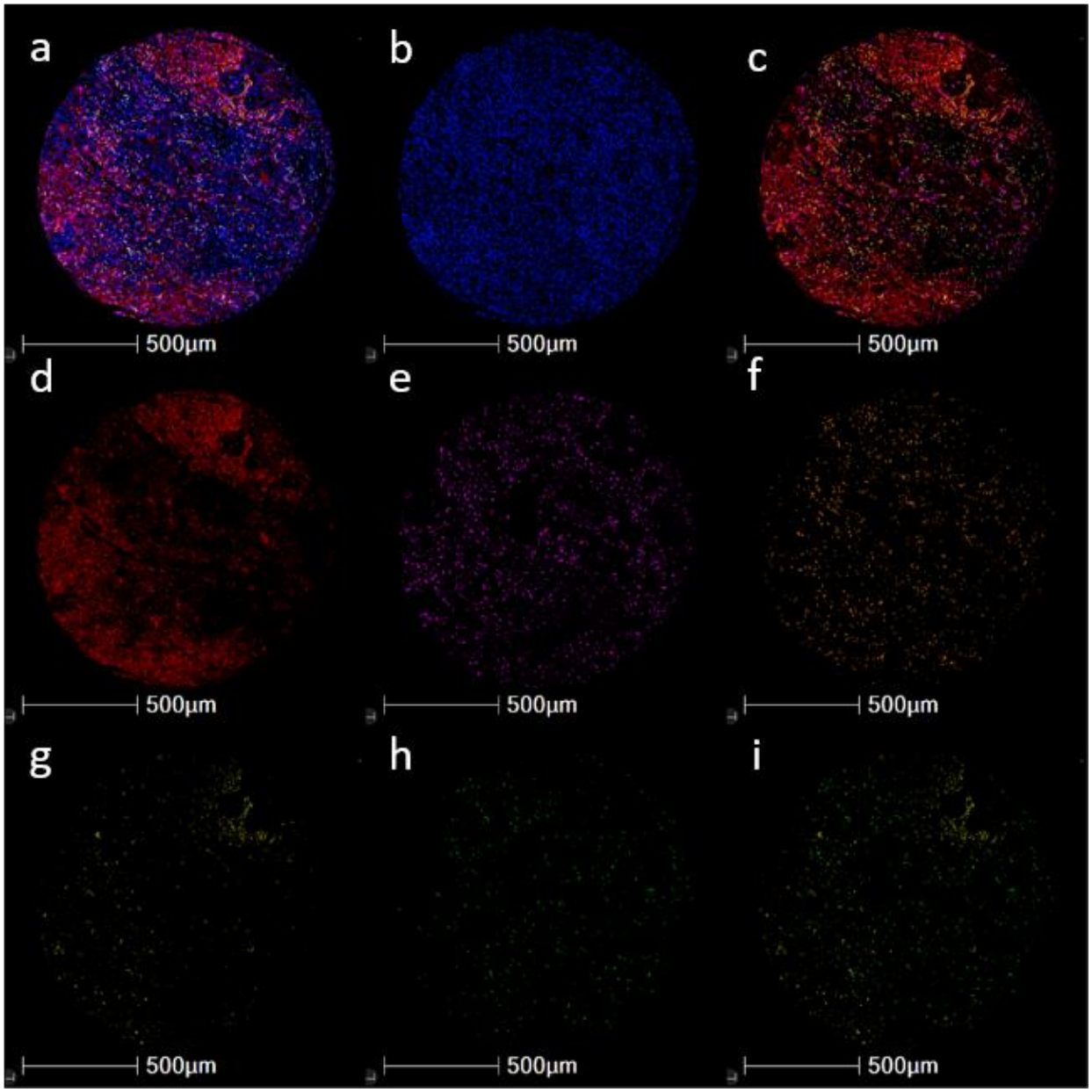

Figure 4.2 Multiplexed IHC image of a representative BCON TMA core.
a) Composite multiplex image of all stains using pseudo-colours with DAPI in blue, PDL1 in red, CD68 in pink, CD8 in orange, CD4 in yellow and FOXP3 in green. c) A composite image of the same core but without the DAPI stain displayed. The following images use the same pseudo-colours on the same core to represent the visualisation of each marker after spectral unmixing b) DAPI, d) PDL1, e) CD68, f) CD8, g) CD4, h) FOXP3, i) CD4 and FOXP3 co-localisation representing Treg cells.

Table 4.1. Table of characteristics comparing the multiplex study and overall trial cohorts

Characteristic	Multiplex (n=116)	Overall (n=296)
Age		
Mean (SD)	73.9 (7.21)	72.4 (7.64)
Median [Min, Max]	75.0 [52.0, 88.0]	74.0 [44.0, 89.0]
Missing	0 (0%)	1 (0.3%)
Gender		
Male	96 (82.8%)	234 (79.1%)
Female	20 (17.2%)	61 (20.9%)
Tumour de-bulking		
Complete	46 (39.7%)	120 (40.5%)
Partial	40 (34.5%)	91 (30.7%)
Biopsy	28 (24.1%)	74 (25.3%)
Missing	2 (1.7%)	10 (3.4%)
Grade		
2	17 (14.7%)	45 (15.2%)
3	98 (84.5%)	249 (84.1%)
Missing	1 (0.9%)	2 (0.7%)
Tumour stage		
2	89 (76.7%)	215 (73.0%)
3	22 (19.0%)	67 (22.6%)
4	5 (4.3%)	12 (4.1%)
Missing	0 (0%)	1 (0.3%)
Treatment		
RT	61 (52.6%)	148 (50.0%)
RT+CON	55 (47.4%)	148 (50.0%)
Ischaemic heart disease		
Absent	105 (90.5%)	264 (89.2%)
Present	11 (9.5%)	31 (10.5%)
Missing	0 (0%)	1 (0.3%)
Hypertension		
Absent	76 (65.5%)	202 (68.2%)
Present	40 (34.5%)	93 (31.4%)
Missing	0 (0%)	1 (0.3%)
Diabetes		
Absent	103 (88.8%)	272 (91.9%)
Present	13 (11.2%)	23 (7.8%)
Missing	0 (0%)	1 (0.3%)

4.4.2 Tumours with low tumour CD8+ cells associate with a poor prognosis

All markers had a non-normal distribution and non-parametric statistics were subsequently used (Figure 4.3). The percentage of CD8+ cells ranged from 0 to 44% per patient (Table 4.2). There was a non-linear relationship between the percentage of CD8+ cells and overall survival. CD8+ T cell counts stratified into quartiles showed a significant but non-linear relationship with overall survival (p=0.014) with the upper quartile as an outlier (Figure 4.4). The upper quartile was used to stratify patients into CD8+ high and low groups. Patients with CD8+ low tumours had significantly worse overall (HR 0.47, 95% CI 0.28-0.78, p=0.003) and local progression free (HR 0.52, 95% CI 0.32-0.87, p=0.011) survival (Figure 4.5).

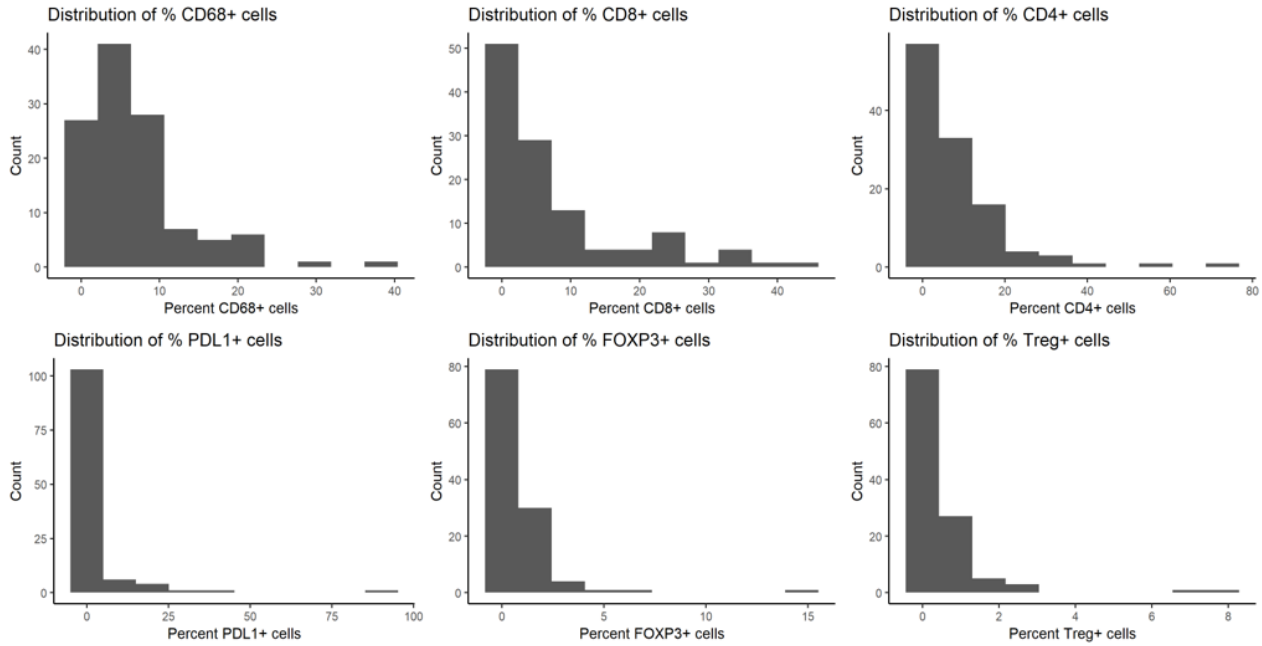

Figure 4.3 The percent of each marker was calculated per patient by dividing the number of cells positive for the marker across all cores of one patient by the total number of cells (DAPI count) across all cores for each patient. Histograms were plotted using R Studio.

Table 4.2. The differences in range (min, max), mean and median population densities for each marker (n=116).

Marker	Min	Max	Mean	Median
PDL1+	0	90.26	2.78	0.06
CD68+	0	38.29	6.74	4.68
CD8+	0	43.52	7.54	3.09
CD4+	0	72.73	8.54	4.60
FOXP3+CD4+	0	7.85	0.53	0.19

Values are percentages. Counts of each marker were obtained by calculating the percentage of each marker from the total cell count across all cores of each patient.

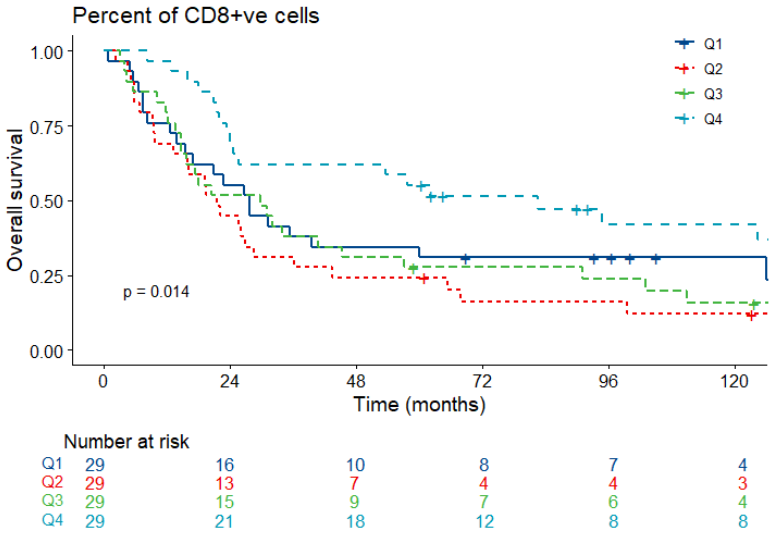

Figure 4.4. Kaplan-Meier survival curves showing the non-linearity between overall survival and percent of CD8 T cells. The percent of CD8+ T cells was stratified into quantiles and Kaplan-Meier curves plotted using the "survival" package in R (n=116).

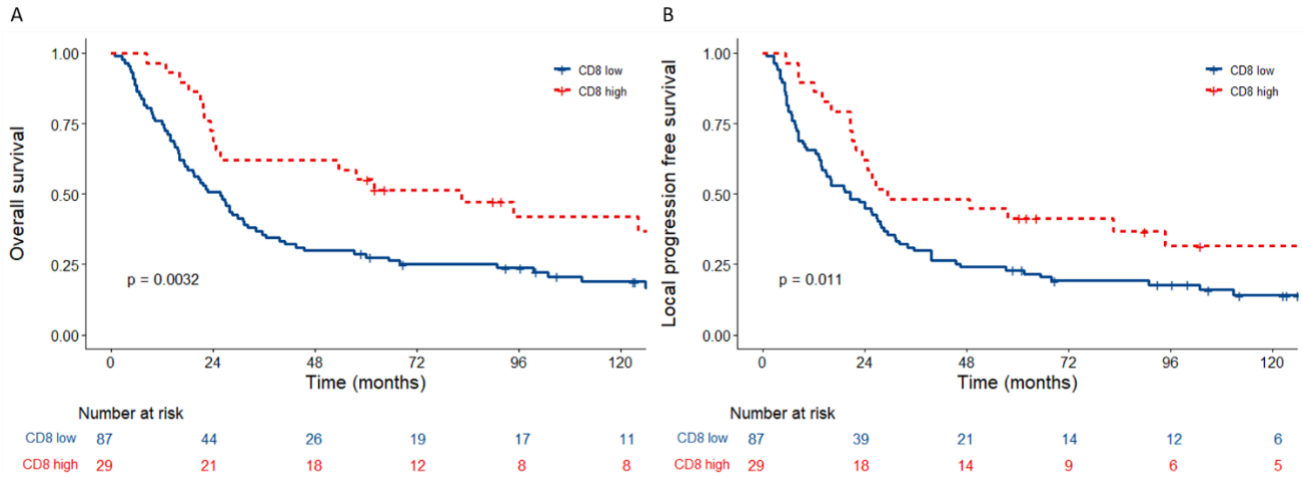

Figure 4.5. Kaplan-Meier plots of survival according to percent CD8+ T cells.
p values are from log-rank tests calculated by R packages "survival" and "survminer". CD8+ T cells are stratified into low and high using the upper quartile as the cut-off. A) Overall survival and B) local progression free survival in the whole cohort according to percent CD8+ T cells low vs percent CD8+ T cells high.

4.4.3 Low tumour CD8+ cell counts predict benefit from hypoxia modification

Low CD8+ cells were an adverse prognostic factor in patients who received radiotherapy alone for overall (n=61; HR 0.39, 95% CI 0.19-0.76, p=0.005) and local progression free (HR 0.38, 95% CI 0.19-0.75, p=0.004) survival (Figure 4.6 A, C). Low counts were not prognostic in patients who had radiotherapy plus CON for both overall (p=0.17) and local progression free (p=0.55) survival (Figure 4.6 B, D). Patients with low CD8+ T cell counts had better overall (HR 0.63, 95% CI 0.4-1.0, p=0.05) and local progression free (HR 0.63, 95% CI 0.4-1.0, p=0.052) survival when CON was given with radiotherapy (Figure 4.7 A, C). Those with high CD8+ T cell counts derived no benefit from hypoxia modification (Figure 4.7 B, D). Table 4.3 shows similar clinicopathologic characteristics between the RT versus RT+CON groups and low versus high tumour CD8 counts groups.

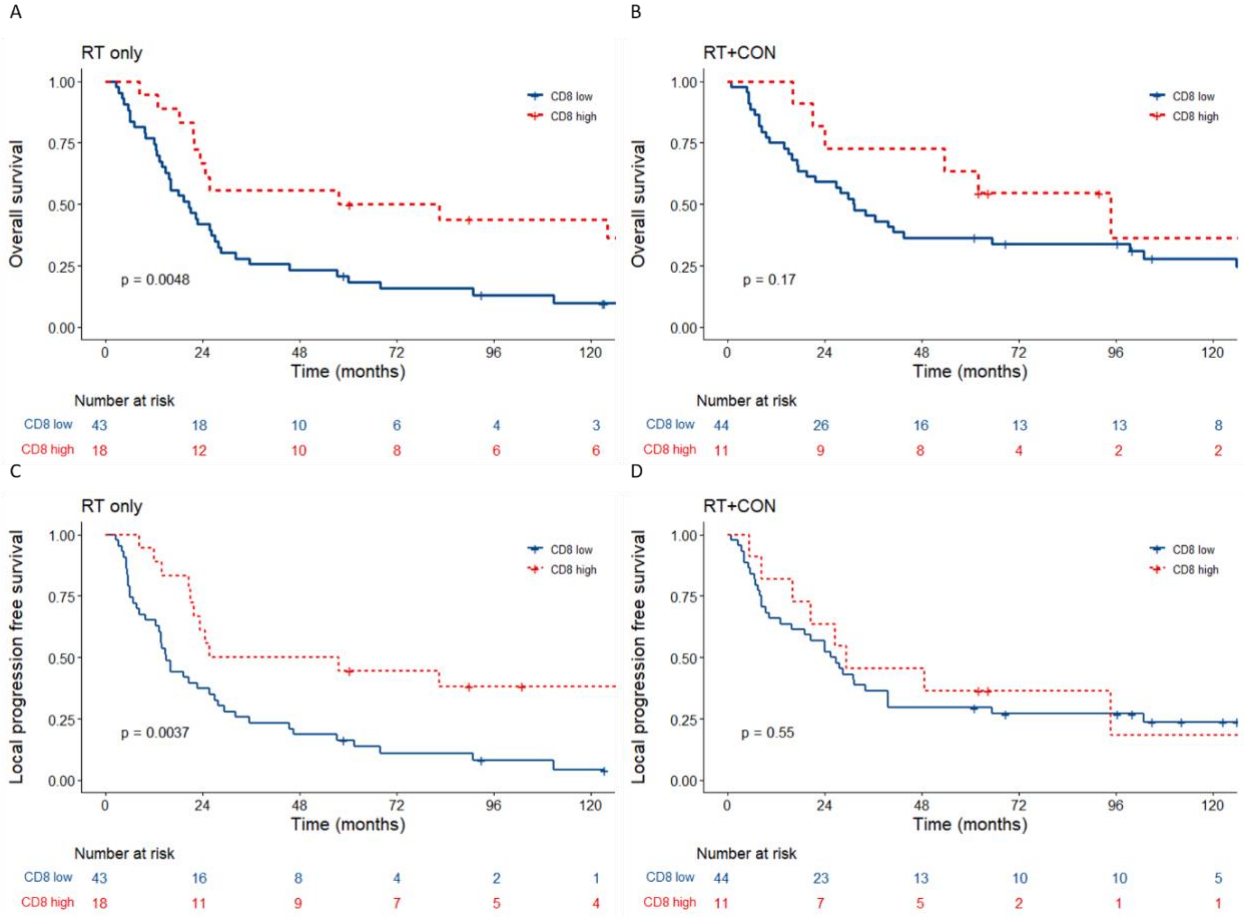

Figure 4.6. Kaplan-Meier curves for the two treatment arms of BCON with patients stratified by the upper quartile of the percentage of CD8+ T cells.
p values are from log-rank tests calculated by R packages "survival" and "survminer". Overall survival for patients receiving A) RT only or B) RT+CON; and local progression free survival for patients receiving B) RT only or D) RT+CON.

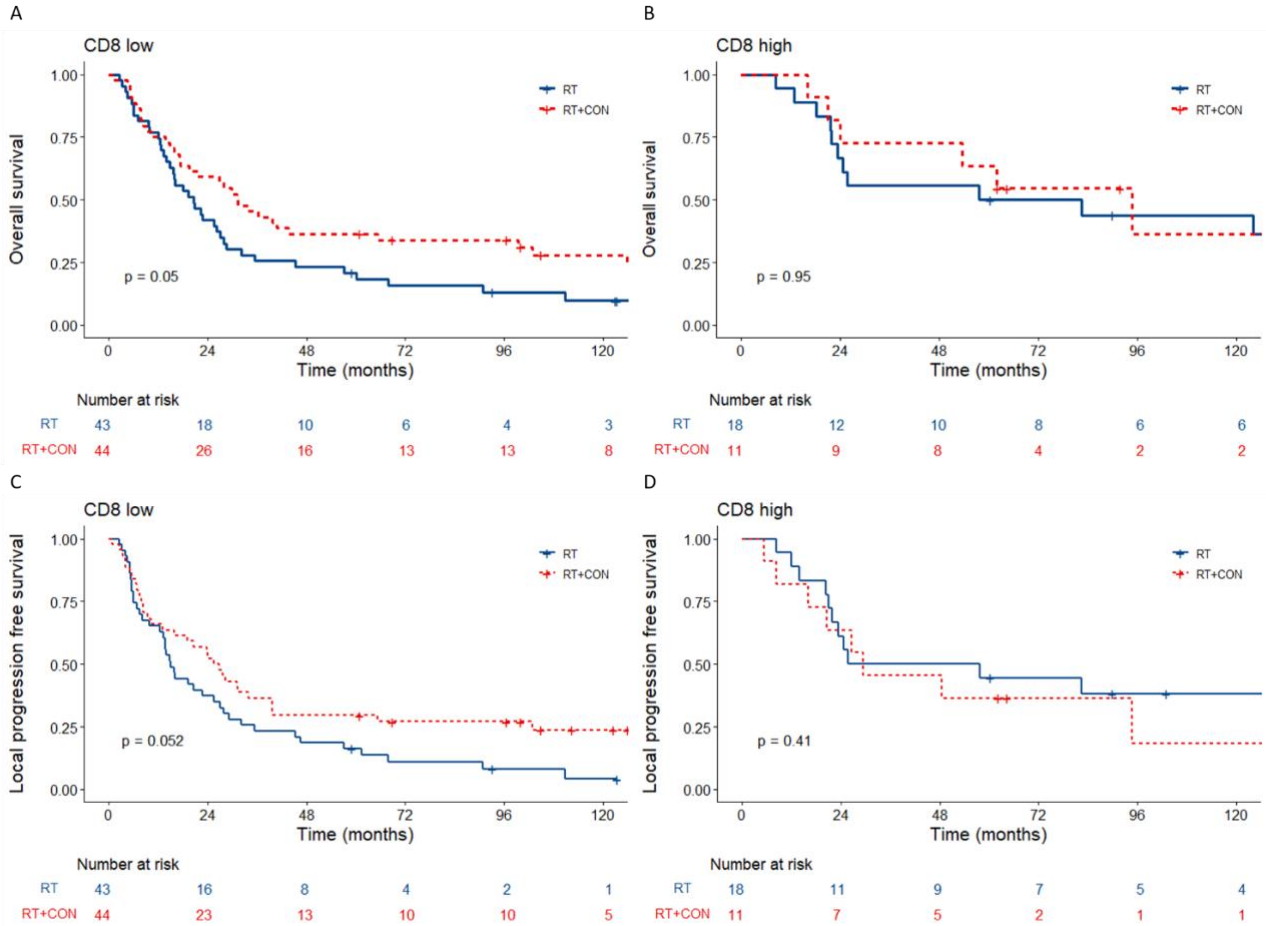

Figure 4.7. Kaplan-Meier curves for patients with low versus high CD8+ T cells with patients stratified by treatment with RT or RT+CON.

p values are from log-rank tests calculated by R packages “survival” and “survminer”. Overall survival for tumours stratified as A) CD8+ low and B) CD8+; and local progression free survival for C) CD+8 low and D) CD8+ high.

Table 4.3. Clinicopathologic characteristics of the multiplex study cohort.

Characteristic	RT (N=61)	RT+CON (N=55)	CD8 low (N=87)	CD8 high (N=29)	Overall (N=116)
Age (years)					
Mean (SD)	74.7 (7.24)	72.9 (7.13)	73.5 (7.63)	75.0 (5.74)	73.9 (7.21)
Median [Min, Max]	76.0 [53.0, 88.0]	74.0 [52.0, 85.0]	75.0 [52.0, 86.0]	75.0 [64.0, 88.0]	75.0 [52.0, 88.0]
Gender					
Male	49 (80.3%)	47 (85.5%)	73 (83.9%)	23 (79.3%)	96 (82.8%)
Female	12 (19.7%)	8 (14.5%)	14 (16.1%)	6 (20.7%)	20 (17.2%)
Tumour stage					
2	44 (72.1%)	45 (81.8%)	67 (77.0%)	22 (75.9%)	89 (76.7%)
3	14 (23.0%)	8 (14.5%)	16 (18.4%)	6 (20.7%)	22 (19.0%)
4	3 (4.9%)	2 (3.6%)	4 (4.6%)	1 (3.4%)	5 (4.3%)
Grade					
2	8 (13.1%)	9 (16.4%)	14 (16.1%)	3 (10.3%)	17 (14.7%)
3	53 (86.9%)	45 (81.8%)	72 (82.8%)	26 (89.7%)	98 (84.5%)
Missing	0 (0%)	1 (1.8%)	1 (1.1%)	0 (0%)	1 (0.9%)
Tumour debulking					
Complete	22 (36.1%)	24 (43.6%)	35 (40.2%)	11 (37.9%)	46 (39.7%)
Partial	23 (37.7%)	17 (30.9%)	30 (34.5%)	10 (34.5%)	40 (34.5%)
Biopsy	15 (24.6%)	13 (23.6%)	20 (23.0%)	8 (27.6%)	28 (24.1%)
Missing	1 (1.6%)	1 (1.8%)	2 (2.3%)	0 (0%)	2 (1.7%)
Hypertension					
Absent	40 (65.6%)	36 (65.5%)	57 (65.5%)	19 (65.5%)	76 (65.5%)
Present	21 (34.4%)	19 (34.5%)	30 (34.5%)	10 (34.5%)	40 (34.5%)
CA9					
Absent	34 (55.7%)	30 (54.5%)	47 (54.0%)	17 (58.6%)	64 (55.2%)
Present	24 (39.3%)	23 (41.8%)	37 (42.5%)	10 (34.5%)	47 (40.5%)
Missing	3 (4.9%)	2 (3.6%)	3 (3.4%)	2 (6.9%)	5 (4.3%)
Necrosis					
Absent	28 (45.9%)	26 (47.3%)	39 (44.8%)	15 (51.7%)	54 (46.6%)
Present	33 (54.1%)	26 (47.3%)	46 (52.9%)	13 (44.8%)	59 (50.9%)
Missing	0 (0%)	3 (5.5%)	2 (2.3%)	1 (3.4%)	3 (2.6%)
Percent CD8+ T cells					
Low	43 (70.5%)	44 (80.0%)	n/a	n/a	87 (75.0%)
High	18 (29.5%)	11 (20.0%)	n/a	n/a	29 (25.0%)
Treatment					
RT	n/a	n/a	43 (49.4%)	18 (62.1%)	61 (52.6%)
RT+CON	n/a	n/a	44 (50.6%)	11 (37.9%)	55 (47.4%)

n/a=not applicable

4.4.4 Low CD8+T cell counts associate with CA9 positivity but retain independent prognostic significance

Analysis of CA9 IHC staining previously performed on the samples and used as a marker of hypoxia showed positive versus negative tumours had fewer CD8+ cells (p=0.03, n=111; Figure 4.8). The patients were further stratified into four groups according to both CA9 status and CD8+ counts. Cumulative incidence curves showed that regardless of the hypoxia status, both groups with high CD8+ had significantly fewer events for both overall (p=0.011) and local progression free (p=0.029) survival compared to those groups with low CD8+ counts (Figure 4.9). A multivariable Cox proportional hazard model analyses for overall survival taking into account other clinicopathologic factors showed the percentage of CD8+ T cells maintained prognostic significance (HR 0.33 95% CI 0.18-0.59; p<0.001) alongside necrosis (p=0.006), tumour de-bulking (p=0.038), treatment arm (p=0.033) and age (p=<0.001; Table 4.4). The presence of CA9 had no independent prognostic significance in the multiplex cohort (HR 0.65, 95% CI 0.39-1.08, p=0.1).

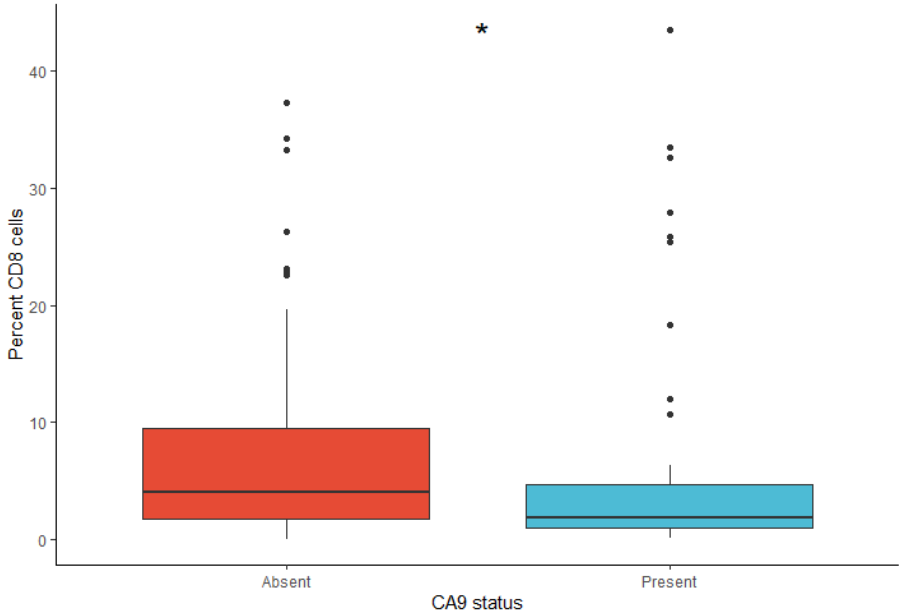

Figure 4.8. Boxplot showing the population density for CD8+ T cells when grouped into CA9 absent or present. p values are represented as: ns = not significant, *<0.05, **<0.01, ***<0.001

A

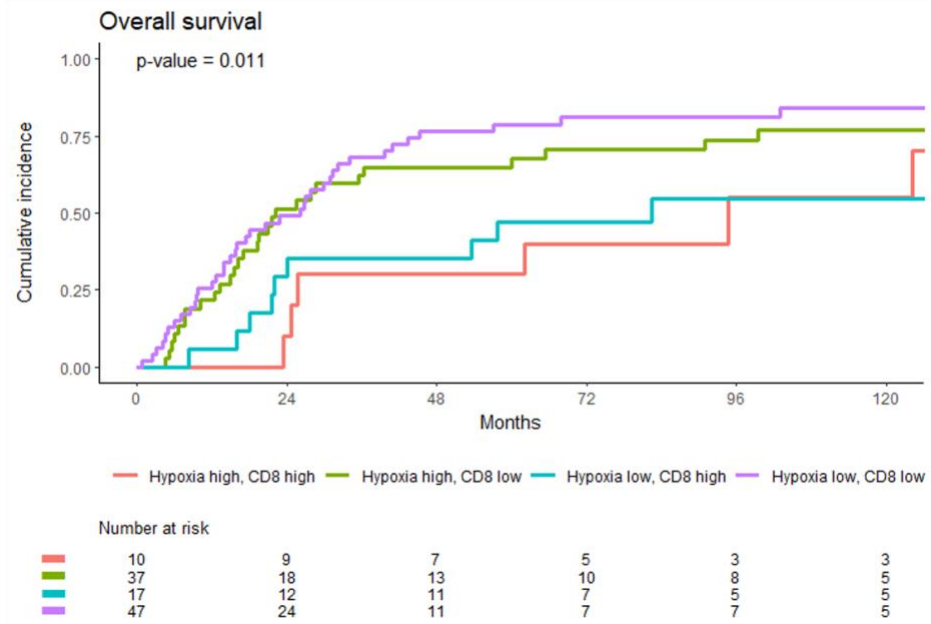

B

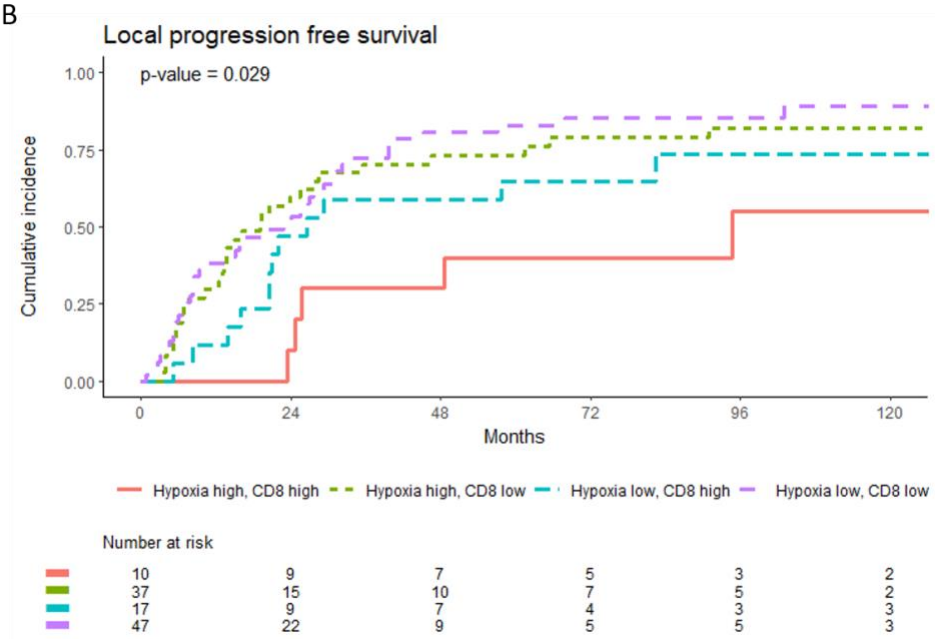

Figure 4.9. Cumulative incidence of events for A) overall survival and B) local progression free survival according to percent CD8+ T cell low/high, hypoxia low/high.
Tumours were stratified into hypoxia high or low using the CA9 IHC status and CD8+ high or low using the upper quartile as done previously. Graphs and p values were plotted using the "cmprsk" package in R.

Table 4.4. Multivariable Cox proportional hazard model analyses of CD8+ T cell counts with other clinicopathologic variables for overall survival.

Characteristic	HR[1]	95% CI[1]	p-value
Age	1.05	1.02, 1.08	<0.001
Gender			
Male	—	—	
Female	1.36	0.70, 2.61	0.36
Tumour stage			
2	—	—	
3,4	1.14	0.66, 1.96	0.65
Grade			
2	—	—	
3	0.76	0.39, 1.46	0.41
Treatment			
RT	—	—	
RT+CON	0.60	0.38, 0.96	0.033
Tumour de-bulking			
Complete	—	—	
Partial	0.93	0.54, 1.58	0.78
Biopsy	1.94	1.04, 3.63	0.038
Hypertension			
Absent	—	—	
Present	1.48	0.89, 2.48	0.13
CA9			
Absent	—	—	
Present	0.65	0.39, 1.08	0.10
Necrosis			
Absent	—	—	
Present	2.03	1.23, 3.37	0.006
Percent of CD8+ T cells			
Low	—	—	
High	0.33	0.18, 0.59	<0.001

[1] HR = Hazard Ratio, CI = Confidence Interval. p values represent log-rank tests as calculated by the 'survival' package in R.

4.4.5 Tumours with low CD8+ T cell counts are more likely to have a luminal molecular subtype

Tumours were assigned a molecular subtype using the consensus class subtyping (Kamoun *et al.*, 2020). Percentages of tumour CD8+ T cells were higher in the basal/squamous and stroma-rich subtypes (Figure 4.10 A). I further stratified the subtypes into either luminal or basal and excluded the five NE-like patients. The percentage of CD8+ cells were significantly higher in tumours with a basal versus a luminal molecular subtype (p=0.02; Figure 4.10 B). Kaplan-Meier curves using the first order subtyping showed no prognostic significance for survival between the two subtypes in our cohort (n=80; p=0.26; Figure 4.11).

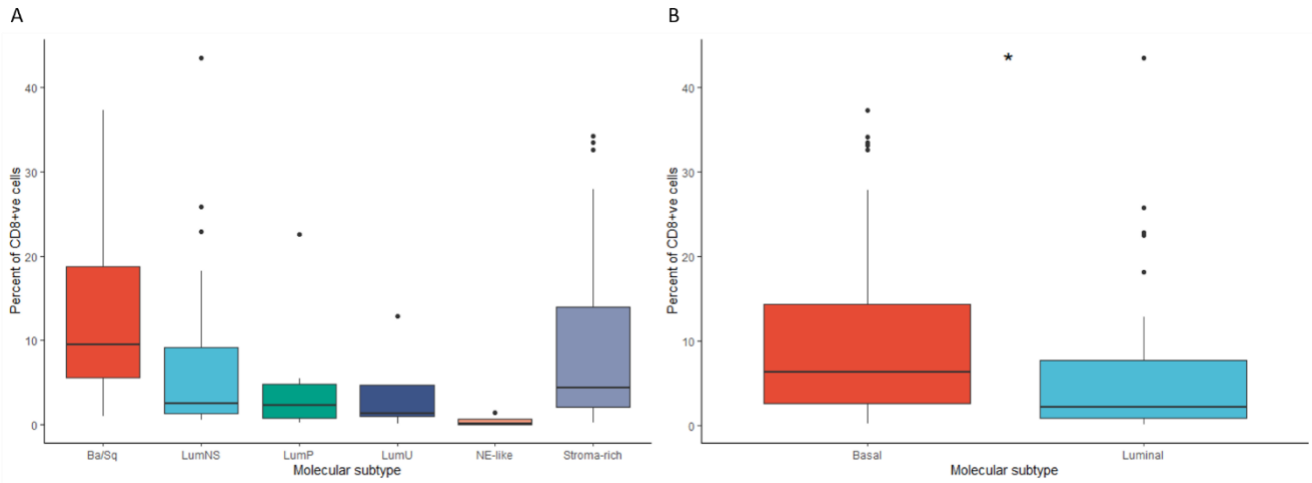

Figure 4.10. Boxplots showing the association between the percent of CD8+ T cells and the molecular subtype. Molecular subtypes are assigned as A) using "consensusMIBC" package in R (n=80) and B) further stratification into basal (basal/squamous and stroma-rich) and luminal (LumP, LumU, LumNS) sub subtypes with NE-like excluded (n=75). Statistical tests are Wilcox tests with p values represented as: ns = not significant, *<0.05, **<0.01, ***<0.001.

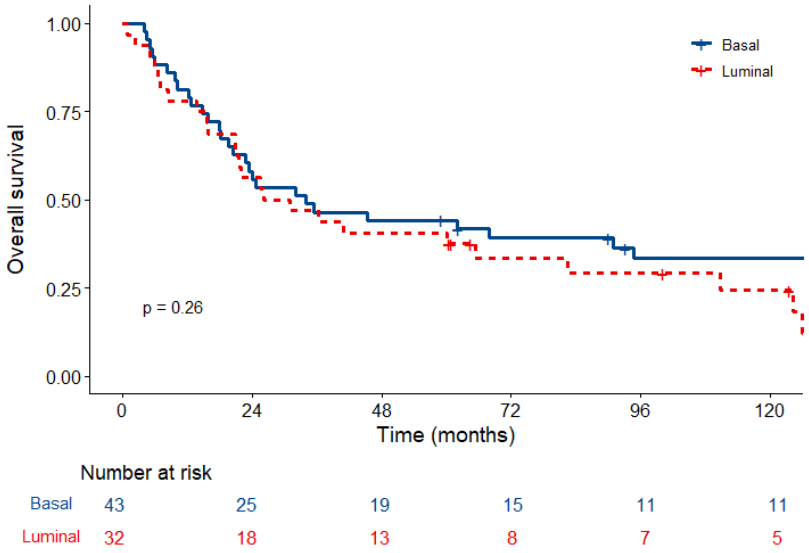

Figure 4.11. Kaplan-Meier plots for overall survival according to first order molecular subtype. Subtypes are stratified from consensus class classifications into basal (basal/squamous and stroma-rich) and luminal (LumP, LumU, LumNS) subtypes with NE-like excluded (n=75). p values are log rank tests calculated using "survival" and "survminer" packages in R.

4.4.6 Exploratory analyses with PD-L1, macrophages and other T cell types

Of the other markers, only CD4+ T helper cells counts were positively associated with CA9 expression (p=0.007;Table 4.5). However, there was no significant association with overall survival (p=0.36). None of the other markers showed any significant prognostic relevance. Table 4.2 summarises the range of counts obtained with the other multiplexed immune markers studied. There was significantly higher expression of CD68 and PDL1 in the basal group compared to the luminal group (p=0.037, p<0.001, respectively; Figure 4.12).

Table 4.5. Relationships between immune markers and hypoxia in 116 BCON patients.

Marker	All patients (116)	CA9 absent (64)	CA9 present (47)	p value
PDL1+	0.06	0.06	0.07	0.79
CD68+	4.68	5.70	4.39	0.59
CD8+	3.09	4.49	1.72	0.03
CD4+	4.60	7.23	2.10	0.01
CD4+FOXP3+	0.19	0.19	0.19	0.71

Values are the median of the percentage of each marker, as described in Section 4.3.3, according to all tumours in the cohort or stratified by tumours classified as CA9 absent or present. p values are results from Wilcox tests performed comparing the median values between CA9 present or absent.

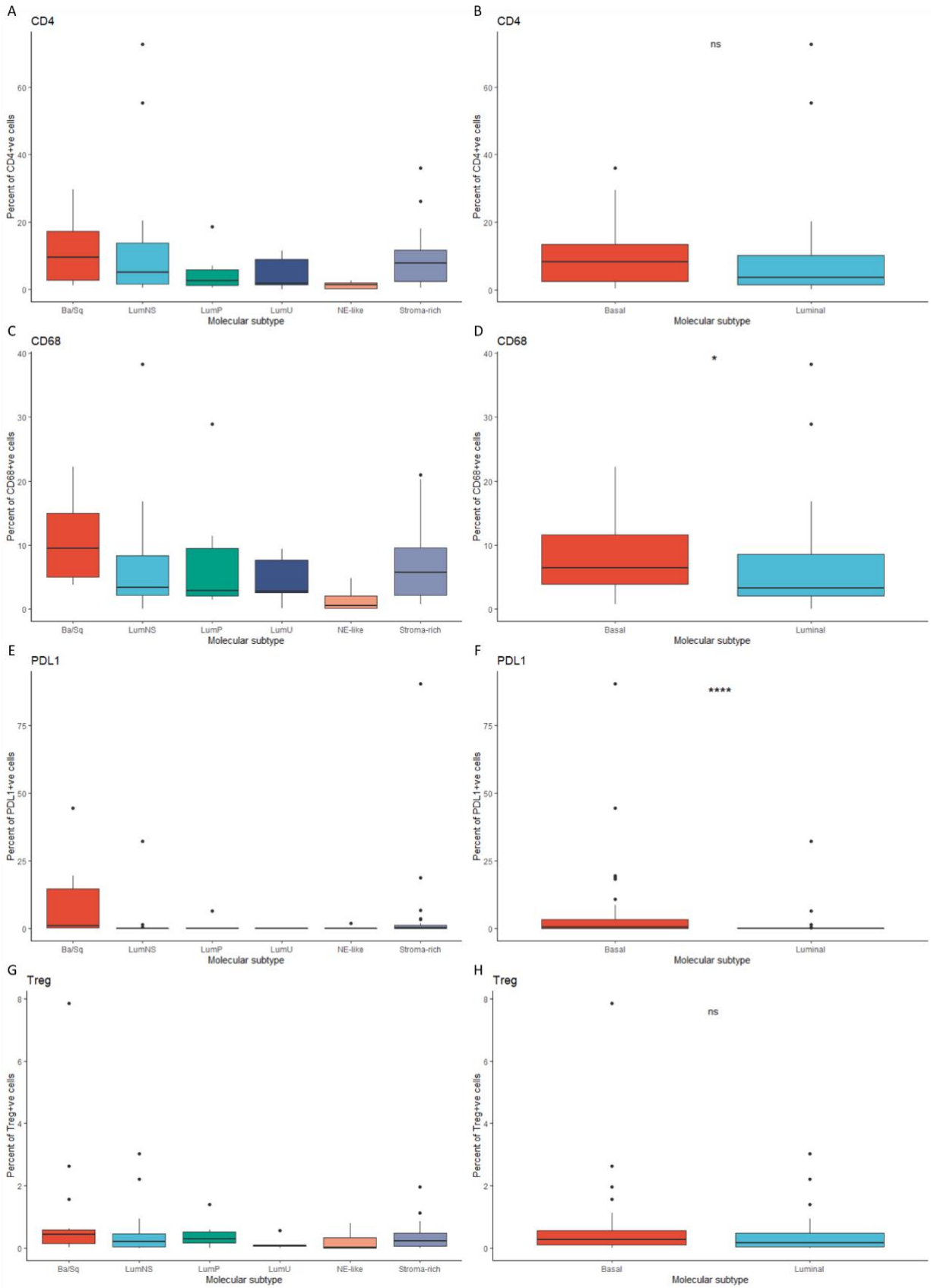

Figure 4.12. Boxplots showing the association between molecular subtype and the density of each marker. Molecular subtypes were assigned using "consensusMIBC" package in R and correlated with the percent of each marker (n=80; A-D). Subtypes were then grouped into luminal (LumP, LumU, LumNS), basal (basal/squamous and stroma-rich) and NE-Like subtypes were excluded and correlated with the percent of each marker (n=75; E-H). Statistical tests are Wilcoxon tests with p values represented as: ns = not significant, *<0.05, **<0.01, ***<0.001.

4.5 Discussion

This study found low tumour CD8+ T-cell counts associate with a poor overall prognosis, in keeping with previously published findings in bladder cancers (Sharma *et al.*, 2007; van Wilpe *et al.*, 2020). Whole TMA cores were used with no tumour/stroma differentiation. Some authors reported that tissue compartmentalisation is important when using CD8+ T cells as a prognostic marker. However, a recent meta-analysis found that, although there is a slight superiority to quantifying stromal T cells, CD8+ T cell levels are prognostic regardless of localisation pattern (F. Li *et al.*, 2021). Deng *et al.* also demonstrated prognostic significance of CD8+ T cells on FFPE whole tumour sections in bladder cancer (Deng *et al.*, 2018). In these results, I show for the first time that patients with low CD8+ T cells benefit from hypoxia modifying therapy, CON. Another novel finding from this study is that bladder tumours with low CD8+ counts have higher CA9 expression, but that CD8+ T cell count retains independent prognostic significance in multivariable analysis.

Hypoxia is an adverse prognostic factor in bladder cancer. Previous research has shown that the presence of necrosis associates with hypoxia, is a negative prognostic factor in the BCON cohort and that patients with high necrosis benefit from CON (Eustace, Irlam, *et al.*, 2013; Song *et al.*, 2021). Similarly, patients with a high expression of the hypoxia markers HIF-1α and CA9 had significantly improved 5-year local relapse free survival with RT+CON compared to RT alone (Hunter *et al.*, 2014). An existing 24-gene bladder cancer hypoxia-associated signature showed that a high hypoxia score was a negative prognostic factor and predicted benefit of therapeutic intervention with CON (Yang, Taylor, *et al.*, 2017).

These results show that assessing CD8+ T cell status provides additional information to assessing tumour hypoxia. Whilst the results presented here show that patients with low CD8+ T cell counts benefit from having CON with radiotherapy, the literature indicates that a high CD8+ T cell count predicts benefit from ICIs in both bladder and other cancer types (Wang *et al.*, 2019; F. Li *et al.*, 2021). Therefore, using CD8+ T cell counts as a biomarker could stratify patients to receive radiotherapy plus CON (low CD8+ tumours) or standard-of-care treatment with/without an ICI (high CD8+ tumours). A recent paper showed MIBC patients with low stromal TILs (which correlated with CD8+ levels) have a poor prognosis following radical cystectomy suggesting it should not be a treatment option (Sikic *et al.*, 2022). Further research is needed to investigate the prognostic significance of CD8+ counts in MIBC patients undergoing radiotherapy with chemotherapy (another standard-of-care

treatment), but I would hypothesise that low CD8+ counts would also be an adverse prognostic factor.

I found that MIBC with low CD8+ counts were more hypoxic than those with high CD8+ counts. Hypoxia might reduce CD8+ T cell infiltration via a mechanism involving increased adenosine signalling. Adenosine accumulation occurs in tissue as hypoxia increases and this has a strong role in the regulation of tumour inflammation. Specifically, extracellular adenosine has been linked with decreasing T cell differentiation and activity in hypoxic environments. It has been shown that T cells either avoid going into, or are inhibited by, hypoxic and adenosine rich areas due to the adenosine receptor signalling pathway (Hatfield *et al.*, 2015). Adenosine has been shown to bind to adenosine receptors on effector T cells reducing activity and differentiation (Bowser *et al.*, 2017). Further to this, hypoxia has been shown to induce T cell apoptosis by the adenosine receptor signalling pathway (Sun *et al.*, 2009).

Importantly these results show that CON improves outcomes in low CD8+ MIBC patients. Increasing oxygenation with CON might reduce adenosine signalling and promote T cell infiltration to increase anti-tumour immunity. It has previously been shown in a murine model that hyperoxic breathing (60% oxygen) decreased levels of HIF-1α and extracellular adenosine. The hyperoxic breathing was also shown to upregulate MHC class I on the tumours cells, which is known to enable CD8+ T cell anti-tumour effects (Hatfield *et al.*, 2014). A recent study demonstrated that locally delivered oxygen reduced adenosine accumulation in hypoxic cells and restored the cytotoxic ability of CD8+ T cells both *in vitro* and *in vivo* (Colombani *et al.*, 2021). Another study in a murine model demonstrated that hyperbaric oxygen directly increased T cell infiltration (X. Liu *et al.*, 2021). Both carbogen and nicotinamide could be recapitulating these effects to restore anti-tumour capacity of CD8+ T cells in the tumour.

As molecular subtype is increasingly of interest as a biomarker in bladder cancer, I assigned a molecular subtype to the tumours in BCON using the consensus classification and discovered a higher proportion of most infiltrates in the basal/squamous and stroma-rich subtypes, as reported by others (Kamoun *et al.*, 2020). However, molecular subtype was not prognostic in this study cohort. Molecular subtypes were previously examined on a larger BCON sub-cohort with available transcriptomic data where tumours were stratified into basal and luminal subtypes using a different methodology (BASE47) and it was also

found not to be prognostic (Song *et al.*, 2021). In this study, I also investigated other suppressive immune markers including PD-L1, CD68+ macrophage populations and Treg populations characterised by CD4+ and FOXP3+ co-localisation. In agreement with published literature I found PD-L1 had no clinical relevance as a biomarker in this context (Faraj *et al.*, 2015). None of the other markers showed any prognostic relevance or link with CA9. This was unexpected as it has been shown in other cancer types and *in vivo* models that hypoxia drives an increase in both Tregs and macrophages (Hasmim *et al.*, 2013; B. Wang *et al.*, 2021).

The limitations of this study include the relatively low numbers of samples and limited tissue available for analysis. Further work is needed to elucidate mechanisms of hypoxia causing low CD8+ T cells. Analysis needs to be done on a bladder cancer ICI clinical trial cohort with transcriptomics and available FFPE blocks. It could then be determined if those tumours with low CD8+ T cells are more hypoxic and if those patients with high CD8 T cells benefitted from the ICI. Tumour/stroma stratification could be evaluated to see if prognostic strength can be further improved. However, current analysis shows prognostic significance is independent of tissue differentiation, which would make any future test simpler and cheaper as it would allow use of the tissue and stain indiscriminately, reducing costs and turnaround time.

These results are hypothesis generating and inform the design of clinical a trial where patients are stratified using CD8+ T cell count as a biomarker to receive either RT+CON or other oxygen modifying approaches (in patient tumours with low CD8+ counts) or randomised to standard-of-care alone or with an ICI (high CD8+ counts).

5 Hypoxia associates with inflammatory signalling and increased immune infiltrates in muscle-invasive bladder cancer

5.1 Abstract

Introduction: Hypoxia and a suppressive TME are both independent negative prognostic factors in MIBC that contribute to radiotherapy resistance. Hypoxia has been shown to induce an immune suppressive TME by recruiting myeloid cells that inhibit anti-tumour T cell responses. Recent transcriptomic analyses showed hypoxia increases suppressive and anti-tumour immune signalling and infiltrates in bladder cancer. I sought to investigate the relationship between HIF, hypoxia and immune signalling and infiltrates in MIBC.

Materials and methods: ChIPseq was performed to identify HIF-1α, HIF-2α, and HIF-1β binding in the genome of the MIBC cell line T24 cultured in 1% and 0.1% oxygen for 24 h. Microarray data from four MIBC cell lines (T24, J82, UMUC3, and HT1376) cultured under 1%, 0.2% and 0.1% oxygen for 24 h was used. Differences in the immune contexture between hypoxia high and low tumours were investigated using *in silico* analyses of two bladder cancer cohorts (BCON and TCGA) filtered to only include MIBC cases. GO and GSEA were used with the R packages "limma" and "fgsea". Immune deconvolution was performed using ImSig and TIMER algorithms. RStudio was used for all analyses.

Results: In hypoxia, HIF-1α and HIF-2α bound to ~11.5-13.5% and ~4.5-7.5% of immune-related genes, respectively (1-0.1% O_2). HIF-1α and HIF-2α both bound to genes associated with T cell differentiation signalling pathways. HIF-1α and HIF-2α had distinct roles in immune-related signalling. HIF-1α associated with interferon production specifically, whilst HIF-2α associated with generic cytokine signalling as well as humoral and toll-like receptor immune responses. Neutrophil and myeloid cell signalling was enriched under hypoxia, alongside Hallmark pathways associated with Tregs and macrophages. High hypoxia MIBC tumours had increased expression of suppressive and anti-tumour immune gene signatures and associated with increased immune infiltrates.

Conclusion: Hypoxia associates with inflammation as there was a positive correlation between hypoxia and both immune-related signalling and the presence of immune infiltrates in MIBC. This immune-related increase occurs for both suppressive and anti-tumour related immune signalling as seen *in vitro* and *in situ* using patient tumours.

5.2 Introduction

In the UK, the standard-of-care treatment option for MIBC patients is either radical cystectomy or radiotherapy with a radiosensitiser, and neoadjuvant chemotherapy if the patient is fit enough (National Institute for Health and Care Excellence, 2015). In addition to direct cancer cell killing, radiotherapy effectiveness depends on eliciting an anti-tumour immune response driven by DCs and T cells. However, radiotherapy can also induce a pro-tumour inflammatory response by the proportional increase of Treg cells alongside the release of cytokines and chemokines that recruit myeloid cell populations such as neutrophils, macrophages and MDSCs (Kachikwu *et al.*, 2011; Barker *et al.*, 2015). Recruited Tregs and myeloid cells suppress anti-tumour T cell responses and contribute to disease progression and recurrence (Grivennikov, Greten and Karin, 2010). Therefore, an existing suppressive TME potentiates the pro-tumour capabilities of radiotherapy-induced immune responses and is a poor prognostic factor for radiotherapy outcomes (Barker *et al.*, 2015). Hypoxia is also a poor prognostic factor that contributes to radiotherapy resistance, disease progression and recurrence in many solid tumours including bladder cancer (Höckel *et al.*, 1996; Theodoropoulos *et al.*, 2004; Hunter *et al.*, 2014).

Cellular responses to hypoxia are mostly regulated by HIF transcription factors, which are heterodimers consisting of alpha and beta subunits. There are three different HIFs, driven by different HIF-α isoforms binding to the HIF-1β subunit, of which HIF1 and HIF2 are the best studied (Vaupel and Harrison, 2004). Hypoxia has been linked to driving a suppressive immune TME by altering the phenotypes and activities of different immune cells (Manoochehri Khoshinani, Afshar and Najafi, 2016). Hypoxia inhibits antigen uptake of DCs and alters their cytokine and chemokine expression, which reduces T cell and increases neutrophil recruitment to create a suppressive immune TME (Elia *et al.*, 2008). Hypoxia has also been shown to inhibit neutrophil apoptosis to prolong their normal survival time, and promote MDSC inhibition of T cell proliferation and their differentiation into TAMs (Walmsley *et al.*, 2005; Corzo *et al.*, 2010). Moreover, HIF can drive the inflammatory potential of neutrophils and TAMs (Cramer *et al.*, 2003), and the latter are found in the highest densities in hypoxic regions and tend to have a T cell inhibiting suppressive M2 phenotype (Talks *et al.*, 2000; Murdoch *et al.*, 2004; Doedens *et al.*, 2010). Hypoxia, and associated adenosine accumulation, can also inhibit CD8+ T cell proliferation and infiltration into hypoxic areas, and induce CD8+ T cell apoptosis (Ohta *et al.*, 2006; Sun *et al.*, 2009;

Hatfield *et al.*, 2015; Jayaprakash *et al.*, 2018). Little has been reported specifically for human bladder cancer, aside from a study showing macrophage infiltration positively correlated with HIF-1α expression, angiogenesis and a poor prognosis (Chai *et al.*, 2008).

Recently, a meta-analysis investigated the relationship between *HIF1A* gene expression and the immune TME in ten TCGA cohorts. The authors showed that in bladder cancer there was a positive correlation between *HIF1A* expression and both immune suppressive (PD-L1, Tregs, MDSCs and M2 macrophages) and anti-tumour immune (CD8+ T cells, NK cells, M1 macrophages and IFN response) gene signatures (Chen *et al.*, 2020). A high correlation between *HIF1A* expression, EMT gene signatures and a poor prognosis in the bladder cancer cohort provided further support that hypoxia contributes to disease progression and is a poor prognostic factor in bladder cancer (Chen *et al.*, 2020).

The overall aim in this chapter was to investigate the relationship between HIF, hypoxia and immune-related signalling in MIBC. The first objective was to investigate hypoxia-associated, and HIF-specific, regulation of immune-related genes and signalling pathways in MIBC using *in vitro* approaches. The second objective was to investigate differences in immune signalling and infiltrates between hypoxia high and low MIBC tumours using *in silico* approaches.

5.3 Materials and methods

5.3.1 ChIPseq data generation

ChIPseq was performed as detailed in 2.6. In brief, T24 bladder cancer cells were cultured for 24 h in both 0.1% and 1% O_2. The protein-DNA interactions were cross-linked using ChIP cross-link gold and 1% formaldehyde before lysing the cells and shearing the chromatin into 200-300bp fragments using a Biorupter Pico. Antibodies against HIF-1α, HIF-2α and HIF-1β and Dynabeads Protein G were used for immunoprecipitation (IP). The fragments were de-cross-linked and the DNA eluted using the phenol chloroform method. qPCR was used to validate the ChIP experiment before the samples were sequenced and mapped by the CRUK MI core facilities. DNA with no IP was processed and sequenced in parallel as the input control.

5.3.2 Microarray data generation

As described in 2.7, microarray data were generated for a panel of MIBC cell lines (T24, J82, UMUC3 and HT1376) under various oxygen concentrations (21%, 1%, 0.2% and 0.1%). Cells were cultured for 24 h in each condition and RNA was extracted using RNeasy Plus Mini Kit. Gene expression arrays were generated using Clariom S pico HT human assay by Yourgene Health and batch corrected using ComBat function from the R package "sva" to produce $\log_2$ summarised gene level expression.

5.3.3 Data analysis

R and RStudio were used throughout, alongside the package "tidyverse". All ChIPseq data analysis was performed using the most stringent filtering parameter (peaks close to transcriptional start site and protein coding). Over representation analysis was performed using the "clusterProfiler" to generate the top 20 significant (adjusted p value < 0.05) gene ontology biological processes and graphically represented using "enrichplot".

Gene signatures from published literature were used as described in 2.8.6. Hypoxia scores were assigned using the Yang *et al* bladder cancer hypoxia gene signature using the median score across the genes in the signature and stratifying into low and high groups by the median score of each cohort (Yang, Taylor, *et al.*, 2017).

The R package "limma" was used to obtain differentially expressed genes (DEGs; $p<0.1$) across any of the cell lines in each oxygen concentration compared to normoxia. The function "goana" was used with the DEGs to investigate gene ontologies annotated using the search term "immun" that were significantly ($p<0.05$) enriched under hypoxia. The R package "fgsea" was used to perform the GSEA with Hallmark pathways from "msigdb" and the DEGs to investigate which Hallmark pathways were significantly ($p<0.05$) enriched under hypoxia.

ImSig was applied using the R package "ImSig" (Nirmal *et al.*, 2016) and TIMER deconvolution was performed using the website http://timer.cistrome.org/ with BLCA as the cancer type (Li *et al.*, 2016). Further details are in Section 2.8.5.

5.4 Results

5.4.1 ChIPseq identified HIF binding sites with high specificity and low background

To identify genome wide HIF binding sites I performed ChIP sequencing for HIF-1α, HIF-2α and HIF-1β in the T24 MIBC cell line cultured under 1% and 0.1% oxygen. Figure 5.1 shows heatmaps of input, HIF-1α, HIF-2α and HIF-1β signal intensity demonstrating high signal for each sample at transcriptional start sites (TSS) and high specificity compared to input background signal intensity. Figure 5.2 shows an enrichment of mapped reads around transcriptional start sites for each sample over the input, further illustrating specificity of the ChIP samples. Peaks were filtered according to four different filtering parameters: all significant peaks; protein coding peaks; near TSS; and both protein coding and near TSS (hereby termed stringent). Table 5.1 shows that different numbers of peaks were identified when comparing oxygen concentrations (0.1% and 1%) and samples (HIF-1α, HIF-2α and HIF-1β). According to the highest stringency filtering level, there were more HIF bound genes at 0.1% oxygen compared to 1% oxygen, and ~3 fold more genes bound by HIF-1α than HIF-2α (Table 5.1).

A

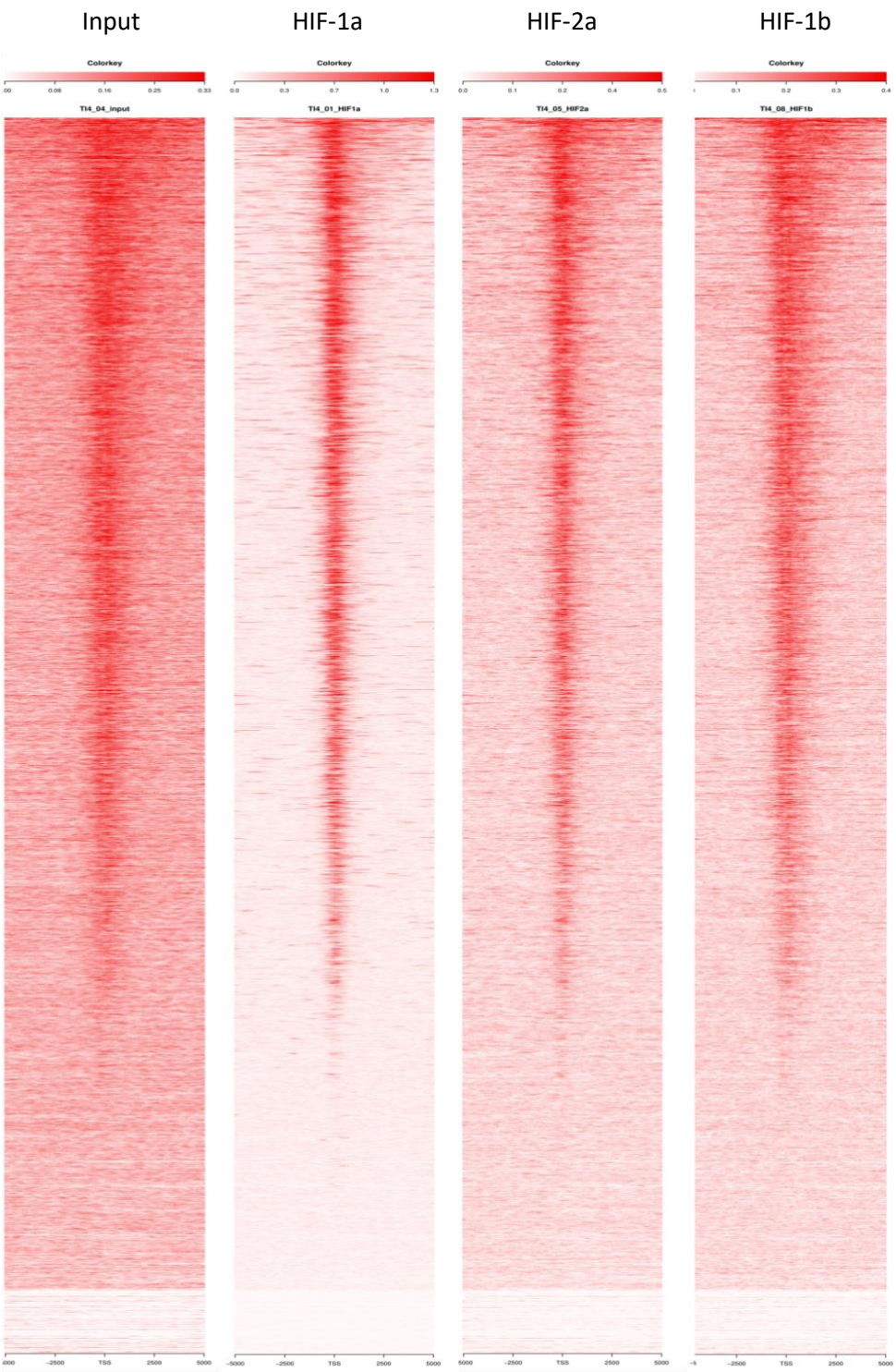
Input
HIF-1a
HIF-2a
HIF-1b
Colorkey
TI4_04_input
TI4_01_HIF1a
TI4_05_HIF2a
TI4_08_HIF1b
TSS

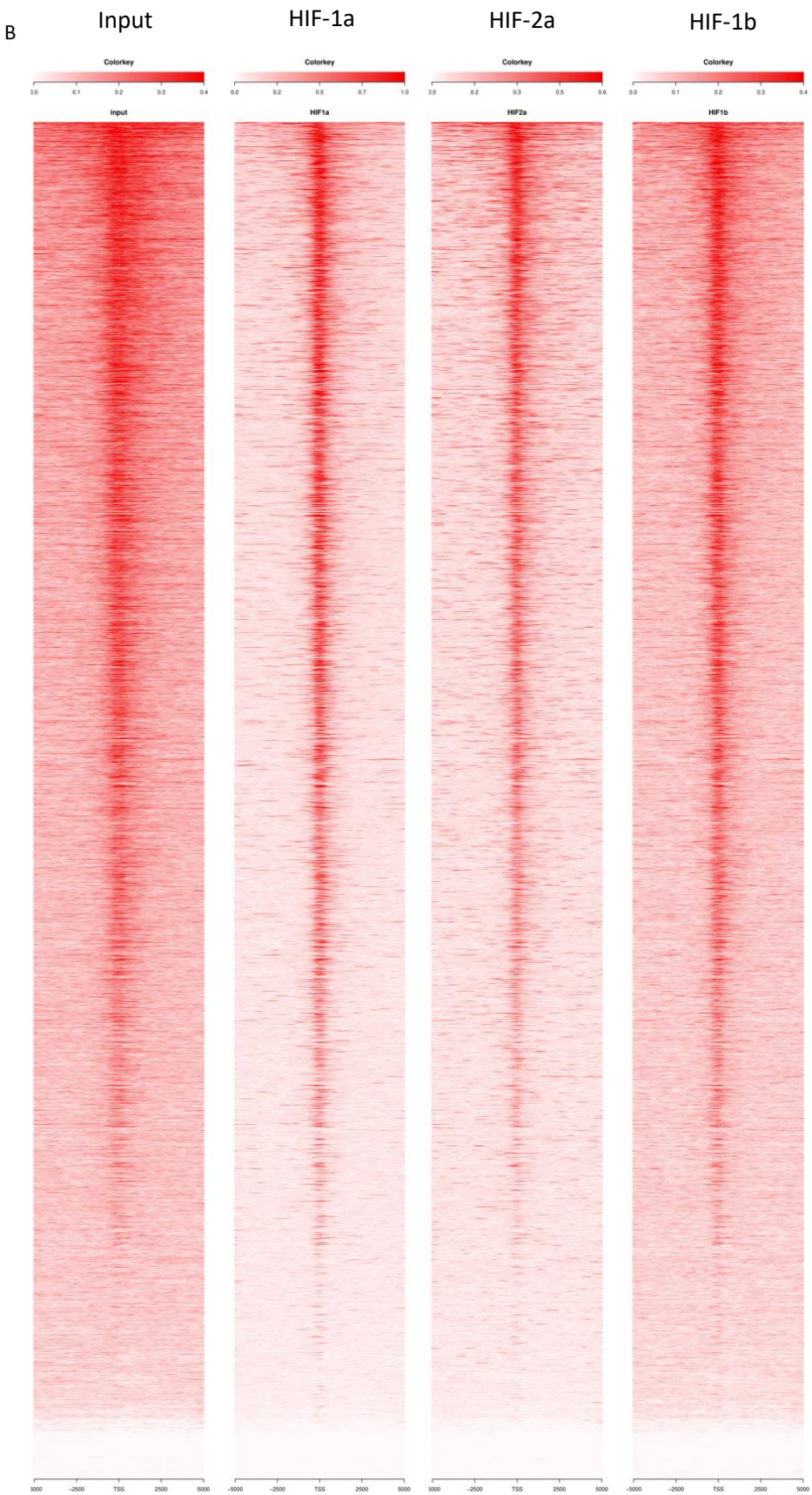

Figure 5.1 Heatmaps of signal intensities for T24 cells cultured under A) 1% O_2 and B) 0.1% O_2.
Binding sites for each sample were identified by MACS peak caller and ordered on the y-axis according to signal intensity. Heatmaps show the signal (read counts per million mapped reads) expressed as colour intensity (darker colour = higher signal). The x-axis shows genomic region of mapped reads at the transcriptional start sites and across flanking ± 5kb regions. Graphs were generated using R package "ngsplot". Left to right: input DNA, HIF-1α, HIF-2α and HIF-1β ChIP.

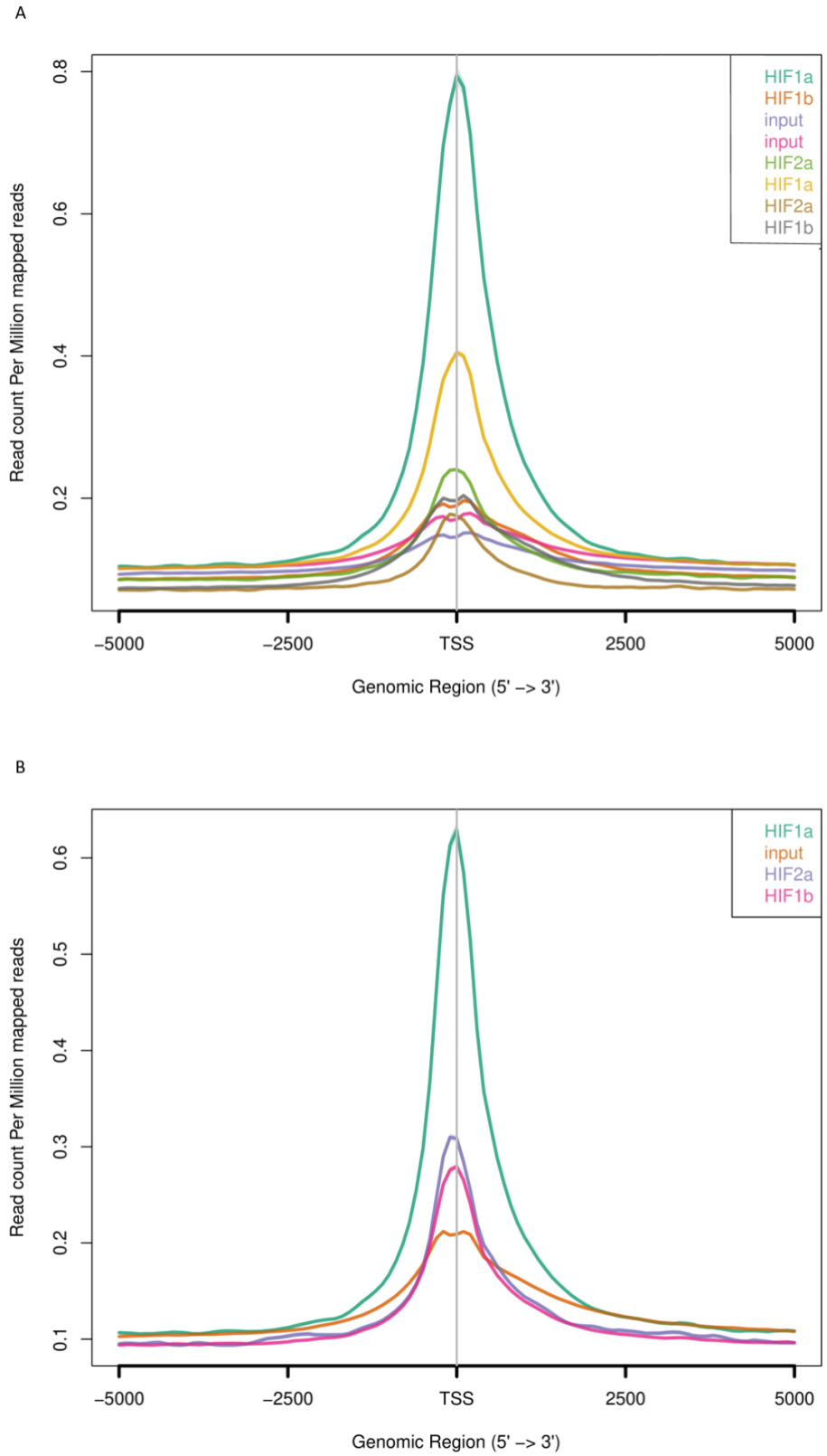

Figure 5.2 Enrichment of mapped reads around the transcriptional start site for each sample under A) 1% O_2 and B) 0.1% O_2.
The signal reads are expressed as counts per million mapped reads (y-axis) across flanking ± 5kb regions (x-axis). Graphs were generated using package "ngplpots". 1% O_2 data were generated in duplicate, 0.1% O_2 data were single replicates.

Table 5.1 Number of peaks according to different filtering parameters for T24 cells cultured in different oxygen levels.

Oxygen	Sample	AllSigPeaks	Protein coding	Near TSS	Protein coding and near TSS
0.1%	HIF-1α	30486	23536	7514	6801
	HIF-1β	4857	3539	975	848
	HIF-2α	72520	48438	3435	2883
1%	HIF-1α	32123	24728	6712	6043
	HIF-1β	5963	4291	990	847
	HIF-2α	36505	24713	1974	1612

AllSigPeaks = all significant peaks, TSS = transcriptional start site and near TSS is identified as within x distance from an annotated transcriptional start site of a promoter region in the genome.

5.4.2 HIF1 and HIF2 are associated with distinct biological processes

The large number of identified peaks (Table 5.1) makes analysis at the individual gene level difficult. Therefore, over representation analysis was performed using the genes identified by the most stringent filtering level to look at gene sets found more frequently than expected by chance. The top 20 gene sets enriched for HIF-1β show that it affects, as expected, processes associated with metabolism and oxygen level (Figure 5.3). HIF-1α and HIF-2α associate with distinct biological processes, which differ depending on the severity of hypoxia as shown in Figure 5.4 and Figure 5.5. Interestingly, in the top 20 enriched gene sets for HIF-2α is myeloid cell differentiation under 1% oxygen and TGF-β signalling under 0.1% oxygen (Figure 5.5).

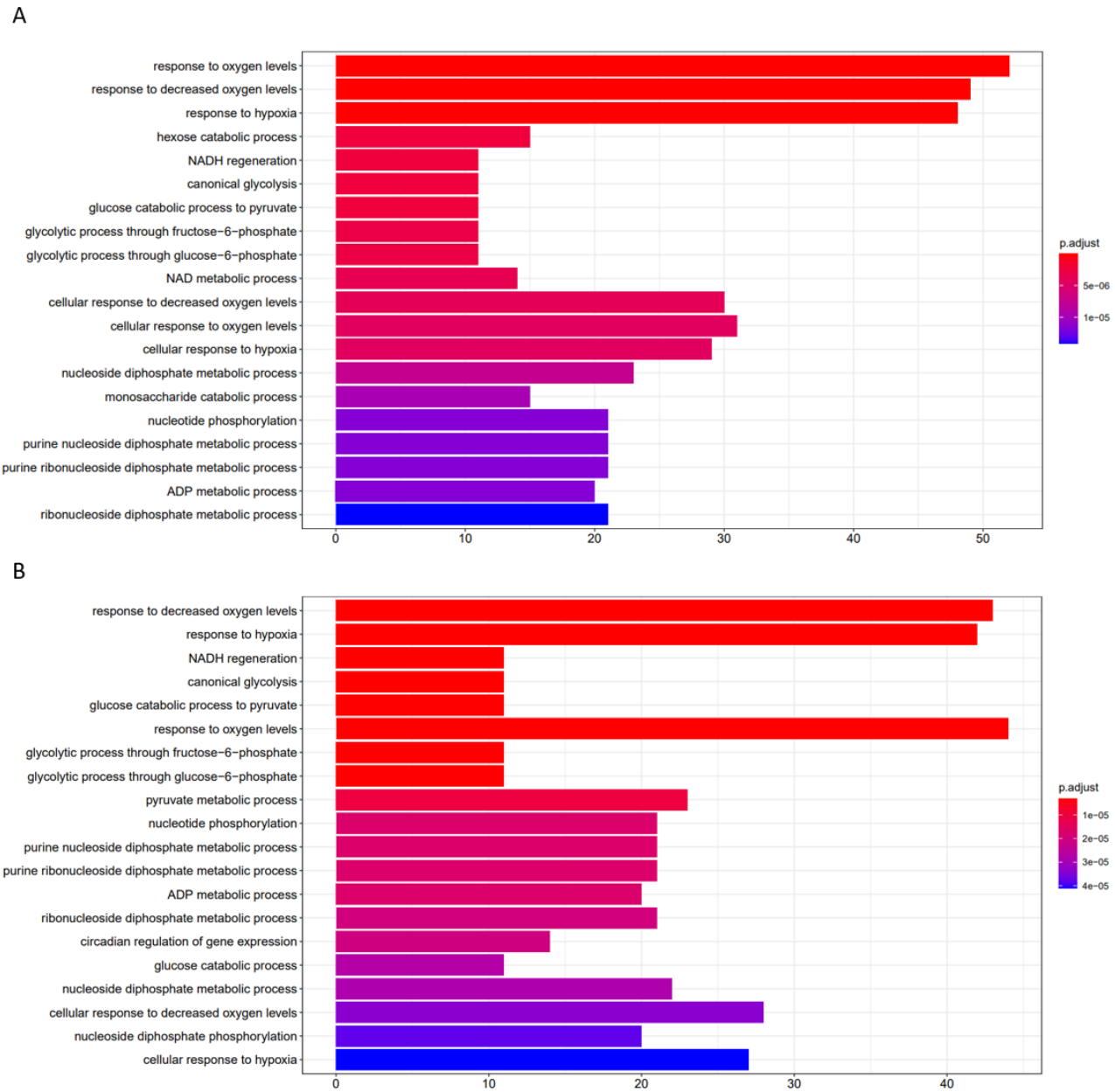

Figure 5.3 HIF-1β targeted pathways enriched in T24 cells cultured in A) 1% and B) 0.1% oxygen.
Enriched Gene Ontology (GO) biological processes terms were identified with R package "clusterProfiler". Each term was ordered according to statistical significance (BH) and the top-20 results were visualised as bar plots. X-axis refers to the number of HIF-1β bound genes from the dataset that were mapped onto that given GO term.

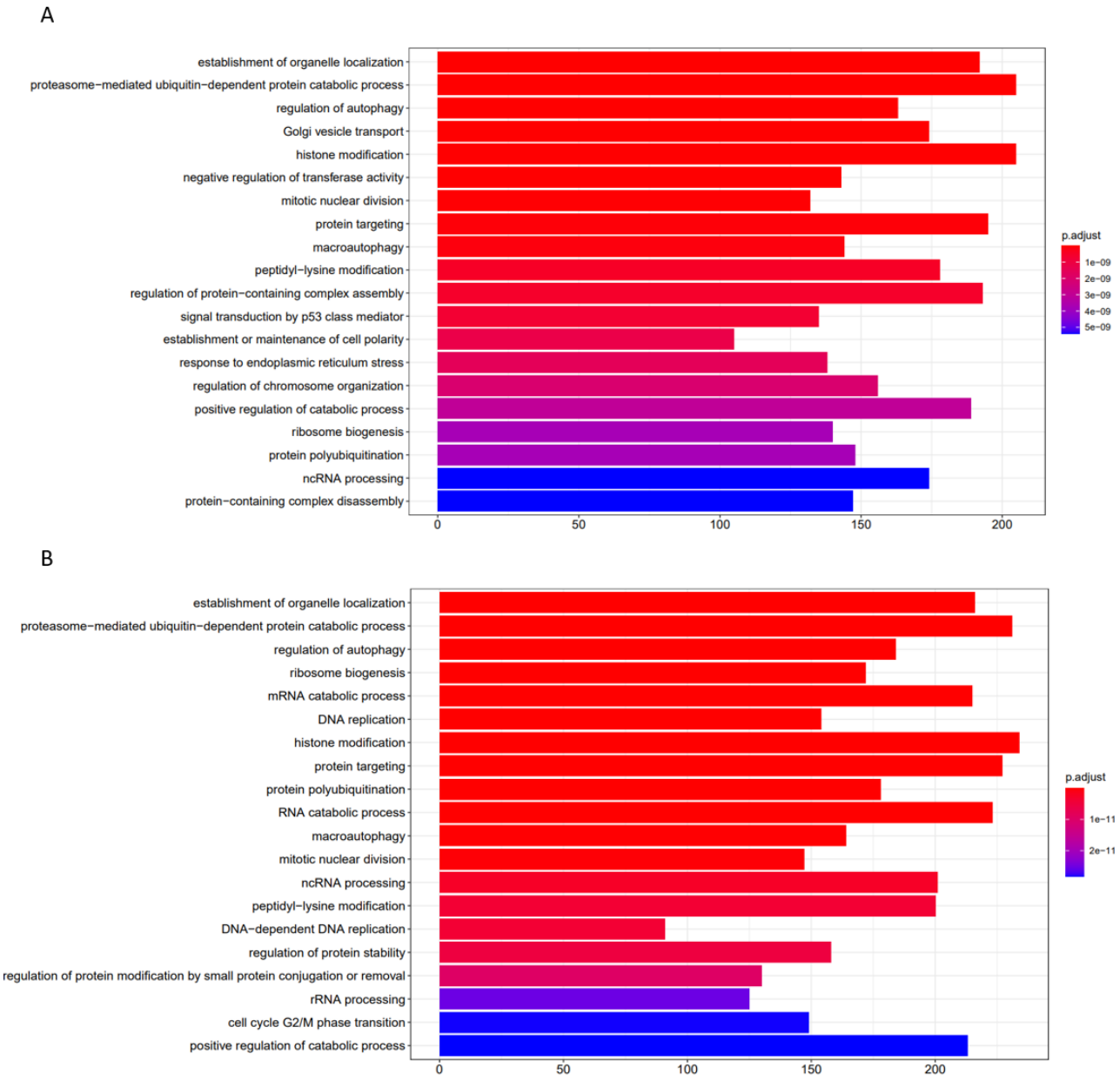

Figure 5.4 HIF-1α targeted pathways enriched in T24 cells cultured in A) 1% and B) 0.1% oxygen.
Enriched Gene Ontology (GO) biological processes terms were identified with R package "clusterProfiler". Each term was ordered according to statistical significance (BH) and the top-20 results were visualised as bar plots. X-axis refers to the number of genes from the dataset that were mapped onto that given GO term.

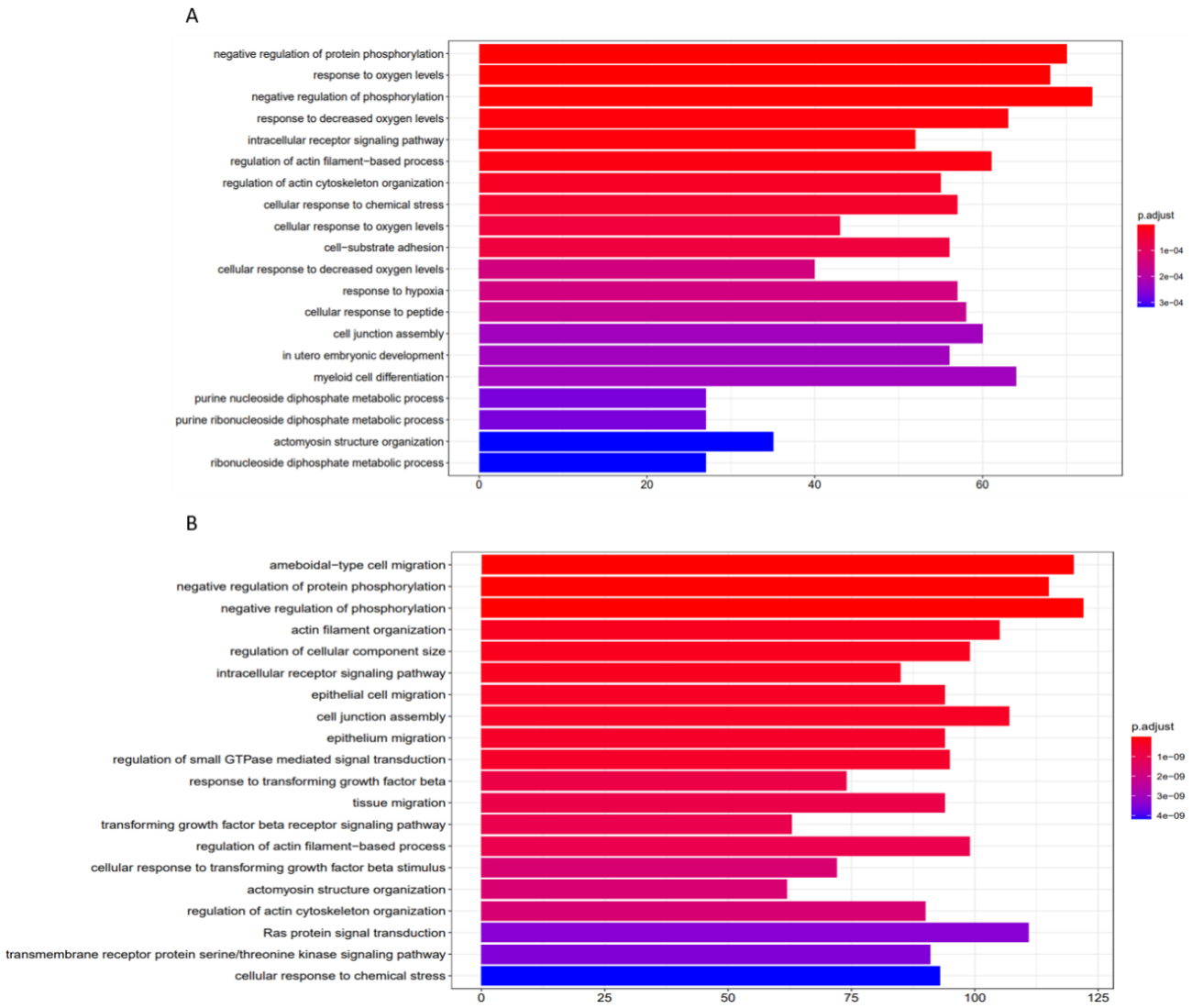

Figure 5.5 HIF-2α targeted pathways enriched in T24 cells cultured in under A) 1% and B) 0.1% oxygen. Enriched Gene Ontology (GO) biological processes terms were identified with R package "clusterProfiler". Each term was ordered according to statistical significance (BH) and the top-20 results were visualised as bar plots. X-axis refers to the number of genes from the dataset that were mapped onto that given GO term.

5.4.3 HIF1 and HIF2 associate with unique immune-related processes

To identify which HIF-bound genes are immune-related, the EBI QuickGO resource was used to cross-reference ChIPseq identified genes with those annotated as "immune response" (n=2494; Figure 5.6). The proportion of HIF-bound genes that were immune-related was higher in HIF-1α than HIF-2α samples and increased as the oxygen concentration decreased from ~4.5-11.5% in 1% oxygen for HIF-2α and HIF-1α, respectively, to ~7.5-13.5% in 0.1% hypoxia (Table 5.2). Most of the genes identified from the 1% dataset are also present in the 0.1% dataset as shown in Figure 5.7. Figure 5.8 shows that a number of these immune-related genes were unique to either HIF-1α or HIF-2α. HIF-2α is enriched at an enhancer region of the PD-L1 gene (*CD274*) under 1% and 0.1% hypoxia, which was visualised using University of California Santa Cruz (UCSC) genome browser resource (Figure 5.9). Over representation analysis was performed on the subunit unique genes to identify enriched immune-related gene sets. The results from the top 20 gene sets for the unique immune-related genes bound to each subunit indicate that HIF-1α associates with signalling related to adaptive immune responses such as interferon-associated signalling and HIF-2α with signalling associated with innate immune responses such as humoural and toll-like receptor signalling (Figure 5.10 and Figure 5.11). Both HIFs are enriched for gene sets associated with T cell activation/differentiation in their top 20 enriched immune-related pathways.

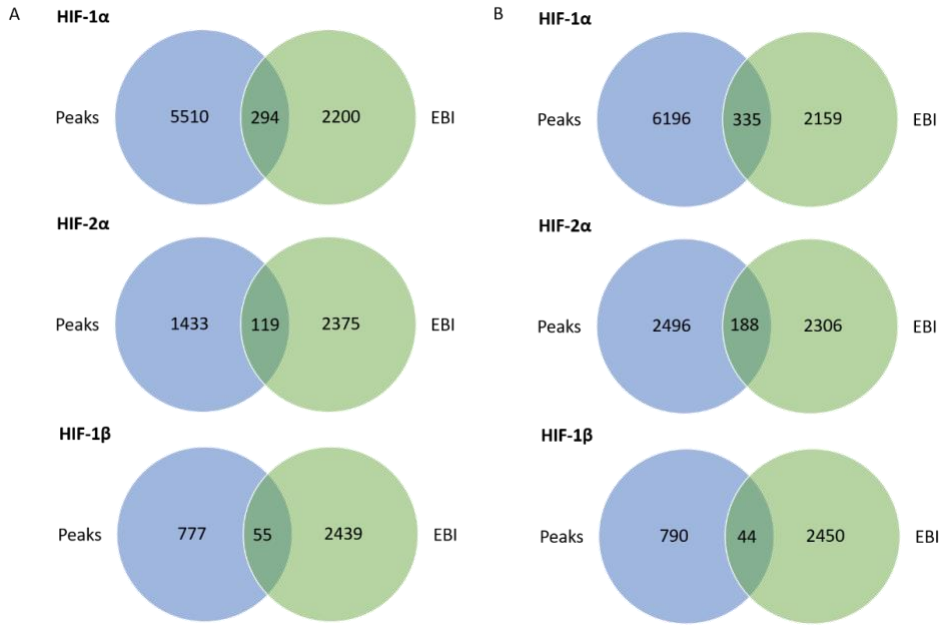

Figure 5.6 Venn diagrams showing the number of genes overlapping between ChIPseq genes and immune response genes in T24 cells grown in A) 1% oxygen and B) 0.1% oxygen.
The most stringent filtering parameter for each sample under both oxygen concentrations was cross-referenced with genes annotated as "immune response" from the EBI QuickGO resource.

Table 5.2 Percentage of immune-related genes bound to each HIF subunit.

Oxygen concentration	HIF subunit	Percent of immune genes bound
1%	HIF-1α	11.79
	HIF-1β	2.20
	HIF-2α	4.77
0.1%	HIF-1α	13.43
	HIF-1β	1.76
	HIF-2α	7.54

Values are the percentages of genes annotated as immune-related by EBI Quick GO (n=2494) for genes identified as bound by each HIF subunit according to the stringent filtering level.

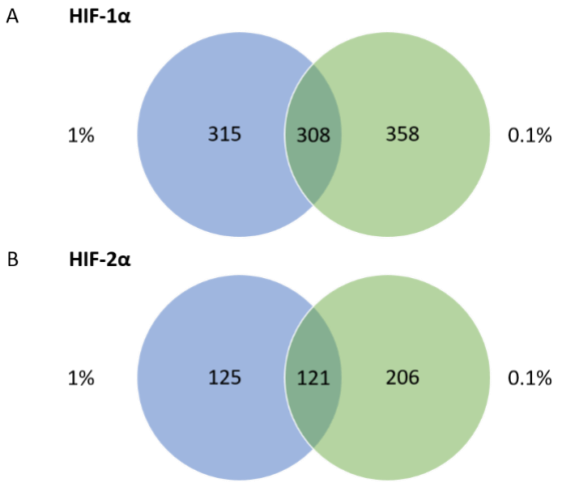

Figure 5.7 Venn diagrams showing the overlap between immune response genes identified from each oxygen concentration for A) HIF-1α and B) HIF-2α.
The most stringent filtering parameter for each sample under both oxygen concentrations was used. Immune response genes were defined using those annotated as "immune response" from the EBI QuickGO resource.

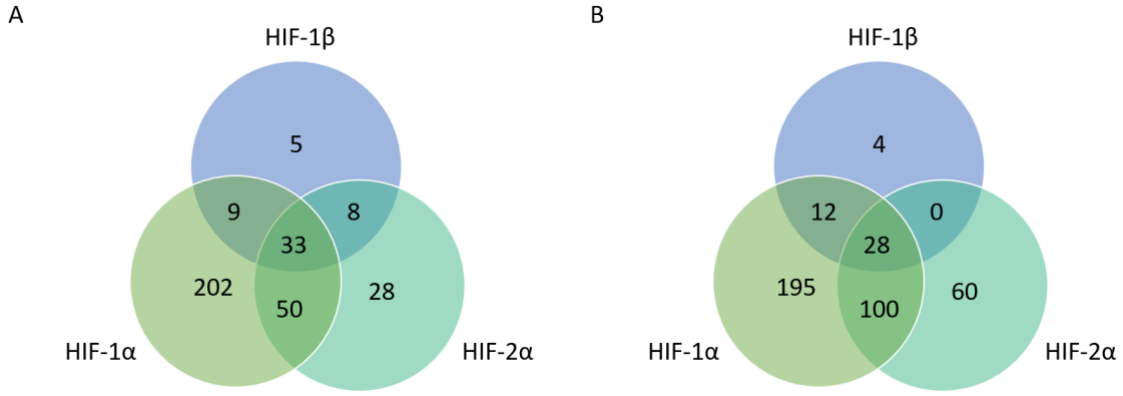

Figure 5.8 Venn diagrams showing the number of immune response genes overlapping between the HIF subunits for A) 1% oxygen and B) 0.1% oxygen.
The most stringent filtering parameter for each sample under both oxygen concentrations was used. Immune response genes were defined using those annotated as "immune response" from the EBI QuickGO resource.

A

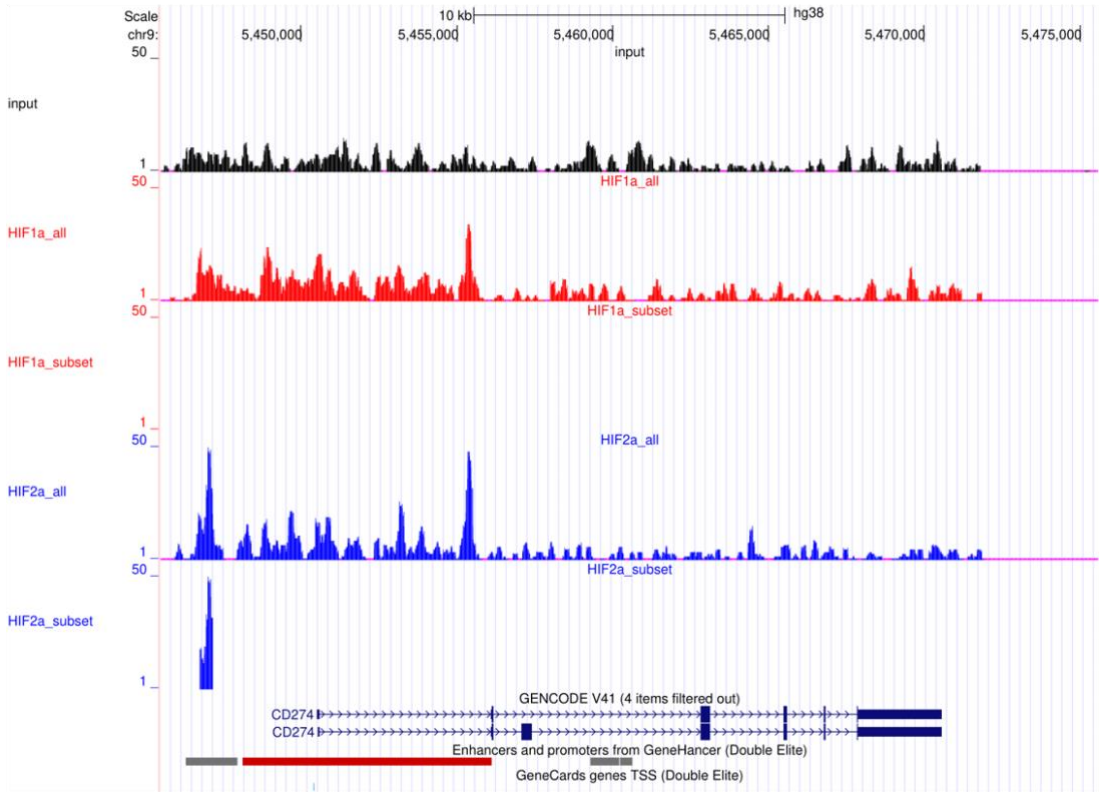

B

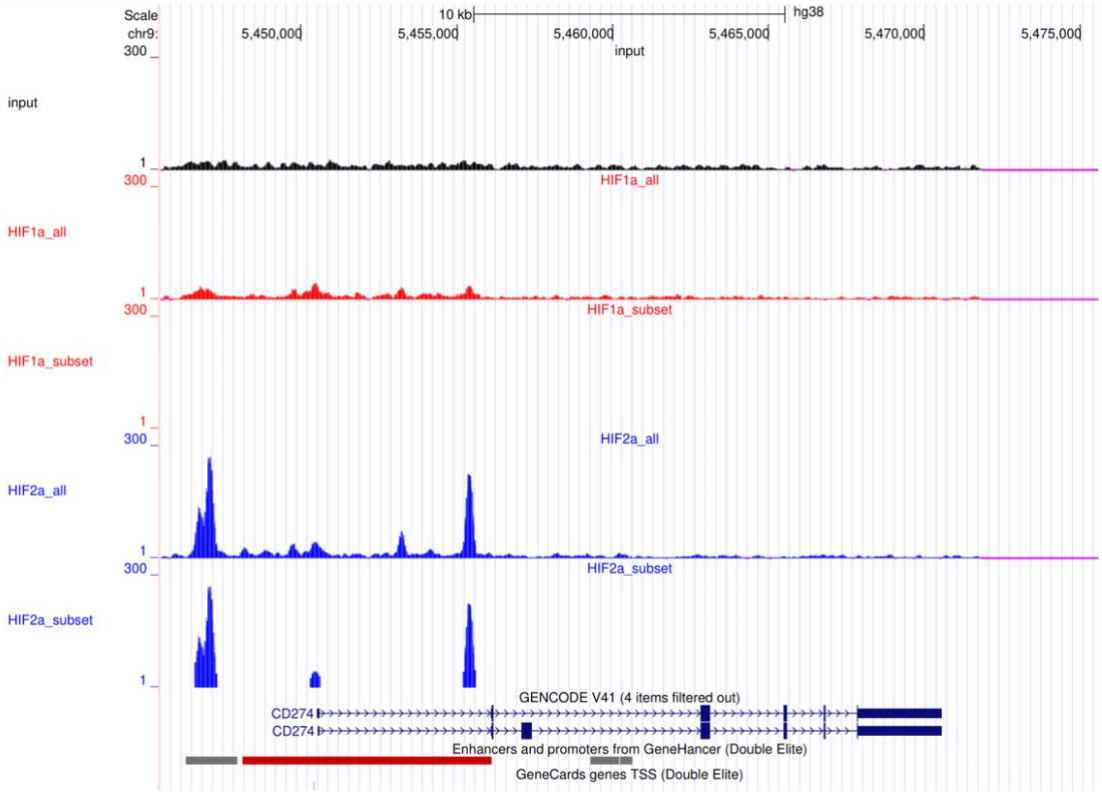

Figure 5.9 ChIPseq tracks for the CD274 gene (encoding the PD-L1 protein) shown using the UCSC genome browser for A) 1% and B) 0.1% samples.
Representative tracks are displayed from top to bottom in each image for input: HIF-1α (no filtering), HIF-1α (filtering), HIF-2α (no filtering), and HIF-2α (filtering). The track shown at the bottom annotates known enhancers and promoters from the GeneHancer database where: grey = enhancer and red = enhancer/promoter. The corresponding peaks above the CD274 enhancer region for the HIF-2α tracks demonstrate the enrichment of HIF-2α in this genomic region in T24 cell line.

A

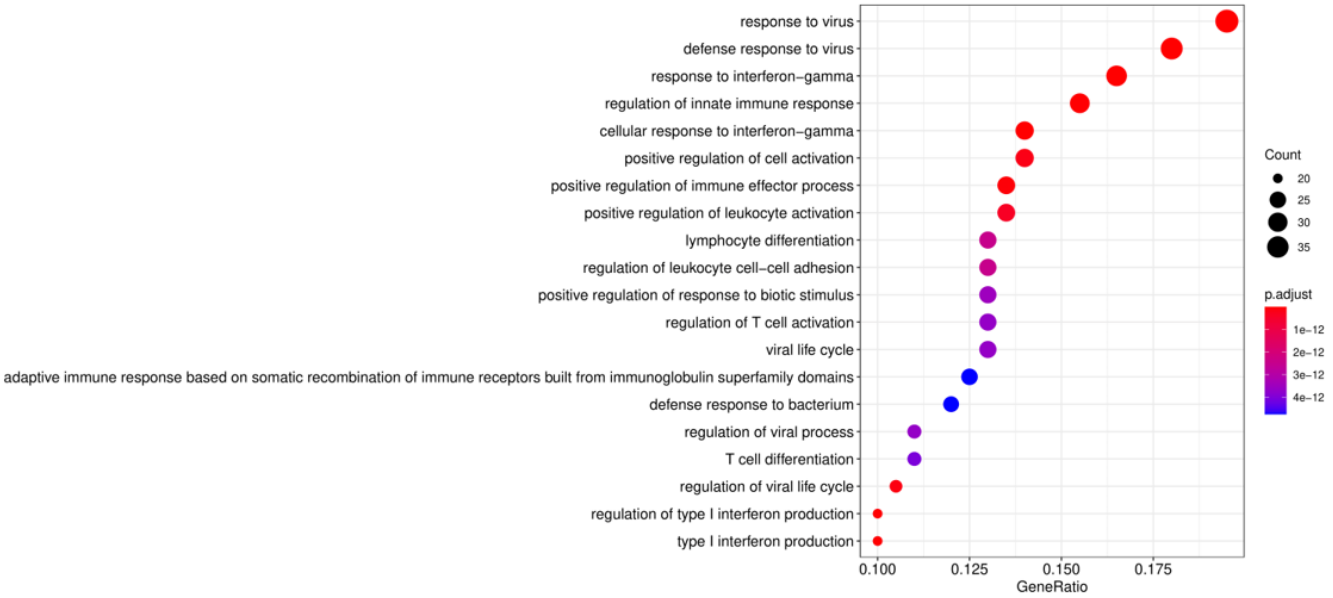

B

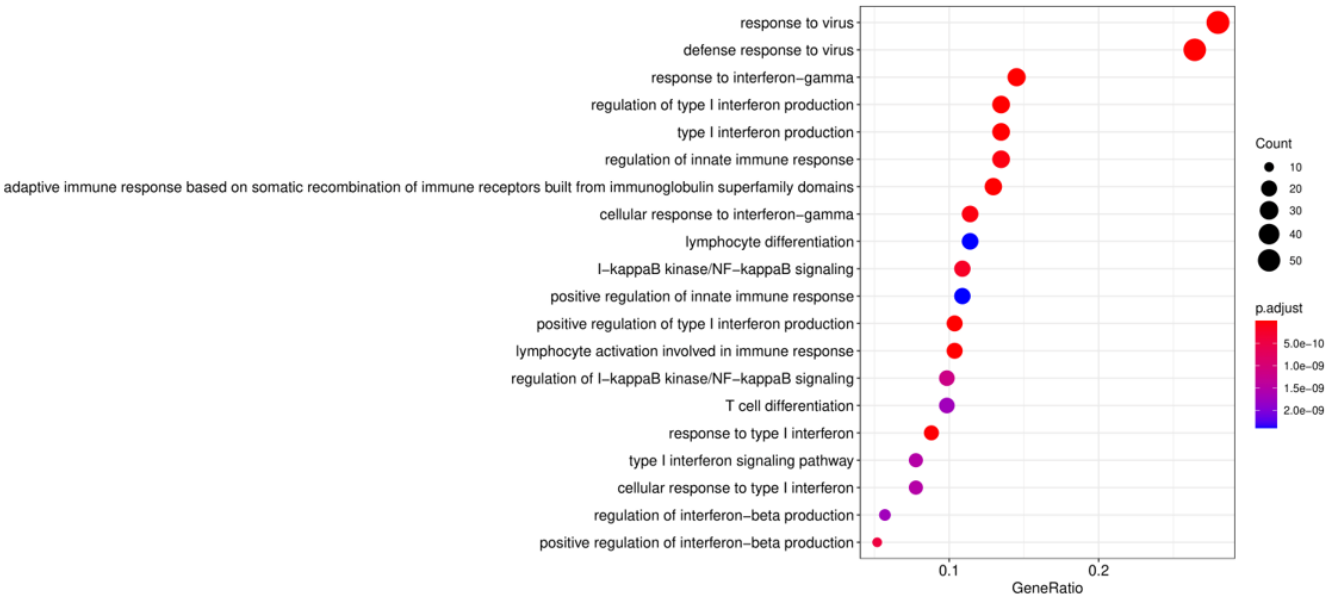

Figure 5.10 Over representation analysis for HIF-1α unique immune genes in A) 1% and B) 0.1% oxygen.
Enriched Gene Ontology (GO) biological processes terms were identified with R package "clusterProfiler". The top 20 terms were plotted and ordered according to count. Count is the number of genes in this dataset that mapped onto the given GO term. X-axis is the gene ratio, which is the count divided by the total number of genes annotated to the given GO term, presented as a ratio.

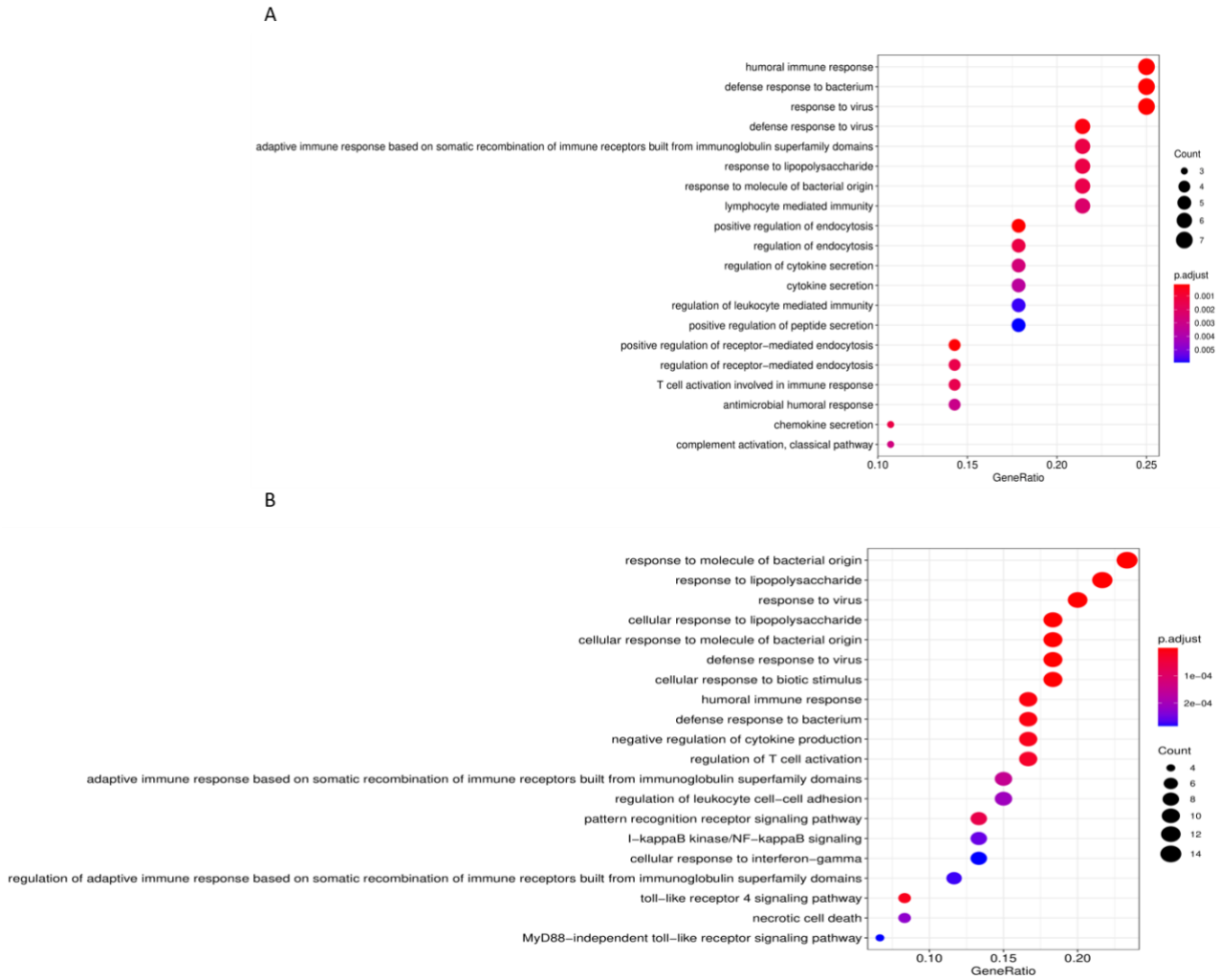

Figure 5.11 Over representation analysis for HIF-2α unique immune genes in A) 1% and B) 0.1% oxygen. Enriched Gene Ontology (GO) biological processes terms were identified with R package "clusterProfiler". The top 20 terms were plotted and ordered according to count. Count is the number of genes in this dataset that mapped onto the given GO term. X-axis is the gene ratio, which is the count divided by the total number of genes annotated to the given GO term, presented as a ratio.

5.4.4 Hypoxia associates with myeloid, neutrophil and CD4+ T cell signalling processes

Microarray transcriptomics was used to investigate differentially expressed genes (DEGs) under hypoxia (0.1%, 0.2%, and 1% O_2) compared to normoxia (21% O_2) in a panel of MIBC cell lines (T24, J82, UMUC3 and HT1376). Gene ontology (GO) over representation analysis was used to investigate DEGs ($p<0.1$) that were significantly ($p<0.05$) enriched for biological processes under the GO search term “immun” for any of the cell lines under each oxygen concentration. Biological processes associated with myeloid and neutrophil signalling were enriched in cells cultured in all three low oxygen concentrations (Table 5.3-5). Gene set enrichment analysis (GSEA) using the Hallmark pathways showed that under hypoxia Hallmark_TNFα_signalling_via_NFkB (1%, 0.2%, 0.1% O_2) and

Hallmark_IL2_STAT5_signalling (1%, 0.2% O_2) were in the top ten significantly enriched pathways alongside Hallmark_hypoxia and Hallmark_glycolysis (1%, 0.2%, 0.1% O_2) and Hallmark_epithelial_to_mesemchymal_transition signalling (0.2%, 0.1% O_2; Figure 5.12).

Table 5.3 GO terms filtered by the search term "immun" significantly enriched under 1% hypoxia.

Term	ID	Ont	N	DE	P.DE
somatic diversification of immune receptors via germline recombination within a single locus	GO:0002562	BP	66	7	0.05
neutrophil mediated immunity	GO:0002446	BP	501	43	<0.001
neutrophil activation involved in immune response	GO:0002283	BP	490	42	<0.001
myeloid leukocyte mediated immunity	GO:0002444	BP	555	46	<0.001
myeloid cell activation involved in immune response	GO:0002275	BP	549	43	0.003
leukocyte activation involved in immune response	GO:0002366	BP	716	51	0.01
cell activation involved in immune response	GO:0002263	BP	720	51	0.01

Ont is the gene ontology term, BP = biological process. N = number of genes in the GO term. DE = number of differentially expressed genes from dataset present in the GO term. P.DE = p value for over representation of the GO term in the set.

Table 5.4 GO terms filtered by the search term "immun" significantly enriched under 0.2% hypoxia.

Term	ID	Ont	N	DE	P.DE
somatic recombination of immunoglobulin genes involved in immune response	GO:0002204	BP	51	15	0.01
somatic diversification of immunoglobulins involved in immune response	GO:0002208	BP	51	15	0.01
somatic recombination of immunoglobulin gene segments	GO:0016447	BP	56	15	0.02
immunoglobulin production involved in immunoglobulin-mediated immune response	GO:0002381	BP	61	15	0.05
somatic diversification of immune receptors via germline recombination within a single locus	GO:0002562	BP	66	16	0.05
somatic diversification of immunoglobulins	GO:0016445	BP	66	16	0.05
neutrophil mediated immunity	GO:0002446	BP	501	100	0.006
neutrophil activation involved in immune response	GO:0002283	BP	490	95	0.02
myeloid leukocyte mediated immunity	GO:0002444	BP	555	105	0.02

Ont is the gene ontology term, BP = biological process. N = number of genes in the GO term. DE = number of differentially expressed genes from dataset present in the GO term. P.DE = p value for over representation of the GO term in the set.

Table 5.5 GO terms filtered by the search term “immun” significantly enriched under 0.1% hypoxia.

Term	ID	Ont	N	DE	P.DE
mitigation of host immune response by virus	GO:0030683	BP	2	2	0.04
positive regulation of tolerance induction dependent upon immune response	GO:0002654	BP	2	2	0.04
positive regulation of immune response to tumor cell	GO:0002839	BP	13	6	0.03
positive regulation of myeloid leukocyte cytokine production	GO:0061081	BP	19	8	0.02
neutrophil mediated immunity	GO:0002446	BP	501	127	<0.001
neutrophil activation involved in immune response	GO:0002283	BP	490	121	0.003
myeloid leukocyte mediated immunity	GO:0002444	BP	555	136	0.003
myeloid cell activation involved in immune response	GO:0002275	BP	549	127	0.02

Ont is the gene ontology term, BP = biological process. N = number of genes in the GO term. DE = number of differentially expressed genes from dataset present in the GO term. P.DE = p value for over representation of the GO term in the set.

A

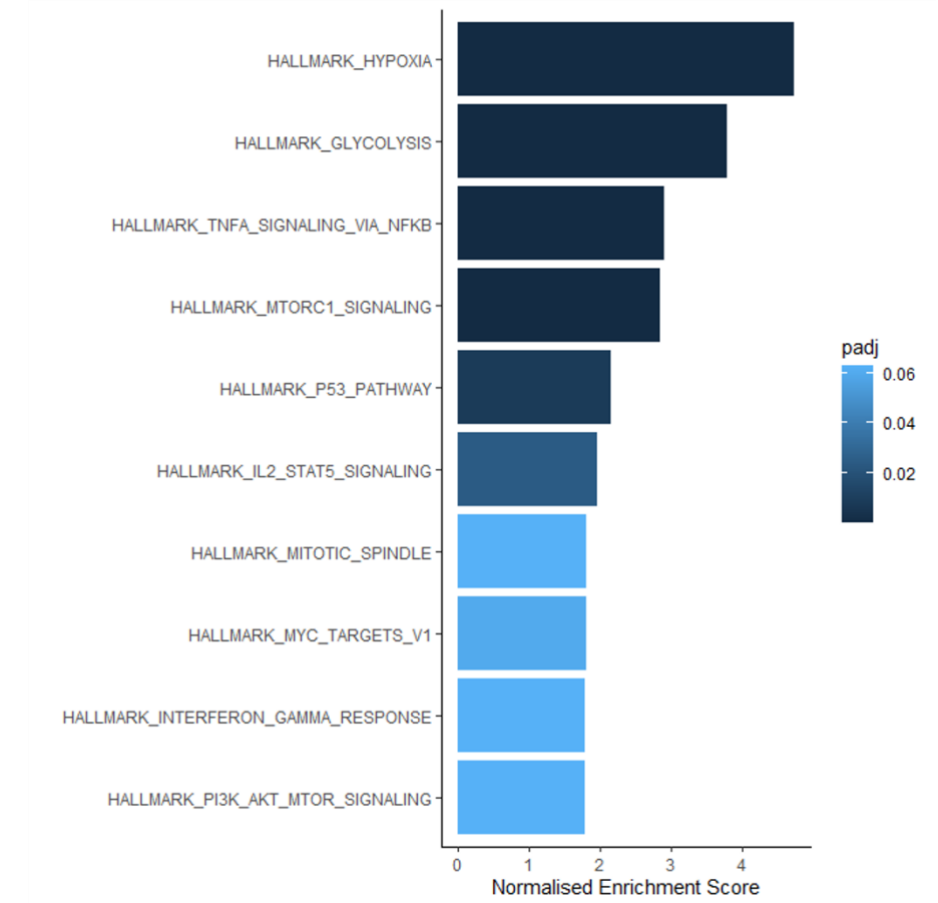
HALLMARK_HYPOXIA
HALLMARK_GLYCOLYSIS
HALLMARK_TNFA_SIGNALING_VIA_NFKB
HALLMARK_MTORC1_SIGNALING
HALLMARK_P53_PATHWAY
HALLMARK_IL2_STAT5_SIGNALING
HALLMARK_MITOTIC_SPINDLE
HALLMARK_MYC_TARGETS_V1
HALLMARK_INTERFERON_GAMMA_RESPONSE
HALLMARK_PI3K_AKT_MTOR_SIGNALING
0
1
2
3
4
Normalised Enrichment Score
padj
0.06
0.04
0.02

B

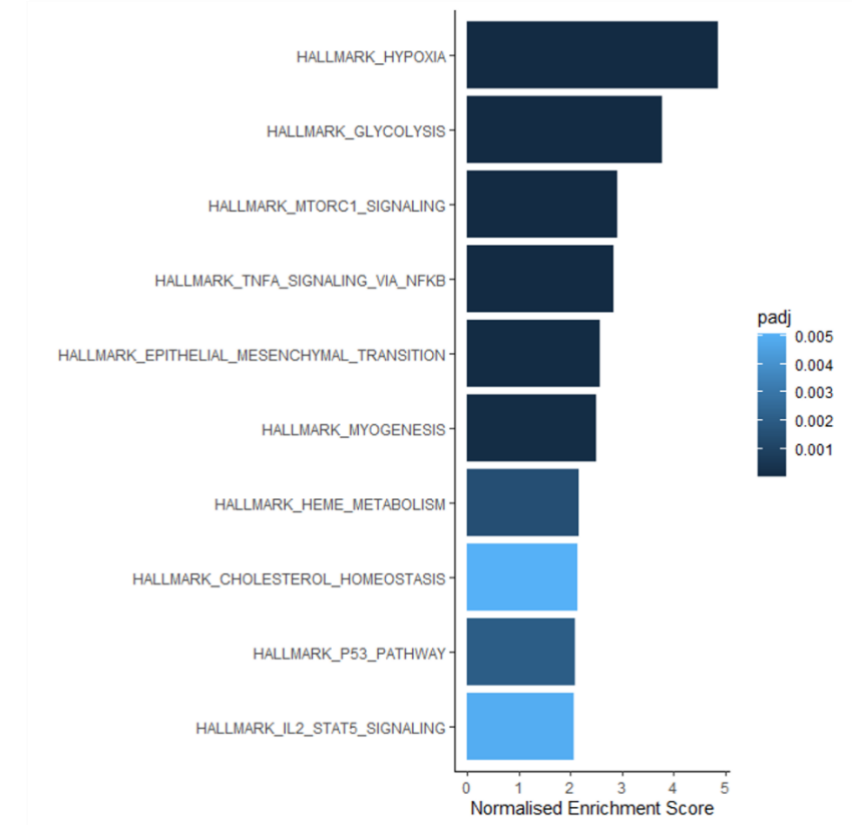
HALLMARK_HYPOXIA
HALLMARK_GLYCOLYSIS
HALLMARK_MTORC1_SIGNALING
HALLMARK_TNFA_SIGNALING_VIA_NFKB
HALLMARK_EPITHELIAL_MESENCHYMAL_TRANSITION
HALLMARK_MYOGENESIS
HALLMARK_HEME_METABOLISM
HALLMARK_CHOLESTEROL_HOMEOSTASIS
HALLMARK_P53_PATHWAY
HALLMARK_IL2_STAT5_SIGNALING
0
1
2
3
4
5
Normalised Enrichment Score
padj
0.005
0.004
0.003
0.002
0.001

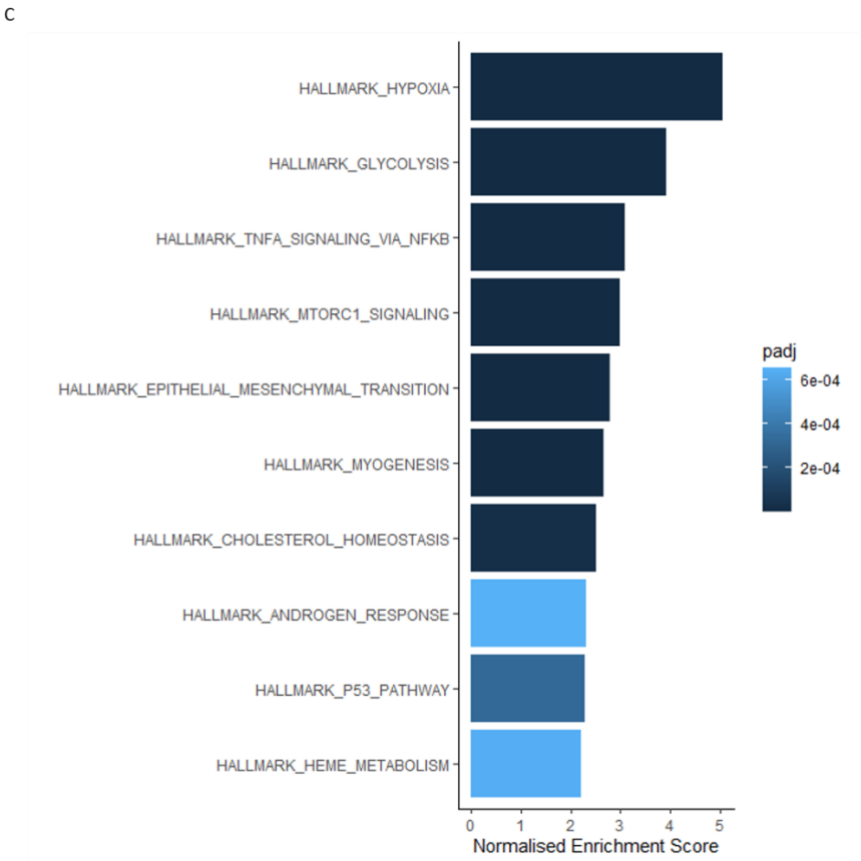

Figure 5.12 Gene set enrichment analysis showing the hallmark pathways significantly enriched under A) 1% B) 0.2%, C) 0.1% hypoxia ordered according to normalised enrichment score.
R package "fgsea" was used for the analysis and significance was defined as p value of <0.05, with adjusted p values shown in the figure legend using the colour key.

5.4.5 Hypoxia associates with increased immune signalling in tumours

To assess how hypoxia affects immune signalling in human tumours *in situ*, BCON and TCGA-BLCA MIBC gene expression datasets were used to correlate hypoxia scores with expression of immune signalling pathways. The bladder cancer 24-gene hypoxia gene signature was correlated with the scores of various published immune-related gene signatures. Heatmaps show there is a higher expression of the immune-related gene signatures in high hypoxia tumours (hypoxia scores greater than the median), and low expression in low hypoxia samples in the BCON (Figure 5.13 A) and TCGA cohorts (Figure 5.13 B). Boxplots shown in Figure 5.14 show that MIBC with high versus low hypoxia have significantly increased expression of the immune-related signatures, apart from mast cell signalling and NK cell signalling in the BCON cohort.

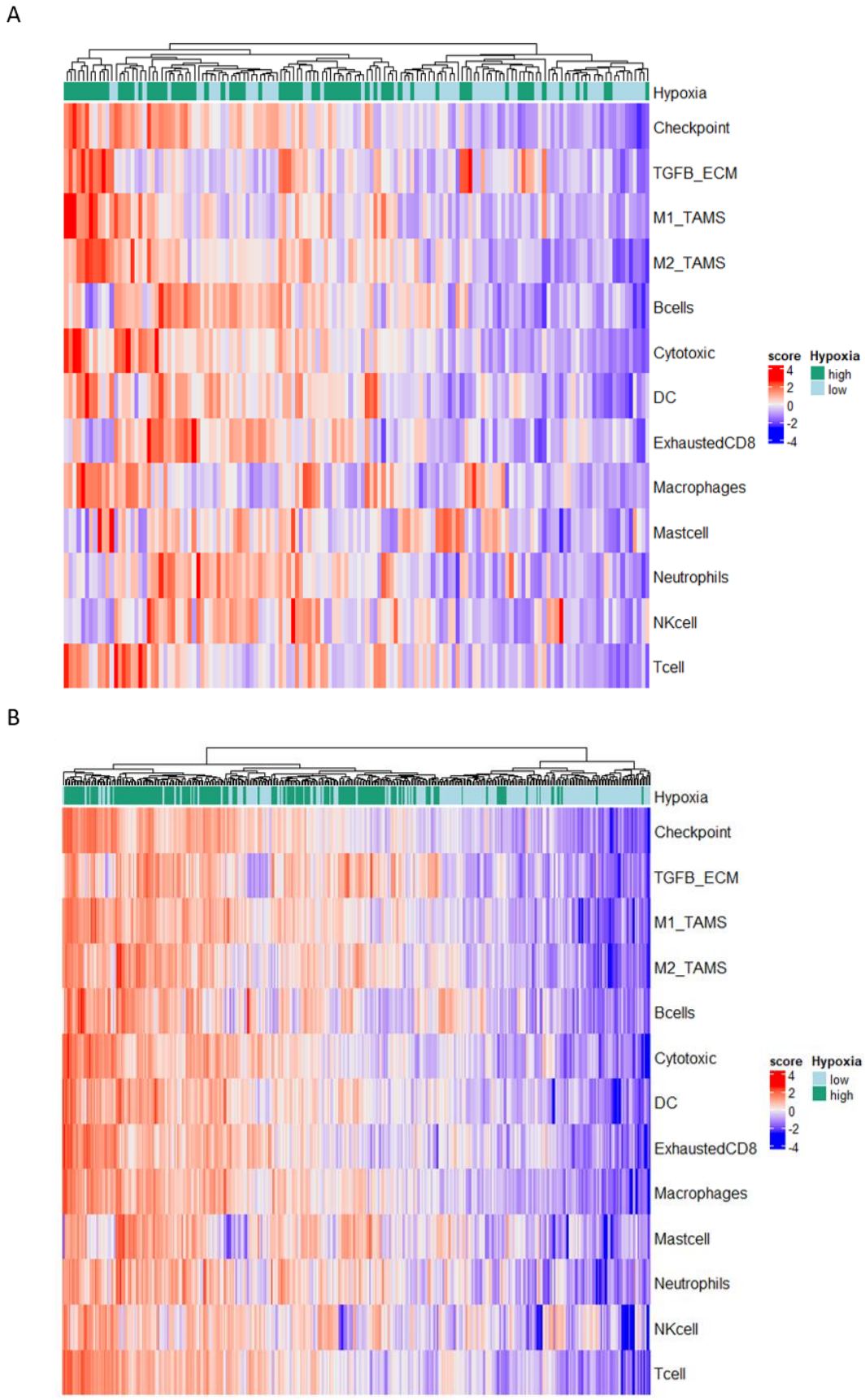

Figure 5.13 Heatmaps showing the clustering of immune-related signature scores in relation to hypoxia status high or low in A) BCON and B) TCGA cohort. R package "ComplexHeatmap" was used to generate the graph. Hypoxia status was stratified by the median hypoxia score of the cohort.

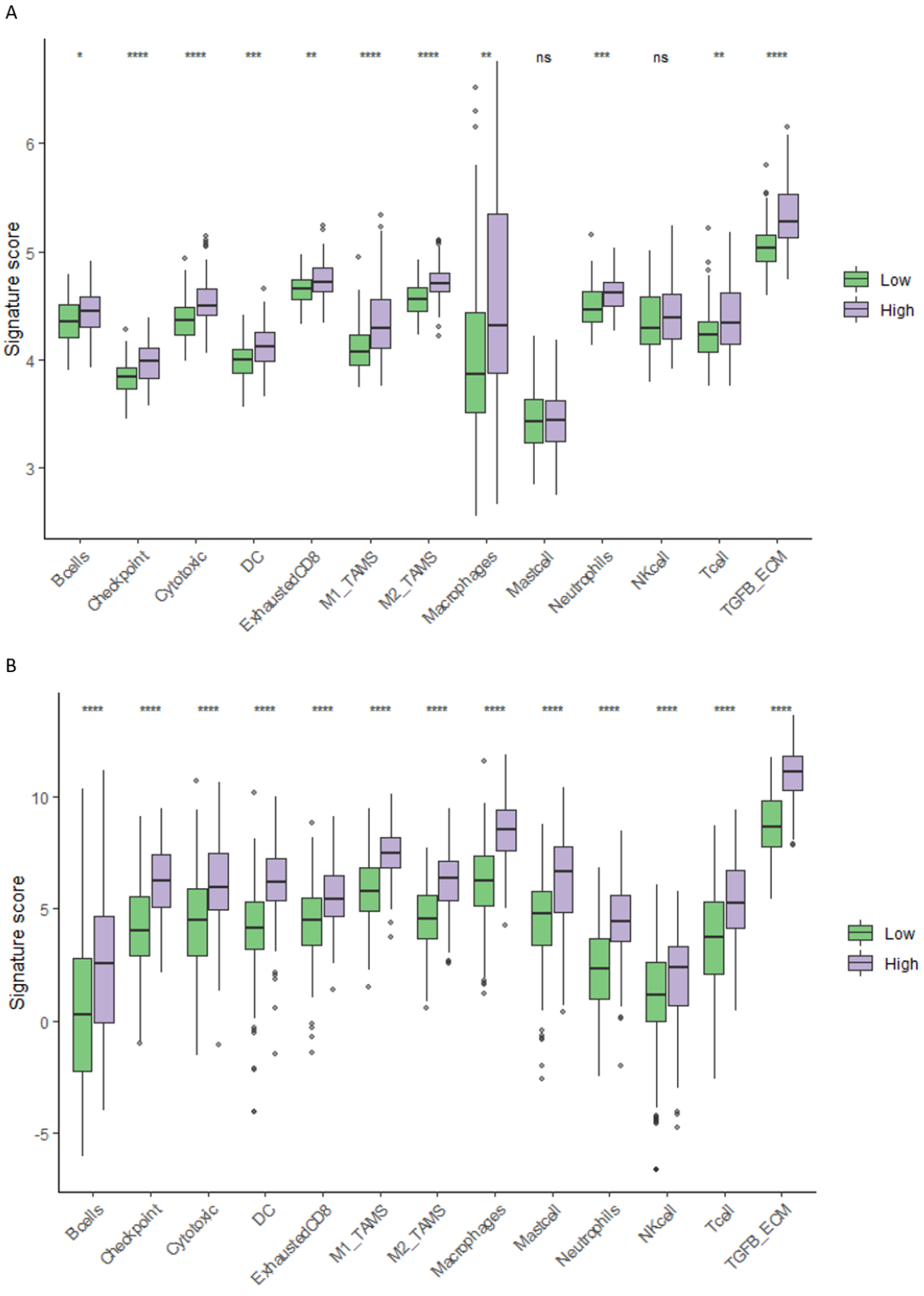

Figure 5.14 Boxplots showing the score of immune-related signatures according to hypoxia score for A) BCON and B) TCGA. Signature scores were calculated using the mean expression of the genes in the signature. Hypoxia status was stratified by the median hypoxia score of the cohort. Statistics are p values from t tests with p values represented as: ns = not significant, *<0.05, **<0.01, ***<0.001, ****<0.0001.

5.4.6 Hypoxia associates with an inflamed immune TME

ImSig and TIMER immune cell deconvolution algorithms were used to assess the presence of immune cell infiltrates for low versus high hypoxia tumours in the BCON and TCGA-BLCA datasets. As shown in Figure 5.15 and Figure 5.16, high hypoxia tumours had significantly more T cells and neutrophils, as shown by both algorithms. ImSig further shows high hypoxia tumours have significantly more monocytes and NK cells, whilst TIMER shows significantly more myeloid dendritic cells. Macrophages were significantly increased in high hypoxia tumours when analysed by ImSig, but not significantly different when using TIMER for the BCON cohort (Figure 5.15). Macrophages were significantly increased in high hypoxia tumours as seen by both algorithms in the TCGA cohort (Figure 5.16). There were differences in the levels of B cell infiltrates between the two algorithms, with TIMER showing a significant decrease in hypoxic tumours (not significant in TCGA) and ImSig showing a significant increase (Figure 5.15-16).

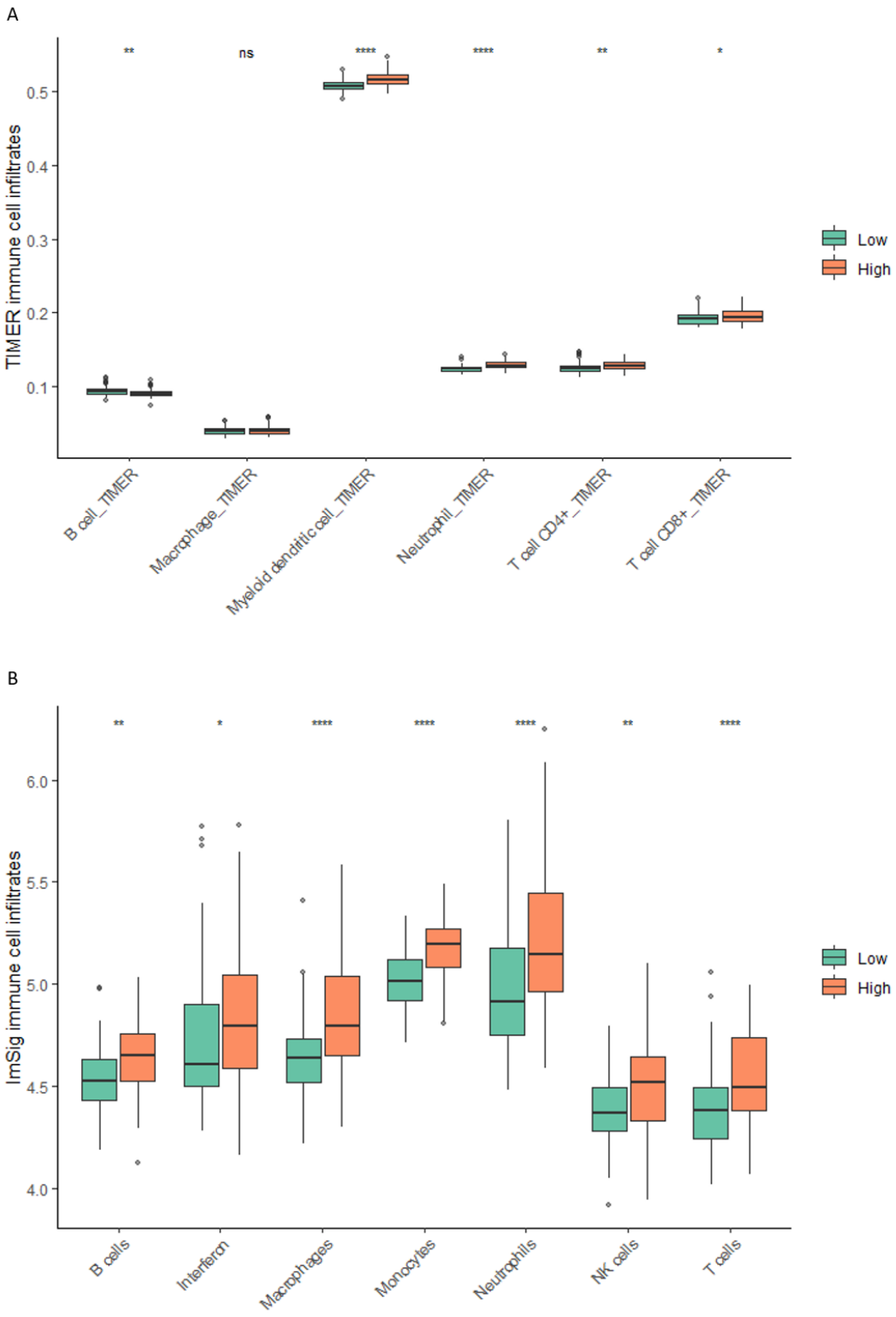

Figure 5.15 Boxplots showing the fraction of immune cell population according to hypoxia status for the BCON cohort. Immune cell populations were deconvoluted by A) TIMER and B) ImSig algorithms. Hypoxia status was stratified by the median hypoxia score of the cohort. Statistics are adjusted p values (BH) from t tests with p values represented as: ns = not significant, *<0.05, **<0.01, ***<0.001, ****<0.0001

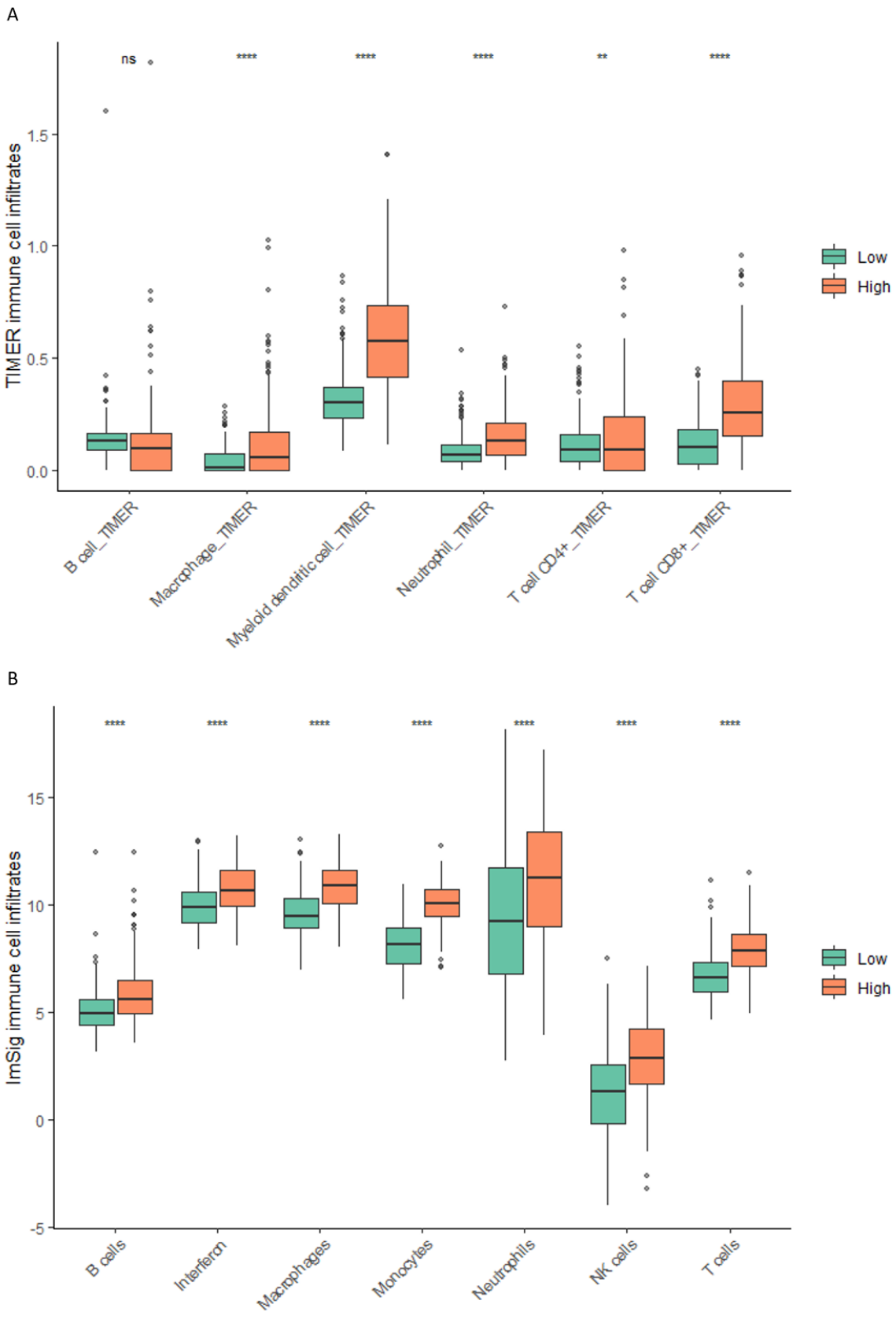

Figure 5.16 Boxplots showing the fraction of immune cell population according to hypoxia status for the TCGA cohort. Immune cell populations were deconvoluted by A) TIMER and B) ImSig algorithms. Hypoxia status was stratified by the median hypoxia score of the cohort. Statistics are adjusted p values (BH) from t tests with p values represented as: ns = not significant, *<0.05, **<0.01, ***<0.001, ****<0.0001

5.5 Discussion

There are several novel findings from the work described in this chapter regarding the role of HIF and hypoxia in immune-related processes in MIBC. First, I show that in 1% hypoxia, 11.8% of immune-related genes bind to HIF-1α, increasing to 13.4% in 0.1% hypoxia. HIF-2α binds to 4.8% and 7.5% of all immune-related genes under 1% and 0.1% hypoxia, respectively. Second, I show that HIF-1α and HIF-2α bind uniquely to some immune-related genes, which associate with distinct immune-related processes. HIF-1α is enriched for immune gene binding associated with T cell activation pathways and related interferon production. Third, I show that in the T24 MIBC cell line HIF-2α is enriched at an enhancer region of the PD-L1 gene. I also consolidate recent findings to demonstrate that hypoxia upregulates signalling related to both anti-tumour and immune suppressive pathways, and I show this in MIBC specifically.

In a similar manner to this study, Symthies *et al* performed a HIF ChIPseq experiment on kidney and liver cancer cell lines cultured in 0.5% and 3% oxygen for 6, 16 and 48 h (Smythies *et al.*, 2019). They found that the strongest binding occurred at 16 h, providing the basis for the chosen 24 h time point in this study. Whilst Smythies *et al* found that the oxygen concentration did not alter HIF binding locations, my results show an increase in HIF binding sites as the oxygen level decreases. This could be due to increased strength of binding at 0.1% vs 1% oxygen manifesting as increased signal intensity, which lowers the number of binding sites removed through the stringent filtering. I also show a higher proportion of binding sites for HIF-1α compared to HIF-2α, which is consistent with literature (Mole *et al.*, 2009; Schödel *et al.*, 2011; Smythies *et al.*, 2019).

Smythies *et al* found that HIF1 and HIF2 heterodimers bind to distinct regions of the genome without competing and this was conserved across four human cancer cell lines (HKC-8 and RCC4, renal; HepG2, liver; and MCF-7, breast) (Smythies *et al.*, 2019). My work showed that HIF1 and HIF2 associate first with common processes of oxygen consumption and sugar glycolysis and then with distinct biological processes. Smythies *et al* also showed that wherever HIF-1β bound it was with an HIF-α isoform, in concordance with published literature (Hill *et al.*, 2015; Smythies *et al.*, 2019). The HIF-1β sample obtained in my study is of worse quality than the HIFα isoforms, as seen in Figure 5.1-5.2. The lower quality decreased the number of significant genes bound by HIF-1β compared to HIF-1α and HIF-2α that made it through the stringent filtering. However, the results for the subunit unique

immune binding sites show that most of the HIF-1β binding sites overlap with either of the HIF-α isoforms, confirming the binding of the subunits to form heterodimers as expected and in line with the findings presented by Smythies *et al* (Smythies *et al.*, 2019).

The results presented in this chapter show for the first time in MIBC that HIF1 and HIF2 bind to some unique immune-related gene binding. My results show that ~10% of all immune-related genes are bound by HIF in the T24 MIBC cell line. Although it is known that HIF has a role in directly regulating many different immune-related genes, a comprehensive list of HIF-regulated immune genes has not been generated previously, so no comment can be made on whether this proportion of immune-related gene binding is expected. Published literature tends to focus on the immune suppressive effects of HIF and its binding of specific genes that contribute towards immune evasion mechanisms due to their important effects on tumour progression and resistance to treatments (Barker *et al.*, 2015). These HIF-driven immune evasion mechanisms include, but are not limited to: binding of *CCL28* to recruit Tregs; *CXCL12* to recruit TAMs and MDSCs; *CD47* to prevent phagocytosis of immune cells; *5NTE* to increase the adenosine generating protein CD73 that induces T cell anergy; and *CD274* to increase the expression of checkpoint molecule PD-L1 that also induces T cell anergy (Semenza, 2021). In accordance with results from Chapter 3 and other published results as discussed, I show here that HIF binds to the PD-L1 gene (*CD274*) in the T24 MIBC cell line. Previous studies showed that HIF-1α binds to the PD-L1 promoter, and Noman *et al* further showed that HIF-2α does not (Barsoum *et al.*, 2014; Noman *et al.*, 2014). In my results, there are binding peaks for both HIFs when using the most lenient filtering parameter, but only HIF-2α is retained when filtering becomes more stringent. Under both 1% and 0.1% oxygen HIF-2α binding was enriched for an enhancer region of the PD-L1 gene (*CD274)*. Studies investigating the mechanisms governing PD-L1 expression at a genomic level give rise to discrepancies and have rarely included bladder cancer (Fabrizio *et al.*, 2018). As discussed in Section 3.5, there are potential differences in the interaction between HIF and PD-L1 across different tissue types, so the discrepancy is likely to be cell line/cancer type dependent. A study by Funk *et al* analysing transcription factor binding sites across 27 different tissue types found strong tissue-specific enrichments of transcription factor occupancy associated with gene regulation and disease risk (Funk *et al.*, 2020). A recent study by Bruns *et al* showed that *HIF1A* induced CD274 expression in TCGA lung, but neither breast nor melanoma cancers, which further indicates the potential for

tissue-specific HIF regulation of PD-L1 (Bruns and Beltman, 2022). A study analysing the role of HIF-1α and -2α in inducing PD-L1 expression suggests that in kidney cancer HIF-2α is the main regulator of PD-L1 expression, and not HIF-1α (Ruf, Moch and Schraml, 2016). Additional studies are needed to explore the interaction between HIF and PD-L1 in more MIBC cell lines and to further elucidate the molecular mechanisms of PD-L1 expression overall.

The results in this chapter showed that immune-related processes most enriched by HIF binding in a MIBC cell line *in vitro* are those associated with immune stimulatory pathways, not immune suppressive pathways. Interferon is a class of cytokine that has a key role in the induction of anti-tumour immune responses (Jorgovanovic *et al.*, 2020). Enrichment of immune-related pathways reveal different immune-related activities between HIF1 and HIF2. Unique HIF-1α immune-related processes are enriched for positive regulation of various interferon signalling pathways and T cell activation and differentiation. Unique HIF-2α immune-related processes are enriched for humoral responses, generic cytokine and chemokine regulation (some negative), complement activation, some innate immune responses such as toll-like receptor and lipopolysaccharide sensing signalling, as well as T cell activation and differentiation. Non-unique over represented immune-related pathways for HIF-2α specifically included associations with immune suppressive roles such as myeloid cell differentiation and TGF- β signalling. The enrichment of these immune pathways implies a broader role for HIF-2α, whilst HIF-1α was enriched for pathways involved in the stimulation of anti-tumour immune responses. These results are in agreement with published literature showing the role of both HIFs, but mostly HIF-1α, in the activation and effector functions of T cells (Doedens *et al.*, 2013; Palazon *et al.*, 2017).

Expanding on the HIF-specific results, immune-related signalling in a panel of MIBC cells under hypoxic conditions was enriched for myeloid and neutrophil signalling as seen by gene ontology analysis. Whilst still being fully elucidated, TNFα is known to have a role in tumour promoting immune signalling via the induction of NF-kB (Aggarwal, 2003). TNFα via NF-kB has been shown to inhibit anti-tumour immune responses of leukocytes and to contribute to tumour cell proliferation, migration and metastasis (Montfort *et al.*, 2019). TNFα regulates macrophage activation and function and can induce pro-inflammatory cytokine signalling (Parameswaran and Patial, 2010). IL-2 STAT5 signalling has a role in the differentiation of CD4+ cells, which is mostly well characterised for its role in maintaining

Treg differentiation (Mahmud, Manlove and Farrar, 2013; Jones, Read and Oestreich, 2020). As shown by GSEA analysis using Hallmark pathways, both TNFα via NF-kB and IL2 STAT5 signalling was significantly enriched under hypoxia, along with EMT and hypoxia-related signalling. These results indicate the potential difference between HIF-dependent and hypoxia-associated effects on immune-related signalling by tumour cells. As considerable cross-talk occurs between immune cells present in the TME, it is important to expand from *in vitro* analysis to consider relationships between the immune TME and hypoxia in the context of patient tumours.

Different immune gene signatures were used to associate immune signalling with hypoxia using transcriptomic data for MIBC from the BCON and TCGA cohorts. A 24-gene bladder cancer hypoxia gene signature assigned tumours as hypoxia high or low (Yang, Taylor, *et al.*, 2017). Heatmaps showed that tumours assigned as hypoxia high associated with higher expression of both immune suppressive (checkpoint, TGFβ -ECM, M2 TAM, exhausted CD8, macrophage, and neutrophil) and anti-tumour (M1 TAM, cytotoxic, DC, NK cell, and T cell) gene signatures. Boxplots confirmed the statistical significance of the hypoxia high versus low increases in immune-related signature expression. Hypoxia-associated increases in tumour inflammation is supported by a study performed by Chen *et al* (Chen *et al.*, 2020).

To investigate if tumour hypoxia affects the presence of immune infiltrates, I used two different immune cell deconvolution algorithms, ImSig and TIMER (Li *et al.*, 2016; Nirmal *et al.*, 2016). There was a high level of concordance between the two cohorts and algorithms, with the exception of B cells where hypoxia associated with increases using ImSig and decreases using TIMER. All of the other immune infiltrates (monocytes, macrophages, DCs, neutrophils, NK cells, and T cells) increased significantly in MIBC assigned as hypoxia high versus low. These results are further supported by three recently published bladder cancer hypoxia-associated prognostic gene signatures. All three studies showed that tumours assigned as hypoxic had increased infiltration of immune cells and an enrichment of immune-related signalling (F. Zhang *et al.*, 2021; M. Jiang *et al.*, 2021; Z. Liu *et al.*, 2021).

The lack of analysis at the protein level is a limitation of this study. The work is also limited by studying just one MIBC cell line.

In conclusion, HIF-1 and HIF-2 associate with distinct immune-related signalling in MIBC, but this is likely to be tissue type dependent and requires further elucidation. As discussed

in Section 1.4, current literature indicates that hypoxia drives an immune suppressive role in the TME. The work here expands on more recently published literature to show that hypoxia drives immune-related signalling and increases the presence of immune infiltrates in the TME of MIBC (Chen *et al.*, 2020). This immune signalling increase occurs for both suppressive and anti-tumour related immune signalling and highlights the need to consider the balance between the two when analysing hypoxia-driven immune signalling. Further work is needed to investigate the mechanisms and differences between HIF-dependent and HIF-independent hypoxia-related immune signalling in MIBC and to investigate how these affect patient survival and response to treatments.

6 A prognostic hypoxia-driven immune gene signature predicts benefit from hypoxia-modifying therapy and reflects hypoxic and inflamed tumours

6.1 Abstract

Introduction: Hypoxia and the immune tumour microenvironment (TME) are both therapeutically targetable in muscle-invasive bladder cancer (MIBC) using hypoxia-modifying therapy and immune checkpoint inhibitors (ICIs), respectively. As there is currently no single biomarker that stratifies patients for both treatments, I sought to develop an hypoxia-driven immune gene signature that could be used as one.

Materials and methods: ChIPseq and microarray experiments on MIBC cell lines produced a list of immune response-related genes that were regulated by HIF and/or differentially expressed under hypoxia (n=577). The TCGA-BLCA cohort identified genes with prognostic significance (n=8). After fitting a LASSO regression model a final six-gene signature was derived (*AHNAK, EMP1, FGF10, SMAD6, SPNS1, TRIM26*). The weighted mean was used to assign gene signature scores, which were tested in four bladder cancer cohorts (TCGA, GSE32894, GSE13507 and BCON). BCON randomised patients to radiotherapy +/- hypoxia-modifying carbogen and nicotinamide (CON). Hypoxia scores were calculated using a published hypoxia 24-gene signature and immune infiltrate fractions were determined using Cibersort. Molecular subtypes were assigned using the R package "consensusMIBC", and GSEA was performed using the "fgsea" package with Hallmark signalling pathways from MSigDB.

Results: High vs low gene signature scores associated with significantly worse overall survival in TCGA-BLCA MIBC (n=401, HR 2.71, 95% CI 1.96-3.74, p<0.001), GSE32894 (n=224, HR 8.72, 95% CI 2.6-29.12, p<0.001) and GSE13507 (n=165, HR 1.96, 95% CI 1.2-3.18, p=0.005). Scores were not prognostic in BCON (n=141, p=0.37) for the overall cohort, however, patients with high scores had a significantly better survival when given radiotherapy plus CON (RT+CON; HR 0.57, 95% CI 0.33-0.99, p=0.043). In the CON arm, the gene signature maintained prognostic significance in multivariable analyses (HR 0.52, 95% CI 0.25-1.10, p=0.085). Tumours with high versus low gene signature scores had higher hypoxia scores (p≤0.01 for all four cohorts) and associated with basal/squamous and stroma-rich molecular subtypes. High scores associated with enriched inflammation, hypoxia signalling pathways, and depleted TGF-β signalling.

Conclusion: My six-gene hypoxia-driven immune gene signature predicts poor prognosis MIBC patients who benefit from CON with radiotherapy. The signature reflects a hypoxic and inflamed TME and associates with phenotypes that are likely to respond to ICIs.

6.2 Introduction

Hypoxia is a poor prognostic factor that contributes to radiotherapy and chemotherapy resistance in MIBC (Theodoropoulos *et al.*, 2004). Hypoxic MIBC tumours benefit from the addition of hypoxia-modifying carbogen and nicotinamide (CON) (Hoskin *et al.*, 2010; Song *et al.*, 2021). A bladder cancer-specific hypoxia-associated 24-gene signature can be used as a biomarker to identify those hypoxic tumours that benefit from the addition of CON to radiotherapy to improve overall survival outcomes (Yang, Taylor, *et al.*, 2017).

The immune TME has a role in tumour response to radiotherapy and chemotherapy (Barker *et al.*, 2015). Anti-tumour immune effects are essential for the successful therapeutic clearing of tumours. These anti-tumour immune effects can be inhibited by phenotypically exhausted CD8+ T cells via the upregulation of checkpoint molecules such as PD-L1 and CTLA-4 (Chen and Mellman, 2013). A treatment option for MIBC that ameliorates immune-associated poor responses is immune checkpoint inhibitors (ICIs) (Cheng *et al.*, 2018). Currently, six ICIs are approved for advanced bladder cancer, but only ~20% of patients have sustained responses to treatment (Wołącewicz *et al.*, 2020). Therefore, there is a need to find biomarkers that predict benefit of ICIs.

There is evidence that bladder cancers with an inflamed TME benefit from ICIs and that inflamed TMEs are represented by a basal molecular subtype (Pfannstiel *et al.*, 2019; Kamoun *et al.*, 2020; H. Zhang *et al.*, 2021). Tumours with high TGF-β signalling and few immune infiltrates in bladder cancer are less likely to benefit from ICIs (Mariathasan *et al.*, 2018). It has recently been shown that ICI responders had high immune response signalling and basal/squamous features whilst non-responders had increased angiogenesis and TGF-β signalling (Powles *et al.*, 2021).

A TCGA based study that correlated *HIF1A* gene expression with tumour immunity and clinical outcomes showed patients with high versus low *HIF1A* gene expression had worse survival outcomes. The authors showed that in bladder cancer *HIF1A* associated with increased expression of both anti-tumour immune signatures such as such as CD8+ T cells, IFN response, and M1 macrophages as well as immune suppressive signatures such as TGF-β signalling and M2 macrophages, but that the correlations with immune suppressive signatures were stronger. The authors showed that high *HIF1A* expression associated with response to ICI treatment in a kidney cancer cohort (Chen *et al.*, 2020). Three bladder cancer hypoxia-associated gene signatures were published in 2021 that showed high

signature scores represent inflamed TMEs by associating with increased immune infiltrates and signalling. All of the signatures were prognostic and hypothesised that patients with high scores would benefit from ICIs (F. Zhang *et al.*, 2021; M. Jiang *et al.*, 2021; Z. Liu *et al.*, 2021).

Gene signatures are useful biomarkers that can be used to personalise treatment strategies to improve overall survival outcomes (Yang and West, 2019). The aim of this study was to develop a prognostic hypoxia-driven immune gene signature that would identify patients likely to fail standard-of-care treatments and predict benefit from additional targeted therapies, specifically hypoxia-modifying therapies, to improve survival.

6.3 Materials and methods

6.3.1 Cohorts used

The cohorts were obtained as described in Section 2.8.1. TCGA (n=405), GSE32894 (n=224), GSE13507 (n=187) and BCON cohorts (n=141) were used. BCON was a prospective multicentre phase III clinical trial registered as CRUK/01/003 of which the protocol and conclusions are published in the initial report (Hoskin *et al.*, 2010) and updated for long-term clinical outcomes (Song *et al.*, 2021). Patients were randomised to receive radiotherapy (RT) +/- CON (RT+CON). The updated long-term clinical outcomes were used in all analyses. TCGA and BCON were filtered to include MIBC only.

6.3.2 ChIPseq data generation

ChIPseq was performed as detailed in Section 2.6. In brief, T24 bladder cancer cells were cultured for 24 h in both 0.1% and 1% O_2. The protein-DNA interactions were cross-linked using ChIP cross-link gold and 1% formaldehyde before lysing the cells and shearing the chromatin into 200-300bp fragments using a Biorupter Pico. Antibodies against HIF-1α, HIF-2α and HIF-1β and Dynabeads Protein G were used for immunoprecipitation. The fragments were de-cross-linked and the DNA eluted using the phenol chloroform method. qPCR was used to validate the ChIP experiment before the samples were sequenced and mapped by the CRUK MI core facilities.

6.3.3 Muscle-invasive bladder cancer cell line microarray data generation

As described in Section 2.7, microarray data were generated for a panel of MIBC cell lines (T24, J82, UMUC3 and HT1376) under various oxygen concentrations (21%, 1%, 0.2% and 0.1%). Cells were cultured for 24 h in each condition and RNA was extracted using RNeasy

Plus Mini Kit (Qiagen). Gene expression arrays were generated using Clariom S pico HT human assay by Yourgene Health and batch corrected using ComBat function from the R package "sva" to produce $\log_2$ summarised gene level expression.

6.3.4 LASSO regression model

The LASSO regression model was used as described in Section 2.8.4. In brief, the LASSO model was applied using the R package "glmnet" and those genes with a coefficient shrunken to 0 were removed from the list before running the model again. The final coefficients were used to apply the weighted mean to each sample using the predict function.

6.3.5 Assigning molecular subtypes

Consensus molecular subtypes were applied using the R package "consensusMIBC", as detailed in Section 2.8.2. First order subtyping was applied by assigning all three luminal subtypes (LumP, LumNS and LumU) to luminal, and basal/squamous and stroma-rich subtypes to basal. NE-like were removed from the first order analyses due to small numbers.

6.3.6 GSEA, Cibersort and use of published gene signatures

Section 2.8.5 describes how immune cell fractions were imputed for each sample using the Cibersort algorithm. The R package "limma" was used to obtained significant ($p<0.1$) differentially expressed genes for high vs low scores. Hallmark pathways were downloaded using "msigdb" and the package "fgsea" was used to perform GSEA. The results show which Hallmark pathways were significantly (p value <0.05) up/down regulated, which is further detailed in Section 2.8.8. Hypoxia scores and CD8 and IFNγ signalling scores were assigned using the relevant gene signatures as described in Section 2.8.6.

6.3.7 Statistics

All of the analyses were performed using R version and RStudio and stated packages used to analyse data and calculate significance. Parametric statistics (t-test, Pearson) were used when data were normally distributed and non-parametric statistics (Wilcoxon test, Spearman) were used when the data were non-normally distributed. Kaplan-Meier curves were used to assess relationships with overall survival using the "survival" and "survminer" packages which use Cox proportional hazard models and log-rank tests to calculate p values.

Survival significance, multivariable analysis and statistical tests were performed using the "survival" package and the results were tabulated using the "gtsummary" package.

6.4 Results

6.4.1 Curating bladder-specific hypoxia-driven immune-related seed genes

A list of seed genes (expressed at the RNA level) that are hypoxia-driven and immune-related in bladder cancer cell lines was obtained using a ChIPseq and a microarray dataset as shown in Figure 6.1. A manually curated list of immune-related genes was obtained using unique immune-related gene lists from ImmPort, Hallmark and published literature (n=2954; Table 6.1). Those immune-related genes where HIF-1α, HIF-2α or HIF-1β had bound were identified using the ChIPseq protein coding peaks from T24 MIBC cell line cultured under both 0.1% and 1% O_2 (n=1872). The immune-related genes that were differentially expressed in any of four MIBC cell lines (T24, HT1376, J8, UMUC3) under either 0.1%, 0.2% or 1% O_2 were identified using microarray gene expression data (n=731). Those bladder cancer-specific hypoxia-driven immune-related genes expressed in both derived lists (n=577) were used as the seed genes for deriving a prognostic gene signature.

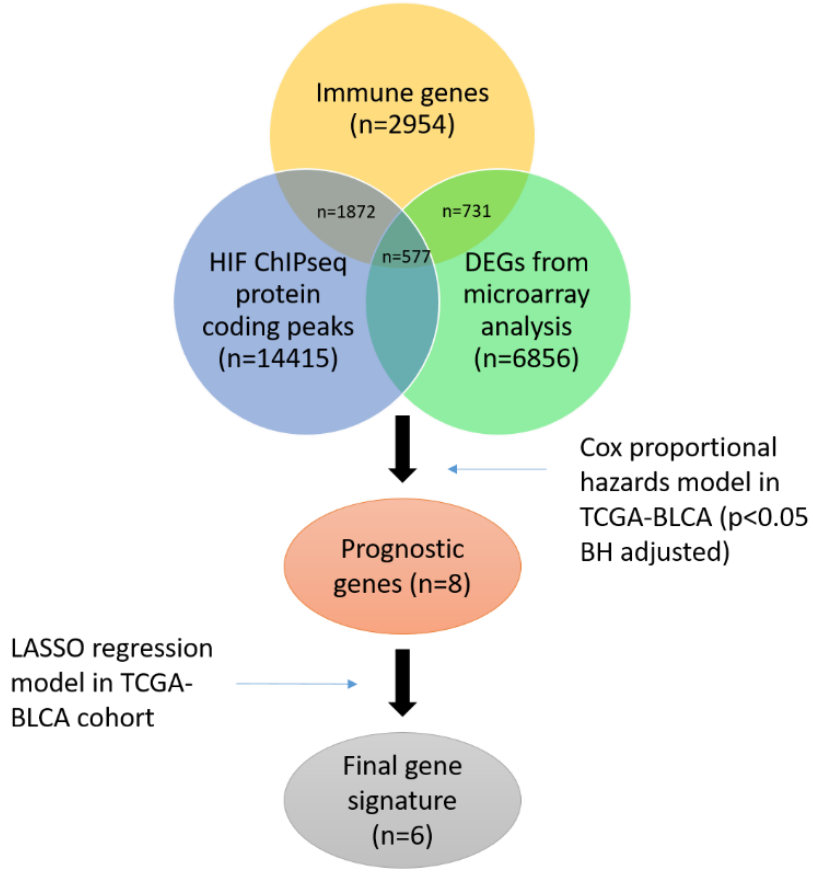

Figure 6.1 Schematic illustrating how the gene signature was derived.

Table 6.1. The names and sources of lists that were used to curate a list of immune-related genes.

Name	Source	Number of genes
Antigen processing and presentation	ImmPort	148
Antimicrobials	ImmPort	535
BCR signalling pathway	ImmPort	272
Chemokines	ImmPort	102
Chemokines receptors	ImmPort	53
Cytokines	ImmPort	456
Cytokines receptors	ImmPort	307
Interferons	ImmPort	17
Interferons receptors	ImmPort	3
Interleukins	ImmPort	47
Interleukins receptors	ImmPort	42
Natural killer cell	ImmPort	134
TCR signalling pathway	ImmPort	291
TGF-β family members	ImmPort	33
TGF-β family members receptors	ImmPort	12
TNF family members	ImmPort	12
TNF family members receptors	ImmPort	19
Immune-related genes	He *et al*	706
Immune suppressive markers	Lei *et al*	133
Complement	Hallmark	200
IL2 STAT5 signalling	Hallmark	199
IL6 JAK STAT3 signalling	Hallmark	87
Inflammatory response	Hallmark	200
Interferon alpha response	Hallmark	97
Interferon gamma response	Hallmark	200
PI3K Akt MTOR signalling	Hallmark	105
TGF-β signalling	Hallmark	54
TNFα signalling via NFκB	Hallmark	200
P53 pathway	Hallmark	200
WNT ß-catenin signalling	Hallmark	42

6.4.2 Deriving a prognostic gene signature

The curated list of seed genes were tested for prognostic significance (adjusted p value < 0.05) using Cox proportional hazard models on the TCGA bladder cancer cohort (n=8). A LASSO regression model resulted in a final six-gene signature: *AHNAK, EMP1, FGF10, SPNS1, SMAD6* and *TRIM26*. Gene scores were calculated as the weighted mean using the LASSO coefficients. Evaluation of the median vs the upper quartile as the cut-off for stratification showed the median best separated the cohort and was used to stratify patients into low or

high score thereafter. Kaplan-Meier curves show that in the TCGA bladder cancer cohort patients with a high vs low score had a worse prognosis (HR 2.71, 95% CI 1.96-3.74, p<0.001; Figure 6.2). Multivariable Cox proportional hazard models for overall survival in the TCGA cohort showed the derived gene signature maintained independent prognostic significance (HR 2.06, 95% CI 1.40-3.03, p<0.001) alongside tumour stage four (HR 2.37, 95% CI 1.52-3.69, p<0.001). No significance was seen for molecular subtype (HR 1.20, 95% CI 0.76-1.88, p=0.43) nor the 24-gene hypoxia score (HR 1.10, 95% CI 0.71-1.70, p=0.67; Table 6.2).

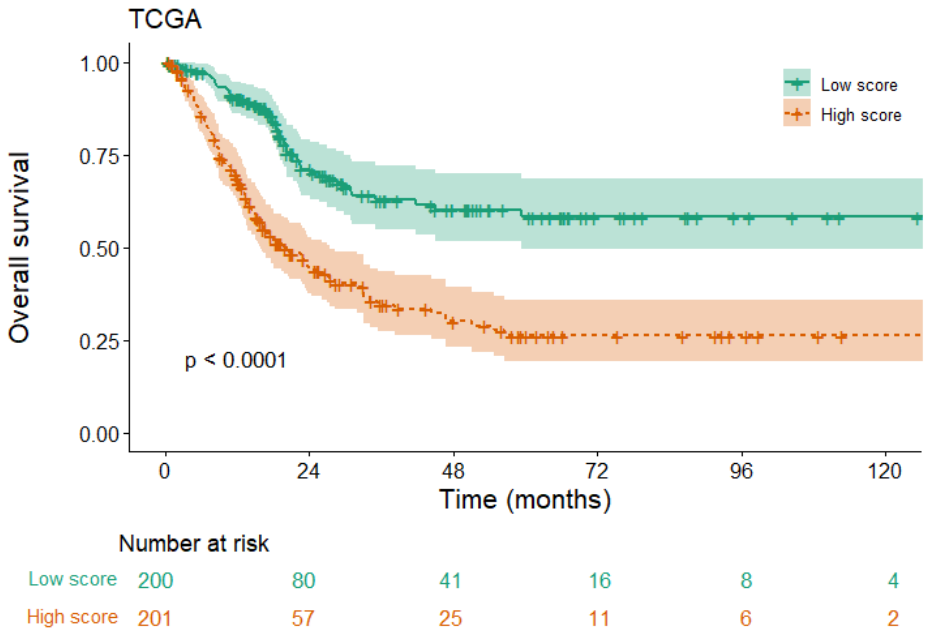

Figure 6.2. A six-gene hypoxia-driven immune gene signature is prognostic in the TCGA-BLCA cohort.
Kaplan-Meier plot showing 10-year overall survival for the TCGA-BLCA cohort with patients stratified by 6-gene scores. Scores were applied using the weighted mean and stratified using the median as the cut-off. p values are log-rank tests as calculated by the R packages "survival" and "survminer".

Table 6.2. Multivariable analyses for overall survival in the TCGA-BLCA cohort

Characteristic	HR[1]	95% CI[1]	p-value
Gender			
Male	—	—	
Female	1.24	0.87, 1.78	0.23
Stage			
2	—	—	
3	1.37	0.86, 2.18	0.19
4	2.37	1.52, 3.69	<0.001
Radiotherapy			
Yes	—	—	
No	0.67	0.31, 1.45	0.31
Hypoxia score			
Low	—	—	
High	1.10	0.71, 1.70	0.67
Molecular subtype			
Luminal	—	—	
Basal	1.20	0.76, 1.88	0.43
Gene signature			
Low score	—	—	
High score	2.06	1.40, 3.03	<0.001

[1] HR = Hazard Ratio, CI = Confidence Interval. p values represent log-rank tests as calculated by the 'survival' package in R.

6.4.3 Validation of the gene signature

The gene signature was validated in three external cohorts (GSE32894, GSE13507, and BCON). In all cohorts, apart from BCON, the six genes separated the samples into two distinct clusters (Figure 6.3). One out of six genes was missing in GSE32894 data (*FGF10*). All six genes were present in GSE13507. Two of the six genes were missing in BCON data (*EMP1* and *SMAD6*). Figure 6.4 shows high vs low scores associated with a significantly worse survival in GSE32894 (n=224, HR 8.72, 95% CI 2.6-29.12, p<0.001) and GSE13507 (n=165, HR 1.96, 95% CI 1.2-3.18, p=0.005), but not in the overall BCON cohort (n=141, p=0.37). In multivariable analysis for the GSE32894 and GSE13507 cohorts the derived score did not retain independent significance (Table 6.3-6.4). In the GSE32894 cohort (n=224), tumours were disproportionately of a low stage (non-muscle invasive) as 173 were <T2 (Ta=110, T1=63), 49 were ≥ T2 (T2=3, T3=7, T4=1) and 1 was of an unknown stage. In the GSE13507 cohort (n=165) tumours were also more represented by non-muscle-invasive tumours as 104 were < T2 (Ta=24, T1=80) and 61 were ≥ T2 (T2=31, T3=19, and T4=11).

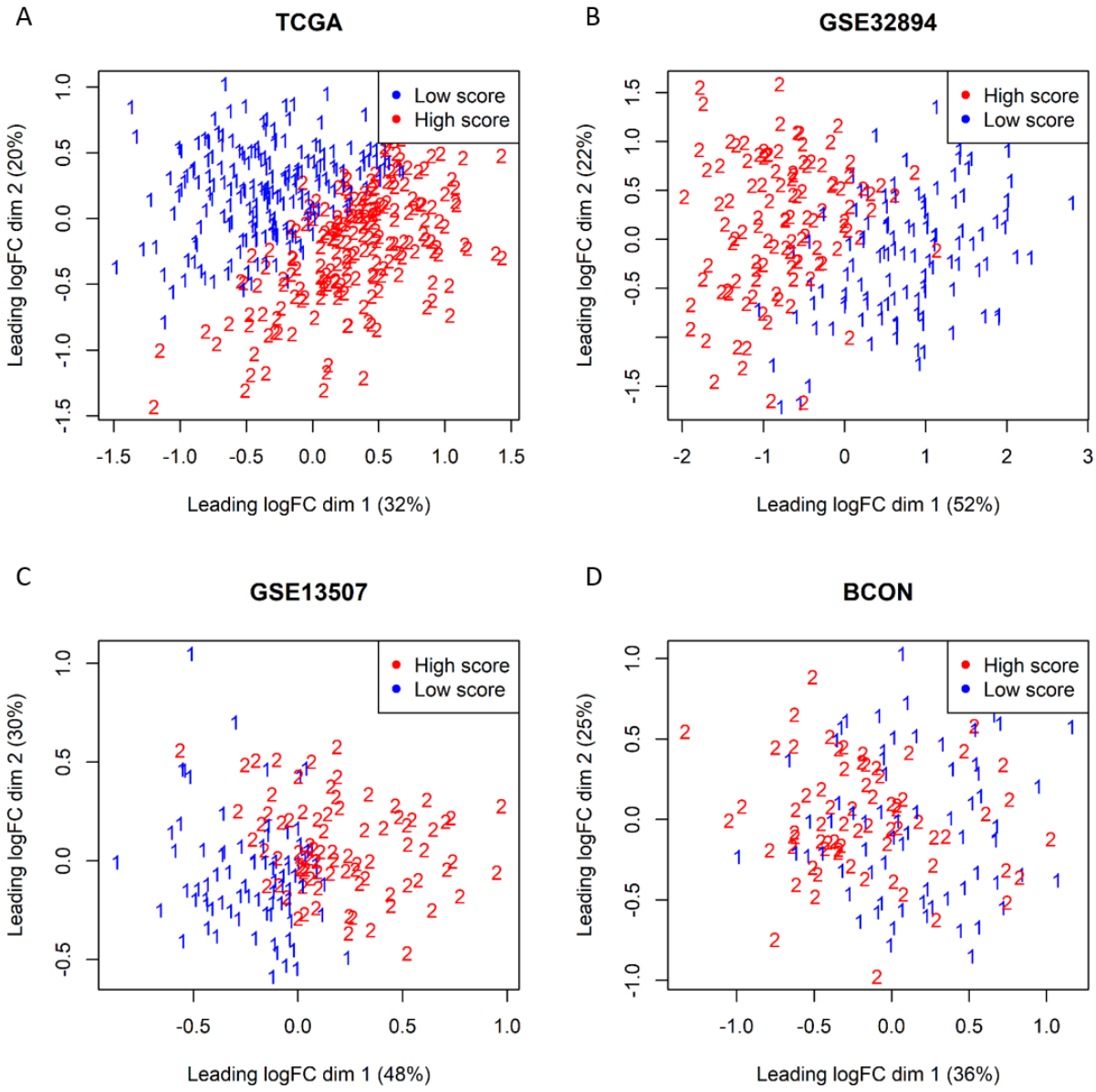

Figure 6.3 Multidimensional scaling (MDS) plots illustrating how the expression of the six signature genes separate the samples when labelled low and high scores in A) TCGA, B) GSE32894, C) GSE13507 and D) BCON cohorts.
MDS was calculated using "limma" package in R.

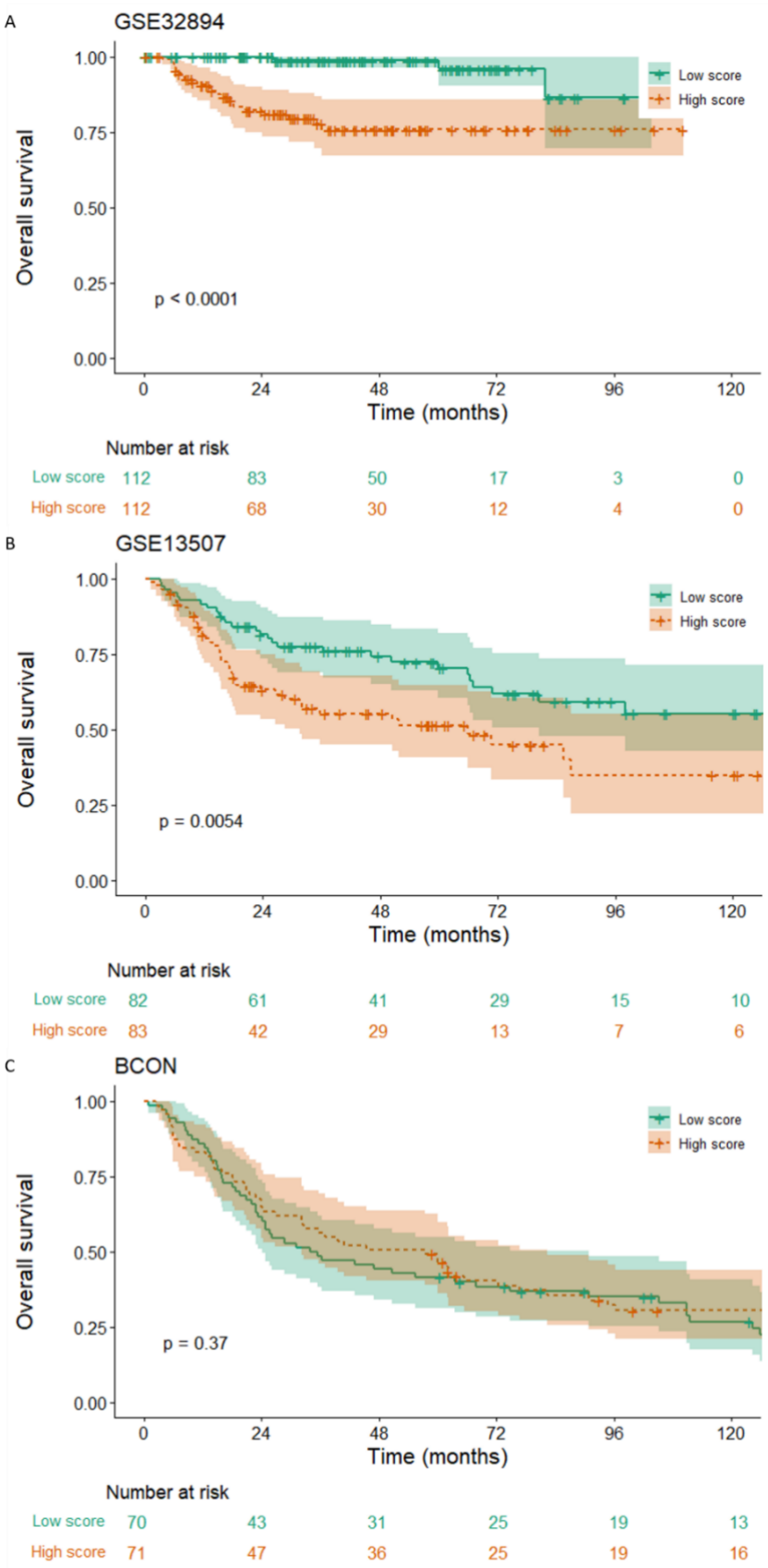

Figure 6.4. Kaplan-Meier plots showing 10-year overall survival according to gene signature scores for A) TCGA-BLCA cohort, B) GSE32894 cohort and C) GSE13507 cohort.
Score is applied using the weighted mean and stratified using the median as the cut-off. p values are log-rank tests as calculated by the R packages "survival" and "survminer".

Table 6.3 Multivariable analyses for overall survival in the GSE32894 cohort

Characteristic	HR[1]	95% CI[1]	p-value
Age	1.00	0.94, 1.06	0.90
Gender			
Male	—	—	
Female	0.53	0.18, 1.58	0.26
Stage			
<T1	—	—	
≥T2	34.9	7.16, 170	<0.001
Gene signature			
Low score	—	—	
High score	1.50	0.40, 5.67	0.55

[1] HR = Hazard Ratio, CI = Confidence Interval. p values represent log-rank tests as calculated by the 'survival' package in R.

Table 6.4 Multivariable analyses for overall survival in the GSE13507 cohort

Characteristic	HR[1]	95% CI[1]	p-value
Age	1.08	1.05, 1.11	<0.001
Gender			
Male	—	—	
Female	1.13	0.61, 2.07	0.70
Stage			
<T1	—	—	
≥T2	2.33	1.22, 4.45	0.010
Grade			
Low	—	—	
High	1.25	0.69, 2.24	0.46
Chemotherapy			
No	—	—	
Yes	1.48	0.70, 3.10	0.30
Gene signature			
Low score	—	—	
High score	0.94	0.54, 1.63	0.82

[1] HR = Hazard Ratio, CI = Confidence Interval. p values represent log-rank tests as calculated by the 'survival' package in R.

6.4.4 The gene signature is bladder cancer specific

The signature was tested for prognostic significance in six other cancers available from TCGA: breast invasive carcinoma (BRCA), cervical squamous cell carcinoma and endocervical adenocarcinoma (CESC), esophageal carcinoma (ESCA), lung squamous cell carcinoma (LUSC), pancreatic adenocarcinoma (PAAD), and prostate adenocarcinoma (PRAD). The signature had no prognostic relevance (BRCA, p=0.38; CESC = 0.85; ESCA, p=0.97; LUSC, p=0.66; PAAD, p=0.53, PRAD = 0.55; Figure 6.5).

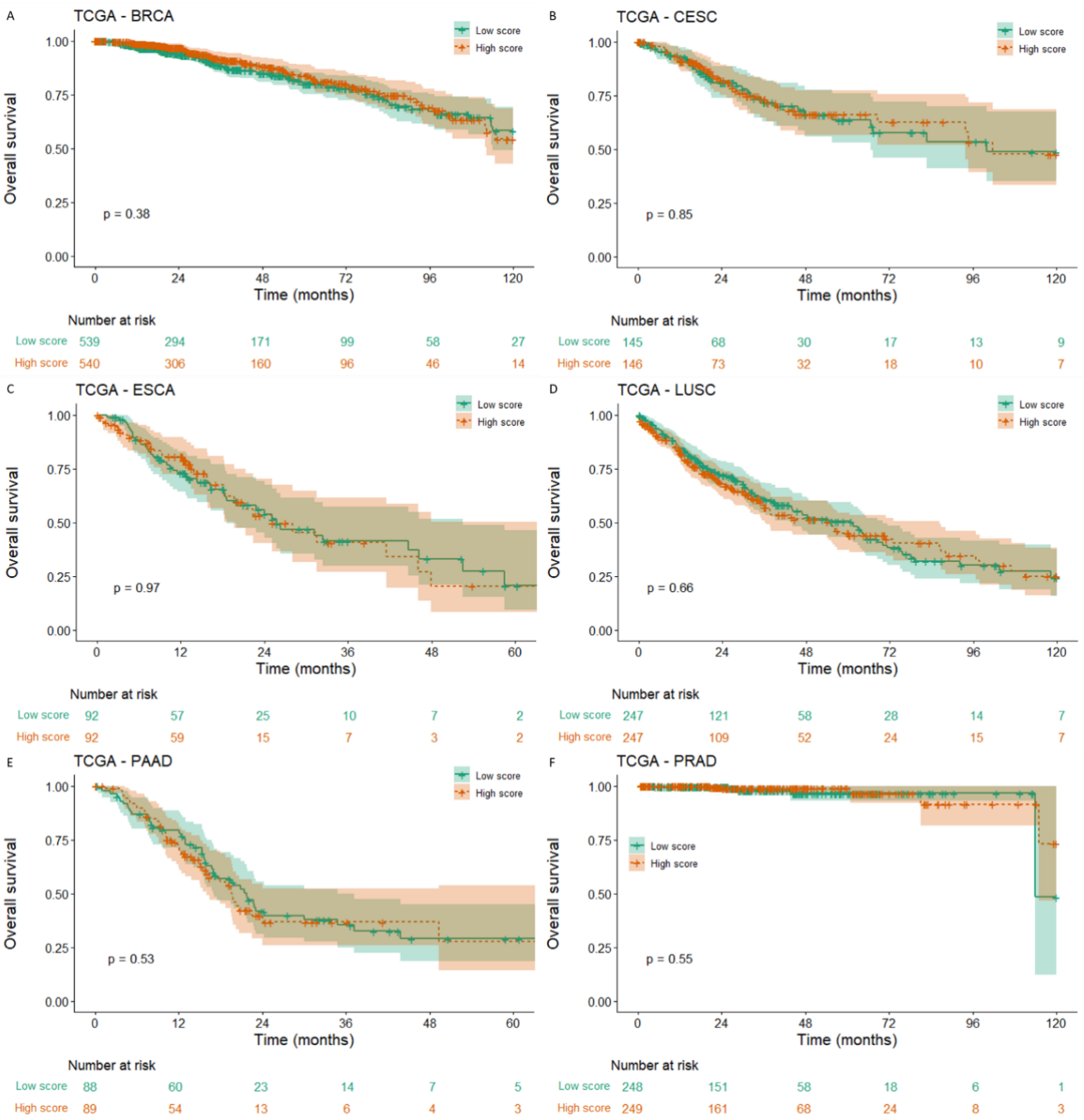

Figure 6.5 Kaplan-Meier plots showing overall survival according to gene signature score for the TCGA cohorts: A) breast invasive carcinoma, B) cervical squamous cell carcinoma and endocervical adenocarcinoma, C) lung squamous cell carcinoma, D) esophageal carcinoma, E) pancreatic adenocarcinoma, and F) prostate adenocarcinoma.
Scores were applied using the weighted mean and stratified using the median as the cut-off. p values are log-rank tests as calculated by the R packages “survival” and “survminer”.

6.4.5 High gene signature scores predict response to hypoxia-modifying therapy and reflect hypoxic tumours

High gene signature scores associated with an improved overall survival for the RT+CON arm of the BCON trial (HR 0.55, 95% CI 0.31-0.97, p=0.035), but no difference was observed between low and high scores in the RT arm (p=0.32; Figure 6.6 A, B). In the RT arm high score patients had a significantly worse local progression free survival (HR 1.73, 95% CI 1.04-2.89, p=0.033), but no difference was observed in the RT+CON arm (p=0.69; Figure 6.6 C, D). No prognostic difference was observed regarding treatment when patients had a low gene signature score for either overall (p=0.37; Figure 6.7 A) or local progression free survival (p=0.60; Figure 6.7 C). However, patients with a high gene signature score had a significantly better overall survival when given RT+CON vs RT alone (HR 0.57, 95% CI 0.33-0.99, p=0.043; Figure 6.7 B), and a non-significantly better local progression free survival (HR = 0.63, 95% CI 0.38-1.1, p=0.075; Figure 6.7 D).

Gene signature scores positively correlated with the 24-gene hypoxia score and high scores had a significantly higher 24-gene hypoxia scores in all four cohorts (TCGA, p<0.001; GSE32894, p<0.001; GSE13507, p<0.001; BCON, p=0.004; Figure 6.8). In the separate treatment arms of BCON the derived hypoxia-driven immune gene signature outperformed the existing 24-gene hypoxia score shown by univariable Cox proportional hazard models to analyse overall survival for high versus low scores (Table 6.5). Table 6.6 summarises the findings from a multivariable analysis of overall survival in the CON arm of the BCON cohort showing the trend for the immune signature to retain prognostic significance (HR 0.52, 95% CI 0.25-1.10, p=0.085) alongside age (HR 1.05, 95% CI 1.01-1.09, p=0.013). No significance was seen for necrosis (p=0.54), molecular subtype (p=0.86), or tumour stage four (p=0.92).

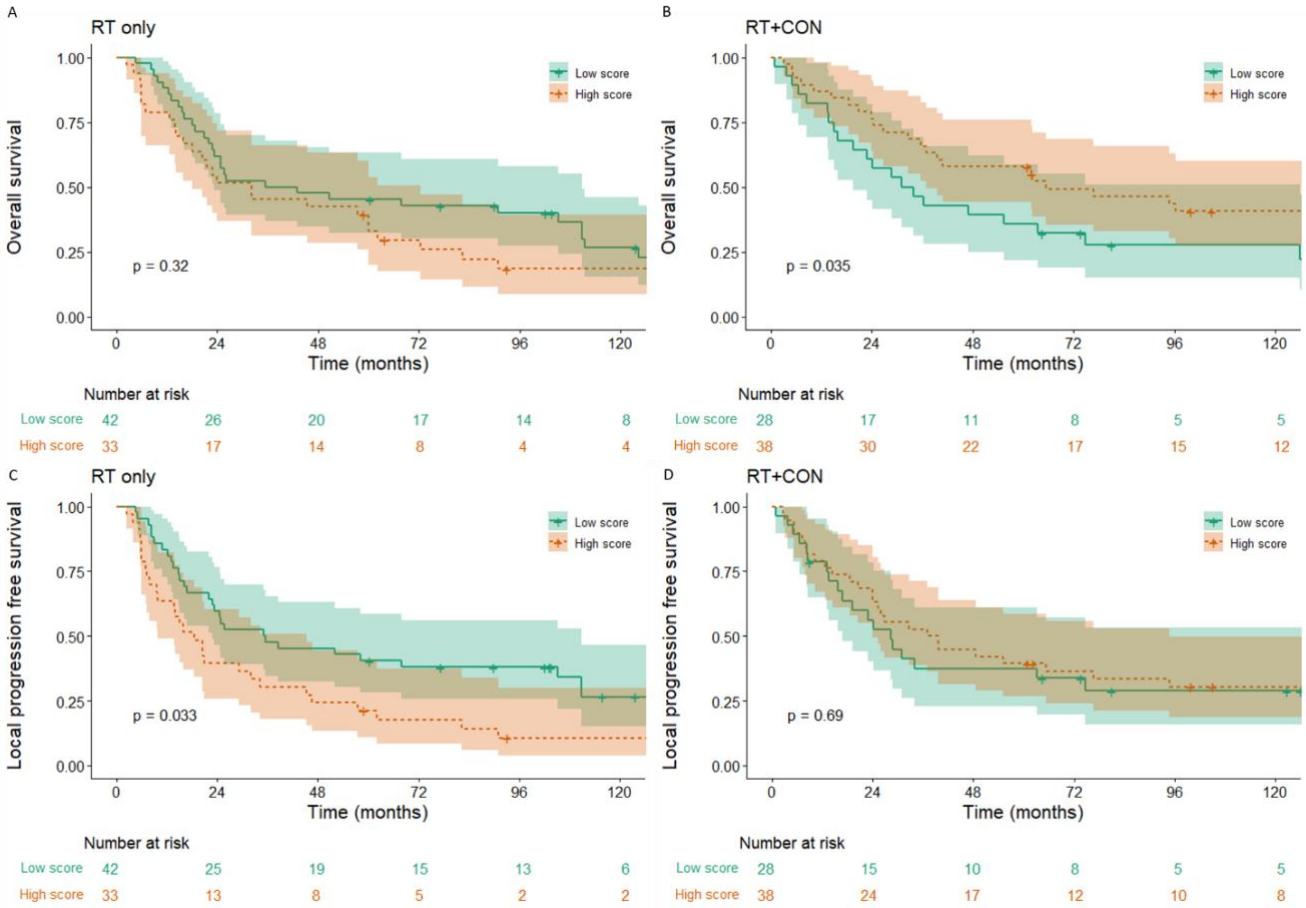

Figure 6.6 Kaplan-Meier plots for treatment arms of BCON according to gene signature scores.
Overall 10-year survival for A) RT only treatment arm and B) RT+CON treatment arm. Local progression free survival for C) RT only treatment arm and D) RT+CON treatment arm. Score is applied using the weighted mean and stratified using the median as the cut-off. p values are log-rank tests as calculated by the R packages “survival” and “survminer”.

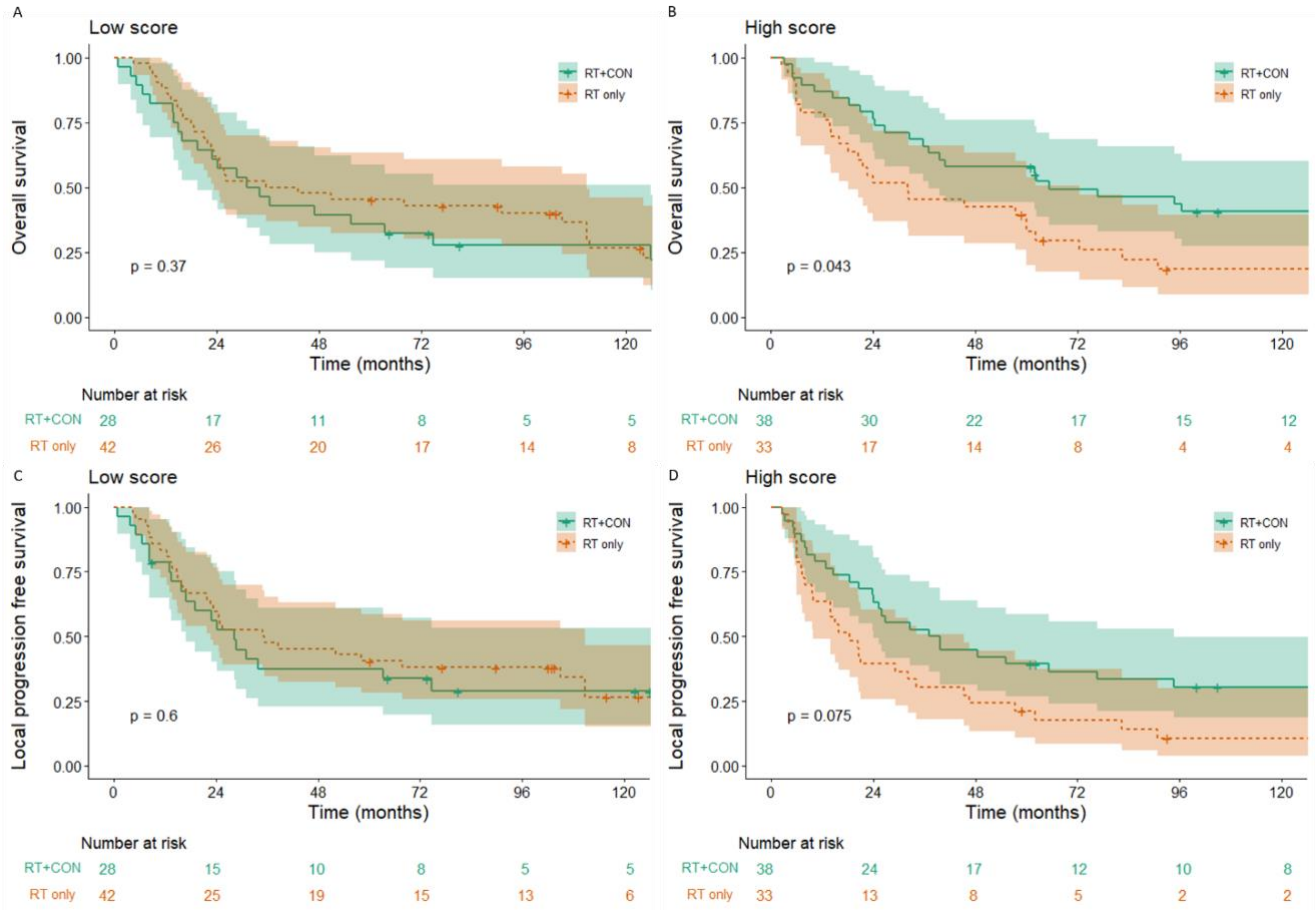

Figure 6.7. Kaplan-Meier plots for gene signature score high and low according to treatment arm of BCON. Overall 10-year survival for A) low gene signature score patients and B) high gene signature score patients. Local progression free survival for C) low gene signature score patients and D) high gene signature score patients. Score is applied using the weighted mean and stratified using the median as the cut-off. p values are log-rank tests as calculated by the R packages “survival” and “survminer”.

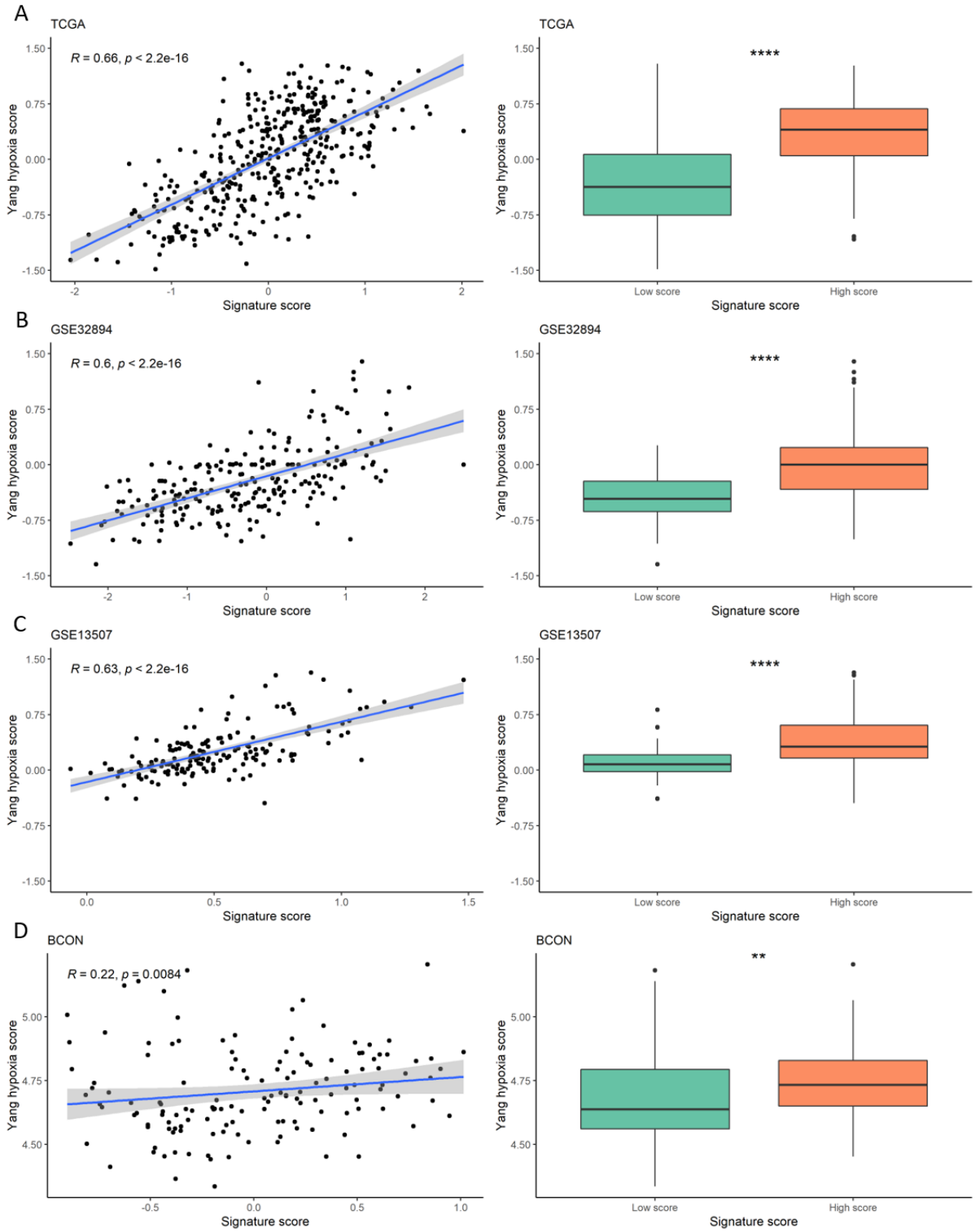

Figure 6.8. Graphs showing the correlation between 24-gene hypoxia signature scores and the immune signature scores in the A) TCGA, B) GSE23894, C) GSE13507, and D) BCON cohorts.
Hypoxia scores were calculated as defined by Yang *et al.* and plotted against gene signature scores. R^2 values were calculated using Spearman's correlation coefficient and the p values represent a linear model analysis. Boxplot statistical tests are Wilcox tests with p values represented as follows: ns = not significant, *<0.05, **<0.01, ***<0.001, ****<0.0001.

Table 6.5 Univariable analysis for overall survival in the treatment arms of the BCON cohort

Treatment arm	Characteristic	HR[1]	95% CI[1]	p-value
RT only	Continuous hypoxia signature score	5.22	1.10, 24.75	0.037
	High hypoxia signature score	1.59	0.95, 2.66	0.077
	Continuous immune signature score	1.75	1.03, 2.99	0.039
	High immune signature score	1.30	0.78, 2.18	0.32
RT+CON	Continuous hypoxia signature score	1.20	0.21, 6.96	0.84
	High hypoxia signature score	0.99	0.57, 1.73	0.98
	Continuous immune signature score	0.58	0.30, 1.11	0.099
	High immune signature score	0.55	0.31, 0.97	0.035

[1] HR = Hazard Ratio, CI = Confidence Interval. p values represent log-rank tests as calculated by the 'survival' package in R.

Table 6.6. Multivariable analysis of overall survival in the CON arm of the BCON cohort

Characteristic	HR[1]	95% CI[1]	p-value
Age	1.05	1.01, 1.09	0.013
Gender			
Male	—	—	
Female	0.89	0.41, 1.95	0.77
Tumour stage			
2	—	—	
3	1.14	0.53, 2.46	0.74
4	1.12	0.13, 9.63	0.92
Grade			
2	—	—	
3	0.68	0.31, 1.52	0.35
Hypertension			
Absent	—	—	
Present	0.86	0.40, 1.86	0.71
Necrosis			
Absent	—	—	
Present	0.82	0.44, 1.54	0.54
Molecular subtype			
Luminal	—	—	
Basal	0.95	0.50, 1.79	0.86
Gene signature			
Low score	—	—	
High score	0.52	0.25, 1.10	0.085

[1] HR = Hazard Ratio, CI = Confidence Interval. p values represent log-rank tests as calculated by the 'survival' package in R.

6.4.6 The gene signature associates with molecular subtypes and stems from stromal/immune cells

The consensus molecular classifier was used to assign molecular subtypes and basal/squamous and stroma-rich subtypes associated with higher gene signature scores, whilst lower gene signature scores associated with the three luminal subtypes (LumP, LumNS and LumU; Figure 6.9 A, C, E). Further stratification into first order luminal and basal molecular subtypes demonstrated basal subtypes have a significantly higher gene signature score than luminal ($p<0.001$ for TCGA, GSE32894, and GSE13507; Figure 6.9 B, D, F). High gene signatures scores also associated with higher ESTIMATE immune and stromal scores and lower tumour purity in all three cohorts (Figure 6.10-6.12).

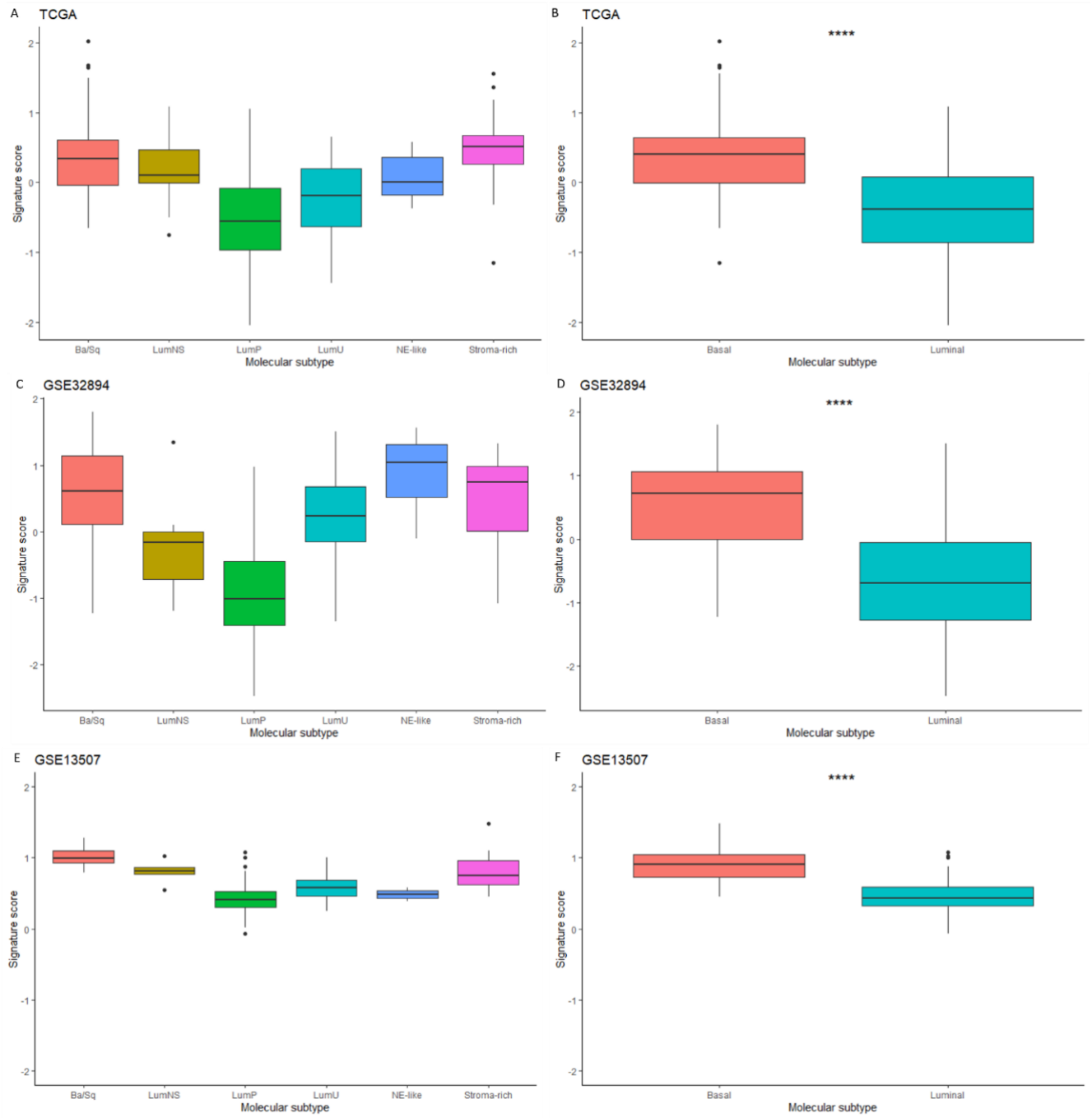

Figure 6.9. Boxplots showing the associations between molecular subtype and the gene signature scores. Molecular subtypes were assigned using "consensusMIBC" package in R and plotted against the gene signature score for A) TCGA, C) GSE32894, and E) GSE13507 cohorts. Subtypes were then grouped into luminal (LumP, LumU, LumNS), basal (basal/squamous and stroma-rich), and NE-Like subtypes were excluded, and correlated with the gene signature score for B) TCGA, D) GSE23894, and F) GSE13507 cohorts. Statistical tests are wilcox tests with p values represented as follows: ns = not significant, *<0.05, **<0.01, ***<0.001, ****<0.0001.

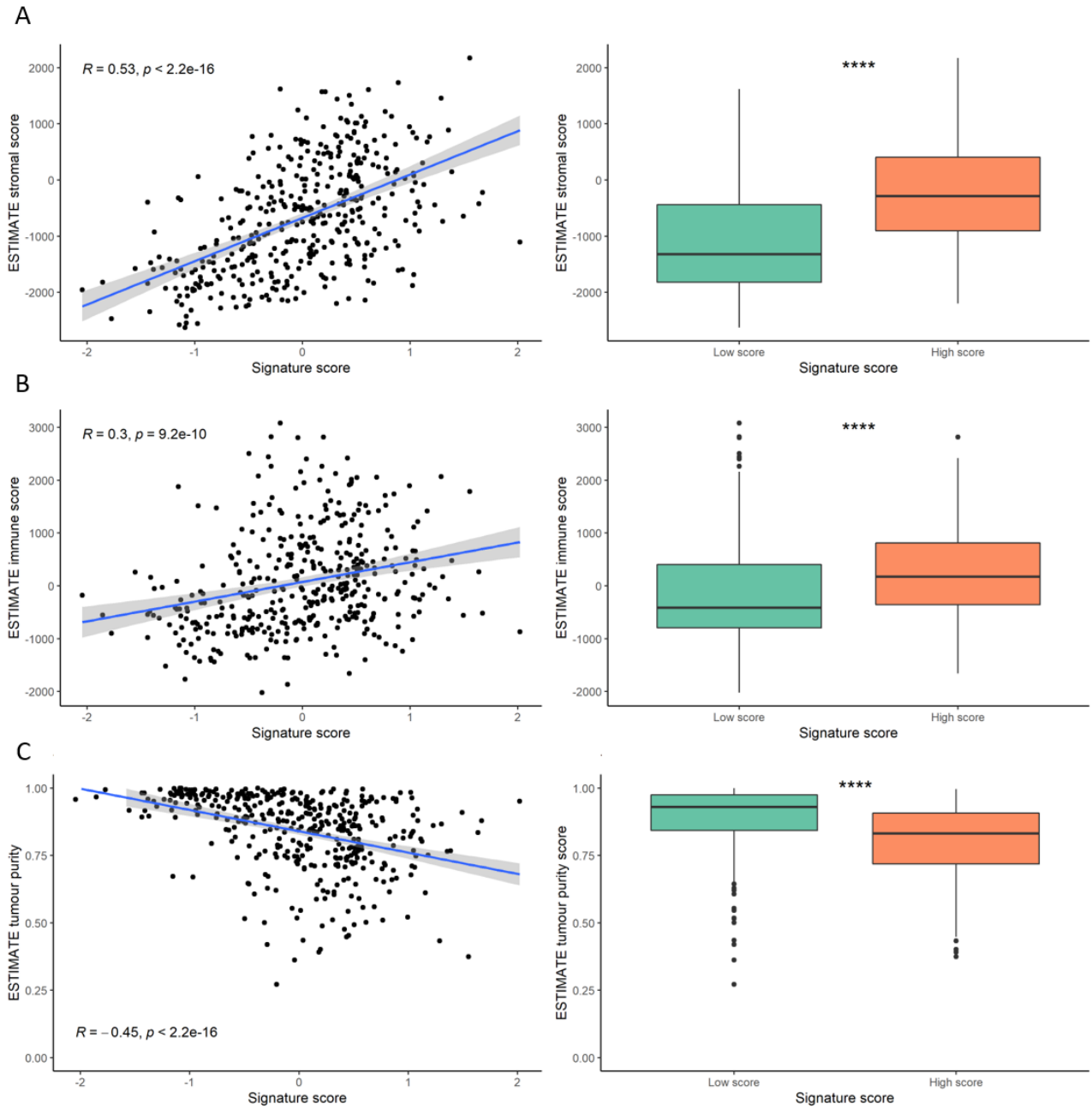

Figure 6.10 Signature scores associate with higher ESTIMATE stromal (A) and immune (B) and lower tumour purity (C) scores in the TCGA cohort.
ESTIMATE scores were plotted using the R package "estimate". R^2 values were calculated using Spearman's correlation coefficient and the p values represent a linear model analysis. Boxplot statistical tests are wilcox tests with p values represented as follows: ns = not significant, *<0.05, **<0.01, ***<0.001, ****<0.0001.

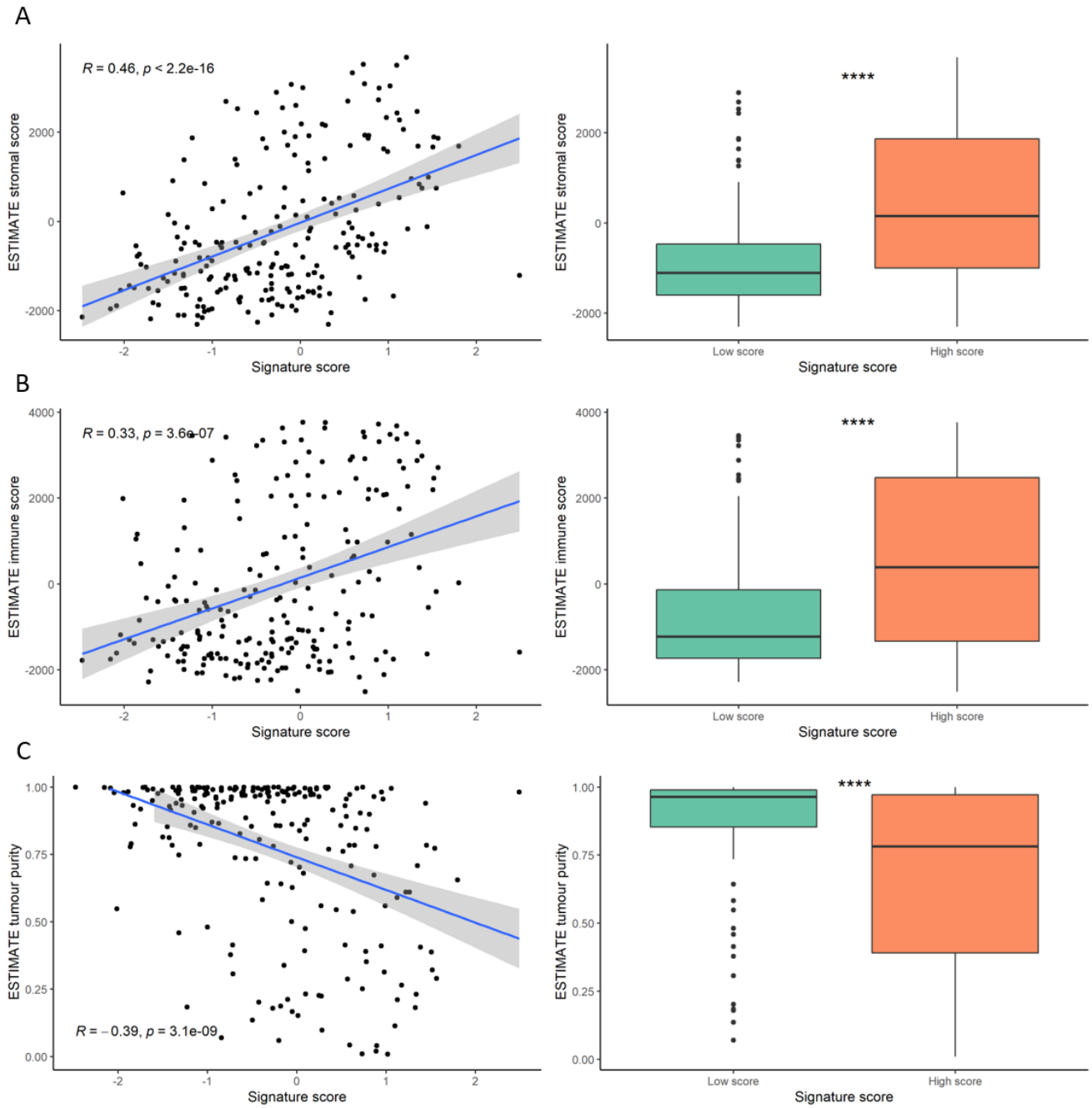

Figure 6.11 Signature scores associate with higher ESTIMATE stromal (A) and immune (B) and lower tumour purity (C) scores in the GSE32894 cohort.
ESTIMATE scores were plotted using the R package "estimate". R^2 values were calculated using Spearman's correlation coefficient and the p values represent a linear model analysis. Boxplot statistical tests are wilcox tests with p values represented as follows: ns = not significant, *<0.05, **<0.01, ***<0.001, ****<0.0001.

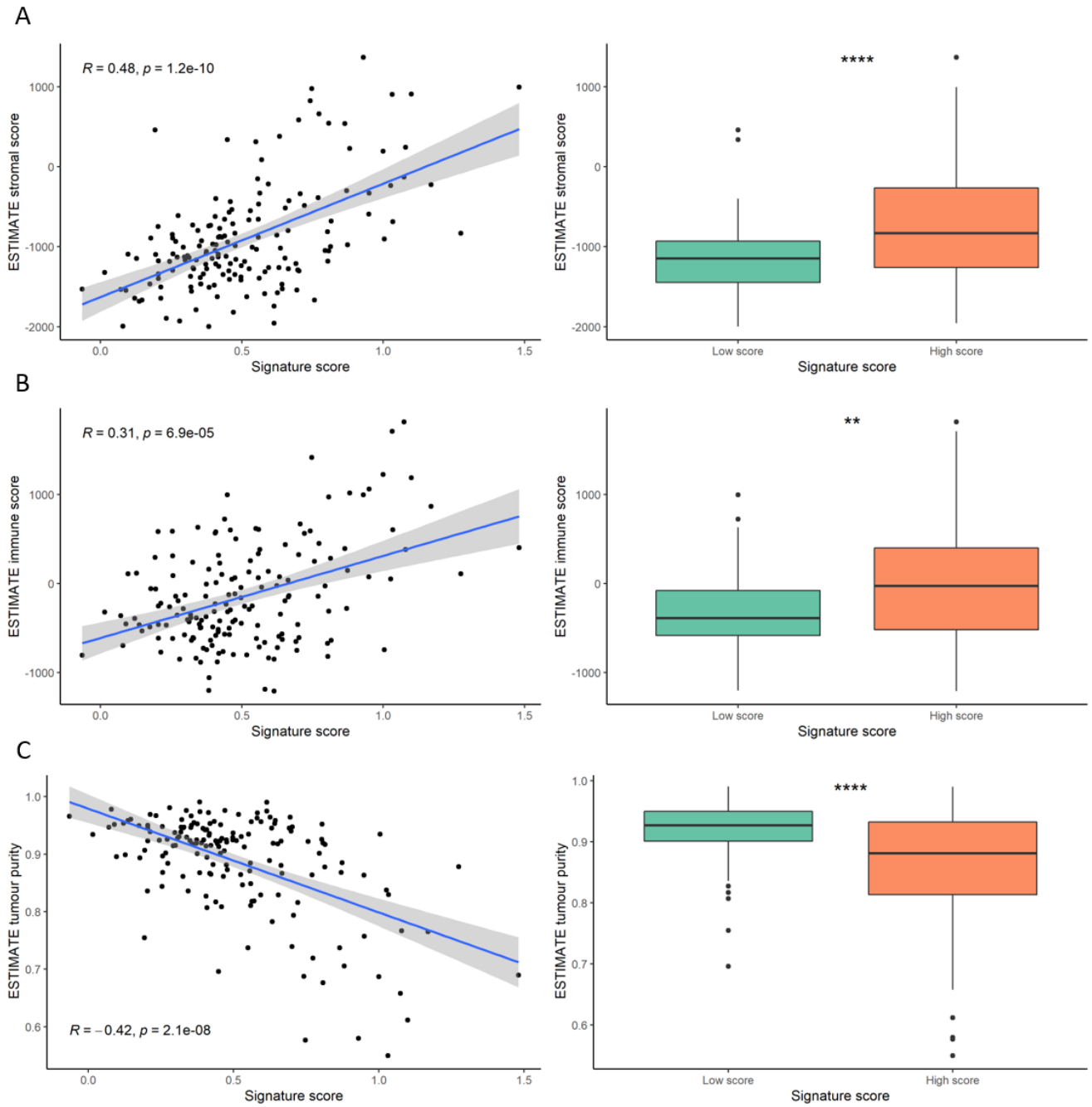

Figure 6.12. Signature scores associate with higher ESTIMATE stromal (A) and immune (B) and lower tumour purity (C) scores in the GSE13507 cohort.
ESTIMATE scores were plotted using the R package "estimate". R^2 values were calculated using Spearman's correlation coefficient and the p values represent a linear model analysis. Boxplot statistical tests are wilcox tests with p values represented as follows: ns = not significant, *<0.05, **<0.01, ***<0.001, ****<0.0001.

6.4.7 High gene signature scores represent an inflamed tumour microenvironment

Gene set enrichment analysis (GSEA) was performed on the cohorts to evaluate which Hallmark pathways had significantly (adjusted p value <0.05) up/down regulated expression in tumours with high versus low gene signature scores (Table 6.7-6.9). Hallmark_hypoxia signalling was significantly upregulated in all three cohorts ($p \leq 0.001$ for all). Pathways associated with hypoxia: Hallmark_unfolded protein_response and Hallmark_glycolysis, were upregulated in both GSE32894 ($p=0.03$ and $p=0.007$, respectively) and GSE13507 ($p=0.01$ and $p<0.001$). Hallmark_epithelial_to_mesemchymal_transition was the most highly expressed signalling pathway in all three cohorts ($p<0.001$ for all). Pathways associated with inflammation: Hallmark_inflammatory_response, Hallmark_interferon_gamma_response, Hallmark_TNFa_signalling_via_NFkB, Hallmark_IL2_STAT5_signalling, IL6_JAK_STAT3_signalling, and Hallmark_complement were significantly upregulated in all three cohorts ($p<0.001$ for all). GSE32894 and GSE13507 both had significantly decreased Hallmark_TGF_beta_signalling ($p<0.001$ and $p=0.02$). This inflamed TME seen in tumours with high vs low gene scores also associated with increased M0 and M1 macrophages, CD4 cells and decreased Tregs as measured using the Cibersort algorithm (Figure 6.13). High versus low gene signature scores had significantly increased CD8 T cell signalling and IFNγ signalling in all three cohorts ($p<0.01$ for all; Figure 6.14).

Table 6.7. Gene set enrichment analysis showing the hallmark pathways ranked by normalised enrichment score when gene signature score was high versus low in the TCGA cohort.

Pathway	p val	p adj	NES	Size
HALLMARK_EPITHELIAL_MESENCHYMAL_TRANSITION	1.00E-10	5.56E-10	4.76	174
HALLMARK_INFLAMMATORY_RESPONSE	1.00E-10	5.56E-10	3.41	155
HALLMARK_APICAL_JUNCTION	1.00E-10	5.56E-10	3.19	137
HALLMARK_COAGULATION	1.00E-10	5.56E-10	3.17	102
HALLMARK_MYOGENESIS	1.00E-10	5.56E-10	3.10	153
HALLMARK_TNFA_SIGNALING_VIA_NFKB	1.00E-10	5.56E-10	3.09	157
HALLMARK_ALLOGRAFT_REJECTION	1.00E-10	5.56E-10	2.96	142
HALLMARK_COMPLEMENT	1.00E-10	5.56E-10	2.91	151
HALLMARK_IL6_JAK_STAT3_SIGNALING	3.36E-10	1.53E-09	2.81	70
HALLMARK_KRAS_SIGNALING_UP	1.00E-10	5.56E-10	2.80	142
HALLMARK_UV_RESPONSE_DN	1.68E-09	7.01E-09	2.67	104
HALLMARK_IL2_STAT5_SIGNALING	1.33E-10	6.65E-10	2.64	136
HALLMARK_ANGIOGENESIS	9.39E-06	2.93E-05	2.47	30
HALLMARK_INTERFERON_GAMMA_RESPONSE	1.08E-07	4.16E-07	2.33	133
HALLMARK_APOPTOSIS	1.18E-06	4.23E-06	2.25	113
HALLMARK_HYPOXIA	7.48E-06	2.49E-05	2.17	138
HALLMARK_APICAL_SURFACE	9.48E-04	0.002634	2.04	33
HALLMARK_MTORC1_SIGNALING	7.01E-05	2.06E-04	2.01	127
HALLMARK_ANDROGEN_RESPONSE	0.003511	0.00924	1.79	69
HALLMARK_HEDGEHOG_SIGNALING	0.034203	0.070423	1.66	23
HALLMARK_ESTROGEN_RESPONSE_EARLY	0.008581	0.021453	1.54	132
HALLMARK_UNFOLDED_PROTEIN_RESPONSE	0.035211	0.070423	1.50	70
HALLMARK_HEME_METABOLISM	0.024321	0.052871	1.50	121
HALLMARK_ESTROGEN_RESPONSE_LATE	0.016413	0.039079	1.49	128
HALLMARK_GLYCOLYSIS	0.043364	0.080304	1.43	134
HALLMARK_MITOTIC_SPINDLE	0.046419	0.082891	1.41	120
HALLMARK_OXIDATIVE_PHOSPHORYLATION	0.018333	0.041667	-1.51	93
HALLMARK_PEROXISOME	0.037767	0.07263	-1.56	55

p val = enrichment p value, p adj = BH adjusted p value, NES = normalised enrichment score, size = number of the pathway genes present in the dataset.

Table 6.8. Gene set enrichment analysis showing the hallmark pathways ranked by normalised enrichment score when gene signature scores were high versus low in the GSE32894 cohort.

Pathway	p val	p adj	NES	Size
HALLMARK_EPITHELIAL_MESENCHYMAL_TRANSITION	1.00E-10	8.33E-10	3.21	158
HALLMARK_E2F_TARGETS	1.00E-10	8.33E-10	2.97	145
HALLMARK_G2M_CHECKPOINT	1.00E-10	8.33E-10	2.89	135
HALLMARK_INFLAMMATORY_RESPONSE	1.00E-10	8.33E-10	2.77	143
HALLMARK_COMPLEMENT	1.00E-10	8.33E-10	2.59	125
HALLMARK_ALLOGRAFT_REJECTION	1.00E-10	8.33E-10	2.59	138
HALLMARK_KRAS_SIGNALING_UP	2.57E-09	1.84E-08	2.29	136
HALLMARK_INTERFERON_GAMMA_RESPONSE	1.58E-08	8.77E-08	2.25	123
HALLMARK_MTORC1_SIGNALING	4.40E-09	2.75E-08	2.23	130
HALLMARK_IL2_STAT5_SIGNALING	2.51E-08	1.26E-07	2.20	136
HALLMARK_IL6_JAK_STAT3_SIGNALING	6.46E-06	2.69E-05	2.15	61
HALLMARK_ANGIOGENESIS	6.19E-05	2.06E-04	2.13	28
HALLMARK_TNFA_SIGNALING_VIA_NFKB	2.03E-06	9.21E-06	2.03	131
HALLMARK_COAGULATION	1.93E-05	6.90E-05	2.00	84
HALLMARK_INTERFERON_ALPHA_RESPONSE	2.96E-04	7.79E-04	1.94	58
HALLMARK_SPERMATOGENESIS	2.08E-04	5.78E-04	1.93	61
HALLMARK_APOPTOSIS	7.91E-05	2.47E-04	1.85	111
HALLMARK_MITOTIC_SPINDLE	1.23E-04	3.61E-04	1.79	128
HALLMARK_CHOLESTEROL_HOMEOSTASIS	0.001809	0.004307	1.77	42
HALLMARK_HYPOXIA	4.93E-04	0.001232	1.76	109
HALLMARK_GLYCOLYSIS	0.003026	0.006578	1.63	125
HALLMARK_MYOGENESIS	0.003674	0.007653	1.58	132
HALLMARK_APICAL_JUNCTION	0.005023	0.010046	1.56	134
HALLMARK_UNFOLDED_PROTEIN_RESPONSE	0.0144	0.027693	1.56	67
HALLMARK_ESTROGEN_RESPONSE_LATE	0.048465	0.086545	1.34	137
HALLMARK_P53_PATHWAY	0.031054	0.057508	-1.33	137
HALLMARK_ESTROGEN_RESPONSE_EARLY	0.002109	0.004794	-1.58	129
HALLMARK_TGF_BETA_SIGNALING	1.67E-05	6.43E-05	-2.24	38

p val = enrichment p value, p adj = BH adjusted p value, NES = normalised enrichment score, size = number of the pathway genes present in the dataset.

Table 6.9. Gene set enrichment analysis showing the hallmark pathways ranked by normalised enrichment score when gene signature scores were high versus low in the GSE13507 cohort.

Pathway	p val	p adj	NES	Size
HALLMARK_EPITHELIAL_MESENCHYMAL_TRANSITION	1.00E-10	5.56E-10	3.34	145
HALLMARK_E2F_TARGETS	1.00E-10	5.56E-10	2.91	134
HALLMARK_G2M_CHECKPOINT	1.00E-10	5.56E-10	2.73	118
HALLMARK_MTORC1_SIGNALING	1.00E-10	5.56E-10	2.71	100
HALLMARK_COMPLEMENT	1.00E-10	5.56E-10	2.68	108
HALLMARK_INFLAMMATORY_RESPONSE	1.00E-10	5.56E-10	2.66	109
HALLMARK_TNFA_SIGNALING_VIA_NFKB	1.00E-10	5.56E-10	2.61	123
HALLMARK_MYOGENESIS	1.00E-10	5.56E-10	2.60	116
HALLMARK_HYPOXIA	1.00E-10	5.56E-10	2.49	106
HALLMARK_KRAS_SIGNALING_UP	3.06E-08	1.53E-07	2.24	109
HALLMARK_IL2_STAT5_SIGNALING	1.08E-07	4.91E-07	2.22	100
HALLMARK_MYC_TARGETS_V1	5.10E-07	2.13E-06	2.18	98
HALLMARK_COAGULATION	1.58E-06	6.08E-06	2.16	74
HALLMARK_APOPTOSIS	2.99E-06	9.97E-06	2.13	77
HALLMARK_ALLOGRAFT_REJECTION	3.64E-06	1.14E-05	2.12	77
HALLMARK_INTERFERON_GAMMA_RESPONSE	2.42E-06	8.64E-06	2.11	89
HALLMARK_IL6_JAK_STAT3_SIGNALING	5.42E-05	1.51E-04	2.07	43
HALLMARK_MITOTIC_SPINDLE	8.65E-06	2.54E-05	2.02	110
HALLMARK_ANGIOGENESIS	2.77E-04	6.29E-04	2.01	22
HALLMARK_ANDROGEN_RESPONSE	1.64E-04	4.30E-04	2.00	52
HALLMARK_SPERMATOGENESIS	7.27E-04	0.001515	1.87	49
HALLMARK_UV_RESPONSE_DN	4.28E-04	9.31E-04	1.83	76
HALLMARK_APICAL_JUNCTION	2.17E-04	5.43E-04	1.82	107
HALLMARK_GLYCOLYSIS	2.75E-04	6.29E-04	1.80	108
HALLMARK_CHOLESTEROL_HOMEOSTASIS	0.00383	0.007366	1.72	36
HALLMARK_UNFOLDED_PROTEIN_RESPONSE	0.005312	0.009837	1.70	57
HALLMARK_ESTROGEN_RESPONSE_LATE	0.001706	0.003411	1.66	99
HALLMARK_INTERFERON_ALPHA_RESPONSE	0.028884	0.046588	1.56	41
HALLMARK_FATTY_ACID_METABOLISM	0.017525	0.030215	1.55	75
HALLMARK_PROTEIN_SECRETION	0.032288	0.050449	1.51	39
HALLMARK_UV_RESPONSE_UP	0.019293	0.032155	1.48	71
HALLMARK_TGF_BETA_SIGNALING	0.011529	0.020587	-1.64	29

p val = enrichment p value, p adj = BH adjusted p value, NES = normalised enrichment score, size = number of the pathway genes present in the dataset.

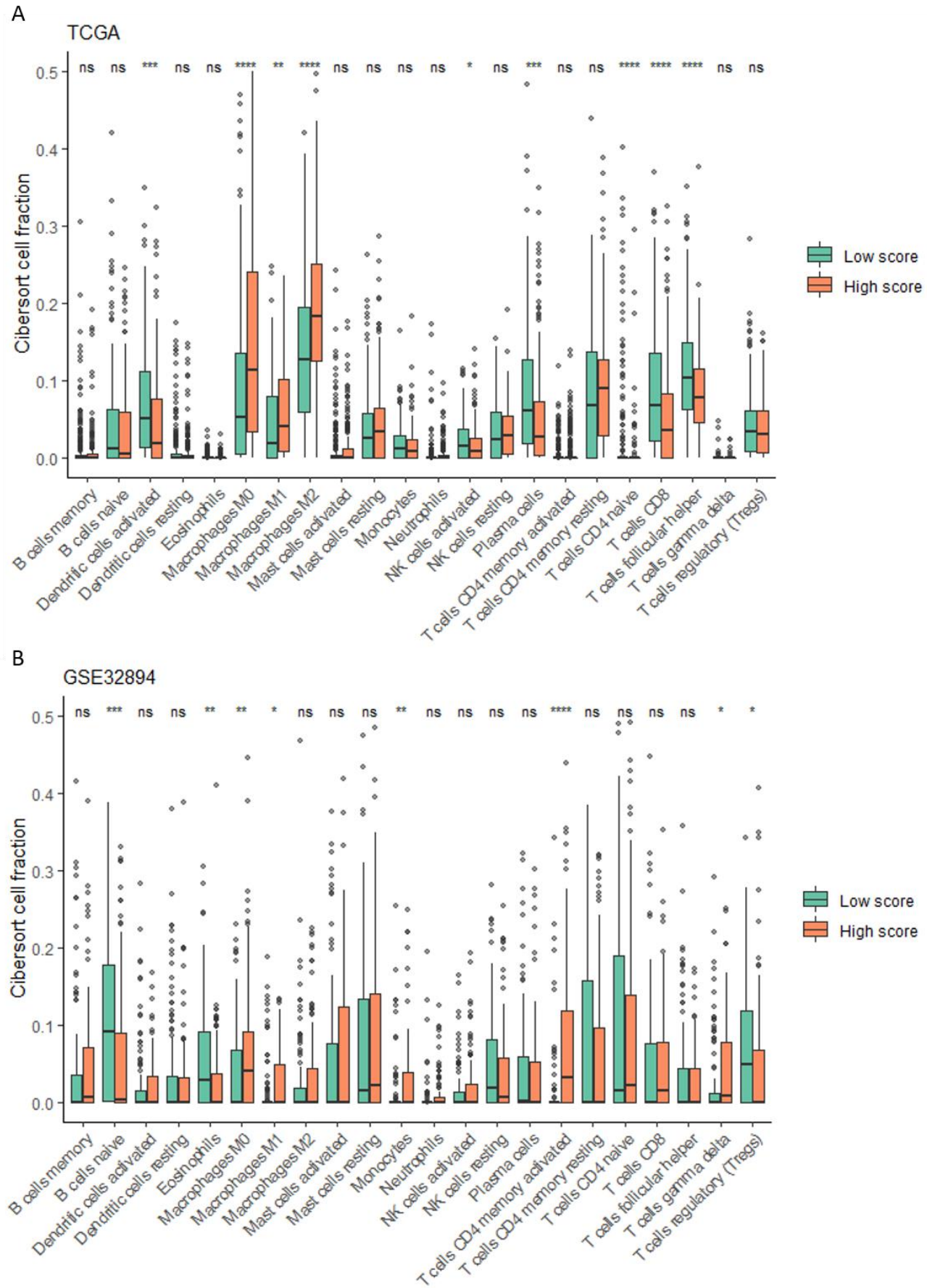
A
TCGA
Cibersort cell fraction
0.0
0.1
0.2
0.3
0.4
0.5
ns ns *** ns ns **** ** **** ns ns ns ns * ns *** ns ns **** **** **** ns ns
B cells memory
B cells naive
Dendritic cells activated
Dendritic cells resting
Eosinophils
Macrophages M0
Macrophages M1
Macrophages M2
Mast cells activated
Mast cells resting
Monocytes
Neutrophils
NK cells activated
NK cells resting
Plasma cells
T cells CD4 memory activated
T cells CD4 memory resting
T cells CD4 naive
T cells CD8
T cells follicular helper
T cells gamma delta
T cells regulatory (Tregs)
Low score
High score
B
GSE32894
Cibersort cell fraction
0.0
0.1
0.2
0.3
0.4
0.5
ns *** ns ns ** ** * ns ns ns ** ns ns ns ns **** ns ns ns ns * *
B cells memory
B cells naive
Dendritic cells activated
Dendritic cells resting
Eosinophils
Macrophages M0
Macrophages M1
Macrophages M2
Mast cells activated
Mast cells resting
Monocytes
Neutrophils
NK cells activated
NK cells resting
Plasma cells
T cells CD4 memory activated
T cells CD4 memory resting
T cells CD4 naive
T cells CD8
T cells follicular helper
T cells gamma delta
T cells regulatory (Tregs)
Low score
High score

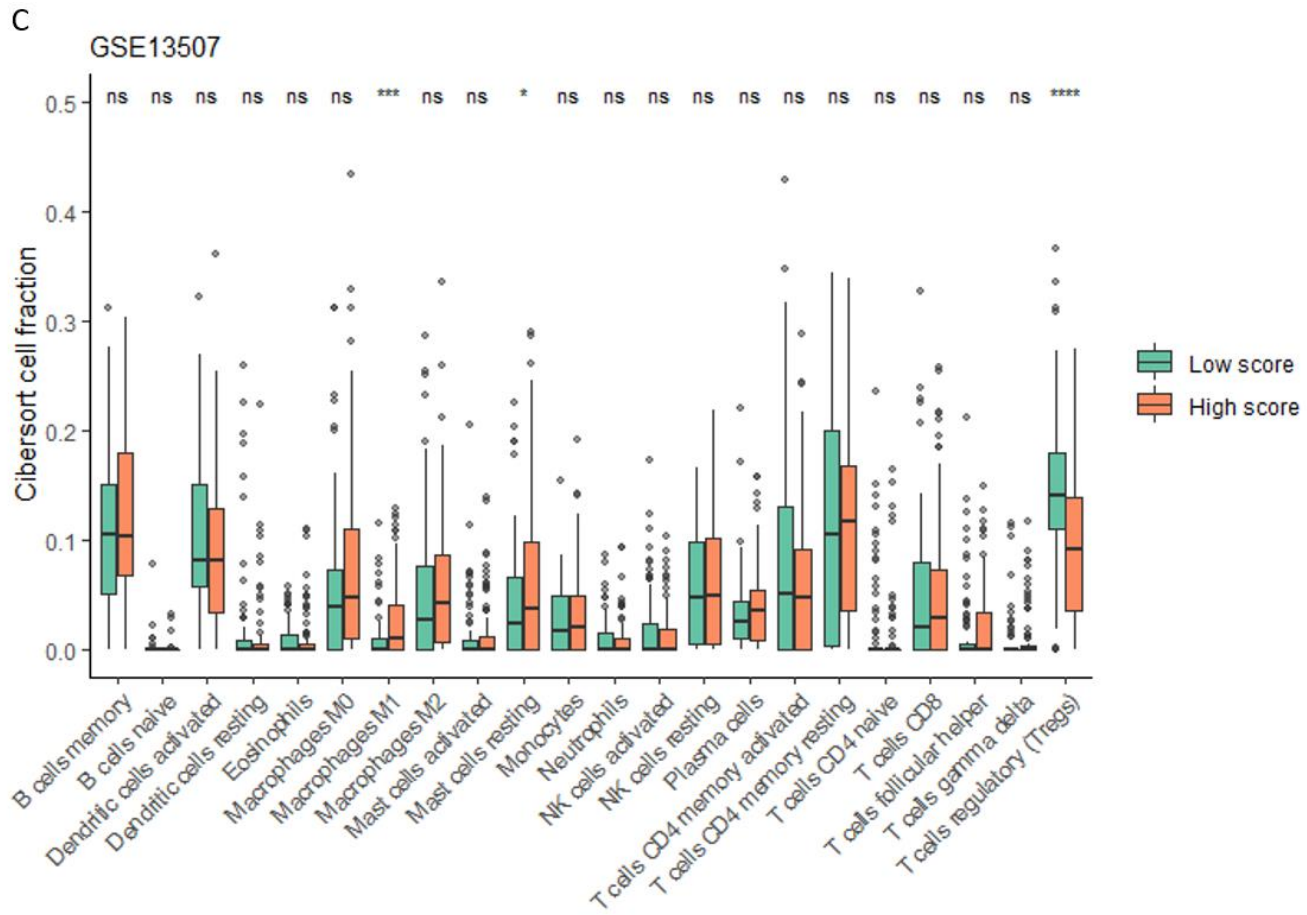

Figure 6.13 Boxplots showing the fraction of each immune cell population according to gene signature score. Immune cell populations were deconvoluted by the Cibersort algorithm. Statistics are p values from t tests with p values represented as: ns = not significant, *<0.05, **<0.01, ***<0.001, ****<0.0001.

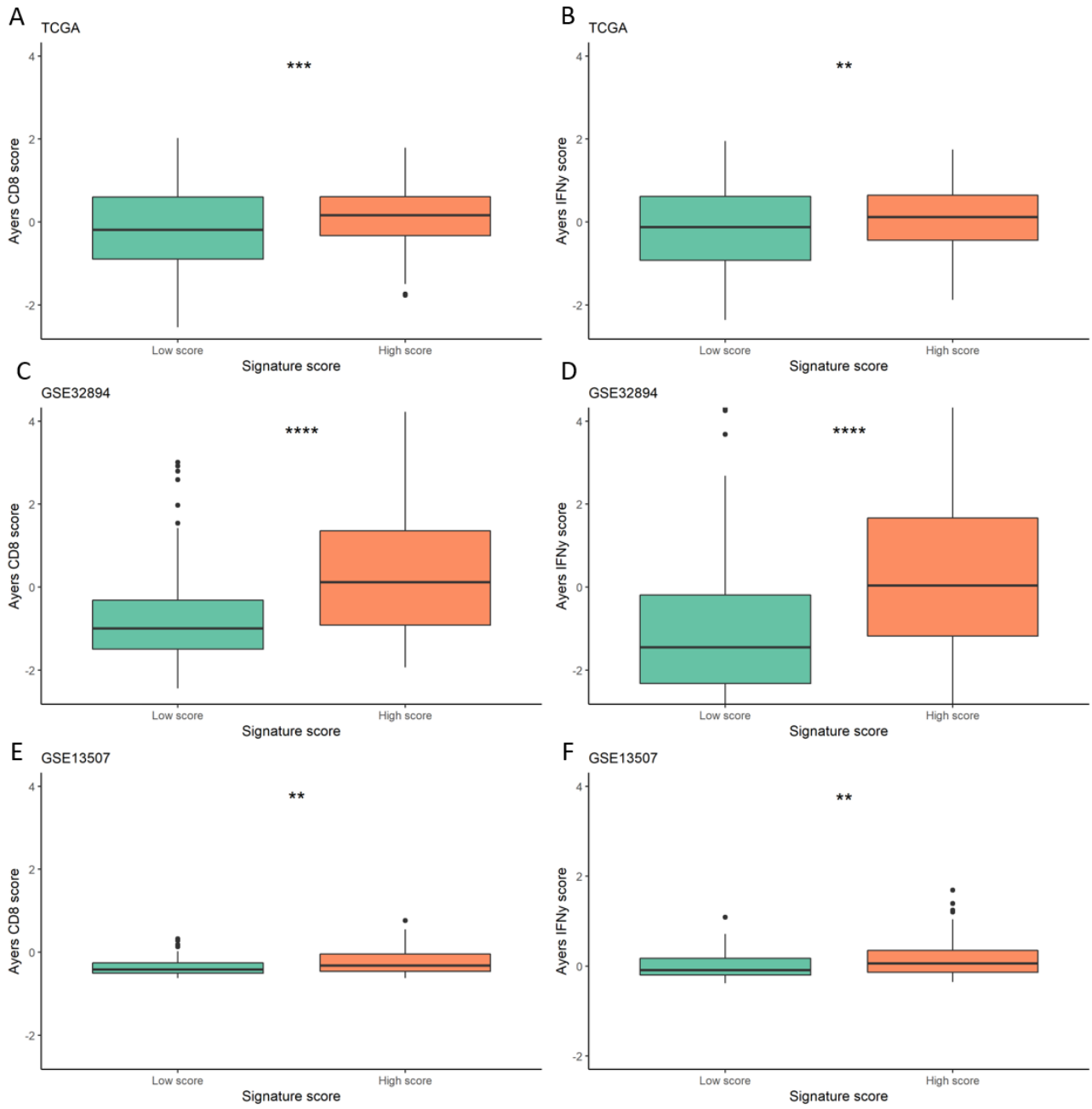

Figure 6.14. Boxplots showing the association between CD8 signalling and IFNγ signalling and the gene signature score. CD8 signalling was calculated using a gene signature defined by Ayers et al. and plotted against the gene signature score for A) TCGA, C) GSE32894, and E) GSE13507 cohorts. IFNγ signalling was calculated using a gene signature defined by Ayers et al. and plotted against the gene signature score for B) TCGA, D) GSE23894, and F) GSE13507 cohorts. Statistical tests are wilcox tests with p values represented as: ns = not significant, *<0.05, **<0.01, ***<0.001, ****<0.0001.

6.5 Discussion

A six-gene hypoxia-driven immune gene signature that is bladder cancer-specific was successfully developed that provides clinically relevant prognostic and predictive information. The derived gene signature was prognostic in three independent bladder cancer cohorts. A number of genes included in the signature (*AHNAK, EMP1, SMAD6*, and *TRIM26*) have been independently identified as prognostic in urothelial cancer using TCGA data (Uhlen *et al.*, 2017). *SMAD6* and *TRIM26* were shown to be prognostic in urothelial cancer alone, whilst *AHNAK* was also prognostic in pancreatic cancer and *EMP1* also prognostic in pancreatic and ovarian cancer (Uhlen *et al.*, 2017). The known function of each of the genes are described in Table 6.10. The bladder-specific prognostic relevance of these genes, combined with the demonstration of a lack of prognostic significance for the gene signature in six other TCGA cancer types, highlights its bladder cancer specificity.

Table 6.10 The functions of the genes present in the derived signature.

Gene	Expression	Function (Uniprot)	Immune function (literature)
AHNAK	↑	Neuronal cell differentiation	Stimulates TGF-β signalling[1]; Required for T cell activation[2]
EMP1	↑	Unknown	Limited data, associates with increased immune infiltrates especially DCs and T cells[3]
FGF10	↑	Cell proliferation and differentiation; wound healing	Released from macrophages and CAFs, upregulates TGF-β signalling[4]
SMAD6	↓	Negatively regulates TGF-β signalling	Inhibits the TGF-β superfamily signalling[5]
SPNS1	↑	Sphingolipid transporter	Limited data, associates with monocytes[6]
TRIM26	↓	Regulates interferon beta production	Induces innate immune responses[7,8]

Expression shows whether the gene expression is up or downregulated in the gene signature (i.e negative or positive coefficients, where ↑ = positive and ↓ = negative. Function is taken from UniProt website resource. Immune/stroma functin is taken from a literature search. 1 = *Lee* et al., *2014*; 2 = *Matza* et al., *2008*; 3 = *Lin* et al., *2020*; 4 = *Clayton and Grose, 2018*; 5 = *Imamura* et al., *1997*; 6 = *Uhlen* et al., *2017*; 7 = *Ran* et al., *2016; 8 = Zhao* et al., *2021*.

AHNAK has further been shown to be prognostic in bladder cancer according to proteomic analysis from urine cytology (Okusa *et al.*, 2008). *AHNAK* is in other bladder cancer gene signatures: one that is prognostic and another that identified poor prognosis tumours with a higher infiltration of CD4+ and CD8+ cells, as well as macrophages, neutrophils and dendritic cells (Qiu *et al.*, 2020; Wu *et al.*, 2020). High expression of *EMP1* has been independently demonstrated to associate with a poor prognosis in bladder cancer

and to positively correlate with increased immune infiltrates and markers (Cheng *et al.*, 2020; Lin *et al.*, 2020). Both *AHNAK* and *EMP1* are included in another six-gene signature that was prognostic in bladder cancer patients and associated with an increased expression of a number of immune-related pathways (Zou *et al.*, 2021). *TRIM26* was shown to drive the proliferation, migration and invasion in MIBC cell lines (Xie *et al.*, 2021).

In 2021, three other hypoxia-associated gene signatures in bladder cancer were published, which show associations with the immune contexture of the TME. The four-gene signature developed by Jiang *et al* was prognostic in three external bladder cancer cohorts, although no confidence intervals were stated. They showed their signature scores positively correlated with ESTIMATE immune and stromal scores and expression of checkpoint molecules such as CTLA-4 and LAG-3 at both a gene and protein level. At the gene level, their signature also positively correlated with *PD-L1* and *PD-1* expression, but they did not explore relationships with other measurements of tumour hypoxia nor show any benefit from hypoxia-targeting treatment. Based on the findings that high signature score tumours have a more inflamed TME they hypothesised that their signature would predict benefit from ICIs, although this was not tested in a clinical cohort (M. Jiang *et al.*, 2021). Another gene signature developed by Zhang *et al* consisted of eight genes, of which one overlapped with Jiang's signature (*HS3ST1*), and was prognostic in the same cohorts. Using Cibersort they found higher infiltration of M0 and M1 macrophages and activated memory CD4+ T cells for high vs low gene signature scores. Whilst no comparison was made with measures of hypoxia or benefit of treatment shown using a clinical cohort, the authors used the resource Genomics of Drug Sensitivity in Cancer database to show that higher scores could potentially identify tumours that are likely develop chemoresistance (F. Zhang *et al.*, 2021). The third bladder cancer hypoxia gene signature was developed by Liu *et al.* They showed that their 16-gene signature was prognostic in two external bladder cancer cohorts and positively correlated with expression of signatures that predicted ICI efficacy. They showed that high gene signature scores associated with basal molecular subtypes as demonstrated by a number of different approaches, including the consensus classification (Z. Liu *et al.*, 2021). They did not correlate their gene signature with other measurements of hypoxia nor show benefit from treatment.

High scores for my 6-gene signature associated with the consensus basal/squamous (ba/sq) and stroma-rich molecular subtypes. Kamoun *et al* show that compared to the

other subtypes, a worse prognosis is seen for ba/sq and NE-like molecular subtypes, consistent with my results (Kamoun *et al.*, 2020). Furthermore, the authors show that in comparison with other subtypes, ba/sq and stroma-rich had higher levels of immune infiltrates and IFNγ signalling, and hypoxia; findings interpreted as indicating a good response to ICIs and poor response to radiotherapy alone, respectively. They further showed that ba/sq subtypes have increased antigen presentation machinery, immune checkpoints and CD8 signalling, which are associated with benefit from ICIs. However, when analysing a clinical cohort they found that LumNS, LumU and NE-like subtypes benefitted most from an anti-PDL1 ICI (atezolizumab), despite these subtypes having decreased expression of the previously mentioned aspects that predict response to ICIs (Kamoun *et al.*, 2020). Therefore, there is a need to use a clinical cohort to investigate whether high gene signature score patients benefit from ICIs, as the existing data gives rise to discrepancies.

Nevertheless, support of the suggestion that high signature score patients are likely to benefit from ICIs comes from further studies using ICI treated clinical cohorts. Ayers *et al.* identified two gene signatures reflecting CD8+ T cell and IFNγ signalling where high expression predicted response to the anti-PD1 ICI pembrolizumab (Ayers *et al.*, 2017). My results show that the gene signature positively correlated with increased CD8+ T cell and IFNγ signalling. Another study showed that a derived immune-related gene signature stratified bladder cancer tumours based on abundance of immune infiltrates and that tumours with increased immune infiltrates had a good response to atezolizumab (P. Li *et al.*, 2021). Here, a high gene signature score associated with increased M0 and M1 macrophages, and CD4+ T cells, as well as ESTIMATE immune score. Mariathasan *et al.* demonstrated that in bladder cancer patients a lack of response to ICIs associated with increased TGF-β signalling expression and in the analyses presented in this chapter, patients with high versus low gene signature scores had significantly decreased TGF-β signalling as shown by GSEA (Mariathasan *et al.*, 2018). Using the same cohort, Powles *et al* expanded on this to show that response to ICIs was associated with high expression of immune response signatures and basal/squamous molecular subtypes, whilst relapse after treatment was associated with increased angiogenesis and TGF-β signalling (Powles *et al.*, 2021). My gene signature also correlated with high ESTIMATE immune scores and expression of multiple signalling pathways associated with inflammation, as well as ba/sq subtypes. These analyses support the suggestion that a high expression of my derived gene signature reflects

tumours that are likely to respond to ICIs, although testing on a clinical cohort is needed to validate this.

In the report outlining the long-term outcomes from the BCON trial, Song *et al.* show that tumours classified as basal compared to luminal (via BASE47 mRNA classifier) had better survival when given CON compared to radiotherapy alone (HR = 0.58, 95% CI 0.32-1.06, p=0.08), and were more hypoxic. The authors saw no difference in survival for basal vs luminal tumours and concluded that a composite biomarker taking into account subtype and hypoxia could improve prognostic and predictive potential (Song *et al.*, 2021). The prognostic gene signature derived here positively correlates with hypoxia, was enriched in basal tumours and predicted benefit from CON addition to radiotherapy. Therefore, the signature could have potential as a composite biomarker. In support of this suggestion, the multivariable analysis of BCON showed only the hypoxia-driven immune gene signature retained prognostic significance when including the 24-hypoxia gene signature and molecular subtype classification.

Radiotherapy can confer either pro or anti-tumour immune effects depending on the immune contexture of the tumour prior to treatment (Barker *et al.*, 2015). A study in MIBC showed that a higher expression of genes reflecting CD8+ T cell infiltration and IFNγ signalling was associated with a better disease specific survival when patients had TMT, but not for those who had radical cystectomy +/- neoadjuvant chemotherapy (Efstathiou *et al.*, 2019). A study by Chen *et al.* demonstrated that *HIF1A* gene expression positively correlated with tumour aggressiveness. In many cancer types, including bladder, *HIF1A* expression was shown to positively correlate with EMT, ESTIMATE stromal scores and immune-promoting and immune-inhibiting gene signatures. They further showed that a kidney cancer cohort receiving an ICI had significantly better response to treatment when *HIF1A* expression was high (Chen *et al.*, 2020).

In mice models, hypoxia reversal by hyperbaric oxygen breathing has been shown to stimulate anti-tumour immune effects including increasing intratumoural infiltration of CD8+ T cells, reducing inhibition of CD8+ T cells and decreasing immune-suppressive molecules such as TGF-β. These effects led to immune-mediated tumour regression, which resulted in improved overall survival (Hatfield *et al.*, 2015). In a prostate cancer mouse model, a hypoxia pro-drug successfully reduced hypoxia and combined with ICIs to drastically improve survival. It was shown that the combination therapy increased levels of

cytotoxic CD8+ T cells and reduced myeloid-derived suppressor cells in the TME to allow for better immune-mediated tumour elimination (Jayaprakash *et al.*, 2018). Taken together, I hypothesise that the signature reflects tumours with an hypoxia-driven inflamed TME that confers pro-tumour immune responses after treatment. The hypoxia-modification through CON enables the shift of the inflamed TME to anti-tumour immune effects, which improve immune-mediated responses to radiotherapy and are likely to combine beneficially with ICIs for increased expansion of immune-mediation tumour clearance (Figure 6.15).

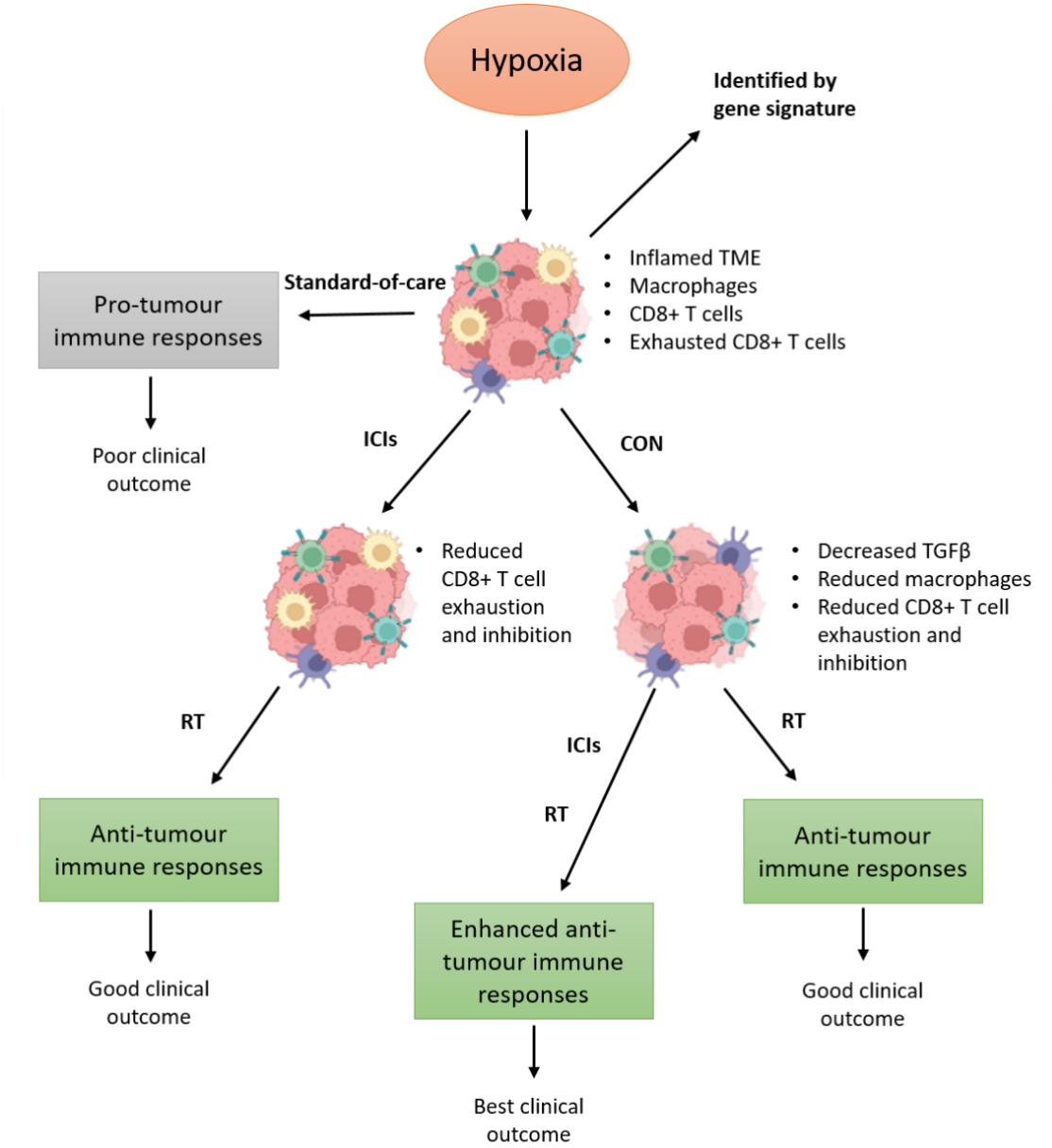

Figure 6.15. Schematic showing the hypothesis of CON and ICI benfit for tumours identified by high hypoxia-driven immune gene signature score. Created with BioRender.

Although other bladder cancer hypoxia-related gene signatures exist that reflect the immune TME, as discussed, the one presented here is the first to my knowledge that is an hypoxia-driven immune gene signature. It also uniquely demonstrates benefit from hypoxia-modifying therapy and shows a strong positive correlation with hypoxia, as well as reflecting increased inflammation in the TME. Furthermore, the signature is bladder cancer-specific. The study is limited by a lack of availability of all the signature genes in the BCON cohort, which limits further analysis of the gene signature in this cohort. Further work needs to be done to elucidate the CON-mediated immune changes in the TME post-radiotherapy.

In summary, I derived a bladder cancer-specific hypoxia-driven immune gene signature that identifies poor prognosis MIBC patients given current standard-of-care treatments alone. The gene signature reflects hypoxic and inflamed tumours and predicts benefit from CON. The gene signature has the potential to also predict tumours likely to benefit from ICIs, but this requires further testing on a bladder cancer cohort treated with ICIs.

7 Discussion

The overall aim of my project was to investigate the effects of hypoxia on the immune tumour microenvironment in MIBC and develop biomarkers for potential use in individualising the use of concurrent treatments with radiotherapy. Four objectives were addressed (see Section 1.5.3) and the key findings from the thesis were:

- Hypoxia led to a cell density dependent decrease in expression of PD-L1 in bladder cancer cells *in vitro,* but in MIBC *in situ,* PD-L1 expression positively correlated with hypoxia.
- Low CD8+ T cell counts confer a poor prognosis in MIBC and predict benefit from addition of hypoxia-modifying therapy, CON, to radiotherapy.
- In MIBC, hypoxia associates with increased suppressive and anti-tumour immune signalling, and presence of immune infiltrates.
- A prognostic bladder cancer-specific hypoxia-driven immune gene signature predicts benefit from CON and represents hypoxic and inflamed tumours.

The findings in this thesis regarding the relationship between hypoxia and PD-L1 expression are important because PD-L1 contributes towards an immune suppressive TME by dampening the CD8+ T cell-mediated anti-tumour immune response, which aids treatment resistance and tumour recurrence and progression (Dovedi *et al.*, 2014; Han, Liu and Li, 2020). Using MIBC cell lines, I show that there is no hypoxia-mediated increase in PD-L1 seen *in* vitro. My results show that when investigating PD-L1 expression *in vitro,* cell density is of importance as PD-L1 expression decreases with increasing cell density and thus should be taken into consideration for future experiments. Using a ChIPseq experiment in the T24 MIBC cell line, I show that HIF-2α binds to an enhancer region of the PD-L1 gene (*CD274*) under 1% and 0.1% hypoxia. The mechanisms governing PD-L1 expression at a genomic level are not well defined and published literature gives rise to discrepancies between cell lines and tissue-types (Fabrizio *et al.*, 2018). More specifically, the HIF-mediated regulation of PD-L1 is poorly defined in the literature and is potentially tissue-type specific. As there are no existing publications analysing the role of hypoxia and HIF on PD-L1 expression in bladder cancer, my data adds to this gap in the literature by providing novel insights into the effect of hypoxia and HIF on PD-L1 expression in MIBC, specifically. More

in-depth research into the roles of HIF-1α and HIF-2α in regulating PD-L1 expression under hypoxia in bladder cancer are lacking in this thesis and these results highlight the need for further studies on this topic. In future work, the *in vitro* experiments should be expanded to increase the number of MIBC cell lines and include the expression of HIF-1α and HIF-2α alongside PD-L1 expression. Knockdown experiments of HIF-2α would provide interesting insights into the role of HIF-2α in PD-L1 expression, as well as ChIP experiments on more MIBC cell lines.

Upon expanding my PD-L1-related research from *in vitro* analysis to investigating the relationship between PD-L1 and hypoxia *in situ* using patient tumours, I found a positive correlation between the two. I found that in MIBC tumours hypoxia also associated with other immune signalling pathways that contribute towards an immune suppressive tumour microenvironment. These results are corroborated by my results using microarray gene expression illustrating that under hypoxia MIBC cell lines are enriched for signalling pathways associated with myeloid and neutrophil activation and differentiation as well as signalling related to Treg maintenance. A suppressive TME is important because it furthers tumour growth and progression and plays an important role in treatment resistance (Hanahan and Weinberg, 2011). The relationship between hypoxia and a suppressive TME has not been thoroughly researched in bladder cancer and I show here that hypoxia contributes towards a suppressive TME in MIBC, specifically. However, in contrast I also show that hypoxia associated with anti-tumour immune signalling processes. Sufficient recruitment and activation of CD8+ T cells is essential to elicit an effective radiotherapy-induced immune-mediated tumour killing, which is vital for tumour clearance and response to treatment (Barker *et al.*, 2015). Immune signalling in the TME is of clinical importance regarding response to treatments. Literature has shown that in bladder cancer an inflamed TME with high levels of immune-related signalling predicts response to ICIs (Mariathasan *et al.*, 2018; Powles *et al.*, 2021). I show that in MIBC tumours there was a positive correlation between hypoxia and various immune-related signalling processes that predict benefit of ICIs. Using HIF ChIP-seq experiments, I also show that HIF binding is enriched for signalling related to CD8+ T cell activation and differentiation, interferon production, humoural immune responses and signalling related to innate immune responses and generic cytokine production. Therefore, not only are the results in this thesis regarding the relationship between HIF-binding, hypoxic conditions, and immune-related signalling in MIBC novel, but

they are of clinical relevance as they indicate that hypoxia could predict response to ICIs in MIBC patients. Analysis of the relationship between the two should be further expanded to see how they relate to patient survival and response to treatments, which is lacking in this thesis.

There is an unmet clinical need to develop biomarkers to personalise treatment strategies for MIBC patients to improve overall survival. I developed two biomarkers that could be studied further for their potential to stratify patients for additional treatments alongside radiotherapy. Both low CD8+ T cell counts and a high hypoxia-driven immune gene signature score predicted poor prognosis patients who had hypoxic tumours and showed benefit from hypoxia-modifying therapy, carbogen and nicotinamide (CON). Of the two, the gene signature provides the more robust option due to the reliability of using a gene signature clinically, as seen by the current use of breast cancer gene signatures such as Oncotype DX in breast cancer, compared to discrepancies seen when trying to adopt an IHC based biomarker across different centres (McVeigh and Kerin, 2017; Walker *et al.*, 2019). The derived hypoxia-driven immune gene signature also reflected inflamed tumours, which are therefore likely to benefit from ICIs. Validation of this hypothesis is needed using an ICI treated MIBC cohort and is lacking in this thesis currently. Collaborations are ongoing to investigate whether high gene signature score predicts patients who respond to ICIs.

Multiplex IHC is a resource-heavy technique as it requires a lengthy optimisation process at a high cost, which I found had to be performed on the same tissue that was going to be used for the experiment. Taken together, this means that optimisation used a lot of clinical trial tissue, and overall the experiment was lengthy and costly. I do not think this was proportional to the breadth of information gleaned from the experiment. Recently, multiplex IHC has been superseded by spatial biology techniques such as digital spatial profiling (DSP) (Merritt *et al.*, 2020). DSP would be interesting to investigate for this project as it has been designed for immune-oncology biomarker discovery, which is pertinent to the topics explored in this thesis (Beechem, 2020). To continue this project, more research is needed to see the effect of CON on the immune TME in MIBC tumours. A phase II clinical trial using the derived gene signature as a biomarker to stratify patients for radiotherapy +/- CON could be used to this effect. Diagnostic biopsies and post-treatment samples could be analysed using digital spatial profiling techniques to provide a wealth of information pertaining to both protein and gene level information investigating how radiotherapy and

CON given synergistically alter the immune TME in MIBC. Mouse models are then needed to investigate the effects of combining radiotherapy and CON with ICIs for hypoxic and inflamed tumours. Literature has shown promising responses for combination of ICIs and hypoxia-modification, but little has been researched into combining them with radiotherapy (Hatfield *et al.*, 2015; Jayaprakash *et al.*, 2018; Colombani *et al.*, 2021; X. Liu *et al.*, 2021). Investigations would first need to be made into the effect of scheduling, dose, toxicities of combinations and the most effective ICI. If the combination treatment is successful in promoting immune-mediated tumour clearing then it would form the basis for a clinical trial where poor prognosis patients with a high gene signature score would be given radiotherapy plus CON with an adjuvant ICI to improve immune-mediated tumour clearance, immunological memory and overall response to treatment. This approach would provide the potential to ameliorate the current poor survival rates for MIBC patients.

Overall, the findings presented in my thesis provide novel insights into the relationship between hypoxia and the immune tumour microenvironment in muscle-invasive bladder cancer. The results provide the basis for further investigations to elucidate the role of HIF-2α on PD-L1 expression in MIBC and take forward the derived gene signature as a potential biomarker to improve MIBC patient survival.

References

Abou Khouzam, R. *et al.* (2021) 'An Eight-Gene Hypoxia Signature Predicts Survival in Pancreatic Cancer and Is Associated With an Immunosuppressed Tumor Microenvironment', *Frontiers in Immunology*. Frontiers Media S.A., 12. doi: 10.3389/FIMMU.2021.680435/FULL.

Aggarwal, B. B. (2003) 'Signalling pathways of the TNF superfamily: a double-edged sword', *Nature Reviews Immunology 2003 3:9*. Nature Publishing Group, 3(9), pp. 745–756. doi: 10.1038/nri1184.

Angelova, M. *et al.* (2015) 'Characterization of the immunophenotypes and antigenomes of colorectal cancers reveals distinct tumor escape mechanisms and novel targets for immunotherapy', *Genome Biology*. BioMed Central, 16(1), p. 64. doi: 10.1186/s13059-015-0620-6.

Aouali, N. *et al.* (2017) 'The Critical Role of Hypoxia in Tumor-Mediated Immunosuppression', in *Hypoxia and Human Diseases*. InTech. doi: 10.5772/65383.

Arneth, B. (2020) 'Tumor Microenvironment', *Medicina*. Multidisciplinary Digital Publishing Institute (MDPI), 56(1). doi: 10.3390/MEDICINA56010015.

Asano, T. *et al.* (2018) 'CD169-positive sinus macrophages in the lymph nodes determine bladder cancer prognosis', *Cancer Science*. John Wiley & Sons, Ltd, 109(5), pp. 1723–1730. doi: 10.1111/CAS.13565.

Ayers, M. *et al.* (2017) 'IFN-γ-related mRNA profile predicts clinical response to PD-1 blockade', *Journal of Clinical Investigation*, 127(8), pp. 2930–2940. doi: 10.1172/JCI91190.

Baras, A. S. *et al.* (2016) 'The ratio of CD8 to Treg tumor-infiltrating lymphocytes is associated with response to cisplatin-based neoadjuvant chemotherapy in patients with muscle invasive urothelial carcinoma of the bladder', *OncoImmunology*. Taylor & Francis, 5(5), pp. 1–7. doi: 10.1080/2162402X.2015.1134412.

Barker, H. E. *et al.* (2015) 'The tumour microenvironment after radiotherapy: Mechanisms of resistance and recurrence', *Nature Reviews Cancer*. doi: 10.1038/nrc3958.

Barsoum, I. B. *et al.* (2014) 'A mechanism of hypoxia-mediated escape from adaptive immunity in cancer cells', *Cancer Research*, 74(3), pp. 665–674. doi: 10.1158/0008-5472.CAN-13-0992.

Becht, E. *et al.* (2016) 'Estimating the population abundance of tissue-infiltrating immune and stromal cell populations using gene expression', *Genome Biology*. BioMed Central,

17(1), p. 218. doi: 10.1186/s13059-016-1070-5.

Beechem, J. M. (2020) 'High-Plex Spatially Resolved RNA and Protein Detection Using Digital Spatial Profiling: A Technology Designed for Immuno-oncology Biomarker Discovery and Translational Research', *Methods in molecular biology (Clifton, N.J.)*. Methods Mol Biol, 2055, pp. 563–583. doi: 10.1007/978-1-4939-9773-2_25.

Bell, C. R. *et al.* (2022) 'Chemotherapy-induced COX-2 upregulation by cancer cells defines their inflammatory properties and limits the efficacy of chemoimmunotherapy combinations', *Nature Communications*. Nature Publishing Group, 13(1). doi: 10.1038/S41467-022-29606-9.

Bosco, M. C. and Varesio, L. (2014) 'Hypoxia and Gene Expression'. Springer, New York, NY, pp. 91–119. doi: 10.1007/978-1-4614-9167-5_5.

Boström, P. J. *et al.* (2016) 'Hypoxia Marker GLUT-1 (Glucose Transporter 1) is an Independent Prognostic Factor for Survival in Bladder Cancer Patients Treated with Radical Cystectomy', *Bladder Cancer*. IOS Press, 2(1), pp. 101–109. doi: 10.3233/BLC-150033.

Bowser, J. L. *et al.* (2017) 'The hypoxia-adenosine link during inflammation', *J Appl Physiol*, 123, pp. 1303–1320. doi: 10.1152/japplphysiol.00101.2017.-Hypoxic.

Bruns, I. B. and Beltman, J. B. (2022) 'Quantifying the contribution of transcription factor activity, mutations and microRNAs to CD274 expression in cancer patients', *Scientific Reports 2022 12:1*. Nature Publishing Group, 12(1), pp. 1–15. doi: 10.1038/s41598-022-08356-0.

Bubeník, J. *et al.* (1973) 'Established cell line of urinary bladder carcinoma (T24) containing tumour-specific antigen', *International Journal of Cancer*, 11(3), pp. 765–773. doi: 10.1002/ijc.2910110327.

Buffa, F. M. *et al.* (2010) 'Large meta-analysis of multiple cancers reveals a common, compact and highly prognostic hypoxia metagene', *British Journal of Cancer*, 102, pp. 428–435. doi: 10.1038/sj.bjc.6605450.

Burnette, B. C. *et al.* (2011) 'The efficacy of radiotherapy relies upon induction of type I interferon-dependent innate and adaptive immunity', *Cancer Research*. American Association for Cancer Research, 71(7), pp. 2488–2496. doi: 10.1158/0008-5472.CAN-10-2820/649508/AM/THE-EFFICACY-OF-RADIOTHERAPY-RELIES-UPON-INDUCTION.

Cairns, R. A. *et al.* (2007) 'Metabolic targeting of hypoxia and HIF1 in solid tumors can enhance cytotoxic chemotherapy', *Proceedings of the National Academy of Sciences of the*

United States of America. National Academy of Sciences, 104(22), p. 9445. doi: 10.1073/PNAS.0611662104.

Cancer Research UK (2022) *Cancer survival statistics*. Available at: https://www.cancerresearchuk.org/health-professional/cancer-statistics/statistics-by-cancer-type/bladder-cancer#heading-Zero (Accessed: 3 May 2022).

Cao, X. *et al.* (2007) 'Glucose uptake inhibitor sensitizes cancer cells to daunorubicin and overcomes drug resistance in hypoxia', *Cancer Chemotherapy and Pharmacology*. Springer, 59(4), pp. 495–505. doi: 10.1007/S00280-006-0291-9/FIGURES/5.

Chai, C. Y. *et al.* (2008) 'Hypoxia-inducible factor-1α expression correlates with focal macrophage infiltration, angiogenesis and unfavourable prognosis in urothelial carcinoma', *Journal of Clinical Pathology*. BMJ Publishing Group, 61(5), pp. 658–664. doi: 10.1136/jcp.2007.050666.

Chakravarthy, A. *et al.* (2018) 'TGF-β-associated extracellular matrix genes link cancer-associated fibroblasts to immune evasion and immunotherapy failure', *Nature Communications*. Nature Publishing Group, 9(1), p. 4692. doi: 10.1038/s41467-018-06654-8.

Chakravarti, A. *et al.* (2005) 'Expression of the epidermal growth factor receptor and Her-2 are predictors of favorable outcome and reduced complete response rates, respectively, in patients with muscle-invading bladder cancers treated by concurrent radiation and cisplatin-based chemotherapy: A report from the Radiation Therapy Oncology Group', *International Journal of Radiation Oncology, Biology, Physics*. Elsevier, 62(2), pp. 309–317. doi: 10.1016/J.IJROBP.2004.09.047.

Chang, W. H., Forde, D. and Lai, A. G. (2019) 'A novel signature derived from immunoregulatory and hypoxia genes predicts prognosis in liver and five other cancers', *Journal of Translational Medicine*. BioMed Central Ltd., 17(1). doi: 10.1186/s12967-019-1775-9.

Chatterjee, S. J. *et al.* (2004) 'Combined effects of p53, p21, and pRb expression in the progression of bladder transitional cell carcinoma', *Journal of Clinical Oncology*. American Society of Clinical Oncology, 22(6), pp. 1007–1013. doi: 10.1200/JCO.2004.05.174.

Chen, B. *et al.* (2018) 'Profiling tumor infiltrating immune cells with CIBERSORT', *Methods in molecular biology (Clifton, N.J.)*. NIH Public Access, 1711, p. 243. doi: 10.1007/978-1-4939-7493-1_12.

Chen, B. *et al.* (2020) 'HIF1A expression correlates with increased tumor immune and

stromal signatures and aggressive phenotypes in human cancers', *Cellular Oncology*. Springer, 43(5), pp. 877–888. doi: 10.1007/s13402-020-00534-4.

Chen, D. S. and Mellman, I. (2013) 'Oncology Meets Immunology: The Cancer-Immunity Cycle', *Immunity*. Elsevier, 39(1), pp. 1–10. doi: 10.1016/J.IMMUNI.2013.07.012.

Cheng, S. *et al.* (2020) 'The prognostic value of six survival-related genes in bladder cancer', *Cell Death Discovery 2020 6:1*. Nature Publishing Group, 6(1), pp. 1–11. doi: 10.1038/s41420-020-00295-x.

Cheng, W. *et al.* (2018) 'Unwrapping the genomic characteristics of urothelial bladder cancer and successes with immune checkpoint blockade therapy.', *Oncogenesis*. Nature Publishing Group, 7(1), p. 2. doi: 10.1038/s41389-017-0013-7.

Choi, W. *et al.* (2014) 'Identification of distinct basal and luminal subtypes of muscle-invasive bladder cancer with different sensitivities to frontline chemotherapy', *Cancer cell*. NIH Public Access, 25(2), p. 152. doi: 10.1016/J.CCR.2014.01.009.

Choudhury, A. *et al.* (2010) 'MRE11 expression is predictive of cause-specific survival following radical radiotherapy for muscle invasive bladder cancer', *Cancer research*. Europe PMC Funders, 70(18), p. 7017. doi: 10.1158/0008-5472.CAN-10-1202.

Choudhury, A. *et al.* (2021) 'Hypofractionated radiotherapy in locally advanced bladder cancer: an individual patient data meta-analysis of the BC2001 and BCON trials', *The Lancet Oncology*, 22(2), pp. 246–255. doi: 10.1016/S1470-2045(20)30607-0.

Clambey, E. T. *et al.* (2012) 'Hypoxia-inducible factor-1 alpha-dependent induction of FoxP3 drives regulatory T-cell abundance and function during inflammatory hypoxia of the mucosa', *Proceedings of the National Academy of Sciences of the United States of America*, 109(41). doi: 10.1073/PNAS.1202366109/SUPPL_FILE/PNAS.201202366SI.PDF.

Clayton, N. S. and Grose, R. P. (2018) 'Emerging Roles of Fibroblast Growth Factor 10 in Cancer', *Frontiers in Genetics*. Frontiers Media SA, 9, p. 499. doi: 10.3389/FGENE.2018.00499.

Colombani, T. *et al.* (2021) 'Oxygen-Generating Cryogels Restore T Cell Mediated Cytotoxicity in Hypoxic Tumors', *Advanced Functional Materials*, 31(37). doi: 10.1002/adfm.202102234.

Colton, M. *et al.* (2020) 'Reprogramming the tumour microenvironment by radiotherapy: implications for radiotherapy and immunotherapy combinations', *Radiation Oncology 2020 15:1*. BioMed Central, 15(1), pp. 1–11. doi: 10.1186/S13014-020-01678-1.

Connolly, K. A. *et al.* (2016) 'Increasing the efficacy of radiotherapy by modulating the CCR2/CCR5 chemokine axes', *Oncotarget*. Impact Journals, 7(52), pp. 86522–86535. doi: 10.18632/ONCOTARGET.13287.

Corzo, C. A. *et al.* (2010) 'HIF-1α regulates function and differentiation of myeloid-derived suppressor cells in the tumor microenvironment.', *The Journal of experimental medicine*. Rockefeller University Press, 207(11), pp. 2439–53. doi: 10.1084/jem.20100587.

Cramer, T. *et al.* (2003) 'HIF-1α Is Essential for Myeloid Cell-Mediated Inflammation', *Cell*. NIH Public Access, 112(5), p. 645. doi: 10.1016/S0092-8674(03)00154-5.

Cumberbatch, M. G. K. *et al.* (2018) 'Epidemiology of Bladder Cancer: A Systematic Review and Contemporary Update of Risk Factors in 2018', *European Urology*. Elsevier, 74(6), pp. 784–795. doi: 10.1016/J.EURURO.2018.09.001.

Danaher, P. *et al.* (2017) 'Gene expression markers of Tumor Infiltrating Leukocytes', *Journal for ImmunoTherapy of Cancer*. BioMed Central Ltd., 5(1), pp. 1–15. doi: 10.1186/S40425-017-0215-8/FIGURES/7.

Datta, A. *et al.* (2021) 'Impact of hypoxia on cervical cancer outcomes', *International journal of gynecological cancer : official journal of the International Gynecological Cancer Society*. NLM (Medline), 31(11), pp. 1459–1470. doi: 10.1136/IJGC-2021-002806.

Dekervel, J. *et al.* (2014) 'Hypoxia-driven gene expression is an independent prognostic factor in stage II and III colon cancer patients', *Clinical Cancer Research*. American Association for Cancer Research Inc., 20(8), pp. 2159–2168. doi: 10.1158/1078-0432.CCR-13-2958/86307/AM/HYPOXIA-DRIVEN-GENE-EXPRESSION-IS-AN-INDEPENDENT.

Demaria, S. and Formenti, S. C. (2012) 'Radiation as an immunological adjuvant: current evidence on dose and fractionation.', *Frontiers in oncology*. Frontiers Media SA, 2, p. 153. doi: 10.3389/fonc.2012.00153.

Deng, B. *et al.* (2018) 'CD8 lymphocytes in tumors and nonsynonymous mutational load correlate with prognosis of bladder cancer patients treated with immune checkpoint inhibitors', *Cancer Reports*. Wiley-Blackwell, 1(1). doi: 10.1002/CNR2.1002.

Deniz, H. *et al.* (2010) 'Evaluation of relationship between HIF-1α immunoreactivity and stage, grade, angiogenic profile and proliferative index in bladder urothelial carcinomas', *International Urology and Nephrology*. Kluwer Academic Publishers, 42(1), pp. 103–107. doi: 10.1007/S11255-009-9590-5/FIGURES/4.

Denko, N. C. *et al.* (2003) 'Investigating hypoxic tumor physiology through gene

expression patterns', *Oncogene 2003 22:37*. Nature Publishing Group, 22(37), pp. 5907–5914. doi: 10.1038/sj.onc.1206703.

Dewan, M. Z. *et al.* (2012) 'Synergy of topical toll-like receptor 7 agonist with radiation and low-dose cyclophosphamide in a mouse model of cutaneous breast cancer', *Clinical Cancer Research*. American Association for Cancer Research, 18(24), pp. 6668–6678. doi: 10.1158/1078-0432.CCR-12-0984/286495/AM/SYNERGY-OF-TOPICAL-TOLL-LIKE-RECEPTOR-7-AGONIST.

DiSilvestro, P. A. *et al.* (2014) 'Phase III randomized trial of weekly cisplatin and irradiation versus cisplatin and tirapazamine and irradiation in stages IB2, IIA, IIB, IIIB, and IVA cervical carcinoma limited to the pelvis: a Gynecologic Oncology Group study.', *Journal of clinical oncology : official journal of the American Society of Clinical Oncology*. American Society of Clinical Oncology, 32(5), pp. 458–64. doi: 10.1200/JCO.2013.51.4265.

Doedens, A. L. *et al.* (2010) 'Macrophage Expression of HIF-1α Suppresses T cell Function and Promotes Tumor Progression', *Cancer research*. NIH Public Access, 70(19), p. 7465. doi: 10.1158/0008-5472.CAN-10-1439.

Doedens, A. L. *et al.* (2013) 'Hypoxia-inducible factors enhance the effector responses of CD8+ T cells to persistent antigen', *Nature Immunology 2013 14:11*. Nature Publishing Group, 14(11), pp. 1173–1182. doi: 10.1038/ni.2714.

Dovedi, S. J. *et al.* (2014) 'Acquired Resistance to Fractionated Radiotherapy Can Be Overcome by Concurrent PD-L1 Blockade', *Cancer Research*. American Association for Cancer Research, 74(19), pp. 5458–5468. doi: 10.1158/0008-5472.CAN-14-1258.

Dovedi, S. J. *et al.* (2016) 'Intravenous administration of the selective toll-like receptor 7 agonist DSR-29133 leads to anti-tumor efficacy in murine solid tumor models which can be potentiated by combination with fractionated radiotherapy', *Oncotarget*. Impact Journals, 7(13), pp. 17035–17046. doi: 10.18632/ONCOTARGET.7928.

Duronio, R. J. and Xiong, Y. (2013) 'Signaling Pathways that Control Cell Proliferation', *Cold Spring Harbor Perspectives in Biology*. Cold Spring Harbor Laboratory Press, 5(3). doi: 10.1101/CSHPERSPECT.A008904.

Efstathiou, J. A. *et al.* (2019) 'Impact of Immune and Stromal Infiltration on Outcomes Following Bladder-Sparing Trimodality Therapy for Muscle-Invasive Bladder Cancer(Figure presented.)', *European Urology*. Elsevier B.V., 76(1), pp. 59–68. doi: 10.1016/j.eururo.2019.01.011.

Elia, A. R. *et al.* (2008) 'Human dendritic cells differentiated in hypoxia down-modulate antigen uptake and change their chemokine expression profile', *Journal of Leukocyte Biology*. John Wiley & Sons, Ltd, 84(6), pp. 1472–1482. doi: 10.1189/jlb.0208082.

Elming, P. B. *et al.* (2019) 'Hyperthermia: The Optimal Treatment to Overcome Radiation Resistant Hypoxia', *Cancers*. Multidisciplinary Digital Publishing Institute (MDPI), 11(1). doi: 10.3390/CANCERS11010060.

European Association of Urology (2018) *Pocket Guidelines*.

Eustace, A., Mani, N., *et al.* (2013) 'A 26-gene hypoxia signature predicts benefit from hypoxia-modifying therapy in laryngeal cancer but not bladder cancer', *Clinical Cancer Research*, 19(17), pp. 4879–4888. doi: 10.1158/1078-0432.CCR-13-0542.

Eustace, A., Irlam, J. J., *et al.* (2013) 'Necrosis predicts benefit from hypoxia-modifying therapy in patients with high risk bladder cancer enrolled in a phase III randomised trial', *Radiotherapy and Oncology*. Elsevier, 108(1), p. 40. doi: 10.1016/J.RADONC.2013.05.017.

Fabrizio, F. P. *et al.* (2018) 'Gene code CD274/PD-L1: from molecular basis toward cancer immunotherapy', *Therapeutic Advances in Medical Oncology*. SAGE Publications, 10. doi: 10.1177/1758835918815598.

Faraj, S. F. *et al.* (2015) 'Assessment of tumoral PD-L1 expression and intratumoral CD8+ T cells in urothelial carcinoma', *Urology*. Elsevier Inc., 85(3), pp. 703.e1-703.e6. doi: 10.1016/j.urology.2014.10.020.

Fardin, P. *et al.* (2010) 'A biology-driven approach identifies the hypoxia gene signature as a predictor of the outcome of neuroblastoma patients', *Molecular Cancer*. BioMed Central, 9(1), pp. 1–15. doi: 10.1186/1476-4598-9-185/FIGURES/5.

Fjeldbo, C. S. *et al.* (2016) 'Integrative analysis of DCE-MRI and gene expression profiles in construction of a gene classifier for assessment of hypoxia-related risk of chemoradiotherapy failure in cervical cancer', *Clinical Cancer Research*. American Association for Cancer Research Inc., 22(16), pp. 4067–4076. doi: 10.1158/1078-0432.CCR-15-2322/128456/AM/INTEGRATIVE-ANALYSIS-OF-DCE-MRI-AND-GENE.

Flaig, T. W. (2019) 'NCCN Guidelines Updates: Management of Muscle-Invasive Bladder Cancer', *Journal of the National Comprehensive Cancer Network : JNCCN*. NLM (Medline), pp. 591–593. doi: 10.6004/jnccn.2019.5017.

Fong, M. H. Y. *et al.* (2020) 'Update on bladder cancer molecular subtypes', *Translational Andrology and Urology*. AME Publications, 9(6), p. 2881. doi: 10.21037/TAU-2019-MIBC-12.

Fridman, W. H. *et al.* (2012) 'The immune contexture in human tumours: impact on clinical outcome', *Nature Reviews Cancer*. Nature Publishing Group, 12(4), pp. 298–306. doi: 10.1038/nrc3245.

Fu, H. *et al.* (2018) 'Identification and validation of stromal immunotype predict survival and benefit from adjuvant chemotherapy in patients with muscle-invasive bladder cancer', *Clinical Cancer Research*. American Association for Cancer Research Inc., 24(13), pp. 3069–3078. doi: 10.1158/1078-0432.CCR-17-2687/87405/AM/IDENTIFICATION-AND-VALIDATION-OF-STROMAL.

Funk, C. C. *et al.* (2020) 'Atlas of Transcription Factor Binding Sites from ENCODE DNase Hypersensitivity Data across 27 Tissue Types', *Cell reports*. NIH Public Access, 32(7), p. 108029. doi: 10.1016/J.CELREP.2020.108029.

Gao, F. *et al.* (2021) 'A Hypoxia-Associated Prognostic Gene Signature Risk Model and Prognosis Predictors in Gliomas', *Frontiers in Oncology*. Frontiers Media S.A., 11, p. 4209. doi: 10.3389/FONC.2021.726794/BIBTEX.

Gao, W. *et al.* (2017) 'Inactivation of the PBRM1 tumor suppressor gene amplifies the HIF-response in VHL-/- clear cell renal carcinoma', *Proceedings of the National Academy of Sciences of the United States of America*. National Academy of Sciences, 114(5), pp. 1027–1032. doi: 10.1073/PNAS.1619726114/SUPPL_FILE/PNAS.1619726114.SAPP.PDF.

Garcia-Diaz, A. *et al.* (2017) 'Interferon Receptor Signaling Pathways Regulating PD-L1 and PD-L2 Expression', *Cell Reports*. ElsevierCompany., 19(6), pp. 1189–1201. doi: 10.1016/j.celrep.2017.04.031.

Gasser, S. *et al.* (2005) 'The DNA damage pathway regulates innate immune system ligands of the NKG2D receptor', *Nature 2005 436:7054*. Nature Publishing Group, 436(7054), pp. 1186–1190. doi: 10.1038/nature03884.

Gérard, C. and Goldbeter, A. (2014) 'The balance between cell cycle arrest and cell proliferation: control by the extracellular matrix and by contact inhibition', *Interface Focus*. The Royal Society, 4(3). doi: 10.1098/RSFS.2013.0075.

Ghazoui, Z. *et al.* (2011) 'Close and stable relationship between proliferation and a hypoxia metagene in aromatase inhibitor-treated ER-positive breast cancer', *Clinical Cancer Research*. American Association for Cancer Research, 17(9), pp. 3005–3012. doi: 10.1158/1078-0432.CCR-10-1704/83536/AM/CLOSE-AND-STABLE-RELATIONSHIP-BETWEEN.

Gray, L. H. *et al.* (1953) 'The concentration of oxygen dissolved in tissues at the time of

irradiation as a factor in radiotherapy', *The British journal of radiology*. The British Institute of Radiology, 26(312), pp. 638–648. doi: 10.1259/0007-1285-26-312-638.

Grimes, D. R. and Partridge, M. (2015) 'A mechanistic investigation of the oxygen fixation hypothesis and oxygen enhancement ratio', *Biomedical Physics & Engineering Express*. IOP Publishing, 1(4), p. 045209. doi: 10.1088/2057-1976/1/4/045209.

Grivennikov, S. I., Greten, F. R. and Karin, M. (2010) 'Immunity, Inflammation, and Cancer', *Cell*. Elsevier Inc., 140(6), pp. 883–899. doi: 10.1016/j.cell.2010.01.025.

Halle, C. *et al.* (2012) 'Hypoxia-induced gene expression in chemoradioresistant cervical cancer revealed by dynamic contrast-enhanced MRI', *Cancer Research*. American Association for Cancer Research, 72(20), pp. 5285–5295. doi: 10.1158/0008-5472.CAN-12-1085/650558/AM/HYPOXIA-INDUCED-GENE-EXPRESSION-IN.

Han, Y., Liu, D. and Li, L. (2020) 'PD-1/PD-L1 pathway: current researches in cancer', *American Journal of Cancer Research*. e-Century Publishing Corporation, 10(3), p. 727. Available at: /pmc/articles/PMC7136921/ (Accessed: 24 September 2021).

Hanahan, D. and Weinberg, R. A. (2000) 'The Hallmarks of Cancer', *Cell*. Elsevier, 100(1), pp. 57–70. doi: 10.1016/S0092-8674(00)81683-9.

Hanahan, D. and Weinberg, R. A. (2011) 'Hallmarks of Cancer: The Next Generation', *Cell*, 144(5), pp. 646–674. doi: 10.1016/j.cell.2011.02.013.

Harris, J. A. *et al.* (2012) 'CD163 versus CD68 in tumor associated macrophages of classical hodgkin lymphoma', *Diagnostic Pathology*. BioMed Central, 7(1), p. 12. doi: 10.1186/1746-1596-7-12.

Hasmim, M. *et al.* (2013) 'Cutting Edge: Hypoxia-Induced Nanog Favors the Intratumoral Infiltration of Regulatory T Cells and Macrophages via Direct Regulation of TGF-β1', *The Journal of Immunology*. American Association of Immunologists, 191(12), pp. 5802–5806. doi: 10.4049/JIMMUNOL.1302140.

Hassanien, O. A. *et al.* (2019) 'Dynamic Contrast-Enhanced Magnetic Resonance Imaging as a Diagnostic Tool in the Assessment of Tumour Angiogenesis in Urinary Bladder Cancer', *Canadian Association of Radiologists Journal*. Canadian Medical Association, 70(3), pp. 254–263. doi: 10.1016/j.carj.2018.11.004.

Hatfield, S. M. *et al.* (2014) 'Systemic oxygenation weakens the hypoxia and hypoxia inducible factor 1α-dependent and extracellular adenosine-mediated tumor protection', *Journal of Molecular Medicine*. NIH Public Access, 92(12), pp. 1283–1292. doi:

10.1007/s00109-014-1189-3.

Hatfield, S. M. *et al.* (2015) 'Immunological mechanisms of the antitumor effects of supplemental oxygenation', *Science Translational Medicine*. American Association for the Advancement of Science, 7(277). doi: 10.1126/SCITRANSLMED.AAA1260/SUPPL_FILE/7-277RA30_SM.PDF.

Hegde, P. S., Karanikas, V. and Evers, S. (2016) 'The Where, the When, and the How of Immune Monitoring for Cancer Immunotherapies in the Era of Checkpoint Inhibition.', *Clinical cancer research : an official journal of the American Association for Cancer Research*. American Association for Cancer Research, 22(8), pp. 1865–74. doi: 10.1158/1078-0432.CCR-15-1507.

Hill, R. P. *et al.* (2015) 'Hypoxia and Predicting Radiation Response', *Seminars in Radiation Oncology*. W.B. Saunders, 25(4), pp. 260–272. doi: 10.1016/J.SEMRADONC.2015.05.004.

Höckel, M. *et al.* (1996) 'Hypoxia and radiation response in human tumors', *Seminars in Radiation Oncology*. W.B. Saunders, 6(1), pp. 3–9. doi: 10.1016/S1053-4296(96)80031-2.

Honeychurch, J. *et al.* (2003) 'Anti-CD40 monoclonal antibody therapy in combination with irradiation results in a CD8 T-cell–dependent immunity to B-cell lymphoma', *Blood*. American Society of Hematology, 102(4), pp. 1449–1457. doi: 10.1182/BLOOD-2002-12-3717.

Horn, T. *et al.* (2016) 'The prognostic effect of tumour-infiltrating lymphocytic subpopulations in bladder cancer', *World Journal of Urology*. Springer Verlag, 34(2), pp. 181–187. doi: 10.1007/S00345-015-1615-3/TABLES/4.

Hoskin, P. J. *et al.* (2003) 'GLUT1 and CAIX as intrinsic markers of hypoxia in bladder cancer: relationship with vascularity and proliferation as predictors of outcome of ARCON', *British Journal of Cancer*. Nature Publishing Group, 89(7), p. 1290. doi: 10.1038/SJ.BJC.6601260.

Hoskin, P. J. *et al.* (2010) 'Radiotherapy with concurrent carbogen and nicotinamide in bladder carcinoma.', *Journal of clinical oncology : official journal of the American Society of Clinical Oncology*. American Society of Clinical Oncology, 28(33), pp. 4912–8. doi: 10.1200/JCO.2010.28.4950.

Hoskin, P. J., Saunders, M. I. and Dische, S. (1999) 'Hypoxic radiosensitizers in radical radiotherapy for patients with bladder carcinoma: hyperbaric oxygen, misonidazole, and accelerated radiotherapy, carbogen and nicotinamide.', *Cancer*, 86(7), pp. 1322–1328. doi:

10.1002/(SICI)1097-0142(19991001)86:7.

Hu, B. *et al.* (2020) 'Blockade of DC-SIGN+ Tumor-associated macrophages reactivates antitumor immunity and improves immunotherapy in muscle-invasive bladder cancer', *Cancer Research*. American Association for Cancer Research Inc., 80(8), pp. 1707–1719. doi: 10.1158/0008-5472.CAN-19-2254/654225/AM/BLOCKADE-OF-DC-SIGN-TUMOR-ASSOCIATED-MACROPHAGES.

Hu, Z. *et al.* (2009) 'A compact VEGF signature associated with distant metastases and poor outcomes', *BMC Medicine*. BioMed Central, 7(1), pp. 1–14. doi: 10.1186/1741-7015-7-9/FIGURES/6.

Hunter, B. A. *et al.* (2014) 'Expression of hypoxia-inducible factor-1α predicts benefit from hypoxia modification in invasive bladder cancer', *British Journal of Cancer*. Nature Publishing Group, 111(3), p. 437. doi: 10.1038/BJC.2014.315.

Imamura, T. *et al.* (1997) 'Smad6 inhibits signalling by the TGF-β superfamily', *Nature 1997 389:6651*. Nature Publishing Group, 389(6651), pp. 622–626. doi: 10.1038/39355.

Infantino, V. *et al.* (2021) 'Cancer Cell Metabolism in Hypoxia: Role of HIF-1 as Key Regulator and Therapeutic Target', *International Journal of Molecular Sciences*. Multidisciplinary Digital Publishing Institute (MDPI), 22(11). doi: 10.3390/IJMS22115703.

James, N. D. *et al.* (2012) 'Radiotherapy with or without Chemotherapy in Muscle-Invasive Bladder Cancer', *New England Journal of Medicine*. Massachusetts Medical Society , 366(16), pp. 1477–1488. doi: 10.1056/NEJMoa1106106.

Janssens, G. O. *et al.* (2012) 'Accelerated radiotherapy with carbogen and nicotinamide for laryngeal cancer: Results of a phase III randomized trial', *Journal of Clinical Oncology*. American Society of Clinical Oncology , 30(15), pp. 1777–1783. doi: 10.1200/JCO.2011.35.9315.

Jayaprakash, P. *et al.* (2018) 'Targeted hypoxia reduction restores T cell infiltration and sensitizes prostate cancer to immunotherapy', *The Journal of Clinical Investigation*. American Society for Clinical Investigation, 128(11), pp. 5137–5149. doi: 10.1172/JCI96268.

Jeong, W. *et al.* (2014) 'Pilot trial of EZN-2968, an antisense oligonucleotide inhibitor of hypoxia-inducible factor-1 alpha (HIF-1α), in patients with refractory solid tumors', *Cancer chemotherapy and pharmacology*. NIH Public Access, 73(2), p. 343. doi: 10.1007/S00280-013-2362-Z.

Jiang, L. R. *et al.* (2021) 'PD-1-Positive Tumor-Associated Macrophages Define Poor

Clinical Outcomes in Patients With Muscle Invasive Bladder Cancer Through Potential CD68/PD-1 Complex Interactions', *Frontiers in Oncology*. Frontiers Media S.A., 11, p. 1810. doi: 10.3389/FONC.2021.679928/BIBTEX.

Jiang, M. *et al.* (2021) 'Identification of a Hypoxia-Related Signature for Predicting Prognosis and the Immune Microenvironment in Bladder Cancer', *Frontiers in Molecular Biosciences*. Frontiers Media S.A., 8, p. 380. doi: 10.3389/FMOLB.2021.613359/BIBTEX.

Jones, D. M., Read, K. A. and Oestreich, K. J. (2020) 'Dynamic Roles for IL-2–STAT5 Signaling in Effector and Regulatory CD4+ T Cell Populations', *The Journal of Immunology*. American Association of Immunologists, 205(7), pp. 1721–1730. doi: 10.4049/JIMMUNOL.2000612.

Jorgovanovic, D. *et al.* (2020) 'Roles of IFN-γ in tumor progression and regression: a review', *Biomarker Research 2020 8:1*. BioMed Central, 8(1), pp. 1–16. doi: 10.1186/S40364-020-00228-X.

Joseph, M. and Enting, D. (2019) 'Immune Responses in Bladder Cancer-Role of Immune Cell Populations, Prognostic Factors and Therapeutic Implications', *Frontiers in Oncology*. Frontiers Media S.A., p. 1270. doi: 10.3389/fonc.2019.01270.

Joshi, M. *et al.* (2021) 'Phase II clinical study of concurrent durvalumab and radiation therapy (DUART) followed by adjuvant durvalumab in patients with localized urothelial cancer of bladder: Results for primary analyses and survival. BTCRC-GU15-023.', *https://doi.org/10.1200/JCO.2021.39.6_suppl.398*. American Society of Clinical Oncology, 39(6_suppl), pp. 398–398. doi: 10.1200/JCO.2021.39.6_SUPPL.398.

Kachikwu, E. L. *et al.* (2011) 'Radiation Enhances Regulatory T Cell Representation', *International Journal of Radiation Oncology*Biology*Physics*, 81(4), pp. 1128–1135. doi: 10.1016/j.ijrobp.2010.09.034.

Kamat, A. M. and Black, P. C. (2021) 'Radical Cystectomy', in *Bladder Cancer A Practical Guide*, pp. 139–140.

Kamoun, A. *et al.* (2020) 'A Consensus Molecular Classification of Muscle-invasive Bladder Cancer', *European Urology*. Elsevier, 77(4), pp. 420–433. doi: 10.1016/J.EURURO.2019.09.006.

Karakashev, S. V. and Reginato, M. J. (2015) 'Progress toward overcoming hypoxia-induced resistance to solid tumor therapy', *Cancer Management and Research*. Dove Press, 7, pp. 253–264. doi: 10.2147/CMAR.S58285.

Karsh, L. *et al.* (2018) 'Double-Blind, Randomized, Placebo-controlled Studies Evaluating Apaziquone (E09, Qapzola™) Intravesical Instillation Post Transurethral Resection of Bladder Tumors for the Treatment of Low-risk Non-Muscle Invasive Bladder Cancer', *Bladder Cancer (Amsterdam, Netherlands)*. IOS Press, 4(3), p. 293. doi: 10.3233/BLC-180166.

Khan, M. T. *et al.* (2021) 'A miRNA signature predicts benefit from addition of hypoxia-modifying therapy to radiation treatment in invasive bladder cancer', *British Journal of Cancer*. Nature Publishing Group, 125(1), p. 85. doi: 10.1038/S41416-021-01326-9.

Kim, W.-J. *et al.* (2011) 'A four-gene signature predicts disease progression in muscle invasive bladder cancer.', *Molecular medicine (Cambridge, Mass.)*. The Feinstein Institute for Medical Research, 17(5–6), pp. 478–85. doi: 10.2119/molmed.2010.00274.

Klatte, T. *et al.* (2009) 'Carbonic anhydrase IX in bladder cancer', *Cancer*. John Wiley & Sons, Ltd, 115(7), pp. 1448–1458. doi: 10.1002/CNCR.24163.

Kolstad, P. (1964) 'Oxygen Tension and Radiocurability in Cancer of the Cervix', *Acta Obstetricia et Gynecologica Scandinavica*. John Wiley & Sons, Ltd, 43(S7), pp. 100–102. doi: 10.3109/00016346409155842.

Kong, D. *et al.* (2005) 'Echinomycin, a Small-Molecule Inhibitor of Hypoxia-Inducible Factor-1 DNA-Binding Activity', *Cancer Research*. American Association for Cancer Research, 65(19), pp. 9047–9055. doi: 10.1158/0008-5472.CAN-05-1235.

Krishnamurthy, P. and Schuetz, J. D. (2005) 'The ABC Transporter Abcg2/Bcrp: Role in Hypoxia Mediated Survival', *Biometals 2005 18:4*. Springer, 18(4), pp. 349–358. doi: 10.1007/S10534-005-3709-7.

Van Kuijk, S. J. A. *et al.* (2016) 'Prognostic Significance of Carbonic Anhydrase IX Expression in Cancer Patients: A Meta-Analysis', *Frontiers in Oncology*. Frontiers Media SA, 6(MAR), p. 69. doi: 10.3389/FONC.2016.00069.

Kummar, S. *et al.* (2011) 'Multihistology, Target-Driven Pilot Trial of Oral Topotecan as an Inhibitor of Hypoxia-Inducible Factor-1α (HIF-1α) in Advanced Solid Tumors', *Clinical cancer research : an official journal of the American Association for Cancer Research*. NIH Public Access, 17(15), p. 5123. doi: 10.1158/1078-0432.CCR-11-0682.

Kuszynski, C. A., Miller, K. A. and Rizzino, A. (1993) 'Influence of cell density and receptor number on the binding and distribution of cell surface epidermal growth factor receptors', *In Vitro Cellular & Developmental Biology - Animal: Journal of the Society for In Vitro Biology*. Springer, 29(9), pp. 708–713. doi: 10.1007/BF02631427.

Lal, N. *et al.* (2015) 'An immunogenomic stratification of colorectal cancer: Implications for development of targeted immunotherapy', *Oncoimmunology*. Taylor & Francis, 4(3), pp. 1–9. doi: 10.4161/2162402X.2014.976052.

Lallemand, D. *et al.* (1998) 'Stress-activated protein kinases are negatively regulated by cell density.', *The EMBO Journal*. European Molecular Biology Organization, 17(19), p. 5615. doi: 10.1093/EMBOJ/17.19.5615.

Lane, B. *et al.* (2022) 'Development and validation of a hypoxia-associated signature for lung adenocarcinoma', *Scientific Reports*. Nature Publishing Group, 12(1), p. 1290. doi: 10.1038/S41598-022-05385-7.

Laurberg, J. R. *et al.* (2012) 'Expression of TIP60 (tat-interactive protein) and MRE11 (meiotic recombination 11 homolog) predict treatment-specific outcome of localised invasive bladder cancer', *BJU International*. John Wiley & Sons, Ltd, 110(11c), pp. E1228–E1236. doi: 10.1111/J.1464-410X.2012.11564.X.

Le, A. *et al.* (2010) 'Inhibition of lactate dehydrogenase A induces oxidative stress and inhibits tumor progression', *Proceedings of the National Academy of Sciences of the United States of America*. National Academy of Sciences, 107(5), p. 2037. doi: 10.1073/PNAS.0914433107.

Leblond, M. M. *et al.* (2021) 'Tumor-Associated Macrophages in Bladder Cancer: Biological Role, Impact on Therapeutic Response and Perspectives for Immunotherapy', *Cancers*. Multidisciplinary Digital Publishing Institute (MDPI), 13(18). doi: 10.3390/CANCERS13184712.

Lee, I. H. *et al.* (2014) 'Ahnak functions as a tumor suppressor via modulation of TGFβ/Smad signaling pathway', *Oncogene 2014 33:38*. Nature Publishing Group, 33(38), pp. 4675–4684. doi: 10.1038/onc.2014.69.

Li, B. *et al.* (2016) 'Comprehensive analyses of tumor immunity: Implications for cancer immunotherapy', *Genome Biology*. BioMed Central Ltd., 17(1), pp. 1–16. doi: 10.1186/S13059-016-1028-7/FIGURES/6.

Li, D. K. and Wang, W. (2020) 'Characteristics and clinical trial results of agonistic anti-CD40 antibodies in the treatment of malignancies', *Oncology Letters*. Spandidos Publications, 20(5). doi: 10.3892/OL.2020.12037.

Li, F. *et al.* (2021) 'The association between CD8+ tumor-infiltrating lymphocytes and the clinical outcome of cancer immunotherapy: A systematic review and meta-analysis',

eClinicalMedicine. Elsevier, 41, p. 101134. doi: 10.1016/j.eclinm.2021.101134.

Li, P. *et al.* (2021) 'Identification of an Immune-Related Risk Signature Correlates With Immunophenotype and Predicts Anti-PD-L1 Efficacy of Urothelial Cancer', *Frontiers in Cell and Developmental Biology*. Frontiers Media S.A., 9, p. 327. doi: 10.3389/fcell.2021.646982.

Van Limbergen, E. J. *et al.* (2017) 'Combining radiotherapy with immunotherapy: the past, the present and the future', *The British Journal of Radiology*. The British Institute of Radiology., 90(1076), p. 20170157. doi: 10.1259/bjr.20170157.

Lin, B. *et al.* (2020) 'High expression of EMP1 predicts a poor prognosis and correlates with immune infiltrates in bladder urothelial carcinoma', *Oncology Letters*. Spandidos Publications, 20(3), p. 2840. doi: 10.3892/OL.2020.11841.

Liu, L. *et al.* (2008) 'Hypoxia-inducible factor-1α contributes to hypoxia-induced chemoresistance in gastric cancer', *Cancer Science*. John Wiley & Sons, Ltd, 99(1), pp. 121–128. doi: 10.1111/J.1349-7006.2007.00643.X.

Liu, X. *et al.* (2021) 'Hyperbaric Oxygen Boosts PD-1 Antibody Delivery and T Cell Infiltration for Augmented Immune Responses Against Solid Tumors', *Advanced Science*. Wiley-Blackwell, 8(15). doi: 10.1002/advs.202100233.

Liu, Z. *et al.* (2021) 'A Robust Hypoxia Risk Score Predicts the Clinical Outcomes and Tumor Microenvironment Immune Characters in Bladder Cancer', *Frontiers in Immunology*. Frontiers Media S.A., 12. doi: 10.3389/FIMMU.2021.725223/FULL.

Lodhi, T. *et al.* (2021) 'Hypoxia and its Modification in Bladder Cancer: Current and Future Perspectives', *Clinical Oncology*. W.B. Saunders, 33(6), pp. 376–390. doi: 10.1016/J.CLON.2021.03.001.

Lugade, A. A. *et al.* (2008) 'Radiation-induced IFN-gamma production within the tumor microenvironment influences antitumor immunity.', *Journal of immunology (Baltimore, Md. : 1950)*, 180(5), pp. 3132–9. Available at: http://www.ncbi.nlm.nih.gov/pubmed/18292536 (Accessed: 10 December 2018).

Luo, J. and Du, X. (2021) 'A promising prognostic signature for lung adenocarcinoma (LUAD) patients basing on 6 hypoxia-related genes', *Medicine (United States)*. Lippincott Williams and Wilkins, 100(50), p. E28237. doi: 10.1097/MD.0000000000028237.

Mabjeesh, N. J. *et al.* (2002) 'Geldanamycin Induces Degradation of Hypoxia-inducible Factor 1 Protein via the Proteosome Pathway in Prostate Cancer Cells 1', *CANCER RESEARCH*, 62, pp. 2478–2482. Available at: http://aacrjournals.org/cancerres/article-

pdf/62/9/2478/2502642/ch0902002478.pdf (Accessed: 10 July 2022).

Mabjeesh, N. J. *et al.* (2003) '2ME2 inhibits tumor growth and angiogenesis by disrupting microtubules and dysregulating HIF', *Cancer cell*. Cancer Cell, 3(4), pp. 363–375. doi: 10.1016/S1535-6108(03)00077-1.

Mahmud, S. A., Manlove, L. S. and Farrar, M. A. (2013) 'Interleukin-2 and STAT5 in regulatory T cell development and function', *JAK-STAT*. Taylor & Francis, 2(1), p. e23154. doi: 10.4161/JKST.23154.

Van Malenstein, H. *et al.* (2010) 'A seven-gene set associated with chronic hypoxia of prognostic importance in hepatocellular carcinoma', *Clinical Cancer Research*. American Association for Cancer Research, 16(16), pp. 4278–4288. doi: 10.1158/1078-0432.CCR-09-3274/83882/AM/A-7-GENE-SET-ASSOCIATED-WITH-CHRONIC-HYPOXIA-OF.

Mangsbo, S. M. *et al.* (2015) 'The human agonistic CD40 antibody ADC-1013 eradicates bladder tumors and generates T-cell-dependent tumor immunity', *Clinical Cancer Research*. American Association for Cancer Research Inc., 21(5), pp. 1115–1126. doi: 10.1158/1078-0432.CCR-14-0913/137095/AM/THE-HUMAN-AGONISTIC-CD40-ANTIBODY-ADC-1013.

Manoochehri Khoshinani, H., Afshar, S. and Najafi, R. (2016) 'Hypoxia: A Double-Edged Sword in Cancer Therapy', *Cancer Investigation*. Taylor & Francis, 34(10), pp. 536–545. doi: 10.1080/07357907.2016.1245317.

Mantovani, A. *et al.* (2004) 'The chemokine system in diverse forms of macrophage activation and polarization', *Trends in Immunology*. Elsevier, 25(12), pp. 677–686. doi: 10.1016/j.it.2004.09.015.

Mantovani, A. *et al.* (2008) 'Cancer-related inflammation', *Nature*, 454(7203), pp. 436–444. doi: 10.1038/nature07205.

Mariathasan, S. *et al.* (2018) 'TGFβ attenuates tumour response to PD-L1 blockade by contributing to exclusion of T cells', *Nature 2018 554:7693*. Nature Publishing Group, 554(7693), pp. 544–548. doi: 10.1038/nature25501.

Masters, J. R. W. *et al.* (1986) *Tissue Culture Model of Transitional Cell Carcinoma: Characterization of Twenty-two Human Urothelial Cell Lines*, *CANCER RESEARCH*.

Matei, D. *et al.* (2009) 'Activity of 2 methoxyestradiol (Panzem® NCD) in advanced, platinum-resistant ovarian cancer and primary peritoneal carcinomatosis: A Hoosier Oncology Group trial', *Gynecologic Oncology*. Academic Press, 115(1), pp. 90–96. doi: 10.1016/J.YGYNO.2009.05.042.

Matza, D. *et al.* (2008) 'A scaffold protein, AHNAK1 is required for calcium signalling during T cell activation', *Immunity*. Howard Hughes Medical Institute, 28(1), p. 64. doi: 10.1016/J.IMMUNI.2007.11.020.

McConkey, D. J. and Choi, W. (2018) 'Molecular Subtypes of Bladder Cancer', *Current Oncology Reports*. Current Medicine Group LLC 1. doi: 10.1007/s11912-018-0727-5.

McVeigh, T. P. and Kerin, M. J. (2017) 'Clinical use of the Oncotype DX genomic test to guide treatment decisions for patients with invasive breast cancer', *Breast Cancer : Targets and Therapy*. Dove Press, 9, p. 393. doi: 10.2147/BCTT.S109847.

Merritt, C. R. *et al.* (2020) 'Multiplex digital spatial profiling of proteins and RNA in fixed tissue', *Nature Biotechnology 2020 38:5*. Nature Publishing Group, 38(5), pp. 586–599. doi: 10.1038/s41587-020-0472-9.

Miao, D. *et al.* (2018) 'Genomic correlates of response to immune checkpoint therapies in clear cell renal cell carcinoma', *Science (New York, N.Y.)*. NIH Public Access, 359(6377), p. 801. doi: 10.1126/SCIENCE.AAN5951.

Michaelson, M. D. *et al.* (2017) 'A Phase I/II Trial of a Combination of Paclitaxel and Trastuzumab with Daily Irradiation or Paclitaxel Alone with Daily Irradiation Following Transurethral Surgery for Non-Cystectomy Candidates with Muscle-Invasive Bladder Cancer (Trial ****)', *International journal of radiation oncology, biology, physics*. NIH Public Access, 97(5), p. 995. doi: 10.1016/J.IJROBP.2016.12.018.

Mills, C. D. *et al.* (2000) 'M-1/M-2 Macrophages and the Th1/Th2 Paradigm', *The Journal of Immunology*. American Association of Immunologists, 164(12), pp. 6166–6173. doi: 10.4049/JIMMUNOL.164.12.6166.

Miranda, A. *et al.* (2019) 'Cancer stemness, intratumoral heterogeneity, and immune response across cancers', *Proceedings of the National Academy of Sciences of the United States of America*. National Academy of Sciences, 116(18), pp. 9020–9029. doi: 10.1073/PNAS.1818210116/-/DCSUPPLEMENTAL.

Mo, Q. *et al.* (2018) 'Prognostic Power of a Tumor Differentiation Gene Signature for Bladder Urothelial Carcinomas', *JNCI: Journal of the National Cancer Institute*. Oxford University Press, 110(5), pp. 448–459. doi: 10.1093/jnci/djx243.

Mo, Z. *et al.* (2020) 'Identification of a Hypoxia-Associated Signature for Lung Adenocarcinoma', *Frontiers in Genetics*. Frontiers Media S.A., 11, p. 647. doi: 10.3389/FGENE.2020.00647/BIBTEX.

Mole, D. R. *et al.* (2009) 'Genome-wide association of hypoxia-inducible factor (HIF)-1α and HIF-2α DNA binding with expression profiling of hypoxia-inducible transcripts', *Journal of Biological Chemistry*, 284(25), pp. 16767–16775. doi: 10.1074/jbc.M901790200.

Mondini, M. *et al.* (2019) 'CCR2-dependent recruitment of Tregs and monocytes following radiotherapy is associated with TNFa-mediated resistance', *Cancer Immunology Research*. American Association for Cancer Research Inc., 7(3), pp. 376–387. doi: 10.1158/2326-6066.CIR-18-0633/470941/AM/CCR2-DEPENDENT-RECRUITMENT-OF-TREGS-AND-MONOCYTES.

Montfort, A. *et al.* (2019) 'The TNF paradox in cancer progression and immunotherapy', *Frontiers in Immunology*. Frontiers Media S.A., 10(JULY), p. 1818. doi: 10.3389/FIMMU.2019.01818/BIBTEX.

Morales, A., Eidinger, D. and Bruce, A. W. (2002) 'Intracavitary Bacillus Calmette-Guerin in the treatment of superficial bladder tumors. 1976.', *The Journal of urology*. No longer published by Elsevier, 167(2 Pt 2), pp. 891–894. doi: 10.1016/s0022-5347(02)80294-4.

Murdoch, C. *et al.* (2004) 'Mechanisms regulating the recruitment of macrophages into hypoxic areas of tumors and other ischemic tissues.', *Blood*. American Society of Hematology, 104(8), pp. 2224–34. doi: 10.1182/blood-2004-03-1109.

Murdoch, C. *et al.* (2008) 'The role of myeloid cells in the promotion of tumour angiogenesis', *Nature Reviews Cancer 2008 8:8*. Nature Publishing Group, 8(8), pp. 618–631. doi: 10.1038/nrc2444.

Murthy, A. *et al.* (2019) 'Intratumoral Hypoxia Reduces IFN-γ–Mediated Immunity and MHC Class I Induction in a Preclinical Tumor Model', *ImmunoHorizons*. The American Association of Immunologists, 3(4), pp. 149–160. doi: 10.4049/immunohorizons.1900017.

National Institute for Health and Care Excellence (2015) *Bladder cancer: diagnosis and management*, *Guidance, 1 Recommendations, 1.5 Treating muscle-invasive bladder cancer*. Available at: https://www.nice.org.uk/guidance/ng2/chapter/1-Recommendations#treating-muscle-invasive-bladder-cancer-2 (Accessed: 8 March 2022).

NHS (2021) *Bladder cancer treatment - NHS*. Available at: https://www.nhs.uk/conditions/bladder-cancer/treatment/ (Accessed: 9 June 2022).

NHS Digital (2019) *Case-mix adjusted percentage of cancers diagnosed at stages 1 and 2 by CCG in England*. Available at: https://crukcancerintelligence.shinyapps.io/EarlyDiagnosis/.

Nie, C., Qin, H. and Zhang, L. (2022) 'Identification and validation of a prognostic

signature related to hypoxic tumor microenvironment in cervical cancer', *PLOS ONE*. Public Library of Science, 17(6), p. e0269462. doi: 10.1371/journal.pone.0269462.

Nirmal, A. J. *et al.* (2016) 'ImSig: A resource for the identification and quantification of immune signatures in blood and tissue transcriptomics data', *bioRxiv*. Cold Spring Harbor Laboratory, p. 077487. doi: 10.1101/077487.

Nirmal, A. J. *et al.* (2018) 'Immune Cell Gene Signatures for Profiling the Microenvironment of Solid Tumors.', *Cancer immunology research*. American Association for Cancer Research, 6(11), pp. 1388–1400. doi: 10.1158/2326-6066.CIR-18-0342.

Noman, M. Z. *et al.* (2014) 'PD-L1 is a novel direct target of HIF-1α, and its blockade under hypoxia enhanced: MDSC-mediated T cell activation', *Journal of Experimental Medicine*, 211(5), pp. 781–790. doi: 10.1084/jem.20131916.

Northern Ireland Cancer Registry (2020) *Bladder cancer statistics 1993-2020*.

Nywening, T. M. *et al.* (2016) 'Targeting tumour-associated macrophages with CCR2 inhibition in combination with FOLFIRINOX in patients with borderline resectable and locally advanced pancreatic cancer: a single-centre, open-label, dose-finding, non-randomised, phase 1b trial', *The Lancet Oncology*. Elsevier, 17(5), pp. 651–662. doi: 10.1016/S1470-2045(16)00078-4.

Office for National Statistics (2019a) *Cancer registration statistics, England Statistical bulletins (2017)*.

Office for National Statistics (2019b) *Cancer survival in England - adults diagnosed (2013-2017 edition)*. Available at: https://www.ons.gov.uk/peoplepopulationandcommunity/healthandsocialcare/conditionsanddiseases/datasets/cancersurvivalratescancersurvivalinenglandadultsdiagnosed (Accessed: 8 July 2020).

Ohta, A. *et al.* (2006) 'A2A adenosine receptor protects tumors from antitumor T cells', *Proceedings of the National Academy of Sciences of the United States of America*. National Academy of Sciences, 103(35), p. 13132. doi: 10.1073/PNAS.0605251103.

Okusa, H. *et al.* (2008) 'Searching for new biomarkers of bladder cancer based on proteomic analysis', *J Electrophoresis*, 52, p. 19.

Overgaard, J. *et al.* (1998) 'A randomized double-blind phase III study of nimorazole as a hypoxic radiosensitizer of primary radiotherapy in supraglottic larynx and pharynx carcinoma. Results of the Danish Head and Neck Cancer Study (DAHANCA) Protocol 5-85',

Radiotherapy and Oncology. Elsevier, 46(2), pp. 135–146. doi: 10.1016/S0167-8140(97)00220-X.

Overgaard, J. (2007) 'Hypoxic radiosensitization: adored and ignored.', *Journal of clinical oncology : official journal of the American Society of Clinical Oncology*. American Society of Clinical Oncology, 25(26), pp. 4066–74. doi: 10.1200/JCO.2007.12.7878.

Palazon, A. *et al.* (2017) 'An HIF-1α/VEGF-A Axis in Cytotoxic T Cells Regulates Tumor Progression', *Cancer Cell*. Cell Press, 32(5), pp. 669-683.e5. doi: 10.1016/J.CCELL.2017.10.003/ATTACHMENT/ED152DCD-EC24-428F-9A47-82834E07B7FC/MMC1.PDF.

Panther, E. *et al.* (2003) 'Adenosine affects expression of membrane molecules, cytokine and chemokine release, and the T-cell stimulatory capacity of human dendritic cells', *Blood*. Content Repository Only!, 101(10), pp. 3985–3990. doi: 10.1182/BLOOD-2002-07-2113.

Parameswaran, N. and Patial, S. (2010) 'Tumor Necrosis Factor-α Signaling in Macrophages', *Critical reviews in eukaryotic gene expression*. NIH Public Access, 20(2), p. 87. doi: 10.1615/CRITREVEUKARGENEEXPR.V20.I2.10.

Pavel, M. *et al.* (2018) 'Contact inhibition controls cell survival and proliferation via YAP/TAZ-autophagy axis', *Nature Communications 2018 9:1*. Nature Publishing Group, 9(1), pp. 1–18. doi: 10.1038/s41467-018-05388-x.

Pelly, V. S. *et al.* (2021) 'Anti-inflammatory drugs remodel the tumor immune environment to enhance immune checkpoint blockade efficacy', *Cancer discovery*. Europe PMC Funders, 11(10), p. 2602. doi: 10.1158/2159-8290.CD-20-1815.

Petridou, S. *et al.* (2000) 'TGF-beta receptor expression and smad2 localization are cell density dependent in fibroblasts', *Invest. Ophthalmol. Vis. Sci*, 41(1), pp. 89–95.

Pfannstiel, C. *et al.* (2019) 'The tumor immune microenvironment drives a prognostic relevance that correlates with bladder cancer subtypes', *Cancer Immunology Research*. American Association for Cancer Research Inc., 7(6), pp. 923–938. doi: 10.1158/2326-6066.CIR-18-0758.

Phillips, R. M. *et al.* (2013) 'EO9 (Apaziquone): from the clinic to the laboratory and back again', *British Journal of Pharmacology*. Wiley-Blackwell, 168(1), p. 11. doi: 10.1111/J.1476-5381.2012.01996.X.

Pocsik, E. *et al.* (1994) 'Cell density-dependent regulation of cell surface expression of two types of human tumor necrosis factor receptors and its effect on cellular response',

Journal of Cellular Biochemistry, 54(4), pp. 453–464. doi: 10.1002/jcb.240540412.

Powell, S. F. *et al.* (2015) 'Phase II study of dichloroacetate (DCA) in combination with chemoradiation (CRT) for unresected, locally advanced squamous cell carcinoma of the head and neck (LA-SCCHN).', *https://doi.org/10.1200/jco.2015.33.15_suppl.e17089*. American Society of Clinical Oncology , 33(15_suppl), pp. e17089–e17089. doi: 10.1200/JCO.2015.33.15_SUPPL.E17089.

Powell, S. F. *et al.* (2022) 'Phase II study of dichloroacetate, an inhibitor of pyruvate dehydrogenase, in combination with chemoradiotherapy for unresected, locally advanced head and neck squamous cell carcinoma', *Investigational New Drugs*. Springer, 40(3), pp. 622–633. doi: 10.1007/S10637-022-01235-5/FIGURES/2.

Powles, T. *et al.* (2021) 'ctDNA guiding adjuvant immunotherapy in urothelial carcinoma', *432 | Nature |*, 595. doi: 10.1038/s41586-021-03642-9.

Public Health Scotland (2020) *Cancer Incidence in Scotland*.

Public Health Wales (2020) *Cancer Incidence Wales, 2002-2019*.

Qian, B.-Z. and Pollard, J. W. (2010) 'Macrophage Diversity Enhances Tumor Progression and Metastasis', *Cell*. Cell Press, 141(1), pp. 39–51. doi: 10.1016/J.CELL.2010.03.014.

Qiu, H. *et al.* (2020) 'Identification and Validation of an Individualized Prognostic Signature of Bladder Cancer Based on Seven Immune Related Genes', *Frontiers in Genetics*. Frontiers Media S.A., 11, p. 12. doi: 10.3389/fgene.2020.00012.

Quail, D. F. and Joyce, J. A. (2013) 'Microenvironmental regulation of tumor progression and metastasis', *Nature Medicine*. Nature Publishing Group, pp. 1423–1437. doi: 10.1038/nm.3394.

Rabie, E. *et al.* (2016) 'Role of Dynamic Contrast-Enhanced Magnetic Resonance Imaging in Staging of Bladder Cancer', *Journal of Clinical and Diagnostic Research : JCDR*. JCDR Research & Publications Private Limited, 10(4), p. TC01. doi: 10.7860/JCDR/2016/17596.7690.

Ragnum, H. B. *et al.* (2015) 'The tumour hypoxia marker pimonidazole reflects a transcriptional programme associated with aggressive prostate cancer.', *British journal of cancer*. Nature Publishing Group, 112(2), pp. 382–90. doi: 10.1038/bjc.2014.604.

Raleigh, J. A. *et al.* (1999) 'Comparisons among pimonidazole binding, oxygen electrode measurements, and radiation response in C3H mouse tumors', *Radiation Research*, 151(5), pp. 580–589. doi: 10.2307/3580034.

Ran, Y. *et al.* (2016) 'Autoubiquitination of TRIM26 links TBK1 to NEMO in RLR-mediated innate antiviral immune response', *Journal of molecular cell biology*. J Mol Cell Biol, 8(1), pp. 31–43. doi: 10.1093/JMCB/MJV068.

Raskovalova, T. *et al.* (2005) 'Gs protein-coupled adenosine receptor signaling and lytic function of activated NK cells', *Journal of immunology (Baltimore, Md. : 1950)*. J Immunol, 175(7), pp. 4383–4391. doi: 10.4049/JIMMUNOL.175.7.4383.

Rath, M. *et al.* (2014) 'Metabolism via arginase or nitric oxide synthase: Two competing arginine pathways in macrophages', *Frontiers in Immunology*. Frontiers Media S.A., 5(OCT), p. 532. doi: 10.3389/FIMMU.2014.00532/BIBTEX.

Rech, A. J. *et al.* (2018) 'Radiotherapy and CD40 activation separately augment immunity to checkpoint blockade in cancer', *Cancer Research*. American Association for Cancer Research Inc., 78(15), pp. 4282–4291. doi: 10.1158/0008-5472.CAN-17-3821/653274/AM/RADIOTHERAPY-AND-CD40-ACTIVATION-SEPARATELY.

Reits, E. A. *et al.* (2006) 'Radiation modulates the peptide repertoire, enhances MHC class I expression, and induces successful antitumor immunotherapy', *Journal of Experimental Medicine*. The Rockefeller University Press, 203(5), pp. 1259–1271. doi: 10.1084/JEM.20052494.

Restifo, N. P. *et al.* (1993) 'Identification of human cancers deficient in antigen processing.', *The Journal of experimental medicine*. Rockefeller University Press, 177(2), pp. 265–72. doi: 10.1084/JEM.177.2.265.

Riera-Domingo, C. *et al.* (2020) 'IMMUNITY, HYPOXIA, AND METABOLISM-THE MÉNAGE A ` TROIS OF CANCER: IMPLICATIONS FOR IMMUNOTHERAPY GRAPHICAL ABSTRACT AUTHORS Physiological Reviews', *Physiol Rev*, 100, pp. 1–102. doi: 10.1152/physrev.00018.2019.

Rischin, D. *et al.* (2008) 'Phase III study of tirapazamine, cisplatin and radiation versus cisplatin and radiation for advanced squamous cell carcinoma of the head and neck', *Journal of Clinical Oncology*. American Society of Clinical Oncology, 26(15_suppl), pp. LBA6008–LBA6008. doi: 10.1200/jco.2008.26.15_suppl.lba6008.

Robertson, A. G. *et al.* (2017) 'Comprehensive Molecular Characterization of Muscle-Invasive Bladder Cancer', *Cell*. Cell Press, 171(3), pp. 540-556.e25. doi: 10.1016/J.CELL.2017.09.007/ATTACHMENT/FAD0F071-6C7E-4BA4-A5F1-E8F84BF6BB7C/MMC3.XLSX.

Rodríguez-Ruiz, M. E. *et al.* (2019) 'TGFb blockade enhances radiotherapy abscopal

efficacy effects in combination with anti-PD1 and anti-CD137 immunostimulatory monoclonal antibodies', *Molecular Cancer Therapeutics*. American Association for Cancer Research Inc., 18(3), pp. 621–631. doi: 10.1158/1535-7163.MCT-18-0558/87711/AM/TGF-BLOCKADE-ENHANCES-RADIOTHERAPY-ABSCOPAL.

Ruf, M., Moch, H. and Schraml, P. (2016) 'PD-L1 expression is regulated by hypoxia inducible factor in clear cell renal cell carcinoma', *International Journal of Cancer*. John Wiley & Sons, Ltd, 139(2), pp. 396–403. doi: 10.1002/IJC.30077.

Salberg, U. B. *et al.* (2022) 'A prognostic hypoxia gene signature with low heterogeneity within the dominant tumour lesion in prostate cancer patients', *British Journal of Cancer 2022*. Nature Publishing Group, pp. 1–8. doi: 10.1038/s41416-022-01782-x.

Satyal, U. *et al.* (2019) 'Clinical implications of molecular subtyping in bladdercancer', *Current opinion in urology*. NIH Public Access, 29(4), p. 350. doi: 10.1097/MOU.0000000000000641.

Schito, L. and Semenza, G. L. (2014) 'Hypoxia and Breast Cancer Metastasis'. Springer, New York, NY, pp. 3–19. doi: 10.1007/978-1-4614-9167-5_1.

Schödel, J. *et al.* (2011) 'High-resolution genome-wide mapping of HIF-binding sites by ChIP-seq', *Blood*, 117(23). doi: 10.1182/blood-2010-10-314427.

Schölch, S. *et al.* (2014) 'Radiotherapy combined with TLR7/8 activation induces strong immune responses against gastrointestinal tumors', *Oncotarget*. Impact Journals, 6(7), pp. 4663–4676. doi: 10.18632/ONCOTARGET.3081.

Seigneuric, R. *et al.* (2007) 'Impact of supervised gene signatures of early hypoxia on patient survival', *Radiotherapy and Oncology*. Elsevier, 83(3), pp. 374–382. doi: 10.1016/J.RADONC.2007.05.002.

Semenza, G. L. (2021) 'Intratumoral hypoxia and mechanisms of immune evasion mediated by hypoxia- inducible factors', *Physiology*. American Physiological Society, 36(2), pp. 73–83. doi: 10.1152/PHYSIOL.00034.2020/ASSET/IMAGES/LARGE/AJ-PHYS200014F006.JPEG.

Sethumadhavan, S. *et al.* (2017) 'Hypoxia and hypoxia-inducible factor (HIF) downregulate antigen-presenting MHC class I molecules limiting tumor cell recognition by T cells', *PLOS ONE*. Edited by G. Simos. Public Library of Science, 12(11), p. e0187314. doi: 10.1371/journal.pone.0187314.

Sharma, P. *et al.* (2007) 'CD8 tumor-infiltrating lymphocytes are predictive of survival in

muscle-invasive urothelial carcinoma', *Proceedings of the National Academy of Sciences of the United States of America*, 104(10), pp. 3967–3972. doi: 10.1073/pnas.0611618104.

Shen, X. *et al.* (2019) 'Recent findings in the regulation of programmed death ligand 1 expression', *Frontiers in Immunology*. Frontiers Media S.A. doi: 10.3389/fimmu.2019.01337.

Shi, M. J. *et al.* (2019) ' High CD3D/CD4 ratio predicts better survival in muscle-invasive bladder cancer ', *Cancer Management and Research*. Dove Press, 11, pp. 2987–2995. doi: 10.2147/CMAR.S191105.

Shin, D. H. *et al.* (2008) 'Bortezomib inhibits tumor adaptation to hypoxia by stimulating the FIH-mediated repression of hypoxia-inducible factor-1', *Blood*. American Society of Hematology, 111(6), pp. 3131–3136. doi: 10.1182/BLOOD-2007-11-120576.

Siemens, D. R. *et al.* (2008) 'Hypoxia increases tumor cell shedding of MHC class I chain-related molecule: Role of nitric oxide', *Cancer Research*. American Association for Cancer Research, 68(12), pp. 4746–4753. doi: 10.1158/0008-5472.CAN-08-0054.

Sikic, D. *et al.* (2022) 'Utility of stromal tumor infiltrating lymphocyte scoring (sTILs) for risk stratification of patients with muscle-invasive urothelial bladder cancer after radical cystectomy', *Urologic Oncology: Seminars and Original Investigations*. Elsevier, 40(2), pp. 63.e19-63.e26. doi: 10.1016/J.UROLONC.2021.07.025.

Sitkovsky, M. and Lukashev, D. (2005) 'Regulation of immune cells by local-tissue oxygen tension: HIF1α and adenosine receptors', *Nature Reviews Immunology*. Nature Publishing Group, 5(9), pp. 712–721. doi: 10.1038/nri1685.

Sjödahl, G. *et al.* (2012) 'A molecular taxonomy for urothelial carcinoma', *Clinical Cancer Research*, 18(12), pp. 3377–3386. doi: 10.1158/1078-0432.CCR-12-0077-T.

Sjödahl, G. *et al.* (2014) 'Infiltration of CD3+ and CD68+ cells in bladder cancer is subtype specific and affects the outcome of patients with muscle-invasive tumors', *Urologic Oncology: Seminars and Original Investigations*. Elsevier Inc., 32(6), pp. 791–797. doi: 10.1016/j.urolonc.2014.02.007.

Sjödahl, G. *et al.* (2017) 'Molecular classification of urothelial carcinoma: global mRNA classification versus tumour-cell phenotype classification', *The Journal of Pathology*. Wiley-Blackwell, 242(1), p. 113. doi: 10.1002/PATH.4886.

Smythies, J. A. *et al.* (2019) ' Inherent DNA -binding specificities of the HIF -1α and HIF -2α transcription factors in chromatin ', *EMBO reports*. EMBO, 20(1). doi: 10.15252/embr.201846401.

Song, Y. P. *et al.* (2019) 'Organ preservation in bladder cancer: an opportunity for truly personalized treatment', *Nature Reviews Urology*. Nature Publishing Group, pp. 511–522. doi: 10.1038/s41585-019-0199-x.

Song, Y. P. *et al.* (2021) 'Long-Term Outcomes of Radical Radiation Therapy with Hypoxia Modification with Biomarker Discovery for Stratification: 10-Year Update of the BCON (Bladder Carbogen Nicotinamide) Phase 3 Randomized Trial (ISRCTN45938399)', *International Journal of Radiation Oncology Biology Physics*, 110(5), pp. 1407–1415. doi: 10.1016/j.ijrobp.2021.03.001.

Spinetti, T. *et al.* (2016) 'TLR7-based cancer immunotherapy decreases intratumoral myeloid-derived suppressor cells and blocks their immunosuppressive function', *OncoImmunology*. Taylor and Francis Inc., 5(11). doi: 10.1080/2162402X.2016.1230578/SUPPL_FILE/KONI_A_1230578_SM3835.ZIP.

Strauss, J. *et al.* (2018) 'Phase I trial of M7824 (MSB0011359C), a bifunctional fusion protein targeting PD-L1 and TGFb, in advanced solid tumors', *Clinical Cancer Research*. American Association for Cancer Research Inc., 24(6), pp. 1287–1295. doi: 10.1158/1078-0432.CCR-17-2653/87424/AM/PHASE-1-TRIAL-OF-M7824-MSB0011359C-A-BIFUNCTIONAL.

Subramanian, A. *et al.* (2005) 'Gene set enrichment analysis: A knowledge-based approach for interpreting genome-wide expression profiles', *Proceedings of the National Academy of Sciences of the United States of America*, 102(43), pp. 15545–15550. doi: 10.1073/PNAS.0506580102/SUPPL_FILE/06580FIG7.JPG.

Suh, Y. E. *et al.* (2017) 'Association between hypoxic volume and underlying hypoxia-induced gene expression in oropharyngeal squamous cell carcinoma', *British journal of cancer*. Br J Cancer, 116(8), pp. 1057–1064. doi: 10.1038/BJC.2017.66.

Sun, J. *et al.* (2009) 'Hypoxia induces T-cell apoptosis by inhibiting chemokine C receptor 7 expression: the role of adenosine receptor A2', *Cellular & Molecular Immunology 2010 7:1*. Nature Publishing Group, 7(1), pp. 77–82. doi: 10.1038/cmi.2009.105.

Sung, H. *et al.* (2021) 'Global Cancer Statistics 2020: GLOBOCAN Estimates of Incidence and Mortality Worldwide for 36 Cancers in 185 Countries', *CA: A Cancer Journal for Clinicians*. American Cancer Society, 71(3), pp. 209–249. doi: 10.3322/CAAC.21660.

Surace, L. *et al.* (2015) 'Complement Is a Central Mediator of Radiotherapy-Induced Tumor-Specific Immunity and Clinical Response', *Immunity*. Cell Press, 42(4), pp. 767–777. doi: 10.1016/J.IMMUNI.2015.03.009/ATTACHMENT/FC25F3E3-5933-4BEE-8645-

69297E97458F/MMC1.PDF.

Takeuchi, Y. and Nishikawa, H. (2016) 'Roles of regulatory T cells in cancer immunity', *International Immunology*. Oxford University Press, 28(8), p. 401. doi: 10.1093/INTIMM/DXW025.

Talks, K. L. *et al.* (2000) 'The expression and distribution of the hypoxia-inducible factors HIF-1alpha and HIF-2alpha in normal human tissues, cancers, and tumor-associated macrophages.', *The American journal of pathology*. Elsevier, 157(2), pp. 411–21. doi: 10.1016/S0002-9440(10)64554-3.

Tharmalingham, H. and Hoskin, P. (2019) *Clinical trials targeting hypoxia*, *Br J Radiol*.

Theodoropoulos, V. E. *et al.* (2004) 'Hypoxia-Inducible Factor 1α Expression Correlates with Angiogenesis and Unfavorable Prognosis in Bladder Cancer', *European Urology*. Elsevier, 46(2), pp. 200–208. doi: 10.1016/J.EURURO.2004.04.008.

Theodoropoulos, V. E. *et al.* (2005) 'Evaluation of hypoxia-inducible factor 1α overexpression as a predictor of tumour recurrence and progression in superficial urothelial bladder carcinoma', *BJU International*. John Wiley & Sons, Ltd, 95(3), pp. 425–431. doi: 10.1111/J.1464-410X.2005.05314.X.

Thiruthaneeswaran, N. *et al.* (2021) 'Lost in application: Measuring hypoxia for radiotherapy optimisation', *European Journal of Cancer*. Pergamon, 148, pp. 260–276. doi: 10.1016/J.EJCA.2021.01.039.

Thomlinson, R. H. and Gray, L. H. (1955) 'The histological structure of some human lung cancers and the possible implications for radiotherapy.', *British journal of cancer*. Nature Publishing Group, 9(4), pp. 539–49. Available at: http://www.ncbi.nlm.nih.gov/pubmed/13304213 (Accessed: 12 December 2018).

Thomson, D. *et al.* (2014) 'NIMRAD – A Phase III Trial to Investigate the Use of Nimorazole Hypoxia Modification with Intensity-modulated Radiotherapy in Head and Neck Cancer', *Clinical Oncology*. Elsevier, 26(6), pp. 344–347. doi: 10.1016/J.CLON.2014.03.003.

Topalian, S. L. *et al.* (2016) 'Mechanism-driven biomarkers to guide immune checkpoint blockade in cancer therapy.', *Nature reviews. Cancer*. NIH Public Access, 16(5), pp. 275–87. doi: 10.1038/nrc.2016.36.

Toustrup, K. *et al.* (2016) 'Validation of a 15-gene hypoxia classifier in head and neck cancer for prospective use in clinical trials', *Acta Oncologica*. Taylor and Francis Ltd, 55(9–10), pp. 1091–1098. doi:

10.3109/0284186X.2016.1167959/SUPPL_FILE/IONC_A_1167959_SM6886.PDF.

Trajkovic, K. *et al.* (2019) 'Fluctuations in cell density alter protein markers of multiple cellular compartments, confounding experimental outcomes', *PLoS ONE*. Public Library of Science, 14(2). doi: 10.1371/journal.pone.0211727.

Tripathi, A., Khaki, A. R. and Grivas, P. (2021) 'Perioperative Immunotherapy in Muscle-invasive Bladder Cancer', *European Urology Oncology*. Elsevier, 4(2), pp. 131–133. doi: 10.1016/J.EUO.2021.01.004.

Tsakiroglou, A. M. *et al.* (2020) 'Spatial proximity between T and PD-L1 expressing cells as a prognostic biomarker for oropharyngeal squamous cell carcinoma', *British Journal of Cancer*. Springer Nature, 122(4), pp. 539–544. doi: 10.1038/s41416-019-0634-z.

Tsakiroglou, A. M. *et al.* (2021) 'Immune infiltrate diversity confers a good prognosis in follicular lymphoma', *Cancer Immunology, Immunotherapy*. Springer Science and Business Media Deutschland GmbH, 70(12), pp. 3573–3585. doi: 10.1007/S00262-021-02945-0/FIGURES/4.

Tuncbilek, N. *et al.* (2012) 'Value of Dynamic Contrast-Enhanced MRI and Correlation with Tumor Angiogenesis in Bladder Cancer', *http://dx.doi.org/10.2214/AJR.08.1332*. American Roentgen Ray Society, 192(4), pp. 949–955. doi: 10.2214/AJR.08.1332.

Turner, K. J. *et al.* (2002) 'The hypoxia-inducible genes VEGF and CA9 are differentially regulated in superficial vs invasive bladder cancer', *British Journal of Cancer 2002 86:8*. Nature Publishing Group, 86(8), pp. 1276–1282. doi: 10.1038/sj.bjc.6600215.

Uhlen, M. *et al.* (2017) 'A pathology atlas of the human cancer transcriptome', *Science*. American Association for the Advancement of Science, 357(6352). doi: 10.1126/SCIENCE.AAN2507/SUPPL_FILE/SUPPLEMENTARY-TABLES.ZIP.

Vanpouille-Box, C. *et al.* (2015) 'TGFβ is a master regulator of radiation therapy-induced antitumor immunity', *Cancer Research*. American Association for Cancer Research Inc., 75(11), pp. 2232–2242. doi: 10.1158/0008-5472.CAN-14-3511/651811/AM/TGF-IS-A-MASTER-REGULATOR-OF-RADIATION-THERAPY.

Vashistha, V. *et al.* (2017) 'Radical Cystectomy Compared to Combined Modality Treatment for Muscle-Invasive Bladder Cancer: A Systematic Review and Meta-Analysis', *International Journal of Radiation Oncology Biology Physics*. Elsevier Inc., 97(5), pp. 1002–1020. doi: 10.1016/j.ijrobp.2016.11.056.

Vaupel, P. and Harrison, L. (2004) 'Tumor hypoxia: causative factors, compensatory

mechanisms, and cellular response.', *The oncologist*. AlphaMed Press, 9 Suppl 5(Supplement 5), pp. 4–9. doi: 10.1634/theoncologist.9-90005-4.

Vaupel, P. and Kelleher, D. K. (2013) 'Blood flow and oxygenation status of prostate cancers', *Advances in Experimental Medicine and Biology*. Springer Science and Business Media, LLC, 765, pp. 299–305. doi: 10.1007/978-1-4614-4989-8_42/TABLES/4.

Vinay, D. S. *et al.* (2015) 'Immune evasion in cancer: Mechanistic basis and therapeutic strategies', *Seminars in Cancer Biology*. Elsevier Ltd, 35, pp. S185–S198. doi: 10.1016/j.semcancer.2015.03.004.

Walker, A. K. *et al.* (2019) 'MRE11 as a Predictive Biomarker of Outcome After Radiation Therapy in Bladder Cancer', *International Journal of Radiation Oncology Biology Physics*. Elsevier Inc., 104(4), pp. 809–818. doi: 10.1016/j.ijrobp.2019.03.015.

Walker, L. S. K. and Sansom, D. M. (2011) 'The emerging role of CTLA4 as a cell-extrinsic regulator of T cell responses', *Nature Reviews Immunology 2011 11:12*. Nature Publishing Group, 11(12), pp. 852–863. doi: 10.1038/nri3108.

Walmsley, S. R. *et al.* (2005) 'Hypoxia-induced neutrophil survival is mediated by HIF-1alpha-dependent NF-kappaB activity', *The Journal of experimental medicine*. J Exp Med, 201(1), pp. 105–115. doi: 10.1084/JEM.20040624.

Walshaw, R. C. *et al.* (2018) 'The anti-PD-1 era — an opportunity to enhance radiotherapy for patients with bladder cancer', *Nature Reviews Urology*. Nature Publishing Group, 15(4), pp. 251–259. doi: 10.1038/nrurol.2017.172.

Walshaw, R. C. *et al.* (2020) 'Toll-Like Receptor Agonists and Radiation Therapy Combinations: An Untapped Opportunity to Induce Anticancer Immunity and Improve Tumor control', *International Journal of Radiation Oncology*Biology*Physics*. Elsevier, 108(1), pp. 27–37. doi: 10.1016/J.IJROBP.2020.04.020.

Wang, B. *et al.* (2021) 'Targeting hypoxia in the tumor microenvironment: a potential strategy to improve cancer immunotherapy', *Journal of Experimental and Clinical Cancer Research*. BioMed Central Ltd, pp. 1–16. doi: 10.1186/s13046-020-01820-7.

Wang, J. *et al.* (2015) 'Effect of TLR Agonists on the Differentiation and Function of Human Monocytic Myeloid-Derived Suppressor Cells', *The Journal of Immunology*. The American Association of Immunologists, 194(9), pp. 4215–4221. doi: 10.4049/JIMMUNOL.1402004/-/DCSUPPLEMENTAL.

Wang, Jianxin *et al.* (2022) 'CCR2/CCR5 inhibitor permits the radiation-induced effector T

cell infiltration in pancreatic adenocarcinoma', *The Journal of Experimental Medicine*. The Rockefeller University Press, 219(5). doi: 10.1084/JEM.20211631.

Wang, L. *et al.* (2019) 'EMT- A nd stroma-related gene expression and resistance to pd-1 blockade in urothelial cancer', *Journal of Urology*. Nature Publishing Group, p. 458. doi: 10.1038/s41467-018-05992-x.

Wang, L. *et al.* (2021) 'Myeloid cell–associated resistance to PD-1/PD-L1 blockade in urothelial cancer revealed through bulk and single-cell RNA sequencing', *Clinical Cancer Research*. American Association for Cancer Research Inc., 27(15), pp. 4287–4300. doi: 10.1158/1078-0432.CCR-20-4574/672427/P/MYELOID-CELL-ASSOCIATED-RESISTANCE-TO-PD-1-PD-L1.

Wang, Y. *et al.* (2020) 'Prognostic value of immune cell infiltration in bladder cancer: A gene expression-based study', *Oncology Letters*, 20(2), pp. 1677–1684. doi: 10.3892/ol.2020.11750.

Wei, S. C., Duffy, C. R. and Allison, J. P. (2018) 'Fundamental mechanisms of immune checkpoint blockade therapy', *Cancer Discovery*, 8(9), pp. 1069–1086. doi: 10.1158/2159-8290.CD-18-0367.

Weichselbaum, R. R. *et al.* (2017) 'Radiotherapy and immunotherapy: a beneficial liaison?', *Nature Reviews Clinical Oncology 2017 14:6*. Nature Publishing Group, 14(6), pp. 365–379. doi: 10.1038/nrclinonc.2016.211.

Williamson, S. K. *et al.* (2005) 'Phase III trial of paclitaxel plus carboplatin with or without tirapazamine in advanced non-small-cell lung cancer: Southwest Oncology Group Trial S0003', *Journal of Clinical Oncology*. American Society of Clinical Oncology, 23(36), pp. 9097–9104. doi: 10.1200/JCO.2005.01.3771.

van Wilpe, S. *et al.* (2020) 'Prognostic and predictive value of tumor-infiltrating immune cells in urothelial cancer of the bladder', *Cancers*, 12(9), pp. 1–22. doi: 10.3390/cancers12092692.

Winerdal, M. E. *et al.* (2018) 'Urinary bladder cancer tregs suppress mmp2 and potentially regulate invasiveness', *Cancer Immunology Research*. American Association for Cancer Research Inc., 6(5), pp. 528–538. doi: 10.1158/2326-6066.CIR-17-0466/470582/AM/URINARY-BLADDER-CANCER-TREGS-SUPPRESS-MMP2-AND.

Winter, S. C. *et al.* (2007) 'Relation of a Hypoxia Metagene Derived from Head and Neck Cancer to Prognosis of Multiple Cancers', *Cancer Research*. American Association for Cancer

Research, 67(7), pp. 3441–3449. doi: 10.1158/0008-5472.CAN-06-3322.

Wołącewicz, M. *et al.* (2020) 'Immunotherapy in bladder cancer: Current methods and future perspectives', *Cancers*. MDPI AG, 12(5). doi: 10.3390/cancers12051181.

Wright Muelas, M. *et al.* (2018) 'Rational cell culture optimization enhances experimental reproducibility in cancer cells', *Scientific Reports*. Nature Publishing Group, 8(1), pp. 1–16. doi: 10.1038/s41598-018-21050-4.

Wu, S.-Q. *et al.* (2018) 'Prognostic roles of tumor associated macrophages in bladder cancer: a system review and meta-analysis', *Oncotarget*. Impact Journals, 9(38), pp. 25294–25303. doi: 10.18632/ONCOTARGET.25334.

Wu, Y. *et al.* (2020) 'Identification of the Six-RNA-Binding Protein Signature for Prognosis Prediction in Bladder Cancer', *Frontiers in Genetics*. Frontiers Media S.A., 11, p. 992. doi: 10.3389/FGENE.2020.00992/BIBTEX.

Xie, J. *et al.* (2013) 'Expression and significance of hypoxia-inducible factor-1α and MDR1/P-glycoprotein in laryngeal carcinoma tissue and hypoxic Hep-2 cells', *Oncology Letters*. Spandidos Publications, 6(1), p. 232. doi: 10.3892/OL.2013.1321.

Xie, X. J. *et al.* (2021) 'Knockdown of TRIM26 inhibits the proliferation, migration and invasion of bladder cancer cells through the Akt/GSK3β/β-catenin pathway', *Chemico-biological interactions*. Chem Biol Interact, 337. doi: 10.1016/J.CBI.2021.109366.

Xu, Z. *et al.* (2018) 'High expression of B7-H3 and CD163 in cancer tissues indicates malignant clinicopathological status and poor prognosis of patients with urothelial cell carcinoma of the bladder', *Oncology Letters*. Spandidos Publications, 15(5), pp. 6519–6526. doi: 10.3892/OL.2018.8173/HTML.

Xue, J. *et al.* (2014) 'Transcriptome-based network analysis reveals a spectrum model of human macrophage activation.', *Immunity*. Elsevier, 40(2), pp. 274–88. doi: 10.1016/j.immuni.2014.01.006.

Xue, Y. *et al.* (2019) 'Tumor-infiltrating M2 macrophages driven by specific genomic alterations are associated with prognosis in bladder cancer', *Oncology Reports*. Spandidos Publications, 42(2), pp. 581–594. doi: 10.3892/OR.2019.7196/HTML.

Yang, L., Taylor, J., *et al.* (2017) 'A gene signature for selecting benefit from hypoxia modification of radiotherapy for high-risk bladder cancer patients', *Clinical Cancer Research*. American Association for Cancer Research Inc., 23(16), pp. 4761–4768. doi: 10.1158/1078-0432.CCR-17-0038/87053/AM/A-GENE-SIGNATURE-FOR-SELECTING-BENEFIT-FROM.

Yang, L., Forker, L., *et al.* (2017) 'Validation of a hypoxia related gene signature in multiple soft tissue sarcoma cohorts', *Oncotarget*. Impact Journals, 9(3), pp. 3946–3955. doi: 10.18632/ONCOTARGET.23280.

Yang, L., Roberts, D., *et al.* (2018) 'Development and Validation of a 28-gene Hypoxia-related Prognostic Signature for Localized Prostate Cancer.', *EBioMedicine*. Elsevier, 31, pp. 182–189. doi: 10.1016/j.ebiom.2018.04.019.

Yang, L., Forker, L., *et al.* (2018) 'Validation of a hypoxia related gene signature in multiple soft tissue sarcoma cohorts', *Oncotarget*. Impact Journals LLC, 9(3), pp. 3946–3955. doi: 10.18632/oncotarget.23280.

Yang, L. J. and West, C. M. L. (2019) 'Hypoxia gene expression signatures as predictive biomarkers for personalising radiotherapy', *British Journal of Radiology*. British Institute of Radiology. doi: 10.1259/bjr.20180036.

Yang, Z. *et al.* (2005) 'Infarct-sparing effect of A2A-adenosine receptor activation is due primarily to its action on lymphocytes', *Circulation*. Circulation, 111(17), pp. 2190–2197. doi: 10.1161/01.CIR.0000163586.62253.A5.

Yokokawa, J. *et al.* (2008) 'Enhanced Functionality of CD4+CD25highFoxP3+ Regulatory T Cells in the Peripheral Blood of Patients with Prostate Cancer', *Clinical Cancer Research*, 14(4), pp. 1032–1040. doi: 10.1158/1078-0432.CCR-07-2056.

Younes, M. *et al.* (2001) 'Glut 1 expression in transitional cell carcinoma of the urinary bladder is associated with poor patient survival.', *Anticancer Research*, 21(1B), pp. 575–578. Available at: https://europepmc.org/article/med/11299807 (Accessed: 20 July 2022).

Young, A. *et al.* (2018) 'A2AR Adenosine Signaling Suppresses Natural Killer Cell Maturation in the Tumor Microenvironment', *Cancer research*. Cancer Res, 78(4), pp. 1003–1016. doi: 10.1158/0008-5472.CAN-17-2826.

Yuan, T. L. *et al.* (2011) 'Cell-to-cell variability in PI3K protein level regulates PI3K-AKT pathway activity in cell populations', *Current Biology*. NIH Public Access, 21(3), p. 173. doi: 10.1016/J.CUB.2010.12.047.

Zelenay, S. *et al.* (2015) 'Cyclooxygenase-Dependent Tumor Growth through Evasion of Immunity', *Cell*. Elsevier, 162(6), p. 1257. doi: 10.1016/J.CELL.2015.08.015.

Zhang, F. *et al.* (2021) 'Development and Validation of a Hypoxia-Related Signature for Predicting Survival Outcomes in Patients With Bladder Cancer', *Frontiers in Genetics*. Frontiers Media S.A., 12. doi: 10.3389/FGENE.2021.670384/FULL.

Zhang, H. *et al.* (2021) 'Tumor Microenvironment Analysis Identified Subtypes Associated With the Prognosis and the Tumor Response to Immunotherapy in Bladder Cancer', *Frontiers in Genetics*. Frontiers Media S.A., 12, p. 134. doi: 10.3389/FGENE.2021.551605/BIBTEX.

Zhang, J. *et al.* (2018) 'Cyclin D-CDK4 kinase destabilizes PD-L1 via Cul3SPOP to control cancer immune surveillance', *Nature*. NIH Public Access, 553(7686), p. 91. doi: 10.1038/NATURE25015.

Zhang, Q. *et al.* (2021) 'A novel hypoxia gene signature indicates prognosis and immune microenvironments characters in patients with hepatocellular carcinoma', *Journal of Cellular and Molecular Medicine*. John Wiley & Sons, Ltd, 25(8), pp. 3772–3784. doi: 10.1111/JCMM.16249.

Zhang, Z. *et al.* (2021) 'Identifying a hypoxia related score to predict the prognosis of bladder cancer: a study with The Cancer Genome Atlas (TCGA) database', *Translational Andrology and Urology*. AME Publications, 10(12), p. 4353. doi: 10.21037/TAU-21-569.

Zhao, J. *et al.* (2021) 'TRIM26 positively regulates the inflammatory immune response through K11-linked ubiquitination of TAB1', *Cell death and differentiation*. Cell Death Differ, 28(11), pp. 3077–3091. doi: 10.1038/S41418-021-00803-1.

Zhou, M. *et al.* (2010) 'Warburg effect in chemosensitivity: Targeting lactate dehydrogenase-A re-sensitizes Taxol-resistant cancer cells to Taxol', *Molecular Cancer*. BioMed Central, 9, p. 33. doi: 10.1186/1476-4598-9-33.

Zou, X. *et al.* (2021) 'A novel 6-gene signature derived from tumor-infiltrating T cells and neutrophils predicts survival of bladder urothelial carcinoma', *Aging (Albany NY)*. Impact Journals, LLC, 13(23), p. 25496. doi: 10.18632/AGING.203770.